

**Improving the Design of Travelling Wave Type
Sloshing Absorbers**

Jayson Allan Grant

A thesis submitted to Victoria University
for the Doctor of Philosophy Degree (Mechanical Engineering)

2014

ACKNOWLEDGEMENTS

I would like to thank the supervisors of this thesis, Dr. Eren Semercigil, Dr. Özden Turan and Dr. Mahesh Prakash. Their valuable guidance, encouragement and assistance helped me immensely in the preparation and completion of this study.

While undertaking my Doctorate of Philosophy I received a Postgraduate Research Scholarship from Victoria University, as well as a top-up Research Scholarship from CSIRO. The financial support of these two scholarships was greatly appreciated.

Finally, I express my sincerest gratitude to my family and friends for their support.

Jayson Allan Grant

ABSTRACT

Liquid sloshing absorbers are simple structures consisting of a partially full container of liquid with a free surface. The primary objective of this thesis is to investigate the potential to improve the design of rectangular sloshing absorbers through attaching surface roughness elements (obstructions) to the absorbers. The potential to increase energy dissipation through intentionally induced liquid sloshing within an absorber for structural control purposes is presented.

Smoothed Particle Hydrodynamics (SPH) is a numerical modelling tool used in this thesis to predict fluid-structure interactions. SPH can accurately predict complex liquid free surface behaviour and liquid velocities. Here SPH is used to successfully model two and three-dimensional liquid sloshing absorbers with predictions validated experimentally. Hence, SPH is proven to be a promising tool for these studies.

The novelty of this thesis consists of using SPH to determine energy dissipation characteristics and the increase of performance in various designs of liquid sloshing absorbers through the introduction of surface roughness elements (obstructions). Attaching obstructions to the base of shallow liquid level rectangular sloshing absorber increases energy dissipation significantly. Varying the inclination alone of two rectangular absorbers attached to a structure is then investigated, giving promising results over various structural frequencies. Normally, varying structural frequencies require different size containers to maintain effective control as the container length is a critical tuning parameter. Hence, there are practical advantages by using the same container, but only varying its inclination. Finally, the novel concept of implementing the geometry of a hen's egg as a sloshing absorber is analysed. Experiments were previously undertaken to analyse the effectiveness of energy dissipation within the egg by reporting on the transient oscillations after it is released, on the ground, from its vertical position. These experiments are compared with three dimensional numerical predictions of the hen's egg and produce acceptable similarities. The egg's unique, natural shape shows great potential producing high damping characteristics.

TABLE OF CONTENTS

	Page
ACKNOWLEDGEMENTS	ii
ABSTRACT	iii
TABLE OF CONTENTS	iv
LIST OF FIGURE CAPTIONS	vi
Chapter 1	1
INTRODUCTION	
Chapter 2	9
ANALYSING AN EFFICIENT LIQUID SLOSHING ABSORBER FOR VIBRATION CONTROL USING SPH	
2.1 INTRODUCTION	9
2.2 SURFACE ROUGHNESS ELEMENTS	11
2.3 FREQUENCY STUDY	13
2.4 INITIAL CONDITION DEPENDENCE	14
2.5 NUMERICAL MODEL	16
2.6 PERFORMANCE INDICATOR	18
2.7 NUMERICAL PREDICTIONS	20
2.7.1 Optimum Ratio Cases	20
2.7.2 ‘Tuned’ cases	24
2.7.3 Comparisons between Summaries of Optimum and ‘Tuned’ Cases	27
2.7.4 Energy Dissipation Characteristics of Optimum Obstruction Case	27
2.7.5 Dependence on Initial Displacement Magnitude	29
2.7.6 Energy Dissipation Characteristics for Different Initial Displacement	34
2.8 CONCLUSIONS	35
Chapter 3	53
A SLOSHING ABSORBER WITH DESIGNED OBSTRUCTIONS TO IMPROVE ENERGY DISSIPATION	
3.1 INTRODUCTION	53
3.2 EXPERIMENTAL SETUP	54
3.3 INITIAL EXPERIMENTS	56
3.3.1 Identifying Effective Obstruction Cases	58
3.3.2 Identifying Effective Obstruction Cases with Respect to r/h_w	63

	Page
3.3.3 Identifying Effective Obstruction Cases With respect to d/L	65
3.4 NUMERICAL MODEL	66
3.5 NUMERICAL PREDICTIONS	67
3.5.1 Numerical and Experimental Displacement History Comparison	67
3.5.2 Numerical and Experimental Liquid Flow Field Comparison	70
3.5.3 Numerical Displacement Histories Analysing Effects of Obstructions	72
3.5.4 Summary of Performance of Numerical Cases	73
3.5.5 Numerical and Experimental Settling Time Ratio Comparison	76
3.5.6 Liquid Flow Field Comparisons – Effects of Obstructions	77
3.6 CONCLUSIONS	78
Chapter 4	99
A STUDY ON THE EFFECT OF INCLINATION ON A SLOSHING ABSORBER USING SPH	
4.1 INTRODUCTION	99
4.2 NUMERICAL MODEL	101
4.3 NUMERICAL PREDICTIONS	104
4.3.1 Numerical Validation	104
4.3.2 Frequency Variation Study	109
4.3.3 Summary of Performance	112
4.3.4 Liquid Velocity Flow Fields	116
4.3.4.1 Energy dissipation Characteristics – Cases Without and With Inclination	116
4.3.4.2 Energy dissipation Characteristics – Inclined Tuned and Un-tuned Cases	121
4.3.5 Inclination Cases with Obstructions	125
4.4 CONCLUSIONS	129
Chapter 5	153
SLOSHING AND ENERGY DISSIPATION IN AN EGG: SPH SIMULATIONS AND EXPERIMENTS	
5.1 INTRODUCTION	153
5.2 NUMERICAL MODEL	155
5.3 DISCUSSION	156
5.3.1 Comparison of Experimental and Numerical Observations	156
5.3.2 Effect of Viscosity	160
5.3.3 The Effects of Obstructions	163
5.3.4 Tuning – A Frequency Study	167
5.4 CONCLUSIONS	170

Chapter 6	186
CONCLUSION	
REFERENCES	192
APPENDIX 1	199
SMOOTHED PARTICLE HYDRODYNAMICS	
APPENDIX 2	204
RESOLUTION STUDY	

LIST OF FIGURE CAPTIONS

- Figure 1.1: Schematic of the structure with an absorber.
- Figure 2.1: (b) Liquid flow past a semi-circular obstruction within the rectangular liquid sloshing absorber and (b) geometry of the rectangular absorber with semi-circular obstructions.
- Figure 2.2: Two snapshots of the velocity contours at particular instances for the 1 obstruction case with a 16 degree initial displacement. (a) High velocities (in red) occur within the liquid and (b) large free surface deformation occurs at the right wall as the structure oscillates from left to right. Velocity scale runs from 0 m/s to 0.8 m/s.
- Figure 2.3: (a) Schematic of the structure with an attached absorber and (b) displacement history of uncontrolled structure (with attached absorber without liquid).
- Figure 2.4: Displacement histories with liquid height of 14.9 mm (— —); and 8 mm without (—) and with one 6 mm obstruction (—) for structural frequencies of (a) 0.36 Hz, (b) 0.5 Hz, (c) 0.64 Hz, (d) 0.78 Hz and (e) 0.92 Hz.
- Figure 2.5: Variation of (a) 10 % and (b) 5 % settling times with the frequency ratio from Figure 2.4. Without (—) and with 1 obstruction (—) at a liquid height of 8 mm and without an obstruction (—) at a liquid height of 14.9 mm.

Figure 2.6: Same as in Figure 2.4, but for varying liquid heights to achieving theoretical tuning.

Figure 2.7: Same as in Figure 2.5, but for ‘tuned’ liquid height cases, from Figure 2.6, without () and with 1 obstruction ().

Figure 2.8: Same as in Figure 2.5, but for cases from Figures 2.5 and 2.7. Horizontal axis is structural frequency, f_s (Hz).

Figure 2.9: Still frames at areas of interest of liquid flow field comparisons of water within a sloshing absorber controlling a structure. Left column shows 1 semi-circular obstruction located in the bottom centre and liquid height of 8 mm case. Right column shows the case without an obstruction with a liquid height of 14.9 mm. Both cases have a 2.5 degrees initial displacement. Fixed velocity scale shows fluid particle velocity ranging from 0 to 0.8 m/s.

Figure 2.10: Numerical displacement histories with structural frequency of 0.64 Hz and liquid height of 14.9 mm without obstructions () and liquid height of 8 mm with 1 () and 2 () obstructions with radius of 6 mm for initial displacements of (a) 1.25, (b) 2.5, (c) 3.75, (d) 6.25, (e) 10 and (f) 16 degrees.

Figure 2.11: Summary of (a) 10 % and (b) 5 % settling times from cases in Figure 2.10 for cases with 1 () and 2 () obstructions at a liquid height of 8 mm and without an obstruction () at a liquid height of 14.9 mm.

Figure 2.12: Still frames at areas of interest of liquid flow field comparisons of water within a sloshing absorber controlling a structure. Left column shows the same 1 obstruction case as in Figure 2.9 with an initial displacement of 2.5 degrees. Right column shows the same case with an initial displacement of 16 degrees. Fixed velocity scale shows fluid particle velocity ranging from 0 to 0.8 m/s.

Figure 3.1: (a) Schematic and (b) photograph of the structure with the absorber.

Figure 3.2: (a) Geometry of the rectangular absorber with 3 semi-circular obstructions (not to scale). (b) 3 semi-circular obstructions attached to the bottom centre of the rectangular container (distance between obstructions centre to centre is 42.5mm). (c) Front and (d) plan views of the semi-circular obstruction with section of tape removed.

Figure 3.3: Schematic plan views of containers with obstructions attached (specified by red lines) for (a) 7 obstructions (even spaced), (b) 2 obstructions (1 obstruction 45 mm from each wall) and (c) 1 obstruction (centre).

Figure 3.4: Settling time ratios for 0 obstructions (—◆—), 7 obstructions (—), 2 obstructions (sides) (—) and 1 obstruction (centre) (—▲—) with a 4 mm obstruction height from 2.6 mm to 10.2 mm liquid height.

Figure 3.5: Schematic plan views of containers with obstructions attached (specified by red lines) for (a) 1 obstruction (centre), (b) 3 obstructions (1 obstruction centre, 2 obstructions (45 mm from each wall) and (c) 3 obstructions (centre, spaced 45 mm from centre obstruction).

Figure 3.6: Same as Figure 3.2 but for 0 obstructions (, 1 obstructions (centre) (, 3 obstructions (1 centre, 2 sides) () and 3 obstructions (centre) () with a 2 mm obstruction height and 1 obstructions (centre) (, 3 obstructions (1 centre, 2 sides) () and 3 obstructions (centre) () with a 4 mm obstruction height.

Figure 3.7: Schematic plan views of containers with obstructions attached (specified by red lines) for (a) 1 obstruction (centre), (b) 3 obstructions (1 obstruction centre, 2 obstructions spaced 45 mm from each wall), (c) 3 obstructions (centre, spaced 45 mm from centre obstruction), (d) 2 obstructions (45 mm from each wall) and (e) 5 obstructions (spaced evenly).

Figure 3.8: Settling time ratios for 2 obstructions (sides) (, 5 obstructions (, 1 obstruction (centre) (, 3 obstructions (1 centre, 2 sides) () and 3 obstructions (centre) () with an 8 mm obstruction height at 7.7 mm to 15.3 mm liquid heights.

Figure 3.9: Schematic plan views of containers with obstructions attached (specified by red lines) for (a) 3 obstructions (1 obstruction centre, 2 obstructions spaced 45 mm from each wall), (b) 3 obstructions (spaced evenly), (c) 3 obstructions (centre, spaced 45 mm from centre obstruction) and (d) 3 obstructions (centre, spaced 22.5 mm from centre obstruction).

Figure 3.10: Same as Figure 3.2 but for 0 obstructions (—◆—), 3 obstructions (1 centre, 2 sides) (—✱—), 3 obstruction (1 centre, 2 middle) (—●—), 3 obstructions (1 centre, 21.25 mm) (—+—) and 3 obstructions (centre) (—+—) with a 4 mm obstruction height.

Figure 3.11: A summary of settling time ratios for cases with obstruction height to liquid height ratio (r/h_w) and obstruction heights (r) of 2 mm (—), 4 mm (—) and 8 mm (—). Inserts are schematic plan views of containers for cases in each figure with varying distance of obstruction to centre of container to free surface length ratio (d/L) of (a) 0 (1 obstruction in the centre), (b) 0.125 (3 obstructions in the centre with 42.5 mm spacing) and (c) 0.375 (3 obstructions with 127.5 mm spacing).

Figure 3.12: Variation of settling time ratio for distance of obstructions to centre of container to free surface length ratio (d/L) for obstruction height to liquid height ratio (r/h_w) of 0.4 ($r = 2$ mm) (—), 0.5 ($r = 4$ mm) (—), 0.8 ($r = 8$ mm) (—).

Figure 3.13: Displacement histories of uncontrolled (-----) and controlled (——) with the rectangular absorber with 3 semi-circular obstructions attached to the bottom centre of the container with obstruction height of 4 mm and a liquid height of 7.7 mm.

Figure 3.14: Displacement histories of the experimental observation (----) and numerical prediction with smoothing lengths of 1.2 (—), 1.6 (—), 2.0 (—) and 2.4 (—). Obstructions are the same as in Figure 4.

Figure 3.15: Still frames at areas of interest of free surface comparisons of water within a sloshing absorber controlling a structure. 3 semi-circular obstructions located in the bottom centre with obstruction height and spacing of 4 mm and 42.5 mm respectively, 16 degrees initial displacement and liquid height of 7.7 mm case is used for this comparison. Left column shows experimental observations. Right column shows numerical predictions obtained with SPH. Experimental error is 1/25 s (+/- 40 ms). Fixed velocity scale shows fluid particle velocity ranging from 0 to 1 m/s.

Figure 3.16: Displacement histories of the structure when coupled to rectangular shaped absorber without (—) and with one (—) and 3 (—) semi-circular obstructions located in the centre (4 mm obstruction height) with obstruction spacing of 42.5 mm, 16 degrees initial displacement and liquid heights of (a) 2.6 mm, (c) 5.1 mm, (e) 7.7 mm, (g) 10.2 mm and (i) 12.8 mm. The right column displays the cases from the left column restricted to +/- 4 degrees

displacement and time from 6 s to 18 s to focus on the effect of obstructions at small displacements (b) 2.6 mm, (d) 5.1 mm, (f) 7.7 mm, (h) 10.2 mm and (j) 12.8 mm.

Figure 3.17: Variation of (a) 10 %, (b) 5 % and (c) 2.5 % settling time ratios with liquid height to free surface length ratio (h_w/L) for absorbers without () and with 1 () and 3 () obstructions. Settling times are taken from cases in Figure 3.14. The settling time ratio for the optimum case from (V.J. Modi and S.R. Munshi, 1998) with a d/L of 0 and an r/h_w of 0.75 ($r = 6$ mm) () is also displayed for comparison.

Figure 3.18: Variation of (a) numerical 2.5 % settling time ratios and (b) experimental settling time ratios with liquid height to free surface length ratio (h_w/L) for absorbers without () and with 1 () and 3 () obstructions. Numerical and experimental settling time ratios are taken from cases in Figures 3.17(c) and 3.6, respectively.

Figure 3.19: Still frames at areas of interest of liquid flow field comparisons of water within the lower half of a sloshing absorber controlling a structure. Left column shows 3 semi-circular obstructions located in the bottom centre with obstruction height and spacing of 4 mm and 42.5 mm respectively, 16 degrees initial displacement and liquid height of 7.7 mm case is used for this comparison. Right column shows same case without obstructions. Fixed velocity scale shows fluid particle velocity ranging from 0 to 1 m/s.

Figure 4.1: An (a) isometric line drawing and (b) photograph of the experimental setup in the wind tunnel, looking upstream. (c) Numerical model of the two inclined containers attached to the bridge deck by two vertical poles. A simplified end view is shown, for clarity.

Figure 4.2: A snapshot of the velocity contours at a particular marked instance for the 20 degree inclination case. Liquid sloshing occurs within the two containers as the structure oscillates. Velocity scale runs from 0 m/s to 0.1 m/s.

Figure 4.3: Numerical (solid line) and experimental (dashed line) displacement histories for 2 containers with free surface (L) of 150mm at structural frequency of 1.8Hz (a) uncontrolled and at inclinations (b) 0, (c) 8, (d) 13, (e) 20 and (f) 26 degrees. (Tuned at 13 degrees (c))

Figure 4.4: Numerical displacement histories of the 0 degree inclination case at a structural frequency of 1.8Hz with particle sizes 0.8 mm x 0.8 mm (— —) from Figure 4.3(b), and 0.4 mm x 0.4 mm (—).

Figure 4.5: Same as Figure 4.3 but for a structural frequency of 0.85Hz. (Tuned at 0 degrees (b))

Figure 4.6: Numerical displacement histories for 2 containers with free surface (L) of 700mm at inclinations (a) 0, (b) 1.5, (c) 2.5, (d) 4, (e) 6, (f) 8, (g) 10 and (h) 12 degrees for structural frequencies of 0.5Hz (— —), 0.7Hz (— —) and 0.9Hz (— —). Structural frequencies of 0.5Hz, 0.7Hz and 0.9Hz are tuned at 4 (d), 8 (f) and 12 (h) degree inclinations respectively.

Figure 4.7: (a) 10 % and (b) 5 % settling times ratios for cases with structural frequencies 0.5 Hz (— —), 0.7 Hz (— —) and 0.9 Hz (— —), from Figure 4.6.

Figure 4.8: Average (a) 10 % and (b) 5 % settling time ratios over structural frequencies 0.5 Hz, 0.7 Hz and 0.9 Hz, for cases from Figure 4.6.

Figure 4.9: (a) 10 % and (b) 5 % settling time ratios with respect to liquid frequency to natural frequency (f_L/f_s) for cases in Figures 4.7(a) and (b).

Figure 4.10: Liquid velocity flow field snapshots for 3 numerical cases approaching first positive structural peak displacement. (a) for 0 degree inclination from Figure 4.5(b) with a structural frequency of 0.85 Hz, (b) for 0 degree inclination from Figure 4.6(a) with a structural frequency of 0.5 Hz, (c) for 4 degrees inclination from Figure 4.6(d) with a structural frequency of 0.5 Hz. Velocity colour scale indicates a range from 0 m/s (blue) to 0.1 m/s (red).

Figure 4.11: Same cases as Figure 4.9 except approaching second negative structural peak displacement.

Figure 4.12: Liquid velocity flow field snapshots at first zero structural displacement for cases with a structural frequency of 0.7 Hz. (a) for 4 degree inclination from Figure 4.6(d), (b) for 8 degree (tuned) inclination from Figure 4.6(f) and (c) for 12 degrees inclination from Figure 4.6(h).

Figure 4.13: Same cases as Figure 4.12 except at first positive structural peak displacement.

Figure 4.14: Same cases as Figure 4.12 except at second zero structural displacement.

Figure 4.15: Same cases as Figure 4.12 except at second negative structural peak displacement.

Figure 4.16: Same cases as Figure 4.12 except at fifth zero structural displacement.

Figure 4.17: Same cases as Figure 4.12 except at third positive structural peak displacement.

Figure 4.18: Same cases as in Figure 4.6 (— —) without obstructions and with a single semi-circular obstruction located in the centre base of the container with obstruction radius of 2.4mm (—) and 5.9mm (—) for inclinations (a) 0, (b) 4, (c) 6 and (d) 8 degrees. (Tuned at 4 degrees (b))

Figure 4.19: Same cases as in Figure 4.6 (— —) without obstructions and with evenly spaced semi-circular obstructions (—) with obstruction radius of 2.4mm for inclinations (a) 0, (b) 1.5, (c) 2.5, (d) 4, (e) 6 and (f) 8 degrees. (Tuned at 4 degrees (d))

Figure 4.20: Liquid velocity flow field snapshots for 2 numerical cases with a structural frequency of 0.5 Hz. (a) and (c) for 4 degrees inclination (repeated from Figure 4.9(c) and 4.10(c)), (b) and (d) for 4 degrees inclination with evenly spaced obstructions with a obstruction height of 2.4 mm from Figure 4.19(d). Velocity colour scale indicates a range from 0 m/s (blue) to 0.1 m/s (red).

Figure 5.1: Angular displacement history of an egg when raw (—) and boiled (---) from (G. So and S.E. Semercigil, 2004).

Figure 5.2: Physiology of egg (Avian Sciences Net, 2012).

Figure 5.3: Geometry of an egg (A. Marsh et al., 2012).

$r_1 = 22$ mm (vertical), $r_2 = 14$ mm (inverted) and $r_3 = 44$ mm (horizontal).

Figure 5.4: Displacement histories for numerical egg friction coefficient of 0.01 (blue thin), 0.05 (red thick) and experimental observations (green dot) for (a) 0.2, (b) 0.4, (c) 0.6, (d) 0.8 and (e) 1 volume fractions.

Figure 5.5: Variation of (a) 10% and (b) 5% settling time and (c) initial potential energy (—▲—) with volume fraction. Settling times given for experimental cases (—●—) and numerical ones with friction coefficient of 0.01 (—◆—) and 0.05 (—■—).

Figure 5.6: Numerical displacement histories for friction coefficient of 0.01, 0.2 volume fraction and a viscosity of (a) 0.001 Pa s, (b) 0.1 Pa s, (c) 1.0 Pa s; and 1.0 volume fraction and a viscosity of (d) 0.001 Pa s, (e) 0.1 Pa s and (f) 1.0 Pa s. Red dots correspond to the instants of the snapshots in Figure 5.7 and 5.8.

Figure 5.7: Liquid velocity flow field snapshots corresponding to marked instances in Figure 5.6 for 0.2 volume fraction. (a) to (d) for viscosity of 0.001 Pa s, and (e) to (h) for viscosity of 1.0 Pa s. Velocity colour scale range from 0 m/s (blue) to 0.3 m/s (red).

Figure 5.8: Same as in Figure 7, but for 1 volume fraction.

Figure 5.9: Egg geometry for 1 (a) and 2 (b) semi-circular obstruction cases with radius 4 mm.

Figure 5.10: Numerical displacement histories without (-----) and with 1 semi-circular obstruction (——) with radius 4 mm and friction coefficient of 0.01, 0.2 volume fraction and a viscosity of (a) 0.001 Pa s, (b) 0.1 Pa s, (c) 1.0 Pa s; and 1.0 volume fraction and a viscosity of (d) 0.001 Pa s, (e) 0.1 Pa s and (f) 1.0 Pa s.

Figure 5.11: Same as Figure 5.10 but for 2 semi-circular obstructions (——) with radius 4 mm.

Figure 5.12: Liquid velocity flow field snapshots for 0.2 volume fraction. (a) to (d) for 2 semi-circular obstructions with 4 mm radius and (e) to (h) without obstruction case. Velocity colour scale indicates a range from 0 m/s (blue) to 0.3 m/s (red).

Figure 5.13: Variation of the structural (■) and liquid frequencies for different fill levels and for (a) upright (◆), (b) horizontal (◇) and (c) inverted (▲) positions of the egg.

Figure 5.14: Variation of the experimental (▲) and numerical (0.01 friction coefficient ◆, 0.05 friction coefficient ■) structural frequency with volume fraction.

Chapter 1

INTRODUCTION

Tall structures, such as towers and bridges, are subject to wind and earthquake loads which can cause them to oscillate at excessive magnitudes. Liquid sloshing absorbers with shallow or deep liquid levels can be used to suppress these excessive oscillations for structural control purposes (Modi et al., 1996; Modi and Munshi, 1998; Tamura et al., 1996) by tuning the frequency of the sloshing to the critical frequency of the structure to be controlled. These absorbers are simple structures consisting of a partially full container of liquid with a free surface. Tuning ensures that significant amounts of harmful energy can be extracted from the structure to the sloshing liquid. However, there needs to be a rapid means of dissipating this energy to avoid its returning back to the structure (then back to the liquid periodically).

A simple configuration of a structure is displayed in Figure 1.1 with an attached shallow liquid level rectangular sloshing absorber. A shallow liquid level refers to a liquid height sufficiently smaller than the sloshing wavelength, defined by the free surface length, such that the liquid motion is governed by travelling waves. Alternatively, a deep liquid level results in primarily standing wave motion. A free surface is marked in the container attached on top of a single degree-of-freedom structure. The structure's motion excites the fluid within the absorber producing sloshing waves. This fluid motion moves out of phase with the structure, causing the fluid to exert counteracting pressure forces on the container walls, controlling the structure. A sloshing absorber has a number of advantages including simple

design, low manufacturing cost and minimal maintenance. Also, a sloshing absorber can be installed into existing and new structures.

Shallow liquid level sloshing absorbers are the main focus of this thesis. This is because sloshing absorbers with shallow liquid levels have been found to be more effective energy dissipaters than deep liquid level sloshing absorbers (Guzel et al., 2005; Modi and Munshi, 1998; Marsh et al., 2010). Rectangular shaped sloshing absorbers with shallow and deep liquid levels have attracted considerable attention in the literature (Modi et al., 1996; Colagrossi et al., 1994; Colagrossi et al., 1996).

Variations of the standard rectangular container sloshing absorber to improve the energy dissipation performance have been the focal point of several previous studies. Some variations include flexible container walls (Gradinscak et al., 2002), a fluid submerged net in the container (Kaneko and Mizota, 2002), baffles attached to container walls (Anderson et al., 2000), wedge shaped fluid obstacles on the bottom of the container (Modi and Akinturk, 2002), container with embossments on the walls (Young-Kyu, 2004) and a study of various shapes including circular and trapezoidal containers (Marsh et al., 2009). However, there is minimal work in the literature on the energy dissipation performance of surface roughness elements (obstructions) attached to the base of a sloshing absorber, other than that of Modi and Munshi (1998). The primary objective of this thesis is to further investigate the potential to improve the design of sloshing absorbers with surface roughness elements for structural control purposes.

The secondary objective of this thesis is to demonstrate the potential of a numerical modelling tool (Smoothed Particle Hydrodynamics – SPH) to predict fluid-structure interactions. The SPH code used in this thesis has been previously developed by CSIRO (Commonwealth Scientific and Industrial Research Organisation) Division of Mathematics, Informatics and Statistics. Due to its Lagrangian nature SPH can accurately capture complex free surface behaviour (Monaghan, 1992; Cleary and Prakash, 2004) without the need for a mesh structure. Consequently, the potential problem of empty control volumes, which would exist with a grid based Computational Fluid Dynamics (CFD) model, as the sloshing of a shallow level liquid exposes the bottom of the container, does not exist with this technique. Here, SPH is used to model two and three-dimensional liquid sloshing absorbers with predictions validated experimentally. A standard form of the quasi-compressible SPH method has successfully been used to model fluid flows for several industrial and environmental applications (Cleary et al., 2007; Cleary and Prakash, 2004). A detailed description of the method can be found in Monaghan (1992). A brief description of the method is presented in Appendix 1. Each chapter's novelty within this thesis is summarised next. Every chapter contains its own introduction, literature review, discussion and conclusions. All tables and figures are given at the end of each chapter.

Earlier work demonstrated the superior energy dissipation efficiency of a rectangular liquid sloshing absorber through the introduction of semi-circular obstructions attached to the base of the absorber (Modi and Munshi, 1998). A parametric free-vibration study was undertaken showing a significant increase in energy dissipation when the obstructions are introduced. Consequently, suggested experimental optimum ratios were given by Modi and Munshi (1998) for a sloshing absorber's container dimensions, liquid height, obstruction height and

location. However, this optimum obstruction case was only analysed at a single structural frequency. As wind and earthquake loads are random in nature, a sloshing absorber that is an effective energy dissipater over a range of structural frequencies and initial structural displacement amplitudes is attractive for design purposes. As a result, in Chapter 2, a sloshing absorber with attached obstructions using optimum ratios, from Modi and Munshi (1998), is compared to optimal cases without an obstruction and analysed over a range of structural frequencies and initial displacements. This study is undertaken numerically, using SPH, with results validated with the experimental results from Modi and Munshi (1998). Comparing improvements in performance with obstructions over a range of structural frequencies has not been undertaken previously in the literature.

An initial structural displacement amplitude study was undertaken in Modi and Munshi, comparing logarithmic damping factors of cases with and without attached obstructions. However, due to uncertainties in determining the damping factor, as discussed in Chapter 2, 10 % and 5 % settling time is used as the main performance indicator throughout this thesis. A 10 % (or 5 %) settling time is the time taken for the structure to oscillate within 10 % (or 5 %) of its initial displacement. Using settling time as the performance indicator gives even more promising results than observed with displacement amplitudes. In the present study, SPH capabilities are utilised to present further improvements with attached obstructions in structural control. In Chapter 2, displacement histories and liquid velocity flow fields are analysed for collision instances and interaction between the liquid and walls or obstructions. Numerical predications are reported in the form of design recommendations^{1,2}.

The main focus of Chapter 3 is to further explore the full potential of the effects of surface roughness elements. Further exploring the effect of size, number and location of these designed obstructions with respect to liquid height is the topic of interest in this chapter. Increased effectiveness is observed in the cases analysed in Chapter 3 compared to the study in Modi and Munshi (1998). An in-depth numerical and experimental comparison study is undertaken to validate the numerical model as well as determine how the attached obstructions enhance energy dissipation. This study consists of structural displacement history and liquid free surface shape comparisons, which have not been undertaken previously in the literature for an absorber with attached obstructions. Both experimental and numerical predictions are presented in the form of design recommendations. The design recommendations contribute to the literature by giving evidence on how to significantly increase energy dissipation within the sloshing absorbers for engineering applications^{3,4}.

An earlier experimental study, in Semercigil et al. (2013), demonstrated that effective control can be achieved by using the inclination of the container as the only design parameter for varying structural frequencies. Varying the inclination of the container varies the static free surface length and therefore the liquid frequency. Generally, optimal energy dissipation is achieved when the liquid frequency equals the frequency with which the structure oscillates (Kareem, 1990; Banerji et al., 2000). Hence, there is potential for the inclination angle to be an effective tuning parameter. Furthermore, the potential for one inclination angle that is effective over a range of structural frequencies is attractive for design purposes. In Chapter 4, two-dimensional numerical predictions, using SPH, are validated with experimental observations from Semercigil et al., (2013). Numerical cases are analysed over varying structural frequencies to identify the physical events occurring within the absorber that are

responsible for effective energy dissipation. An inclination angle that is effective over a range of structural frequencies is established. Surface roughness elements are attached to the base of the absorber to explore the potential to increase energy dissipation⁵.

The raw hen's egg uses liquid sloshing to efficiently dissipate energy to protect its embryo. Determining the effective dissipation characteristics inherent in the egg's unique shape possesses significant advantages for liquid sloshing absorber design in structural control applications. Therefore, determining the egg's effective dissipation characteristics is the main focus of Chapter 5. Three-dimensional numerical predictions in this chapter are undertaken using SPH. These numerical predictions are validated with experimental observations from So and Semercigil (2004). Three-dimensional numerical analysis of the egg, using SPH, has not been undertaken previously in the literature. SPH is also used to analyse complex liquid free surface shapes and identify the natural egg's effective energy dissipation characteristics. Fill volume and viscosity of the sloshing liquid are investigated in this chapter to establish parameters that produce effective dissipation. Attaching surface roughness elements to the egg to improve energy dissipation further is also investigated. Finally, a frequency study is undertaken to provide an understanding of the insensitivity to varying fill levels. This insensitivity implies a form of self tuning, which can potentially provide significant design advantages^{6,7}.

Conclusions of the thesis are summarised in Chapter 6. The thesis also includes two appendices. In Appendix 1, a brief description of the SPH method and numerical modelling technique is given. A resolution study is presented in Appendix 2, justifying the resolution of the SPH fluid particles used in this thesis.

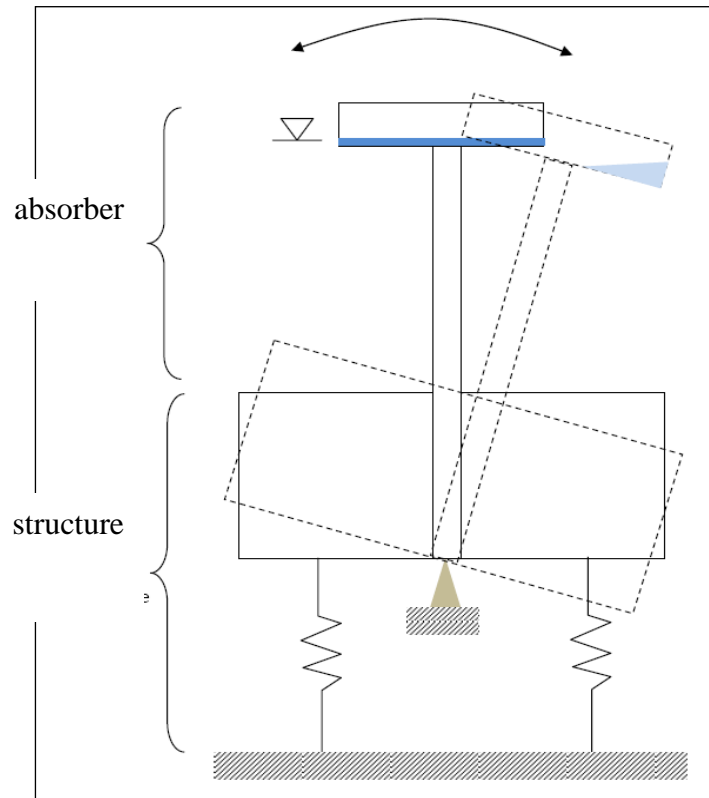


Figure 1.1: Schematic of the structure with an absorber.

¹Grant, J.A., Prakash, M., Semercigil, S.E., Turan, Ö.T., 2010, Analysing an Efficient Liquid Sloshing Absorber for Vibration Control Using SPH, AFMC (Australasian Fluid Mechanics Conference), Auckland, New Zealand.

²Grant, J.A., Prakash, M., Semercigil, S.E., Turan, Ö.T., 2013, Analysing an Efficient Liquid Sloshing Absorber for Vibration Control Using SPH, Journal of Fluids and Structures, under preparation.

³Grant, J.A., Prakash, M., Semercigil, S.E., Turan, Ö.T., 2010, A Rectangular Absorber with Designed Obstructions to Improve Energy Dissipation, 5th International SPHERIC Workshop, Manchester, England.

⁴Grant, J.A., Prakash, M., Semercigil, S.E., Turan, Ö.T., 2013, A Rectangular Absorber with Designed Obstructions to Improve Energy Dissipation Using SPH, Journal of Fluids and Structures, under preparation.

⁵Grant, J.A., Prakash, M., Semercigil, S.E., Turan, Ö.T., 2013, Tuning A Sloshing Absorber Through Inclination Using SPH, Journal of Sound and Vibration, under preparation.

⁶Grant, J.A., Prakash, M., Semercigil, S.E., Turan, Ö.T., 2012, SPH Simulations and Experiments of Sloshing in an Egg-Shaped Shell, 7th International SPHERIC workshop, Prato, Italy.

⁷Grant, J.A., Prakash, M., Semercigil, S.E., Turan, Ö.T., 2012, Sloshing and Energy Dissipation in an Egg: SPH Simulations and Experiments, Submitted to Journal of Sound and Vibration.

Chapter 2

ANALYSING AN EFFICIENT LIQUID SLOSHING ABSORBER FOR VIBRATION CONTROL USING SPH

2.1 Introduction

Large, flexible structures can vibrate at excessive levels due to wind and earthquake loads, causing discomfort to occupants or even structural failure. These structures include tall buildings, long span suspension bridges, communication towers and any section of a machine or building structure that has a significant free span. A sloshing absorber can be attached to a structure to reduce these excessive vibrations. A sloshing absorber is a container partially filled with liquid that has a free surface. A tuned mass damper is another type of absorber, which requires sensors and actuators that control a large solid mass to move in opposition of a structures natural frequency. These sensors and actuators are expensive and require regular maintenance. Sloshing absorbers have a number of advantages compared to a tuned mass damper including simple design, low manufacturing cost and minimal maintenance and therefore sloshing absorbers are the main focus of this thesis. Utilising these advantages would simply be achieved by attaching a sloshing absorber to a large, flexible structure to reduce vibrations instead of a solid mass damper. Liquid sloshing absorbers have been used to reduce vibrations in tall buildings in Japan, United States of America, Canada and Australia (Tamura et al., 1996; Young-Kyu, 2004).

Earlier work demonstrated the superior energy dissipation efficiency of a rectangular liquid sloshing absorber through the introduction of obstructions (Modi and Munshi, 1998). In this work, a parametric free-vibration study was undertaken giving a significant increase in

energy dissipation in the presence of the obstruction. Consequently, suggested experimental optimum ratios were given for a sloshing absorber's container dimensions, liquid height, obstruction height and location. However, this optimum case was only analysed at one structural frequency. As wind and earthquake loads are random in nature, a sloshing absorber that is an effective energy dissipater over a range of structural frequencies and excitation amplitudes is attractive for design purposes in structural applications. As a result, a sloshing absorber with an attached obstruction using optimum ratios from Modi and Munshi, (1998) is compared to optimal cases without an obstruction and analysed over a range of structural frequencies.

Generally, tuning a sloshing absorber to achieve optimum energy dissipation requires the frequency of the sloshing to equal the natural frequency of the structure (Kareem, 1990; Banerji et al., 2000). The key parameters for determining the sloshing frequency within a rectangular absorber are the container length and liquid height. For consistency with the study by Modi and Munshi (1998), container length or free surface length remains constant throughout this chapter and variations in liquid height are investigated. Liquid heights that produce a sloshing frequency that equals the frequency of the structure are analysed over a range of structural frequencies. These 'tuned' liquid height cases, without and with an obstruction using the previously mentioned optimum ratios are compared with the most effective energy dissipation cases without and with an optimum obstruction, from Modi and Munshi (1998). This study is undertaken to determine if the most effective cases, from Modi and Munshi (1998), are more effective than the 'tuned' liquid height cases over a range of structural frequencies.

An initial structural displacement amplitude study was undertaken by Modi and Munshi (1998), comparing cases with and without attached obstructions. However, results from this chapter show differences compared to the study, by Modi and Munshi (1998), analysing the same cases. Therefore, an initial displacement amplitude study is presented in this chapter to determine the potential of the obstructions effectiveness over a range of initial structural displacements.

In this chapter, numerical predictions are undertaken using Smoothed Particle Hydrodynamics (SPH). A standard form of the quasi-compressible SPH method has successfully been used to model fluid flows for several industrial and environmental applications (Cleary et al., 2007; Cleary and Prakash, 2004). In Chapter 3, numerical predictions using this SPH code are validated with experimental observations for a similar setup to this chapter. Due to its Lagrangian nature, SPH can accurately capture complex free surface behaviour (Monaghan, 1992; Cleary and Prakash, 2004). A two-dimensional rectangular sloshing absorber with and without obstructions is modelled here to further investigate the experimental data, from Modi and Munshi (1998). Also, the experimental data is compared with the numerical predictions to validate the SPH model.

2.2 Surface Roughness Elements

Attaching semi-circular surface roughness elements (obstructions) to the base of a rectangular liquid sloshing absorber container were suggested to increase the velocity of the liquid travelling wave. Liquid is accelerated while flowing past an obstruction ($V_2 > V_1$) as displayed in Figure 2.1(a) and was previously reported by (Forbes, 1988). Increasing the

velocity of the travelling wave produces increased potential energy within the liquid at the wave-to-wall interactions. Therefore, enhanced energy dissipation can be achieved through attaching these designed obstructions to a liquid sloshing absorber.

Optimum ratios, for absorber and obstruction geometries, to achieve increased energy dissipation were given by Modi and Munshi (1998). These optimum ratios for a sloshing absorber contain parameters consisting of container length or liquid free surface length (L), liquid height (h_w), obstruction height (r) and location (d) displayed in Figure 2.1(b).

Optimum ratio, obstruction location to container length or free surface length (d/L) equals 0. This suggests that an obstruction located in the centre of a container gives optimum energy dissipation. As a result, a rectangular absorber with 1 obstruction attached in the centre of the absorber's base is analysed in this chapter.

Another obstruction case tested by Modi and Munshi (1998) that shows promising dissipation characteristics is the case with 2 obstructions with a d/L of 0.25. Both cases with 1 and 2 obstructions were analysed at a structural frequency of 0.64 Hz and have an obstruction height of 6 mm, liquid height of 8 mm and free surface length of 370 mm. Therefore, these cases have optimum ratios of obstruction height to liquid height (r/h_w) of 0.75 and liquid height to free surface length (h_w/L) of 0.02. The two obstruction cases are compared to the optimum energy dissipation case without obstructions from Modi and Munshi (1998), which has a liquid height of 14.9 mm. These cases are analysed over structural frequencies of 0.36 Hz to 0.92 Hz and initial displacement amplitudes of 1.25 degrees to 16 degrees.

2.3 Frequency Study

Tuning a sloshing absorber to achieve optimum energy dissipation is usually accomplished by choosing the frequency of the sloshing liquid (f_L) that equals the natural frequency (f_s) of the structure (Kareem, 1990; Banerji et al., 2000). The key parameters for determining the sloshing frequency within a rectangular absorber are the container length and liquid height. For consistency with Modi and Munshi (1998), container length or free surface length remains constant throughout this study and variations in liquid height are investigated. For a given structural frequency, the suggested liquid height to achieve optimal energy dissipation is determined using theoretical tuning, Equation 2.1 (Blevins, 1979). This expression is for a shallow liquid inside a rectangular container.

$$h_w = \frac{(2f_L L)^2}{g}, \quad (2.1)$$

where f_L , L and g are liquid frequency, free surface length and gravitational acceleration, respectively. The free surface length of all cases analysed in this chapter remains constant at 370 mm. However, in liquid heights producing high velocity travelling waves and large free surface discontinuities, this equation may not be as important (Marsh et al., 2009). Instead, efforts to increase energy transfer and dissipation through tuning can produce enhanced effectiveness.

Structural frequencies (f_s) analysed in this chapter are 0.36 Hz, 0.5 Hz, 0.64 Hz, 0.78 Hz and 0.92 Hz. These structural frequencies were chosen as they cover a realistic range of frequencies for a large structure such as a tall building. Therefore, frequencies outside of this range are not of interest. Of course, this small model would not be applied directly to a real structure due to the difference in absorber to structure mass. Effective control can be achieved at an absorber to structure mass ratio of 1 % for a lightly (more than 2 %) damped structure (Banerji et al., 2000). Therefore, to achieve this mass ratio, the absorber's geometries and liquid volumes analysed in this chapter would need to be a part of a larger, compartmentalised arrangement. As a result, the number of absorbers required to produce effective control of the structure would depend entirely on the structure's mass.

The optimum obstruction case, from Modi and Munshi (1998), produces a liquid frequency (f_L) of 0.38 Hz. As a result, for structural frequencies of 0.36 Hz, 0.5 Hz, 0.64 Hz, 0.78 Hz and 0.92 Hz, this case has f_L/f_s of 1.1, 0.76, 0.6, 0.49 and 0.41. Cases with liquid heights using Equation 2.1 for these structural frequencies are 7.2 mm, 14 mm, 22.9 mm, 34 mm and 47.2 mm. An obstruction is then attached to the centre of the container. Obstruction heights of 5.4 mm, 10.5 mm, 17.2 mm, 25.5 mm and 35.4 mm are determined using the optimum ratio, r/h_w of 0.75.

2.4 Initial Condition Dependence

An initial structural displacement amplitude study was undertaken by Modi and Munshi (1998). The displacement amplitude of the structural oscillations affects the liquid motion inside the sloshing absorber. At displacement amplitudes of up to 1 degree, surface ripples

are barely noticeable within the liquid and energy dissipation is negligible. At amplitudes 1 to 2.5 degrees, a single wave is produced accompanied by small ripples in the liquid. Small wave breaking at the wave-to-wall interactions is also observed. At amplitudes from 2.5 degrees to 8.5 degrees (maximum analysed), free surface deformation and high velocity travelling waves of the liquid are observed producing high kinetic energy of the liquid mass. These characteristics result in significantly increased energy dissipation.

Snapshots of the velocity contours, using SPH, at particular instances for the 1 obstruction case with a 16 degree initial displacement are displayed in Figure 2.2. Velocity scale runs from 0 m/s to 0.8 m/s. At displacement amplitudes above 2.5 degrees, high velocities (in red) occur within the liquid, in Figure 2.2(a) and large free surface deformation occurs at the right wall, in Figure 2.2(b) as the structure oscillates from left to right. These predictions agree with the liquid motion characteristics observed at structural displacements above 2.5 degrees by Modi and Munshi (1998). This gives confidence that SPH is a promising numerical tool to further analyse the liquid sloshing absorbers in this chapter.

The study presented in Modi and Munshi (1998) compared cases with and without attached obstructions for varying initial displacement. This study suggested that the case with an obstruction produced increased energy dissipation than compared to the case without an obstruction from initial displacement amplitudes from approximately 0 to about 4 degrees. Above 4 degrees, the case without obstructions produced increased energy dissipation. From experiments and numerical predictions undertaken in Chapter 3, using different optimum ratios for absorber and obstruction geometries, cases with attached obstructions could still

achieve increased energy dissipation at an initial displacement of 16 degrees compared to cases without obstructions. Discrepancies in the effectiveness of the attached obstructions, compared to the study by Modi and Munshi (1998), are due to the difference in the performance indicator used in this chapter, discussed in Section 2.6.

As wind and earthquake loads are random in nature, a sloshing absorber that is an effective energy dissipater over a range of excitation amplitudes is attractive for design purposes in structural applications. Therefore, an initial displacement amplitude study is undertaken in this chapter to determine the potential of the obstructions effectiveness over a range of initial structural displacements. Cases are analysed over initial displacement amplitudes from 1.25 to 16 degrees. Cases outside of this initial displacement history range are not of importance.

2.5 Numerical Model

Numerical predictions are undertaken using Smoothed Particle Hydrodynamics (SPH) to predict fluid-structure interactions. The SPH code used here is developed by CSIRO (Commonwealth Scientific and Industrial Research Organisation) Division of Mathematics, Informatics and Statistics. Due to its Lagrangian nature SPH can accurately capture complex free surface behaviour (Monaghan, 1992; Cleary and Prakash, 2004) without the need for a mesh structure. In this chapter, SPH is used to model two-dimensional liquid sloshing absorbers. A standard form of the quasi-compressible SPH method has successfully been used to model fluid flows for several industrial and environmental applications (Cleary et al., 2007; Cleary and Prakash, 2004). A brief description of the method is presented in Appendix 1.

The two-dimensional structure and the sloshing absorber system are represented by a rigid body, having the same dimensions as the rectangular sloshing absorber from Modi and Munshi (1998) in Figure 2.3(a). The structure's motion is restricted to dynamic rotation about its pivot point. A container to accommodate the sloshing liquid is mounted on top 670 mm above the pivot point. Tethers are attached, representing the structure's stiffness and mechanical damping. Water is used as the sloshing liquid with a density of 1000 kg m^{-3} and dynamic viscosity of 0.001 Pa s .

As this structure is excited, the container on top is subjected to angular oscillations. The uncontrolled structure, for a liquid height of 8 mm, has a mass moment of inertia of 3 kg m^2 . The displacement history of the uncontrolled structure after an initial displacement of 2.5 degrees is displayed in Figure 2.3(b). The uncontrolled structure's slow decay is due to its light damping and critical damping ratio of 1 %. The rectangular absorber's size for the numerical validation remains constant for the study with a length (L) and height (H) of 370 mm and 125 mm respectively. Therefore the wavelength of the fluid or free surface length is also 370 mm. To achieve constant liquid to structure mass ratio, the uncontrolled structure for liquid heights of 7.2 mm to 47.2 mm has a mass of 14.9 kg to 97.9 kg and mass moment of inertia of 2.7 kg m^2 to 17.6 kg m^2 respectively, at rest position.

An SPH particle size of $0.8 \text{ mm} \times 0.8 \text{ mm}$ is suitable to accurately model liquid heights 8mm and above. For liquid heights below 8 mm a particle size of $0.4 \text{ mm} \times 0.4 \text{ mm}$ is used. These resolutions were found to be sufficient from the resolution study (in Appendix 2) for the

shallow liquid levels used in this study and capture all flow characteristics without significantly increasing simulation run time. Time stepping in this code is explicit and is limited by the Courant condition modified for the presence of viscosity, presented in Appendix 1. The time step used for integration is 10^{-6} s. The total real time is 25 seconds for all simulations. The length of simulation time is irrelevant for the reliability of the predictions, as statistical averages are not reported, but simple comparisons of transient vibrations. The number of boundary particles used to model the structure and absorber container is about 8,800. The number of fluid particles used for liquid heights 7.2 mm to 47.2 mm varied from approximately 7,800 to 26,700.

To replicate the experimental initial conditions, from Modi and Munshi (1998), the structure is offset from 0 degrees to an initial displacement amplitude from 1.25 to 16 degrees over 3 seconds. The fluid within the container is given 2 seconds to settle under gravity to reach a state of rest (approaching 0 m/s). The structure is then released, exciting the fluid within the container and allowing the structure to move and respond freely.

2.6 Performance Indicator

Logarithmic damping factor, δ , was the main performance indicator used by Modi and Munshi (1998), given in Equation 2.2.

$$\delta = \frac{1}{n} \ln \frac{x(t)}{x(t+nT)}, \quad (2.2)$$

where n , $x(t)$ and $x(t + nT)$ are number of cycles, initial displacement amplitude and amplitude after 'n' number of cycles, respectively. The damping factor may not give a true representation of the cases' effectiveness to dissipate energy as the damping factor is an assumption of behaviour of a perfectly linear oscillator. As the displacement amplitude decay of the controlled structure is not linear the damping factor will vary depending on where the sample is taken. For example, the displacement history of the case without an obstruction, with a liquid height of 8 mm, in Figure 2.4(c), has a damping factor of 1.6 for the first cycle of oscillation. However, the second and third cycles of oscillation produce damping factors of 0 and 0.9, respectively. Determining a complete cycle of oscillation is also difficult to specify when a distinctive beat is observed in the displacement history as of that in Figure 2.4(c) for the case with a liquid height of 14.9 mm (blue dashed line) at around 2 s. Therefore, in this chapter, 10 % and 5 % settling times are chosen, instead of damping factor, as the key performance indicator. Using settling time as the performance indicator maintains consistency when comparing results of cases with varying structural frequencies and initial displacement amplitudes.

A 10 % (or 5 %) settling time is the time for the peak displacement of the structure to decay within 10 % (or 5 %) of the initial displacement. 10 % and 5 % values are chosen as some indication of performance, and they are not absolute by any measure. Of course, an effective case dissipates its initial energy quickly, resulting in the shortest settling time.

2.7 Numerical Predictions

In the following, SPH predictions using suggested optimum ratio cases, from Modi and Munshi (1998), without and with an attached obstruction, are analysed over structural frequencies 0.36 Hz to 0.92 Hz. Then, the performance of theoretical ‘tuned’ liquid height cases are discussed over the same structural frequencies. Finally, an initial condition dependence study is presented over initial displacement amplitudes of 1.25 to 16 degrees. Liquid velocity flow field snapshots for cases of particular interest are also discussed.

2.7.1 Optimum Ratio Cases

Numerical displacement histories for cases with liquid height of 14.9 mm and 8 mm, without and with 1 semi-circular obstruction located in the centre base of the container are displayed in Figure 2.4. A liquid height of 8 mm is analysed as it was the most effective case, with an obstruction height of 6 mm, at a structural frequency of 0.64 Hz, from Modi and Munshi (1998). The case with a liquid height of 14.9 mm was the most effective without obstructions at the same structural frequency. These cases have an initial displacement amplitude of 2.5 degrees and are analysed over structural frequencies of 0.36 Hz, 0.5 Hz, 0.64 Hz, 0.78 Hz and 0.92 Hz, displayed in Figures 2.4(a), (b), (c), (d) and (e).

Numerical predictions agree with work by Modi and Munshi (1998), where cases with a liquid height of 14.9 mm, without an obstruction, increase energy dissipation as structural frequency increases from 0.36 Hz to 0.64 Hz, in Figures 2.4(a), (b) and (c). This case is most effective at a structural frequency of 0.64 Hz, in Figure 2.4(c). As structural frequencies increase further this case becomes less effective requiring an increased amount of time for the

structure to cease oscillating as displayed in Figures 2.4(d) and (e) for structural frequencies 0.78 Hz and 0.92 Hz, respectively.

A distinctive beat is observed, around 2 s, in the displacement history of the case with a liquid height of 14.9 mm, at a structural frequency of 0.64 Hz, in Figure 2.4(c). A beat in the displacement history gives evidence that the liquid's sloshing frequency is close to the structural frequency. If the sloshing frequency equals the structural frequency, the liquid moves out-of-phase with the structure producing enhanced energy dissipation at the wave-to-wall interactions. However, as the sloshing frequency does not equal the structural frequency, the timing of the wave-to-wall interactions are not optimal. As a result, the liquid is unable to dissipate sufficient energy within the system. Therefore, the energy within the liquid returns to the structure, resulting in continued structural oscillations, after 2.5 s, in Figure 2.4(c).

At a structural frequency of 0.64 Hz, for the case with a liquid height of 14.9 mm, f_L/f_s is approximately 0.8. As suggested in Equation 2.1, to achieve optimal energy dissipation through tuning, f_L/f_s should be approximately 1. This agrees with the observed beat at a structural frequency of 0.64 Hz where tuning is close to being achieved, in Figure 2.4(c). However, at a structural frequency of 0.5 Hz in Figure 2.4(b), f_L/f_s is about 1, but this case becomes less effective requiring increased time to cease oscillating compared to the same case at a structural frequency of 0.64 Hz, in Figure 2.4(c). The reduction in effectiveness for cases with f_L/f_s above 0.8 was also observed by Modi and Munshi (1998). This gives evidence that it is more important to design a shallow liquid level sloshing absorber to enhance energy transfer and dissipation than tuning the liquid sloshing frequency to match the frequency of the structure.

At a structural frequency of 0.5 Hz, the second wave-to-wall interaction begins as the structure travels towards the positive peak displacement, at around 2 s, in Figure 2.4(b). The wave-to-wall interaction, travelling in the same direction as the structure, although dissipating energy, pushes the structure to a larger peak displacement. At a structural frequency of 0.64 Hz, the second wave-to-wall interaction occurs at the positive peak displacement, at about 1.8 s, in Figure 2.4(c). The interaction dissipates increased amounts of energy as the structure has a velocity of approximately 0 m/s. As a result, the interaction causes a beat to occur in the displacement history. However, the liquid is unable to dissipate all the energy from the structure and structural oscillations continue from about 3 seconds, in Figure 2.4(c).

At a liquid height of 8 mm, using the previously mentioned optimum absorber geometry ratios, without obstructions, maximum energy dissipation occurs at a structural frequency of 0.5 Hz, as displayed in Figure 2.4(b). A beat is also observed in the displacement history at about 2.5 s. Also, similar to the case with a liquid height of 14.9 mm, optimum energy dissipation occurs at f_L/f_s of about 0.8, in Figure 2.4(c).

Attaching an obstruction to the same rectangular absorber maximum energy dissipation occurs at a structural frequency of 0.64 Hz displayed in Figure 2.4(c). This is also the most effective case over all the structural frequencies ceasing oscillations within four cycles. Increased velocity gradients in the liquid are observed as the wave travels over the obstruction, also producing increased energy dissipation at the wave-to-wall interactions.

Further analysis on how an attached obstruction increases energy dissipation within the absorber is given later in Section 2.7.4, in the form of liquid flow field snapshots.

10 % and 5 % settling times from cases in Figure 2.4 are displayed in Figures 2.5(a) and 2.5(b). In these figures, the 10 % and 5 % settling times represent the time for the peak displacement to decay within 10 % and 5 % of the initial displacement (2.5 degrees). Cases at liquid heights of 14.9 mm and 8 mm without obstructions give similar trends. Both cases produce similar 10 % settling times, at f_L/f_s of about 0.8, of 4.6 s and 3.2 s respectively. Also, both cases produce increased settling times when structural frequency is varied. As mentioned previously, this gives evidence that it is more important to enhance energy transfer and dissipation than tuning the liquid sloshing frequency to match the frequency of the structure (f_L/f_s of 1).

Attaching an obstruction to the centre of an absorber, using optimum ratios mentioned previously, increases energy dissipation at all structural frequencies or f_L/f_s . This is a significant structural design advantage as wind and earthquake vibrations can cause large structures to oscillate at varying frequencies. Therefore, attaching an obstruction to the absorber is recommended for structural applications.

The obstruction case is most effective at an f_L/f_s of about 0.6 (at the structural frequency of 0.64 Hz), producing a 10 % settling time of 2.3 s, in Figure 2.5(a). This is a substantial improvement compared to the same case without an obstruction with a reduction in 10 % settling time of about 60 %. The results in Modi and Munshi (1998), also suggest a

significant increase, of up to 60 %, in energy dissipation capacity with the introduction of an optimum obstruction to a liquid sloshing absorber.

As a percentage value of the settling time is not absolute, 5 % settling times for cases in Figure 2.4 are given in Figure 2.5(b). Here, almost identical trends are observed as compared to those of a 10 % settling time. This gives confidence that 10 % and 5 % are sufficient values and that settling time is an accurate performance parameter.

2.7.2 ‘Tuned’ Cases

Numerical displacement histories for ‘tuned’ cases with varying liquid heights, without and with 1 semi-circular obstruction are displayed in Figure 2.6(a) to 2.6(e). As a reminder, tuning is achieved by varying the liquid height as the structural frequencies changes. These cases also have an initial displacement amplitude of 2.5 degrees and are analysed over structural frequencies of 0.36 Hz, 0.5 Hz, 0.64 Hz, 0.78 Hz and 0.92 Hz, displayed in Figures 2.6(a), (b), (c), (d) and (e). To achieve ‘tuning’ using Equation 2.1, these cases have liquid heights of 7.2 mm, 14 mm, 22.9 mm, 34 mm and 47.2 mm. Using the optimum ratio r/h_w of 0.75, from Modi and Munshi (1998), the cases with an attached obstruction therefore, have obstruction heights of 5.4 mm, 10.5 mm, 17.2 mm, 25.5 mm and 35.4 mm.

The tuned cases without an obstruction, in Figure 2.6, produce similar effectiveness in dissipating energy over all structural frequencies than compared to the cases without obstructions in Figure 2.4. This is expected as each case’s liquid height was chosen to produce optimal energy dissipation for a given structural frequency through tuning. Attaching

an obstruction increases the frequency of structural oscillations slightly at all structural frequencies analysed. This is most prominently observed at a structural frequency of 0.36 Hz, in Figure 2.6(a), where a phase difference occurs during the first cycle.

At such a low structural frequency of 0.36 Hz, there is insufficient energy for the liquid to travel over the obstruction. As a result, at the initial displacement of 2.5 degrees, the bulk of the liquid remains compartmentalised to one side of the absorber. This significantly reduces the structures first negative peak displacement, at approximately 1.9 s, in Figure 2.4(a), and also increases the damped structure's natural frequency. For structural frequencies above 0.36 Hz, energy within the system is increased and the bulk of the liquid is able to travel over the obstruction. Slight increases in peak displacement amplitudes during the first two to three cycles for cases with an attached obstruction are also observed at structural frequencies of 0.5 Hz to 0.92 Hz in Figures 2.6(b) to 2.6(e). However, an attached obstruction becomes most effective after about 5 s eliminating small displacement oscillations faster than the case without an obstruction.

10 % and 5 % settling times from cases in Figure 2.6 are displayed in Figure 2.7(a) and 2.7(b). The horizontal axis represents liquid height to free surface length (h_w/L). The horizontal axis is different to Figure 2.5, which used f_L/f_s , as each case, in Figure 2.7, has a liquid height 'tuned' so the liquid sloshing frequency equals the structural frequency. As all cases produce an f_L/f_s of 1, this ratio is not meaningful anymore and therefore h_w/L is used.

As mentioned previously, the tuned cases without an obstruction produce similar effectiveness over all structural frequencies than the cases without an obstruction in Figure 2.4. The difference in 10 % settling time for the ‘tuned’ cases without an obstruction over all structural frequencies is about 3 s in Figure 2.7(a), where the cases with a liquid height of 14.9 mm, in Figure 2.5(a), have a difference of around 12 s. Adding an obstruction to the ‘tuned’ liquid height cases reduces settling time, therefore increasing energy dissipation over all structural frequencies or h_w/L . This is also a significant design advantage as it gives evidence that for any liquid height, attaching an obstruction to the centre of the absorber’s base, using the optimum ratio r/h_w of 0.75, increases energy dissipation significantly.

The addition of an obstruction is most effective at a h_w/L of about 0.02 (at a structural frequency of 0.36 Hz), producing a 10 % settling time of 4.2 s. The largest reduction in 10 % settling time, for ‘tuned’ cases, through the addition of an obstruction is 35 % and occurs at h_w/L of about 0.06 (at a structural frequency of 0.64 Hz). Over the range of structural frequencies analysed, adding the obstruction at ‘tuned’ liquid heights produces an average reduction in 10 % settling time of about 30 %.

5 % settling times of the same cases are displayed in Figure 2.7(b) and a similar trend is also observed as compared to the 10 % settling times in Figure 2.7(a). The only exception is at h_w/L of about 0.02, where the case with an obstruction produces a similar 5 % settling time to the case without an obstruction. The obstruction case increases in 5 % settling time, when compared to 10 %, due to some remnant energy which causes small oscillations at the lowest structural frequency of 0.36 Hz (h_w/L of about 0.02). For a 10 % settling time, the remnant

energy is small enough to not indicate this discrepancy, in Figure 2.7(a). The largest reduction in 5 % settling time through the addition of an obstruction is 45 % and occurs at h_w/L of about 0.09 (for a structural frequency of 0.78 Hz). Overall, the 10 % settling times show good agreement with similar trends to the 5 % settling times.

2.7.3 Comparisons between Summaries of Optimum and ‘Tuned’ Cases

A summary of 10 % and 5 % settling times from cases in Figures 2.4 and 2.6 are displayed in Figures 2.8(a) and 2.8(b). The horizontal axis represents the structural frequency, f_s (Hz). These ‘tuned’ and optimum ratio cases are presented again, to determine which case is the most effective energy dissipater by producing the shortest settling time. The most effective case for both 10 % and 5 % settling times, at all structural frequencies, from 0.36 Hz to 0.92 Hz, is the single obstruction case using optimum ratios from Modi and Munshi (1998). The only exception is at a structural frequency of 0.92 Hz, for 10 % settling, in Figure 2.8(a), where the ‘tuned’ case with an attached obstruction produces a slightly reduced settling time. Optimum obstruction geometry ratios are used for both these cases and, therefore, results suggest that attaching an obstruction to a liquid sloshing absorber always increases energy dissipation.

2.7.4 Energy Dissipation Characteristics of Optimum Obstruction Case

The liquid flow field is compared for the most effective energy dissipation cases without and with 1 obstruction, from Figure 2.4(c), in Figure 2.9(a) to (h). Left column shows the 1 obstruction case using optimum ratios with a liquid height of 8 mm and the right column shows the optimum case without obstructions with a liquid height of 14.9 mm. Fixed velocity

scale shows fluid particle velocity ranging from 0 to 0.8 m/s. These frames were chosen to analyse the difference in energy dissipation characteristics from the effects of the attached obstruction. Structural displacements are discussed in this section to give a clearer understanding of how the liquid motion is affected by the structural displacement amplitudes, in Figure 2.4(c), at given points in time.

At approximately 0.9 s, the first negative structural peak displacement occurs in Figure 2.4(c). The first wave-to-wall interaction occurs slightly after this for the obstruction case, at 1.08 s, in Figure 2.9(a). As the structure oscillates from right to left, increased velocity gradients are observed in the wave travelling over the obstruction towards the left wall in Figure 2.9(a). This increase in velocity produces higher amounts of energy dissipation at the wave-to-wall interaction. At the same point in time, the wave-to-wall interaction has just occurred on the left wall for the case without an obstruction, in Figure 2.9(b). A clear wave is observed on the left side of the absorber, travelling right, producing lower velocities than in the obstruction case.

The second wave-to-obstruction interaction occurs at 1.62 s as the absorber rotates clockwise, in Figure 2.9(c). Slight free surface deformation is observed from the travelling wave interacting with the almost stationary liquid (in blue) on the right side of the obstruction, enhancing dissipation efforts. A breaking wave on the right side of the absorber without an obstruction is observed as the structure oscillates from left to right, in Figure 2.9(d). This also produces energy dissipation through shearing of the liquid.

At 1.94 s, the free surface deformation from the wave-to-obstruction interaction, in Figure 2.9(c), has produced a breaking wave travelling towards the right wall in Figure 2.9(e). Increased velocities are again observed in the liquid from the wave travelling over the obstruction, with velocity gradients also occurring in the travelling wave. The wave-to-wall interaction has just occurred for the case without an obstruction in Figure 2.9(f). Energy is still present within the liquid as the breaking wave continues to travel from right to left.

The absorber with an optimum obstruction has dissipated the majority of the structure's initial energy, at 3.68 s, in Figure 2.9(g). This is due to the bulk of liquid having a velocity of almost 0 m/s, displayed in blue. However, a small wave possessing energy is still present on the right side of the absorber without an obstruction, in Figure 2.9(h). As a result, small displacement oscillations occur for the absorber without an obstruction from 3.68 s, in Figure 2.4(c). These SPH observations are consistent with those of Modi and Munshi (1998), at displacement amplitudes from 0 to 2.5 degrees. This gives confidence that SPH produces realistic, complex free surface liquid shapes and can be used to further analyse the liquid sloshing absorbers.

2.7.5 Dependence on Initial Displacement Magnitude

An initial structural displacement amplitude study is undertaken, here, to determine if cases with attached obstructions can produce increased energy dissipation, compared to cases without obstructions, at initial displacements from 1.25 to 16 degrees. A previous study, by Modi and Munshi (1998), suggested cases with an attached obstruction produced increased energy dissipation, compared to the case without an obstruction, from initial displacement

amplitudes of approximately 0 to about 4 degrees. Above 4 degrees, the case without obstructions produced increased energy dissipation. From work presented in Chapter 3, cases with attached obstructions could still achieve increased energy dissipation at an initial displacement of 16 degrees, compared to cases without obstructions. Therefore, cases repeated from Modi and Munshi (1998), without and with 1 and 2 obstructions, are analysed at initial displacements from 1.25 to 16 degrees to determine the potential of the obstructions effectiveness over a range of initial structural displacements.

Numerical displacement histories for cases with a liquid height of 14.9 mm without obstructions and liquid height of 8mm with 1 ($d/L = 0$) and 2 ($d/L = 0.25$) obstructions are displayed in Figures 2.10(a) to 2.10(f). These cases have a structural frequency of 0.64 Hz and are analysed over initial displacements of 1.25, 2.5, 3.75, 6.25, 10 and 16 degrees, displayed in Figures 2.10(a), (b), (c), (d), (e) and (f). Cases without and with 1 obstruction with an initial displacement of 2.5 degrees are repeated in Figure 2.10(b) from Figure 2.4(c).

Differences between cases without and with obstructions are most noticeable at small initial displacements, from 1.25 to 3.75 degrees, in Figures 2.10(a) to (c). Here, a clear beat in the displacement history of the case without obstructions is observed at around 2 s, producing phase differences between cases without and with obstructions. The beat does not occur with both obstruction cases where energy is dissipated more effectively, resulting in the structure ceasing oscillations in a shorter amount of time. The 1 obstruction case is more effective than the case with 2 obstructions at these small initial displacements. This is due to initial energy within the liquid not having sufficient momentum to travel over the 2 obstructions as the

structure oscillates. Consequently, the 1 obstruction case dissipates increased amounts of energy at the wave-to-wall interactions when compared to the case with 2 obstructions.

For initial displacements of 6.25, 10 and 16 degree, cases without and with obstruction have similar displacement histories, displayed in Figures 2.10(d) to (f), compared to those of the smaller initial displacements. The beat does not occur at larger peak displacements above 3.75 degrees for the case without obstructions. This is due to viscous dissipation being the primary form of energy dissipation within the system where momentum opposition is dominate at smaller peak displacements. At large peak displacements, there is too much energy in the structure for the liquid to be able to produce a large enough force on the boundary to vary the natural oscillations of the structure. Once, the liquid absorbs sufficient energy, through viscous dissipation, and peak displacements are reduced, the liquid, if tuned, is able to apply a sufficient counteracting force on the container walls to affect the natural motion of the structure and therefore cause a beat in the displacement history. For the same reason, phase differences also do not occur at these higher initial displacements. Again, a reduction in peak displacements is noticeable for both obstruction cases compared to the case without obstructions.

With larger initial displacements of 10 and 16 degrees, Figures 2.10(e) and (f), the liquid possesses higher velocities. As a result, there is now sufficient momentum within the liquid for the case with 2 obstructions to produce similar effectiveness compared to the case with 1 obstruction. At large initial displacements, above 6.25 degrees, where viscous dissipation is the primary source of effectiveness, energy within the liquid cannot be dissipated as quickly

compared to smaller initial displacements, below 6.25 degrees, where momentum opposition is dominant. Consequently, larger amounts of energy, than compared to smaller initial displacements, are returned from the liquid back to the structure and then back again periodically, producing an increased time for the structure to cease oscillating.

10 % and 5 % settling times, from cases in Figure 2.10, are displayed in Figure 2.11(a) and (b). The study, by Modi and Munshi (1998), suggested an increase in energy dissipation for the case without obstructions above initial displacements of about 4 degrees, compared to the case with obstructions. This study used damping factor as the performance indicator. Using settling time as the performance indicator, both 1 and 2 obstruction cases dissipate energy faster for both 10 % and 5 % settling times at all initial displacements. The case with 1 obstruction is the most effective producing enhanced energy dissipation at all initial displacement amplitudes. This is another significant design advantage as it gives evidence that attaching an obstruction to the centre of the absorber's base, using the optimum ratio r/h_w of 0.75, for any initial displacement, increases energy dissipation significantly.

The case with 1 obstruction is most effective at initial displacements from 2.5 to 3.75 degrees, producing a 10 % settling time of 2.4 s, in Figure 2.11(a). The largest reduction in 10 % settling time through the addition of an obstruction is 50 % and occurs at an initial displacement for 2.5 degrees. Over the range of initial displacements analysed, adding the optimum obstruction produces an average reduction in 10 % settling time of about 30 %.

5 % settling times of the same cases are displayed in Figure 2.11(b) and a similar overall trend is also observed compared to the 10 % settling times in Figure 2.11(a). The only differences in the trend occur at the lower initial displacements of 1.25 and 3.75 degrees. The case without an obstruction produces similar 10 % settling times at initial displacements of 1.25 to 3.75 degrees. This differs to the 5 % settling time cases where initial displacements of 1.25 and 2.5 degrees produce increased settling times compared to 3.75 degrees. Also, the case with 1 obstruction produces a reduction in 10 % settling time at initial displacements of 2.5 and 3.75 degrees when compared to an initial displacement of 1.25 degrees. However, initial displacements of 2.5 and 3.75 degrees produce similar 5 % settling times compared to an initial displacement of 1.25 degrees. As the differences in 10 % and 5 % settling times between cases without and with an obstruction for initial displacements 2.5 and 3.75 degrees are less than 1 s, this slight difference in trend is not of significant importance.

At an initial displacement of 1.25 degrees, 10 % and 5 % settling times are taken when the structure reduces peak oscillations within 0.125 and 0.0625 degrees. At these small displacement amplitudes of less than 1 degree, surface ripples are barely noticeable within the liquid and energy dissipation is negligible. As a result, very small oscillations remain due to surface ripples occurring with minute remnant energy. Therefore, at an initial displacement of 1.25 degrees, an increase of 3.1 s between 10 % and 5 % settling times for the case without an obstruction is not that significant. Overall, the cases with obstructions still produce significantly shorter 10 % and 5 % settling times for all initial displacements. Flow field comparison between initial displacements of 2.5 and 16 degrees for the optimum obstruction case is presented next to further investigate the differences in the dynamics of the liquid motion.

2.7.6 Energy Dissipation Characteristics for Different Initial Displacement

The liquid flow field is compared for the case with 1 obstruction at initial displacements of 2.5 and 16 degrees in Figure 2.12(a) to (h). Left column shows the 1 obstruction case using optimum ratios with a liquid height of 8 mm at an initial displacement of 2.5 degrees. These frames are repeated using the same instances in time from Figure 2.9(a), (c), (e) and (g). The right column shows the same obstruction case with an initial displacement of 16 degrees. Again, fixed velocity scale shows fluid particle velocity ranging from 0 to 0.8 m/s. These frames were chosen to analyse the difference in energy dissipation characteristics from the effects of initial displacement.

At an initial structural displacement of 2.5 degrees, the structure oscillates between 1 to 2.5 degrees from 1.08 s to 1.94 s in Figures 2.12(a), (c) and (e). Small ripples in the liquid are observed with slight variations of liquid velocity and surface elevation at 1.08 s and 1.62 s in Figure 2.12(a) and (c). At 1.94 s, a single wave is travelling from left to right on the right side of the absorber. At displacement amplitude of less than 1 degree, at 3.68 s, in Figure 2.12(g), surface ripples are barely noticeable and energy dissipation is negligible shown by the liquid velocity of almost 0 m/s. These observations predicted with SPH are the same as that observed experimentally at these displacement amplitudes in (V.J. Modi and S.R. Munshi, 1998).

The optimum case with 1 obstruction at an initial structural displacement of 16 degrees produces significantly different dynamics of the liquid motion compared to the same case with an initial displacement of 2.5 degrees. During wave-to-wall interactions, in Figures

2.12(b), (d), (f) and (h), increased velocities (in red) producing large free surface deformation are observed. Severe velocity gradients are also observed in the liquid travelling wave producing high kinetic energy of the liquid mass, in Figure 2.12(d). Sloshing of the liquid with breaking and overturning waves is observed in Figures 2.12(f) and (h). These observations predicted with SPH are also observed experimentally at displacement amplitudes above 2.5 degrees in Modi and Munshi (1998). This gives confidence that SPH produces realistic looking, complex free surface liquid shapes, therefore making SPH a competent design tool for liquid sloshing absorbers in structural control applications.

2.8 Conclusions

Liquid sloshing absorbers using suggested optimum ratios, from Modi and Munshi (1998), to maximize energy dissipation are presented in this chapter. This study gave evidence that energy dissipation is enhanced with the introduction of semi-circular obstructions attached to the base of a rectangular sloshing absorber at a single structural frequency of 0.64 Hz. Large structures, such as tall buildings and bridges, are subject to wind and earthquake loads, which can cause them to oscillate at varying magnitudes. As these loads are random in nature, a sloshing absorber that is effective over a range of structural frequencies and disturbance amplitudes is attractive for design purposes. Therefore, the optimum obstruction case is compared to the optimum case without obstructions, from Modi and Munshi (1998), to determine if enhanced energy dissipation could still be achieved, over a range of structural frequencies.

Logarithmic damping factor was the main performance indicator used by Modi and Munshi (1998). However, damping factor may not give a true representation of the cases' effectiveness to dissipate energy as the formula is an assumption of behaviour of a perfectly linear oscillator. As the displacement amplitude decay of the controlled structure is not linear, the damping factor will vary depending on the number of cycles chosen. Therefore, 10 % and 5 % settling times are used in this chapter, instead of damping factor, as the key performance indicator. A 10 % (or 5 %) settling time is the time for the peak displacement of the structure to decay within 10 % (or 5 %) of the initial displacement.

Attaching an obstruction at the centre of the absorber's base enhances energy dissipation by increasing the velocity gradients of the liquid as it travels over the obstruction. Increasing the velocity gradients of the travelling wave produces increased potential energy within the liquid at the wave-to-wall interactions. The liquid effectively absorbs the energy from the structure, at the wave-to-wall interactions, ceasing structural oscillations in a shorter amount of time compared to the case without an obstruction. Therefore, enhanced energy dissipation can be achieved through attaching these designed obstructions to a liquid sloshing absorber. The case with 1 obstruction has an optimum ratio of obstruction height to liquid height (r/h_w) of 0.75 and is the most effective parameter. This case increases energy dissipation evenly over structural frequencies of 0.36 Hz to 0.92 Hz compared to the optimum case without an obstruction, from Modi and Munshi (1998). Improvements of up to 60 % are achieved with the introduction of an optimum obstruction, which agrees with experimental results in Modi and Munshi (1998).

‘Tuned’ liquid height cases were analysed to determine if energy dissipation could be enhanced further, compared to the optimum obstruction case, from Modi and Munshi (1998), over a range of structural frequencies. The ‘tuned’ cases have liquid heights that produce sloshing frequencies (f_L) that match the frequencies of the structure (f_s) to be controlled, f_L/f_s , of 1. Introducing an obstruction, using optimum ratios, to ‘tuned’ liquid height cases increases energy dissipation up to 35 %. Over the range of structural frequencies analysed (0.36 Hz to 0.92 Hz) these optimum obstruction cases produce an average increase in energy dissipation of 30 % compared to ‘tuned’ cases without obstructions. This gives evidence that introducing an optimum obstruction will increase dissipation at any ‘tuned’ liquid height for any structural application up to 0.92 Hz structural frequency. However, the optimum obstruction case, from Modi and Munshi (1998), was still the most effective case at a f_L/f_s , of about 0.6 (at the structural frequency of 0.64 Hz). Therefore, this gives evidence that it is more important to design a shallow liquid level sloshing absorber to enhance energy transfer and dissipation rather than tune the sloshing frequency to match the frequency of the structure.

Analysis of the most effective energy dissipation cases, from Modi and Munshi (1998), were repeated in this chapter, for varying initial displacement amplitudes due to discrepancies between the results of the performance indicators used. As a result of the previously mentioned issues with using damping factor, settling times gave more promising results with the introduction of obstructions to a liquid sloshing absorber. The optimum case with 1 obstruction gave enhanced energy dissipation over all initial displacement amplitudes from 1.25 to 16 degrees compared to the optimum case without obstructions. Improvements of up to 50 % were achieved with the introduction of an obstruction. Over the range of initial

displacements analysed, adding the optimum obstruction produces an average increase in performance, again, of about 30 %.

Adding obstructions always increases energy dissipation regardless of liquid height, structural frequency or initial displacement amplitudes analysed. The only exception was two ‘tuned’ cases with optimum obstructions where they produced the same effectiveness as the ‘tuned’ cases without obstructions. These are significant structural design advantages as wind and earthquake vibrations can cause large structures to oscillate at varying frequencies and excitation amplitudes. Therefore, attaching an obstruction to the absorber is recommended for structural applications.

Liquid velocity flow field comparisons produce realistic looking; complex free surface shapes with severe velocity gradients in travelling waves, using SPH. The numerical predictions agree with experimental observations made by Modi and Munshi (1998). These details give valuable information that helps explain how energy dissipation occurs within the liquid of the sloshing absorber. As mentioned previously, energy is dissipated effectively with the introduction of the obstruction, by the liquid absorbing the structure’s energy effectively, through increasing the potential energy within the liquid at the wave-to-wall interactions. Increased velocity gradients within the liquid, as the wave travels over the obstruction, produce the increase in energy dissipation at the wave-to-wall interaction. Such a close agreement in the validation results makes SPH a competent design tool for liquid sloshing absorbers in structural control applications.

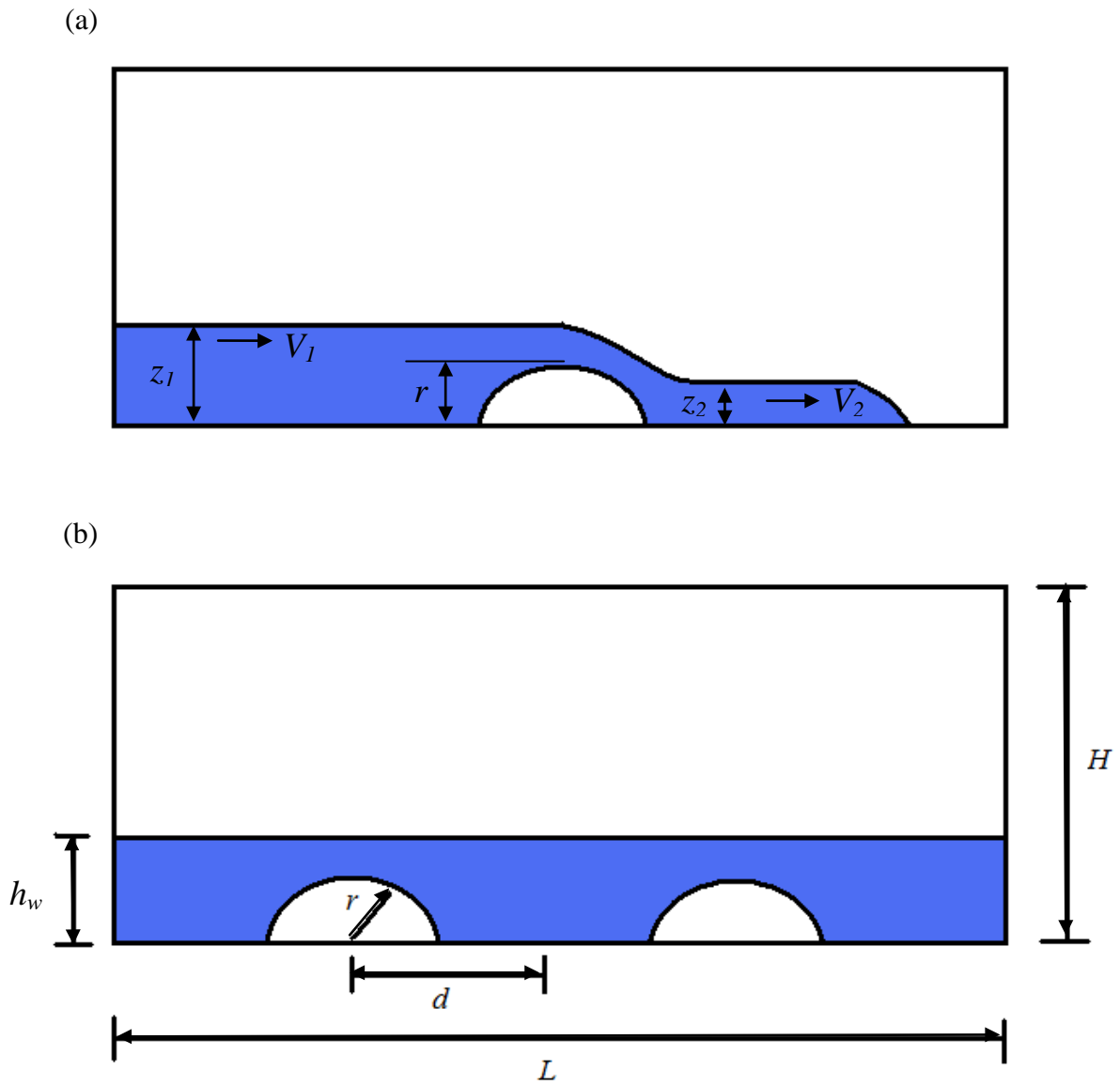


Figure 2.1: (a) Liquid flow past a semi-circular obstruction within the rectangular liquid sloshing absorber and (b) geometry of the rectangular absorber with semi-circular obstructions.

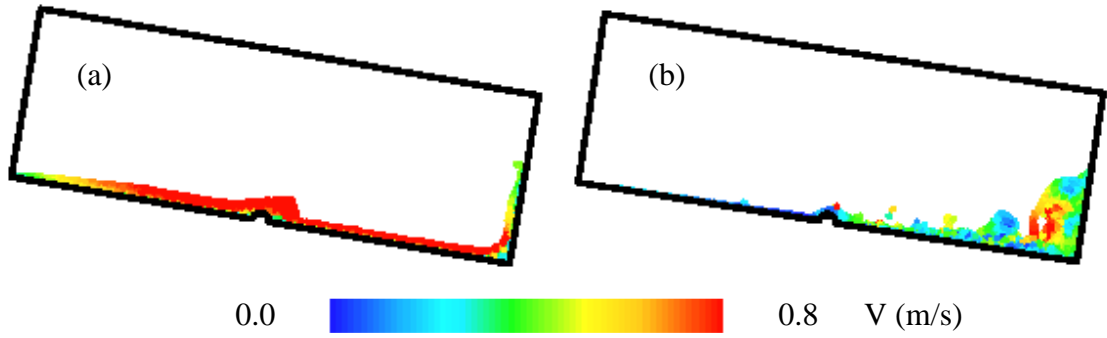


Figure 2.2: Two snapshots of the velocity contours at particular instances for the 1 obstruction case with a 16 degree initial displacement. (a) High velocities (in red) occur within the liquid and (b) large free surface deformation occurs at the right wall as the structure oscillates from left to right. Velocity scale runs from 0 m/s to 0.8 m/s.

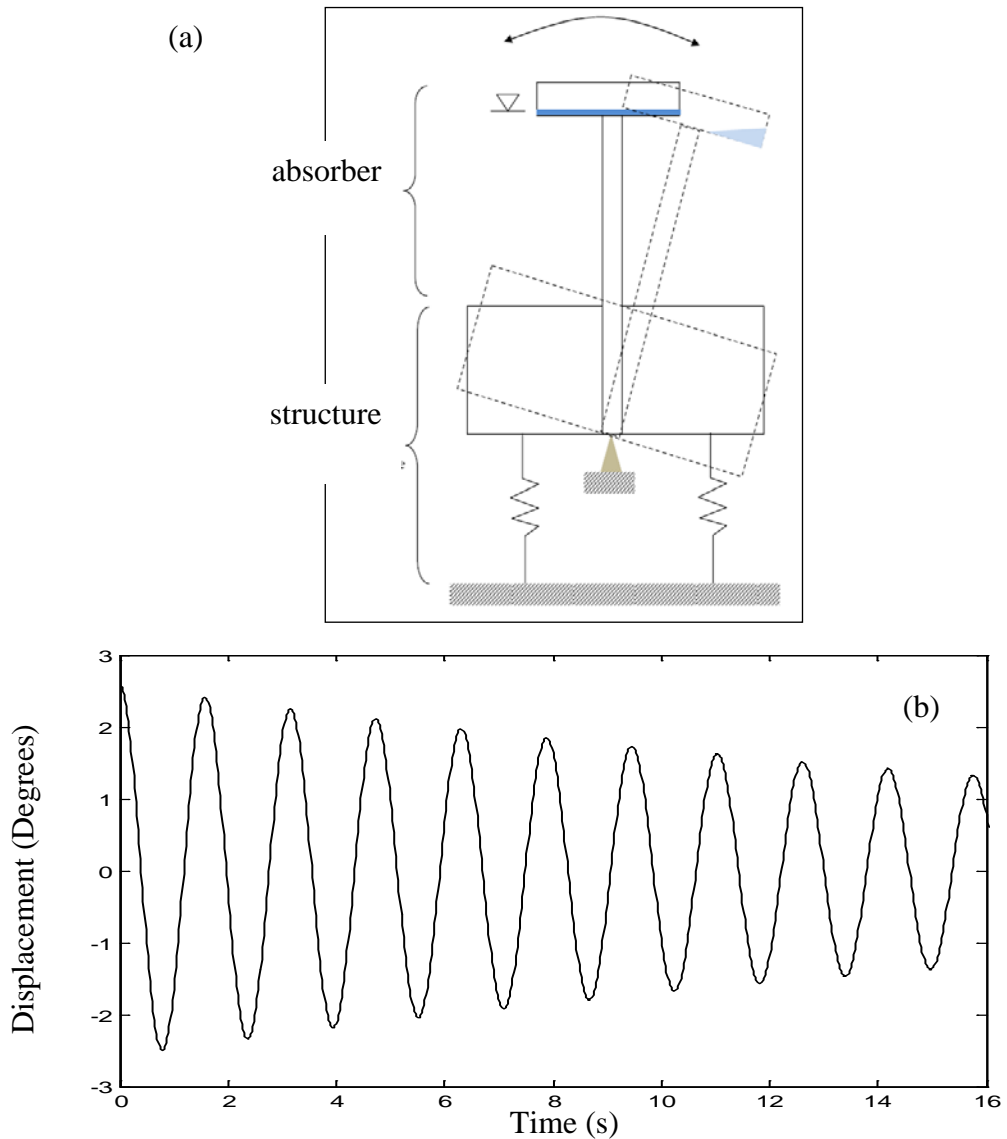


Figure 2.3: (a) Schematic of the structure with an attached absorber and (b) displacement history of uncontrolled structure (with attached absorber without liquid).

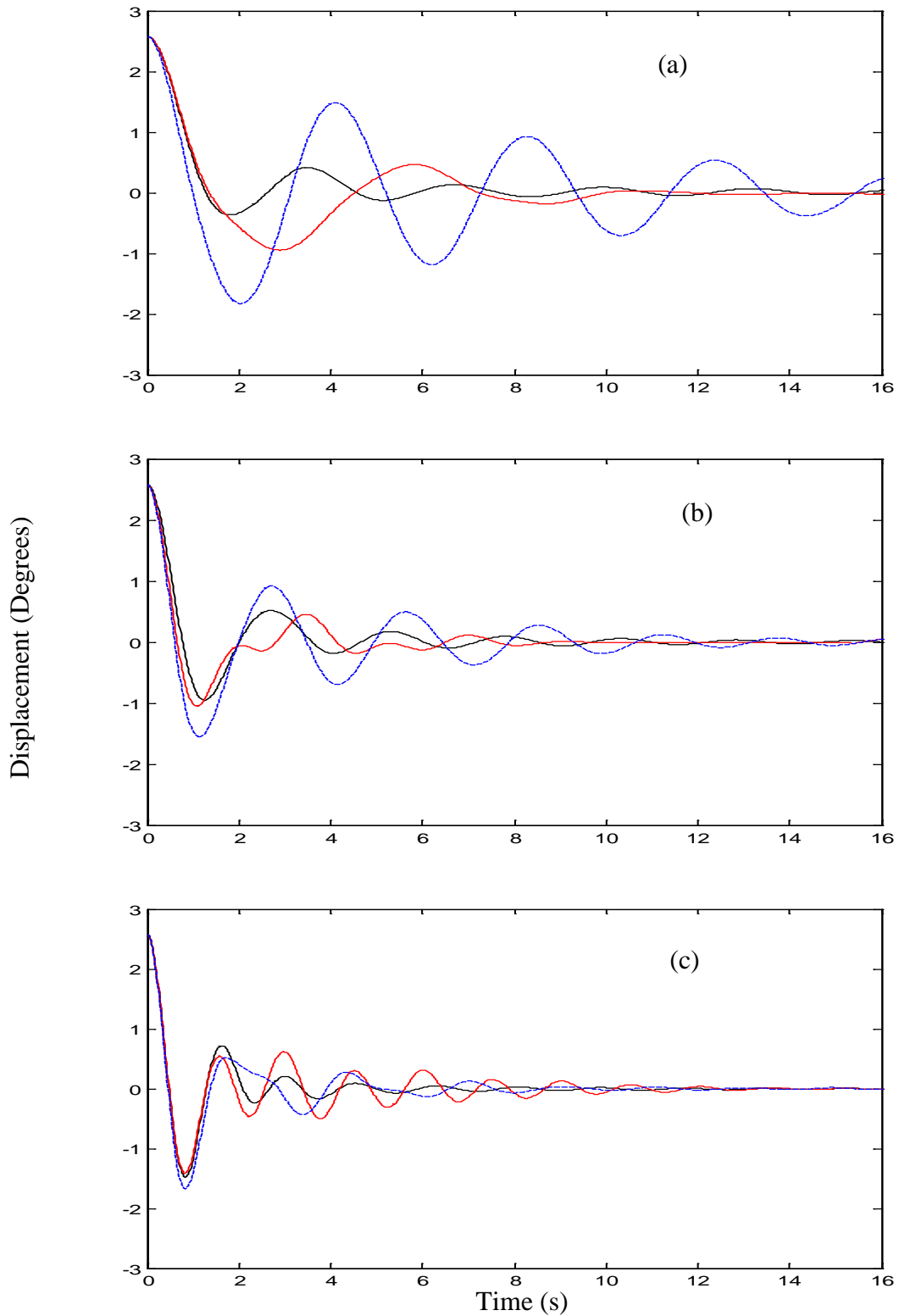


Figure 2.4: Displacement histories with liquid height of 14.9 mm (—); and 8 mm without (—) and with one 6 mm obstruction (—) for structural frequencies of (a) 0.36 Hz, (b) 0.5 Hz, (c) 0.64 Hz, (d) 0.78 Hz and (e) 0.92 Hz.

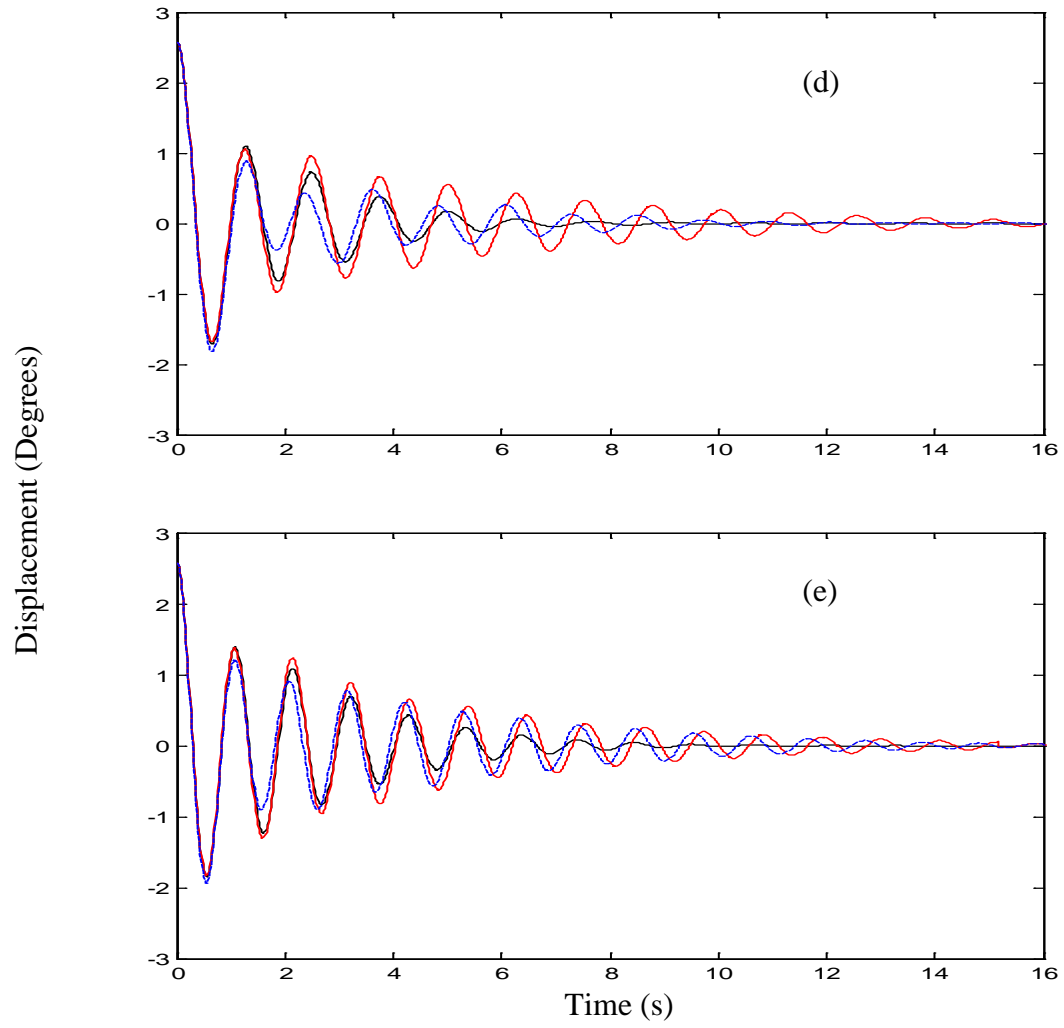


Figure 2.4: Continued.

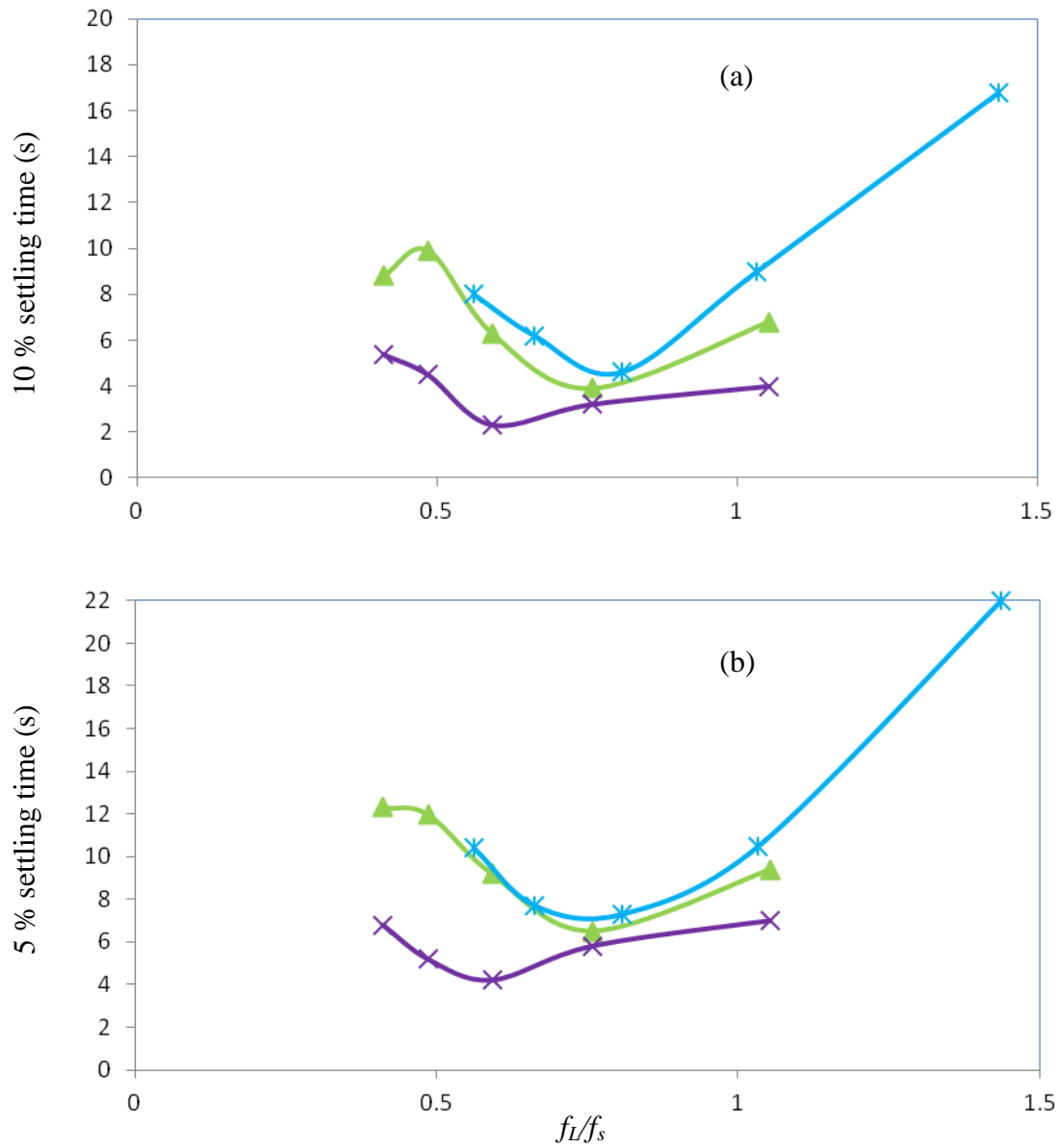


Figure 2.5: Variation of (a) 10 % and (b) 5 % settling times with the frequency ratio from Figure 2.4. Without (—▲—) and with 1 obstruction (—×—) at a liquid height of 8 mm and without an obstruction (—*—) at a liquid height of 14.9 mm.

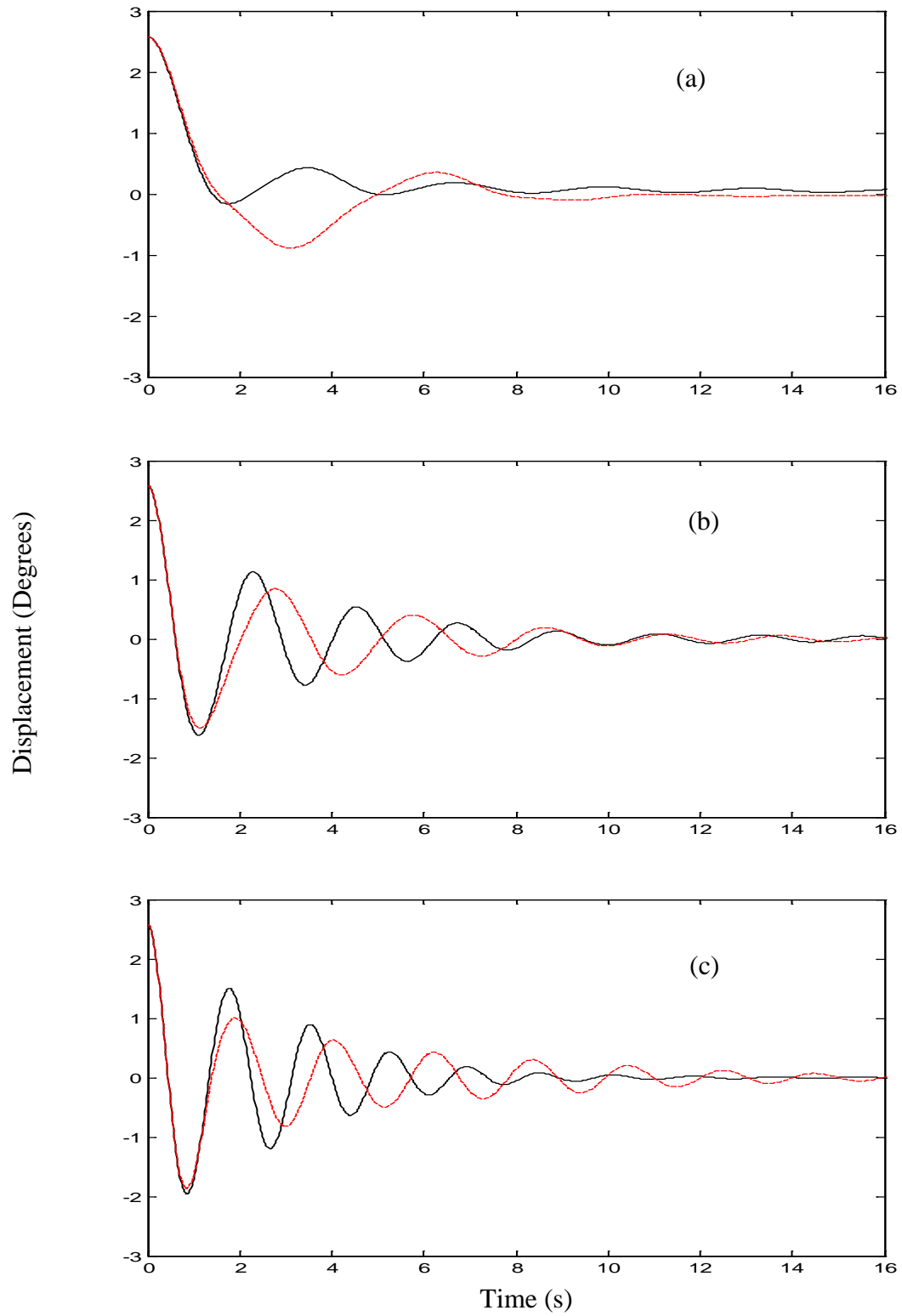


Figure 2.6: Same as in Figure 2.4, but for varying liquid heights to achieving theoretical tuning.

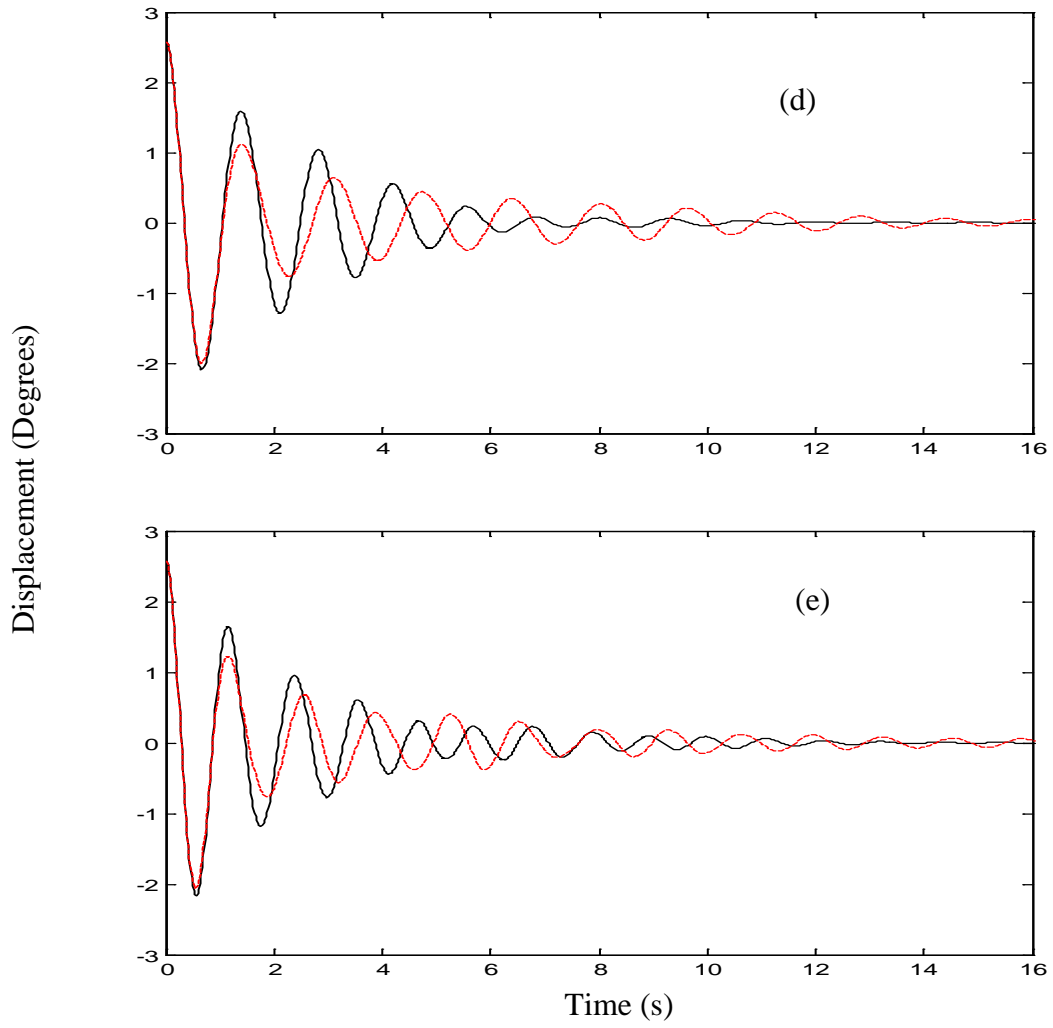


Figure 2.6: Continued.

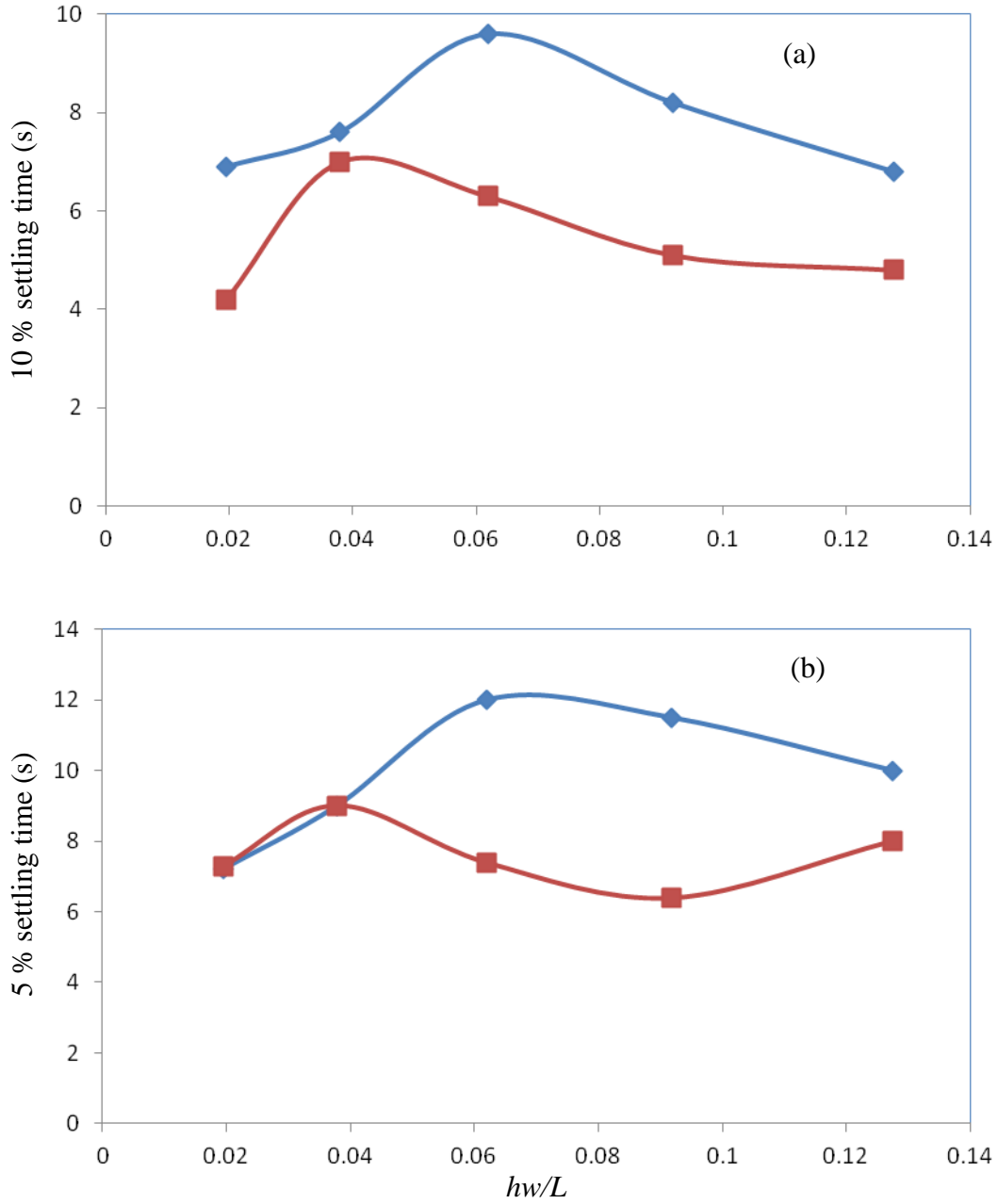


Figure 2.7: Same as in Figure 2.5, but for ‘tuned’ liquid height cases, from Figure 2.6, without (—◆—) and with 1 obstruction (—■—).

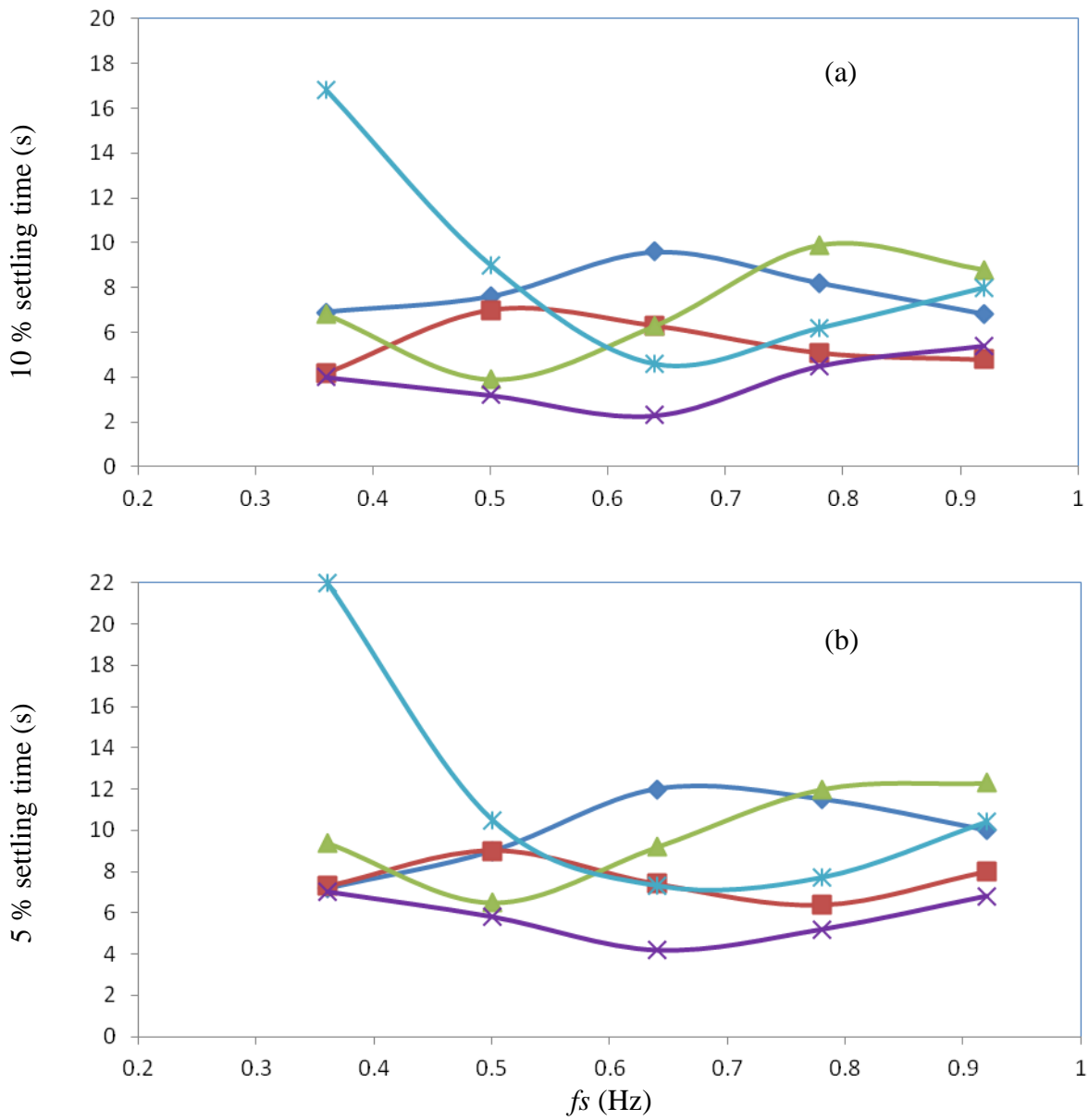


Figure 2.8: Same as in Figure 2.5, but for cases from Figures 2.5 and 2.7. Horizontal axis is structural frequency, f_s (Hz).

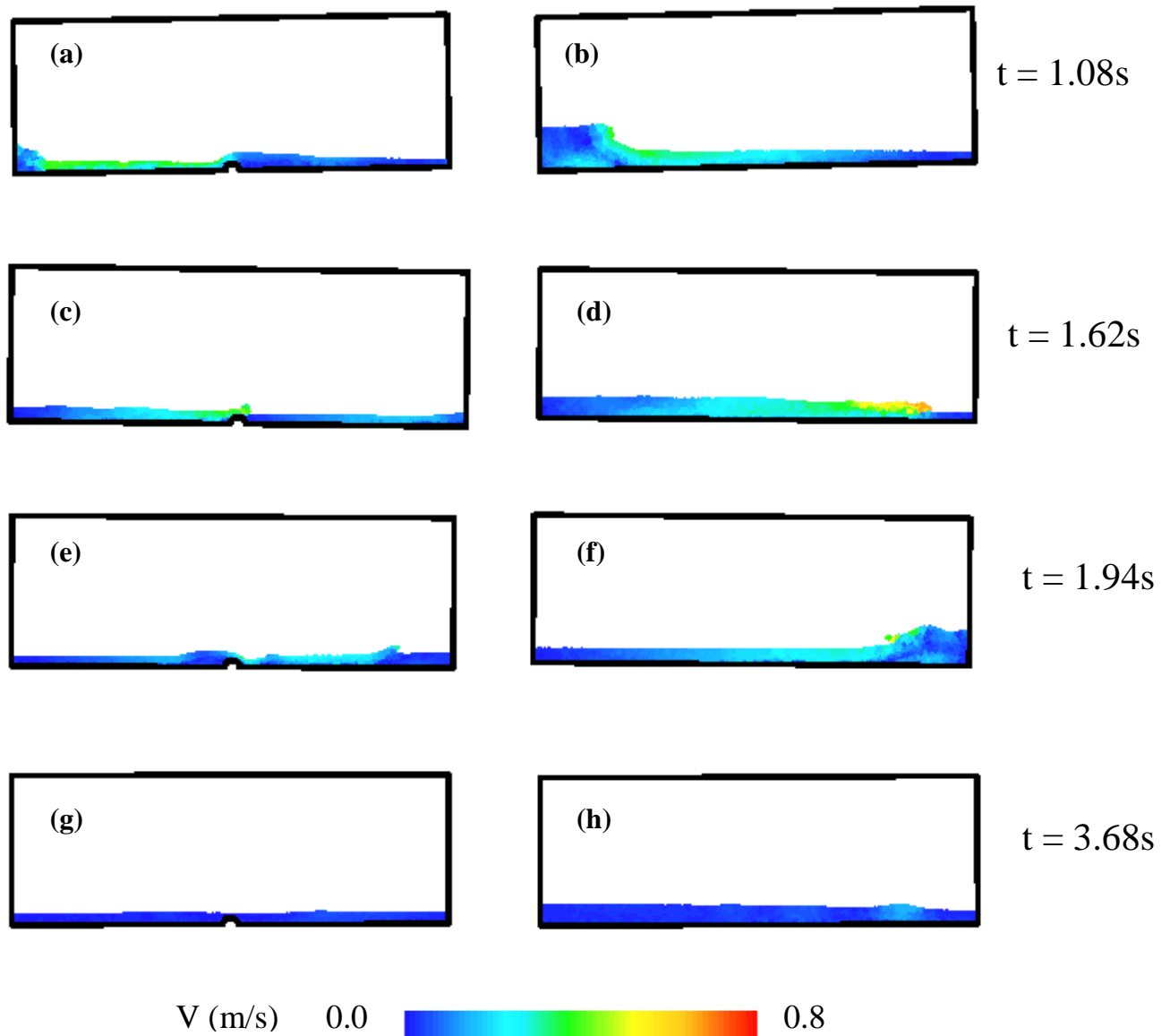


Figure 2.9: Still frames at areas of interest of liquid flow field comparisons of water within a sloshing absorber controlling a structure. Left column shows 1 semi-circular obstruction located in the bottom centre and liquid height of 8 mm case. Right column shows the case without an obstruction with a liquid height of 14.9 mm. Both cases have a 2.5 degrees initial displacement. Fixed velocity scale shows fluid particle velocity ranging from 0 to 0.8 m/s.

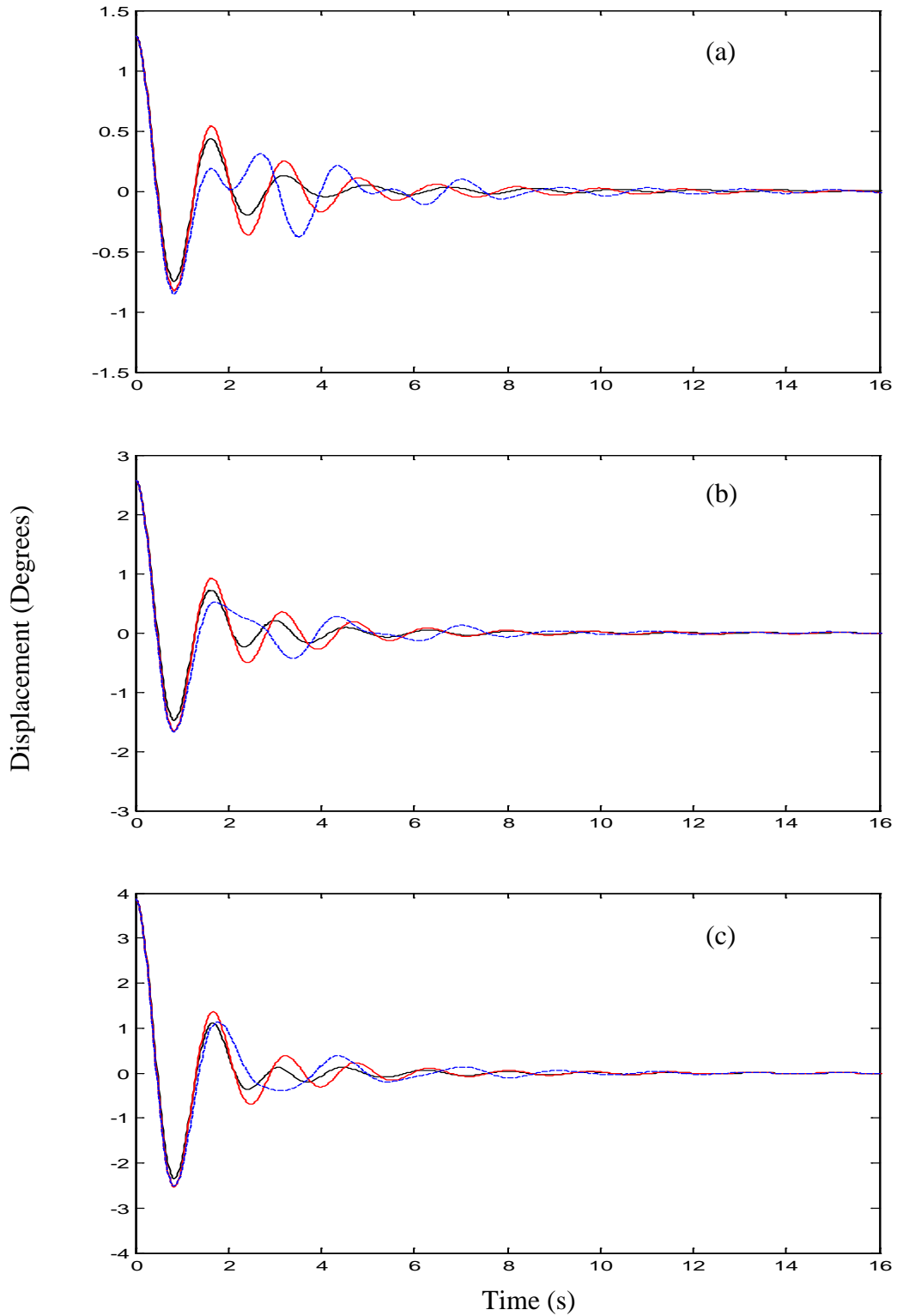


Figure 2.10: Numerical displacement histories with structural frequency of 0.64 Hz and liquid height of 14.9 mm without obstructions (— —) and liquid height of 8 mm with 1 (—) and 2 (—) obstructions with radius of 6 mm for initial displacements of (a) 1.25, (b) 2.5, (c) 3.75, (d) 6.25, (e) 10 and (f) 16 degrees.

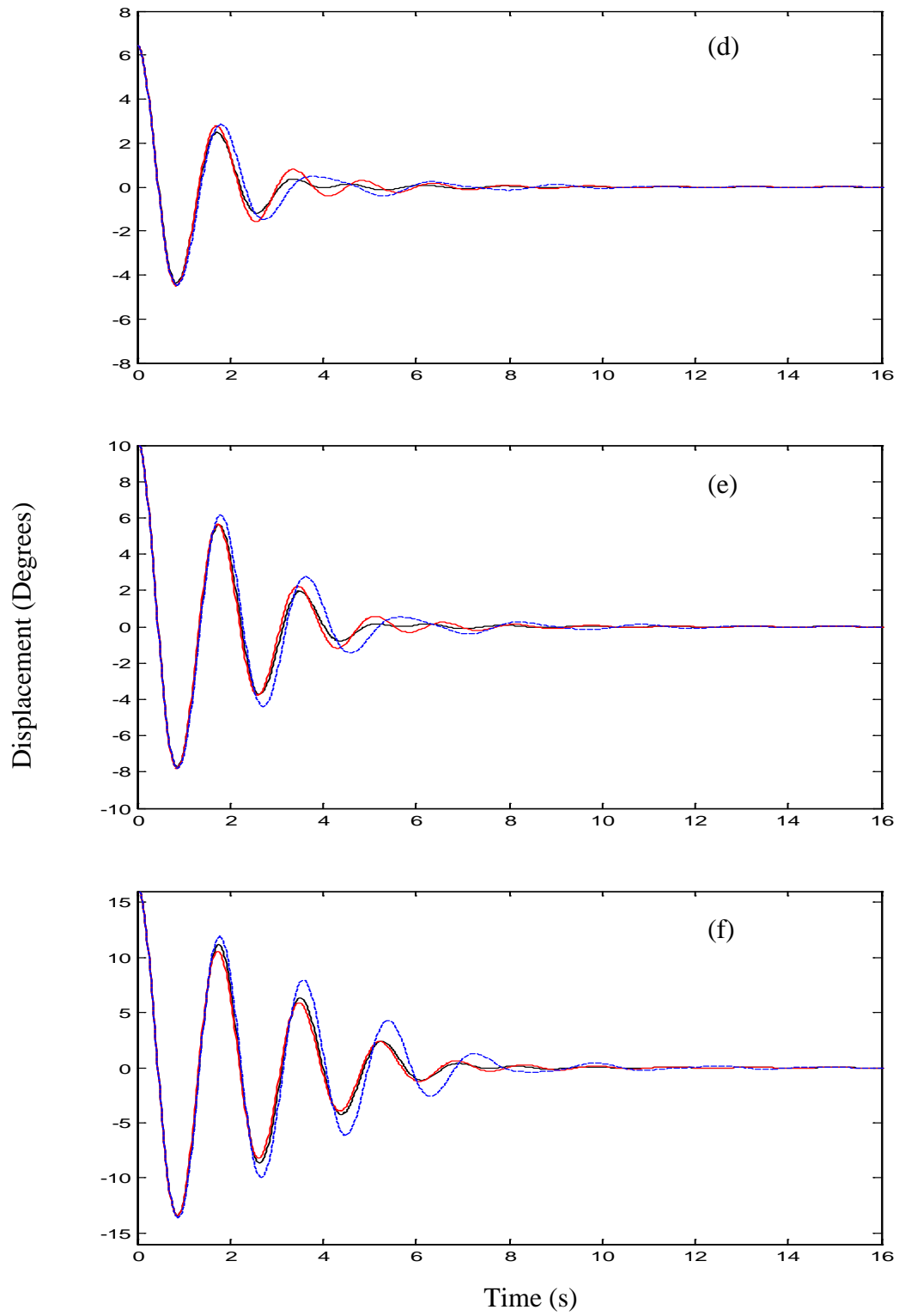


Figure 2.10: Continued.

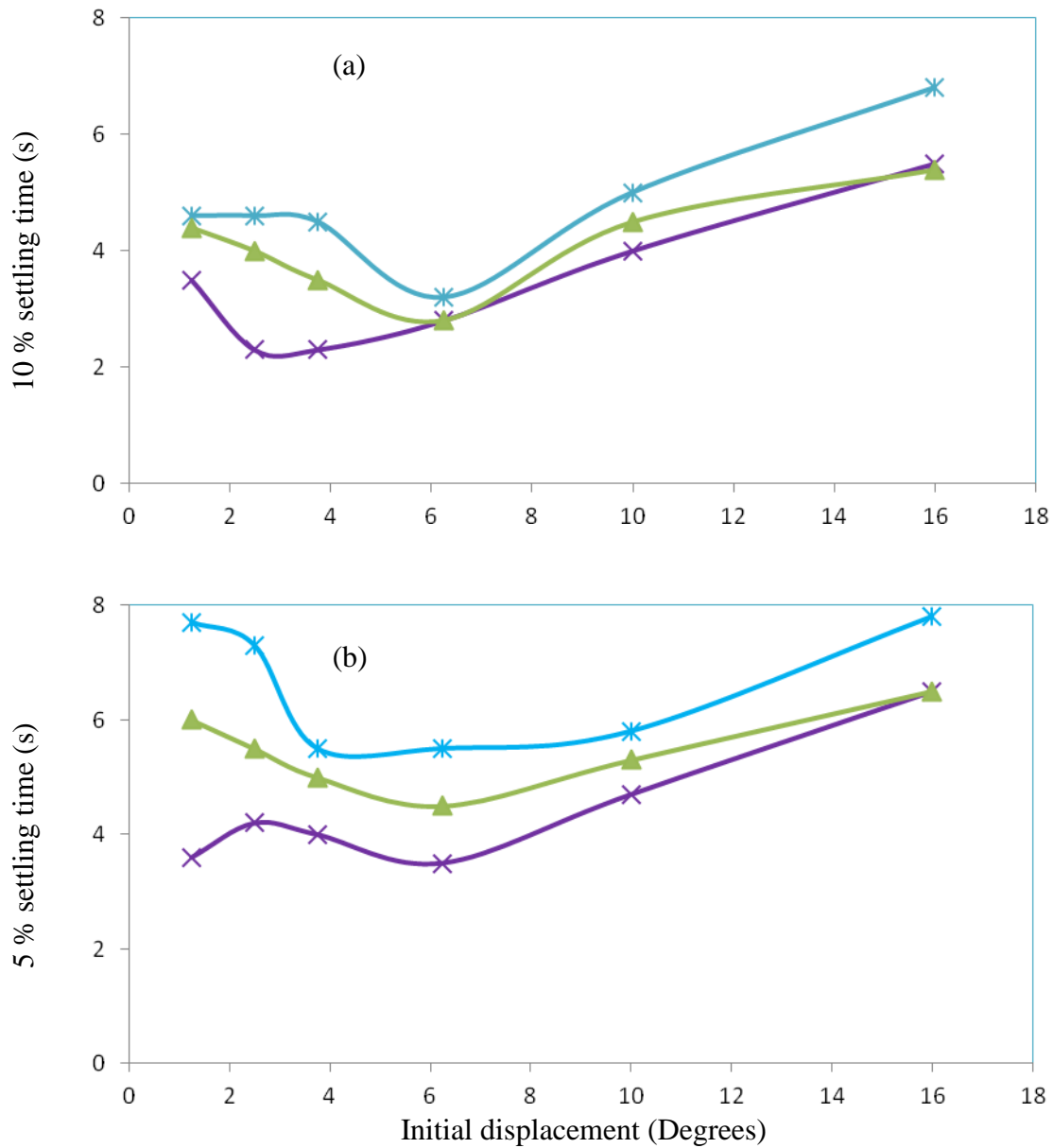


Figure 2.11: Summary of (a) 10 % and (b) 5 % settling times from cases in Figure 2.10 for cases with 1 (—x—) and 2 (—▲—) obstructions at a liquid height of 8 mm and without an obstruction (—*—) at a liquid height of 14.9 mm.

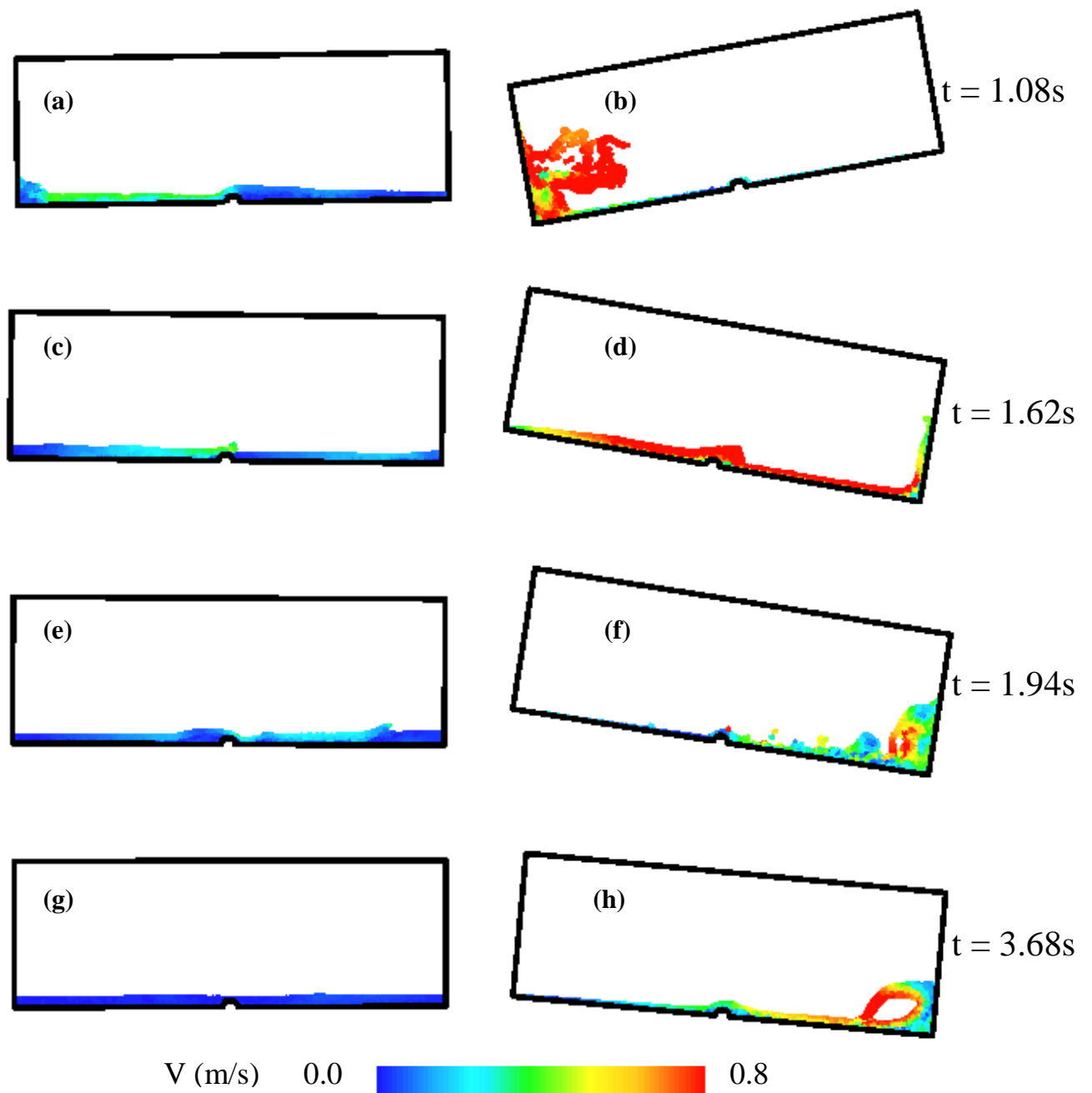


Figure 2.12. Still frames at areas of interest of liquid flow field comparisons of water within a sloshing absorber controlling a structure. Left column shows the same 1 obstruction case as in Figure 2.9 with an initial displacement of 2.5 degrees. Right column shows the same case with an initial displacement of 16 degrees. Fixed velocity scale shows fluid particle velocity ranging from 0 to 0.8 m/s.

Chapter 3

A SLOSHING ABSORBER WITH DESIGNED OBSTRUCTIONS TO IMPROVE ENERGY DISSIPATION

3.1 Introduction

Tall structures, such as towers and bridges, are subject to wind and earthquake loads which can cause them to oscillate at excessive magnitudes. Liquid sloshing absorbers can be used to suppress these excessive oscillations for structural control purposes by tuning the frequency of the sloshing to the critical frequency of the structure to be controlled. These absorbers are simple structures consisting of a partially full container of liquid with a free surface.

Earlier work demonstrated the superior energy dissipation capability of low-level liquid absorbers with travelling sloshing waves, as opposed to deep-level liquids with sustained standing sloshing waves (Marsh et al., 2009). In this work, travelling waves had a clear wavefront with severe velocity gradients to contribute to the dissipation efforts significantly. The presence of this wavefront offer possibilities of enhancing the shear dissipation further, by placing surface roughness elements (obstructions) on the base of the absorber's container.

Attaching surface roughness elements (obstructions) to the base of a sloshing absorber has received minimal attention in the literature. Modi and Munshi (1998) previously analysed select cases involving the number and location of the obstructions experimentally, showing a significant increase in energy dissipation by attaching obstructions to the base of a rectangular sloshing absorber. The main focus of this chapter is to further investigate the full

potential of the effects of obstructions to determine if enhanced energy dissipation can be achieved compared to the select cases analysed by Modi and Munshi (1998).

Comparisons between SPH predictions and experimental observations using a rectangular liquid sloshing absorber without attached obstructions showed good agreement (Marsh, 2010). Here, numerical predictions are validated against experimental observations of a liquid sloshing absorber with attached obstructions for displacement history and free surface behaviour. SPH is used to model two-dimensional rectangular liquid sloshing absorbers with and without attached surface roughness elements to the base of the absorbers. SPH is also used to identify the effective energy dissipation characteristics for the cases with obstructions and give details, such as liquid velocity flow fields, which are not possible through experimental observations. An investigation involving the effects of the height, number and location of these designed obstructions with respect to varying liquid heights is the topic of interest in this chapter. Both experimental and numerical predictions are presented in the form of design recommendations.

3.2 Experimental Setup

A line drawing of the experimental setup is displayed in Figure 3.1(a) and consists of a mechanical oscillator whose structure is configured as an inverted pendulum. The motion of the structure is designed to be rotational around a pivot point. Springs are attached either side of the structure to produce structure stiffness. A container to accommodate the sloshing liquid is mounted on top 670 mm above the pivot point. As this structure is excited, the container on

top is subjected to angular oscillations. An inverted pendulum setup is used as it can increase energy dissipation up to 7 times that experienced in pure translation (Lu et al., 2004).

A photograph of the experimental setup is shown in Figure 3.1(b). Here, the uncontrolled structure has an equivalent viscous damping ratio of 0.015 ± 0.002 , mass moment of inertia calculated to be $3 \pm 0.2 \text{ kg m}^2$, from the measured torsional stiffness of $29.5 \pm 0.5 \text{ N m / rad}$ and frequency of $0.5 \pm 0.05 \text{ Hz}$. The quoted errors for the mass moment of inertia and torsional stiffness are calculated using a method for estimating uncertainty in experimental results by Kline and McClintok (1953). The rectangular absorber's size remains constant for the study with a length, width and height of 340 mm, 230 mm and 180 mm respectively. Therefore the wavelength of the fluid or free surface length is also 340mm. All dimensional measurements have an accuracy of $\pm 0.5 \text{ mm}$.

The structure is offset to an initial displacement amplitude of 16 degrees and is shown in this position by the dashed lines in Figure 3.1(a). A simple stop-block allows for a consistent initial displacement angle of 16 degrees.

After the structure is offset to an initial displacement of 16 degrees, the fluid within the container is then left to settle under gravity until it reaches an initial state of rest. The structure is then released exciting the fluid within the container and allowing the structure to respond freely. The structure and fluid motion are then recorded.

A Canon MV630i Mini digital video camera is used to record the experimental observations. The camera has a frame rate of 12.5 frames/s. Based on this, the experimental error is $1/25$ s (± 40 ms).

3.3 Initial Experiments

A brief description of the initial experiments for the attached obstruction locations is given here. The objective is to explore the effectiveness of various obstruction configurations then further study promising cases numerically to investigate how the obstructions increase energy dissipation. The key parameters investigated are obstruction height (r), liquid height (h_w) and obstruction location or distance from obstruction from the centre of the container (d) displayed in Figure 3.2(a). Three semi-circular obstruction heights consisting of 2 mm, 4 mm, and 8 mm (± 0.5 mm) are analysed. Shallow liquid volumes of 200 ml to 1200 ml in 200 ml (± 5 ml) increments (liquid heights 2.6 mm to 15.3 mm) are used. These liquid heights were chosen as shallow level absorbers produce travelling waves, which increase energy dissipation significantly (Marsh et al., 2009). In addition, it has been reported that optimum energy dissipation can be achieved with an obstruction height slightly less than the liquid height (Modi and Munshi, 1998). Therefore, obstruction heights were chosen to agree with this suggestion.

The mass moment of inertia is given for the initial and final static positions of the liquid. Liquid heights from 2.6 mm to 15.3 mm have initial liquid mass moment of inertia of 0.1 kg m² to 0.66 kg m² and final liquid mass moment of inertia of 0.09 kg m² to 0.56 kg m²,

respectively. Therefore, the liquid to structure mass moment of inertia ranges from 3 % to 22 % in the initial position and 3 % to 19 % in the final position.

Photographs of the rectangular container with one of the semi-circular obstruction cases (3 obstruction in the centre) attached to the bottom of the container with close ups of a single obstruction are displayed in Figure 3.2(b), (c) and (d). Sections of straightened garden hose pipes, sliced length-wise are used as obstructions. Pieces of electrical tape are used to attach them to the bottom of the container. The electrical tape is firmly bound to the bottom of the container to reduce their interference with the fluid flow and to closely approximate a semi-circular profile.

The time required for the structure to cease oscillating is the settling time. The settling time was taken by visually monitoring the structure's oscillations, keeping time with a stop watch.

Each experimental case was run three times and an average was taken to be the settling time. The variation in settling time of the three cases is within ± 1.5 s. This variation corresponds to about 1.2 % of the uncontrolled settling time. All figures' vertical axis in this section is the settling time ratio, which is the settling time normalised by the settling time of the uncontrolled structure.

In this chapter, settling time is chosen as the key performance indicator. However, in the study by Modi and Munshi (1998), logarithmic damping factor was the main performance indicator, given in Equation 3.1.

$$\delta = \frac{1}{n} \ln \frac{x(t)}{x(t+nT)}, \quad (3.1)$$

where n , $x(t)$ and $x(t+nT)$ are number of cycles, initial displacement amplitude and the peak displacement amplitude after ‘n’ cycles, respectively. Due to the displacement amplitude of the structure not having a constant decay, the damping factor will vary depending on where the sampling starts and how many peak displacements are sampled to determine the damping factor. As a result of this discrepancy in determining the damping factor, settling time is used as the performance indicator in this chapter.

3.3.1 Identifying Effective Obstruction Cases

The previous experimental study by Modi and Munshi (1998) analysed select obstruction cases limited to 1 and 2 obstructions. This work concluded that 1 obstruction attached in the centre of the absorber was the most effective in dissipating energy. Therefore, the 1 obstruction case is analysed first. This case is also compared with significantly different obstruction configurations next to determine how the obstruction locations effect energy dissipation and if dissipation can be enhanced further.

Initial experiments consisting of 0 obstructions, 7 obstructions (spaced evenly), 2 obstructions (1 obstruction 45 mm from each side) and 1 obstruction (in the centre) cases are displayed in Figure 3.3. A summary of settling time ratios for these cases with an obstruction

height of 4 mm are displayed in Figure 3.4. As liquid height increases over 10.2 mm so does settling time for all cases. This is because the liquid is too deep for the obstruction to have an effect on the travelling wave. The cases without and with 2 obstructions are effective at a liquid height of 5.1 mm. However, cases with 7 obstructions and 1 obstruction are more effective at 7.7 mm liquid height. The case with 1 obstruction is the most effective producing a settling time ratio of 0.12 at a liquid height of 7.7 mm.

The case with 2 obstructions attached close to the walls of the absorber is superior to the 0 obstruction case at all liquid heights. However, the 1 obstruction case is more effective in dissipating energy than the 2 obstruction case at all liquid heights. The obstructions located near the walls of the container reduce the energy dissipation in the wave-to-wall interactions. This is due to the liquid travelling over the obstruction disrupting the motion and free surface deformation of the liquid during the wave-to-wall interaction. Consequently, the energy dissipated at the wall is reduced. Due to the wave-to-wall interaction producing the most energy dissipation within the system, obstructions near the wall are not recommended.

Liquid height is directly related to initial potential energy within the system. Shallow liquid heights have low mass and therefore, low initial potential energy. Consequently, the case with 7 obstructions is ineffective at low liquid heights as there is not sufficient energy within the liquid to maintain a high velocity travelling wave at the wave-to-wall interaction. The 1 obstruction case is the most effective having a settling time ratio of 0.12. This agrees with Modi and Munshi (1998), where the 1 obstruction case was the most effective energy dissipater of the selected cases analysed. As the wave travels over the obstruction in the

centre of the container, liquid velocity increases, resulting in higher energy dissipation at the wave-to-wall interaction. Obstructions located in the centre of the container are therefore recommended.

Generally, tuning a sloshing absorber to achieve optimum energy dissipation requires the frequency of the sloshing to equal the natural frequency of the structure (Kareem, 1990; Banerji et al., 2000). However, in liquid depths producing high velocity travelling waves and large free surface discontinuities, tuning may not be as important, as discussed in Chapter 2. At shallow liquid heights it is more important to design as sloshing absorber to enhance dissipation than tuning the liquid frequency to equal the frequency that the structure oscillates.

For a structural frequency of 0.5 Hz, the suggested liquid height to achieve tuning is 11.8 mm for a free surface length of 340 mm using Equation 3.2. This expression (Blevins, 1979) is for a shallow liquid inside a rectangular container.

$$h_w = \frac{(2f_L L)^2}{g}, \quad (3.2)$$

where f_L , L and g are liquid frequency (Hz), free surface length (m) and gravitational acceleration (m/s^2), respectively. The 10.2 mm liquid height case without obstructions is similar to the optimal suggested height of 11.8 mm, using Equation 3.2 and achieves a

settling time ratio of 0.28, or a reduction of 72 % compared to the uncontrolled case. The trend from the liquid heights analysed in Figure 3.4 show that optimal liquid height of 11.8 mm using Equation 3.2 is not the most effective case. This is observed as effectiveness decreases and settling time ratio increases as liquid height increases from 7.7 mm for all cases. Therefore, this gives evidence to suggest that choosing a liquid height that maximizes energy dissipation is more important than tuning the sloshing frequency to the structural frequency.

Due to obstructions located in the centre of the container assisting in dissipating energy quickly, a case with 3 obstructions, displayed in Figure 3.5(c), is now analysed to explore efforts to enhance dissipation further. This case has 2 obstructions spaced 45 mm from the centre of the container and is referred to as the 3 obstructions (centre) case. Displacement histories of cases with obstruction heights 2 mm and 4 mm are displayed in Figure 3.6. These cases consist of 1 obstruction, 3 obstructions (1 centre, 2 sides) and 3 obstructions (centre) displayed in Figure 3.5 with the 0 obstruction case for comparison. All of the obstruction cases are more effective in dissipating energy faster than the 0 obstruction case, resulting in reduced settling time ratios. All 2 mm obstruction height cases, except the 3 obstructions (centre) case, produce their shortest settling time ratios at a liquid height of 5.1 mm. All 4 mm obstruction height cases produce their shortest settling time ratios at a liquid height of 7.7 mm. Here, the 3 obstructions (centre) case with an obstruction height of 4 mm is the most effective with a settling time ratio of 0.09.

Cases with an obstruction height of 8 mm are now analysed and consist of 1 obstruction centre, 2 obstructions (1 obstruction 45 mm from each wall), 3 obstructions (1 centre, 2 sides), 3 obstructions (centre) and 5 obstructions (spaced evenly) as displayed in Figure 3.7. Displacement histories of these cases are displayed in Figure 3.8. Settling time ratios increased for all cases for liquid heights lower than 7.7 mm and higher than 15.3 mm. The most effective case for an 8 mm obstruction height was also the 3 obstruction (centre) case with a settling time ratio of 0.11. As obstruction height is increased from 2 mm to 8 mm, an increased liquid height is required to achieve similar effectiveness. As a result, there seems to be a connection between obstruction height and liquid height for effectiveness. For obstruction heights of 4mm and 8 mm, optimum cases occur at r/h_w (obstruction height to liquid height) of 0.5 and 0.8 respectively. The optimum case, from Modi and Munshi (1998), occurs at r/h_w of 0.75 for a single obstruction with a height of 6 mm. This case is within the r/h_w range of 0.5 to 0.8 from the experimental results from this Chapter. Therefore, this gives confidence that the experiments from this Chapter are producing consistent results to the experiments from Modi and Munshi (1998).

Establishing that the 3 obstruction (centre) case is the most effective for all obstruction heights a final investigation is undertaken to determine the optimum distance between the centre obstruction and the 2 obstructions either side. The distance of the 2 side obstructions from the centre of the container (d) is given as a ratio with respect to free surface length (d/L). Four cases, with a d/L ranging from 0 to 0.375 and an obstruction height of 4 mm, are displayed in Figure 3.9. Displacement histories of these cases with 3 obstructions are compared with the 0 obstruction case and are displayed in Figure 3.10. In general, settling time increases for the 3 obstructions cases, as the 2 side obstructions are closer to the walls.

This agrees with the observations from the 2 obstructions case, in Figure 3.4, where obstructions close to the wall disrupt the travelling waves, reducing energy dissipation at the wave-to-wall interactions.

The most effective energy dissipation case is still the 3 obstruction (centre) case with an obstruction height of 4 mm, d/L of 0.125. This case produces shorter settling times than the case without obstructions at all liquid heights analysed (from 2.6 mm to 10.2 mm) and is most effective at a liquid height of 7.7 mm, producing a settling time ratio of 0.09. This case ceases oscillating in under half the time than the most effective case without obstructions with a settling time ratio of 0.2. Hence, optimum energy dissipation is achieved when obstructions are located in the centre of the container and are therefore recommended.

3.3.2 Identifying Effective Obstruction Cases with Respect to r/h_w

A summary of settling time ratios with r/h_w for three d/L cases previously analysed in Figure 3.6 and 3.8 are given in Figure 3.11(a) for d/L of 0, 3.11(b) d/L of 0.125 and 3.11(c) d/L of 0.375. The insert in each figure is the schematic plan view of the container for each d/L case. These cases are now analysed using the three d/L cases with variations in r/h_w to demonstrate the dependence of performance on obstruction location and height.

The shortest settling time ratio case at each obstruction height occurs at the same liquid height independent of d , displayed in Figures 3.11(a), 3.11(b) and 3.11(c). These optimum cases at each obstruction location (d) occur at r/h_w of 0.4, 0.5 and 0.8 for obstruction heights

2 mm, 4 mm and 8 mm respectively. The only exception being the most effective 2 mm obstruction height case at d/L of 0.125, which occurs at a r/h_w of 0.3 in Figure 3.11(b). However, r/h_w of 0.3 and 0.4, have similar settling time ratios of 0.11 and 0.13, and therefore, this trend inconsistency is not significant.

As liquid height increases, to achieve effective energy dissipation, the obstruction height should also increase. From the obstruction heights analysed, displayed in Figures 3.11(a), 3.11(b) and 3.11(c), r/h_w from 0.4 to 0.8 produces a settling time ratio of 0.25 to 0.09 or a reduction in settling time from 75 % to 91 % compared to the uncontrolled case. This increase in effectiveness over a substantial r/h_w range is attractive for design purposes as effective energy dissipation can be achieved with a significant range of liquid heights. The optimal case with an r/h_w of 0.75, from Modi and Munshi (1998), is also within the range of 0.4 to 0.8 from these experiments giving confidence to the validity of these results.

Obstruction height to liquid height, r/h_w , is more important than obstruction location. This is because no matter where the obstructions are located, when the liquid is too deep, the obstructions do not interact with the liquid free surface and therefore there is no change in performance of the absorber. Also, if the liquid is too shallow the obstructions compartmentalise the liquid. Compartmentalisation of the liquid shortens the free surface length to the distance between the obstructions. The shorter free surface length restricts the motion of the liquid reducing the velocity of the travelling wave, hence reducing energy dissipation at the wave-to-wall interactions. The shorter free surface length also varies the liquid sloshing frequency, in Equation 3.2, changing the timing of the wave-to-wall

interactions. As mentioned previously, when r/h_w , ranges from 0.4 to 0.8, the case with 3 obstructions at all liquid heights (2 mm to 8 mm) analysed dissipate energy effectively producing settling time ratios of 0.25 to 0.09, for all d/L cases (0, 0.125 and 0.375). Therefore, obstruction height to liquid height ratio (r/h_w) is more important than the location of the 2 side obstructions or d/L .

3.3.3 Identifying Effective Obstruction Cases With respect to d/L

Variation of settling time ratio with d/L for r/h_w of 0.4 ($r = 2$ mm), 0.5 ($r = 4$ mm) and 0.8 ($r = 8$ mm) displayed in Figure 3.12. These are the shortest settling time ratio cases at each obstruction height from Figure 3.11. The objective of this figure is to determine the optimum obstruction location case. Settling time ratios range from 0.12 to 0.17 for a d/L of 0, from 0.09 to 0.13 for a d/L of 0.125 and from 0.13 to 0.14 for a d/L of 0.375.

The most effective case is the 4 mm obstruction height case with d/L of 0.125 and a r/h_w of 0.5, producing the shortest settling time ratio of 0.09 or 91% reduction in settling time compared to the uncontrolled case, as displayed in Figure 3.12. Two more d/L cases (0.0625 and 0.025) were analysed for the optimum obstruction height of 4 mm. As settling time ratio increases at d/L of 0 and 0.375, compared to d/L of 0.125, these two new cases, closer to d/L 0.125, were chosen to determine if energy dissipation could be enhanced further. However, this was not observed and d/L of 0.125 remained the most effective case. As a result, the d/L of 0.125 (3 obstructions with 2 side obstructions 42.5 mm from the centre) along with the d/L of 0 (1 obstruction located in the centre), both with a 4 mm obstruction height, will be

analysed further both numerically (using SPH) and experimentally. This information acquired through further investigation will be given in the form of design recommendations.

3.4 Numerical Model

The two-dimensional structure and the sloshing absorber system are represented by a rigid body, having the same dimensions as the experimental setup in Figure 3.1(a). The structure's motion is restricted to rotation about its pivot point. Tethers are attached, representing the structure's stiffness and mechanical damping. The numerical model is setup to replicate the experimental initial conditions. Water is used as the sloshing liquid with a density of 1000kg m^{-3} and dynamic viscosity of 0.001 Pa s .

The most effective surface roughness elements (obstructions) are analysed numerically in section 3.6. The first case has one semi-circular obstruction with a 4 mm height located in the centre of the container. The second case has three semi-circular obstructions with a 4 mm height located in the centre of the container, each spaced 42.5 mm apart as displayed in Figure 3.2(b). The locations of the obstructions were chosen to be symmetrical in the centre of the container for this study as to produce the same effective regardless of the direction of excitation. The obstructions were intentionally located away from the container walls in order not to reduce the energy dissipation due to wave-to wall-interactions.

An SPH particle size of 0.8 mm x 0.8 mm is suitable to accurately model liquid heights 8mm and above (as discussed earlier in Chapter 2). For liquid heights below 8 mm, a particle size

of 0.4 mm x 0.4 mm is used. This resolution was found to be suitable (as presented in Appendix 2) for the shallow liquid levels used in this study and captures all flow characteristics without significantly increasing simulation run time. Time stepping in this code is explicit and is limited by the Courant condition modified for the presence of viscosity, as presented in Appendix 1. The time step used for integration is 1×10^{-6} s. The total real time is 25 s for all simulations. The number of fluid particles used for liquid heights 2.6 mm to 12.8 mm varied from approximately 5100 to 26300.

3.5 Numerical Predictions

In the following, numerical predictions of structural displacement amplitudes and liquid flow fields are compared with experimental observations to validate the numerical model. Then, SPH predictions for cases, without and with 1 and 3 attached obstructions, are analysed over liquid heights from 2.6 mm to 12.8 mm, at a structural frequency of 0.5 Hz. Finally, numerical predictions of liquid flow fields, for the optimum obstruction case, are compared to the case without obstructions to determine the effective energy dissipation characteristics.

3.5.1 Numerical and Experimental Displacement History Comparison

The dashed line in Figure 3.13 is the displacement history of an uncontrolled structure after an initial displacement of 16 degrees. The uncontrolled structure's slow decay is due to its light damping and critical damping ratio of 1 %. The solid line in Figure 3.13 is the displacement history of a rectangular sloshing absorber with 3 semi-circular obstructions attached to the bottom centre of the container with obstruction height of 4mm and a liquid

height of 7.7mm. The absorber with attached obstructions displays significant improvements to the energy dissipation response of the structure when compared to the uncontrolled case.

A displacement history comparison of experimental observation and numerical prediction for an absorber with 3 obstructions described previously is displayed in Figure 3.14. The numerical prediction is identical to the experimental observations both in peak amplitude and frequency of the structural oscillation within the first period of oscillation. This occurs when the structure experiences large displacements and the fluid behaviour is energetic. After this point the predicted peak amplitudes begin to decrease at a slightly faster rate than the experimental observations. The predicted frequency of structural oscillation also begins to slightly reduce after this point. As a result, a slightly higher damping is predicted compared to experimental observations.

To reduce the slightly high artificial damping in the numerical model, increasing the smoothing length is investigated. The smoothing length defines the size of the integration domain where a liquid particle interacts with its neighbouring particles. SPH requires a sufficient number of particles to be within this area in order to produce accurate predictions. A smoothing length of 1.2 times the particle separation with a Lennard Jones boundary approximation is most commonly used in this thesis. This boundary approximation is the cheapest method as it only requires a single layer of boundary particles that exert a force on the fluid particles in the normal direction. By using a gradient of kernel approximation for the boundary treatment, the smoothing length can be increased. However, this approximation uses multiple boundary layers that have particles that are included in the summations of the

continuity equation and pressure term in the momentum equation. Therefore, this method requires increased computational efforts. These two boundary treatments and the smoothing length are described further in Appendix 1.

A previous study (A.P. Marsh, 2010) found that increasing the smoothing length to 2.4 times the particle separation resulted in reducing the high numerical damping. However, increasing the smoothing length further resulted in excess loss of information at the free surface. This study suggested that the smoothing length value was sufficient in reducing the high numerical damping while maintaining an acceptable level of free surface detail. Therefore, a smoothing length of 1.2 to 2.4 times the particle separation is investigated. Another method used in this thesis to eliminate the high numerical damping is increasing the resolution by reducing the particle size. Increasing resolution with the variation in boundary treatment and smoothing length is not explored in this chapter due to the effects proving insensitive in a previous SPH study (Cummins et al., 2012).

The number of boundary particles with the Lennard Jones force and gradient of kernel approximation are about 2900 and 8200 respectively. Three layers of boundary particles are needed with the gradient of kernel approximation to allow for the use of larger smoothing lengths. No significant difference in structural behaviour is seen when the treatment of the boundary is changed.

For the current study there was minimal variation in peak amplitude or frequency of oscillation for a smoothing length range of 1.2 to 2.4. The gradient of kernel and Lennard

Jones treatment for the boundary force give almost identical results with all predicted results overlapping in Figure 3.14. However, although there are slight variations in peak displacement amplitudes and structural frequency, both cases produce similar 10 %, 5 % and 2.5 % settling times. The 10 %, 5 % and 2.5 % settling time ratios, taken at the point the structure oscillates within 10 %, 5 % and 2.5 % of its initial displacement, of 16 degrees. These percentage values, also used later in this chapter, are chosen as performance indicators and should not be taken as an absolute measure. The range from 10 % to 2.5 % settling time was chosen to be large enough to accurately validate the numerical model. Numerical and experimental 10 % settling times are 6.1 s and 6.7 s, 5 % settling times are 7.3 s and 8 s and 2.5 % settling times are 8.3 s and 8.9 s. Due to there being a maximum of only 10 % difference between numerical and experimental settling times at a large, 16 degree, initial displacement, comparisons are therefore acceptable.

3.5.2 Numerical and Experimental Liquid Flow Field Comparison

Liquid velocity flow field comparisons between numerical predictions and experimental observations are shown in Figures 3.15(a) to (j). The case with 3 obstructions located in the bottom centre and a liquid height of 7.7mm is used. Two complete cycles of motion of the container is compared at particular moments of interest. These moments of interest mainly consist of wave-to-wall interactions to determine if the numerical model predicts the complex free surface motion of the liquid and wave-to-obstruction interactions to determine how liquid interacts with the obstructions. The left column in Figure 3.15 displays experimental observations of the sloshing absorber controlling a structure. The right column shows numerical predictions. The liquid velocity in the simulations ranges from 0 to 1 m/s.

The first wave to wall interaction (occurring on the left wall) is displayed in Figures 3.15(a) to (d) with the fluid travelling from right to left. A hydraulic jump occurs with large free surface deformation accurately predicted using SPH. Significant swirling occurs close to the left container wall as the fluid falls due to gravity. The swirling pattern is captured effectively by the simulation.

The interaction between liquid and the obstructions is displayed in Figures 3.15(e) and (g). Remarkably good comparisons are achieved using SPH of the obstructions affecting the travelling wave. The first wave to wall interaction on the right wall is displayed in Figure 3.15(f) as the fluid travels from left to right. A hydraulic jump occurs with large free surface deformation. The fluid velocity profile displayed in Figure 3.15(g) is evidence that the obstructions increase the fluid velocity considerably as the wave travels over the obstructions from right to left, at an r/h_w of 0.5.

Figures 3.15(h) and (i) display the second wave to wall interaction on the left wall. Accurate comparisons using SPH display swirling as well as a much smaller hydraulic jump occurring compared to the first wave to wall interaction. The second wave to wall interaction on the right wall is displayed in Figure 3.15(j). By this time the liquid has slowed down considerably due to the effect of the obstructions and the wave to wall interactions. Overall numerical predictions and experimental observations for liquid free surface shapes are almost identical using SPH. Therefore this gives confidence to use SPH to further analyse absorber design with attached obstructions.

3.5.3 Numerical Displacement Histories Analysing Effects of Obstructions

Displacement histories of the structure when coupled to a rectangular shaped absorber without and with 1 and 3 semi-circular obstructions and liquid height of (a) 2.6 mm, (c) 5.1 mm, (e) 7.7 mm, (g) 10.2 mm and (i) 12.8 mm are compared in the left column of Figure 3.16. These cases are re-plotted with changing the scales to ± 4 degrees and from 6 s to 18 s to focus on the effect of obstructions at small displacements at liquid height (b) 2.6 mm, (d) 5.1 mm, (f) 7.7 mm, (h) 10.2 mm and (j) 12.8 mm. Both 1 and 3 obstruction cases are most effective controllers at a liquid height of 7.7mm, Figure 3.16(e). The obstructions become most effective after approximately 10 seconds where they eliminate the small in-phase oscillations, between the liquid travelling wave and the structure, affecting the absorber without obstructions displayed in Figure 3.16(f). Liquid velocity flow field comparisons are presented later to explain how the obstructions eliminate the in phase structural oscillations.

The 1 obstruction case is more effective at decaying the structural displacement than the 3 obstructions case at lower liquid heights of 2.6 mm and 5.1 mm, Figures 3.16(a), (b), (c) and (d). At lower levels there is insufficient momentum for the liquid to travel over the 3 obstructions resulting in significantly reduced velocity of the wave. As a result the travelling wave is unable to dissipate an effective amount of energy at the container walls. As the liquid height increases further, 3 obstructions, becomes more effective in dissipating energy than a single obstruction at the centre. This is due to larger kinetic energy dissipation rates in the deeper liquid levels as well as more wave to obstruction interactions in the 3 obstruction case compared to the 1 obstruction case.

Fluid and structure in phase oscillations occur for liquid heights of 10.2 mm and 12.8 mm in Figures 3.16(d) and (e) respectively as controlling effectiveness decreases. In phase oscillations occur from approximately 8 seconds onward. This is due to the obstructions not being large enough to dissipate an effective amount of energy during wave to obstruction interactions. The obstructions are most effective at small displacements eliminating in phase oscillations. As a result, the effectiveness of the attached obstructions is promising for industrial applications such as liquid damping in a large building that only reaches peak displacements of about 4 degrees. As mentioned previously the 3 obstruction case with a liquid height of 7.7 mm is the most effective energy dissipater ceasing oscillations in the shortest amount of time.

3.5.4 Summary of Performance of Numerical Cases

A summary of performance from the cases in Figure 3.16 are given in Figures 3.17(a), (b) and (c) as settling time ratios (consistent with section 3.4) for different liquid height to free surface length ratios (h_w/L). The vertical axis represents 10 %, 5 % and 2.5 % settling time ratios, taken at the point the structure oscillates within 10 %, 5 % and 2.5 % of its initial displacement, of 16 degrees. An effective case dissipates its initial energy quickly, resulting in the shortest settling time ratio. The 10 % and 5 % values are consistently used as performance indicators in every chapter of this thesis. A 2.5 % value is added as it is chosen to be small enough to enable comparisons with the experimental settling time ratios presented in Section 3.3.

The optimum ratio case from (V.J. Modi and S.R. Munshi, 1998) with r/h_w of 0.75 ($r = 6$ mm), h_w/L of 0.021 and a d/L of 0 is displayed in Figures 3.17(a), (b) and (c) to compare effectiveness between cases. This case is used for comparison to determine if energy dissipation could be enhanced further with attached obstructions. The logarithmic damping factor was used as the main performance indicator for cases in (V.J. Modi and S.R. Munshi, 1998). In order to achieve a direct comparison in performance, the optimum case was run numerically, using SPH, to determine the settling time ratio.

All cases are similar with variations in 10 %, 5 % and 2.5 % settling time ratios. As percentage in settling time ratio reduces the difference in settling time ratio between cases without and with obstructions increases. This is due to the attached obstructions increasing dissipation at small displacement amplitudes by eliminating in phase oscillations. Overall, the 2.5 % settling time ratio cases, in Figure 3.17(c), are in closest agreement to the same cases analysed experimentally, in Figure 3.6. Therefore, the 2.5 % settling time ratio cases are discussed further.

Both 1 and 3 obstruction cases produce faster 2.5 % settling time ratios for all h_w/L variations compared to the cases without obstructions except for the 3 obstruction case with h_w/L of 0.015. As a result, this gives evidence that adding obstructions will always achieve similar or increased effectiveness compared to the same case without obstructions. Also observed in Figure 3.17(c) is that the addition of obstructions produces a wider trough in the reduction of settling time achieving an increased effectiveness over an extended range of liquid heights.

This is a significant structural design advantage as energy dissipation can be increased substantially without a strict tolerance to liquid height.

The case without obstructions has the shortest 2.5 % settling time ratio of 0.21 at h_w/L of 0.015 (h_w of 5.1 mm). The tuned liquid height suggested using Equation 3.2 for a structural frequency of 0.5 Hz has a h_w/L of 0.035 (h_w of 11.8 mm). However, as mentioned previously, at shallow liquid heights it is more important to enhance energy transfer and dissipation than tuning the liquid frequency to equal the frequency of the structure.

The optimum case, from Modi and Munshi (1998), produced a settling time ratio of 0.2. Further reduction in settling time ratio is observed for both the 1 and 3 obstruction cases producing their shortest 2.5 % settling time ratio at h_w/L of 0.023 of 0.15 and 0.16 respectively. The 3 obstruction case gives the most increase in energy dissipation at h_w/L of 0.032, settling 54 % faster than the same case without obstructions.

The 3 obstruction case at h_w/L of 0.022 (h_w of 7.7 mm) is the most effective case with a 2.5 % settling time ratio of 0.15. Therefore, this case settles approximately 40 % faster than the same case without obstructions and about 30 % faster than the most effective case without obstructions with h_w/L of 0.01. Also, this case settles 25 % faster compared to the optimum case from (V.J. Modi and S.R. Munshi, 1998). The 3 obstruction case at h_w/L of 0.02 has a liquid frequency, f_L , of 0.4 Hz and with a structural frequency, f_s , of 0.5 Hz has a f_L/f_s of 0.81. This varies by 19 % compared to a f_L/f_s of 1, which is generally the theory for tuning a sloshing absorber to achieve optimum energy dissipation (Kareem, 1990; Banerji et al.,

2000). However, as stated earlier in section 3.3, choosing a liquid height that maximizes energy dissipation is more important than tuning the sloshing frequency to equal that of the structural frequency. The 3 obstruction case is analysed, in section 3.5.6 with the same case without obstructions using velocity flow field comparisons acquired with SPH to explain how the attached obstructions eliminate the in phase oscillations.

3.5.5 Numerical and Experimental Settling Time Ratio Comparison

Numerical 2.5 % settling time ratios and experimental settling time ratios are displayed in Figures 3.18(a) and 3.18(b) for varying liquid heights without and with 1 and 3 obstructions. The numerical cases are from 3.17(c) and experimental cases are from Figure 3.6. As mentioned previously, a 2.5 % value is chosen to be small enough to enable comparisons with the experimental settling time ratios presented in Section 3.3. These numerical and experimental cases' settling time ratios are compared to determine the accuracy of the numerical predictions.

Both numerical and experimental cases produce their shortest settling time ratios at the same h_w/L values without and with 1 and 3 obstructions. The case without obstructions produces the shortest settling time ratio at a h_w/L of 0.015. The cases with 1 and 3 obstructions produce the shortest settling time ratios at a h_w/L of 0.023. Overall, comparisons between numerical and experimental settling time ratios are acceptable and give confidence to the accuracy of the numerical model.

3.5.6 Liquid Flow Field Comparisons – Effects of Obstructions

Still frames at areas of interest of liquid flow field comparisons between cases without and with 3 obstructions from Figure 3.16(e) and (f) are displayed in Figure 3.18(a) to (h). These still frames only display the lower half of the container to display the liquid motion more clearly. Left column shows the 3 obstruction case with a liquid height of 7.7 mm and the right column shows same case without obstructions. Fixed velocity scale shows fluid particle velocity ranging from 0 to 1m/s. These frames were chosen to analyse the increased energy dissipation from the effects of the attached obstructions eliminating the small displacement oscillations from 6.1 s.

The third negative peak displacement occurs at approximately 6.1 s displayed in Figure 3.16(e). Here, the majority of the liquid mass is to the left side of the absorber pushing the structure to the left for the case without obstructions in Figure 3.18(b). The absorber with obstructions however has the liquid mass distributed over the whole base of the container as the obstructions compartmentalise some of the liquid, in Figure 3.18(a). As a result the reduction of liquid mass pushing the structure left reduces the peak displacement compared to the case without obstructions at about 6 s in Figure 3.16(e).

The liquid travels from left to right interacting with the left obstruction and almost stationary liquid (shown in blue velocity colour scale) to the right of that obstruction therefore dissipating energy at 6.38 s displayed in Figure 3.18(c). As liquid continues to travel left to right the majority of the remaining energy is dissipated, displayed with the blue velocity colouring in Figure 3.18(e). However for the case without obstructions, liquid still possesses

energy with velocity gradients still visible in Figure 3.18(f). At 9 s the 3 obstruction case has dissipated all its energy displayed in Figure 3.18(g) and has ceased oscillating in Figure 3.16(f). Whereas the case without obstructions still possesses noticeable energy within the liquid at the same point in time in the form of velocity gradients with variations of light blue to navy blue velocity colour scaling in Figure 3.18(h). A wave is also observed for the case without obstructions on the left side of the absorber travelling right indicating energy within the liquid and as a result small structural displacement oscillations occur after 9 s in Figure 3.16(f).

3.6 Conclusions

Investigating the full potential of the effects of surface roughness elements (obstructions) was the main focus of this chapter. In general, introducing obstructions close to the centre of the absorber improves the effectiveness of structural control. The central obstructions, increase shear energy dissipation due to wave-to-obstruction interactions and increase liquid velocity as the wave travels over the obstruction, resulting in superior energy dissipation at the wave-to-wall interactions. Hence, small in phase structural oscillations are eliminated.

Obstruction heights from 2 mm to 8 mm were analysed experimentally, for shallow liquid levels from 2.6 mm to 15.3 mm. As a result, obstruction height to liquid height ratios (r/h_w) from 0.4 to 0.8 increase energy dissipation from 75 % to 91 % compared to the uncontrolled case. This increase in effectiveness over a substantial r/h_w range is attractive for design purposes as effective energy dissipation can be achieved with a significant range of liquid heights.

Liquid height is more important than obstruction location for the 3 obstruction case when varying the distance of the 2 side obstructions to the centre of the container (d). Effectiveness is maintained for all variations of d , from 0 to 0.375, while r/h_w remains within 0.4 to 0.8. However, if r/h_w is outside of this range, effectiveness is significantly decreased.

Generally, 1 and 3 obstruction cases give significantly increased energy dissipation, both experimentally and numerically, when compared to the case without obstructions. Optimal energy dissipation is achieved using three obstructions with an obstruction location to free surface length (d/L) of 0.125. This case, with a liquid height to free surface length (h_w/L) of 0.022 and r/h_w of 0.5, dissipates energy approximately 40 % faster than the same liquid height case without obstructions, approximately 30 % faster than the most effective case without obstructions at a liquid height of 5.1 mm and 25 % faster than the optimum case, from Modi and Munshi (1998), with a h_w/L of 0.21 and r/h_w of 0.75. The 3 obstruction case also gives the most improvement in energy dissipation at h_w/L of 0.03 with an increase of 54 % compared to the same case without obstructions.

Displacement history comparisons between experimental observations and numerical predictions using SPH were promising. Slight variations were seen in predicted peak amplitude and frequency of structural oscillations. These slight variations were due to higher predicted numerical damping. Increasing the smoothing length and using a gradient of kernel approximation for the boundary treatment to amend the high numerical damping proved insignificant. Accurate free surface shape comparisons were achieved between experimental

observations and numerical predictions. Flow features such as hydraulic jumps, severe velocity gradients around the obstructions and swirling flow during wave to wall interactions were captured effectively in the simulation. Although slight variations in peak amplitudes were observed, the high accuracy of the liquid flow field comparison gives confidence that these small peak amplitudes are insignificant. As a result, SPH is a competent design tool and is capable of being used to further investigate energy dissipation in liquid sloshing absorbers.

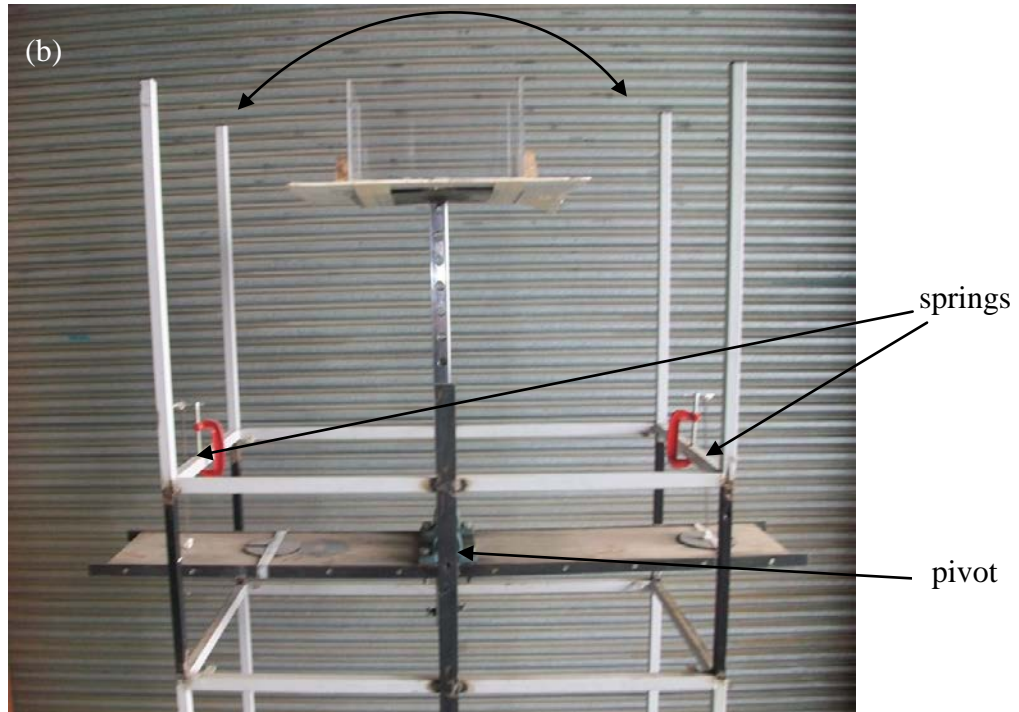
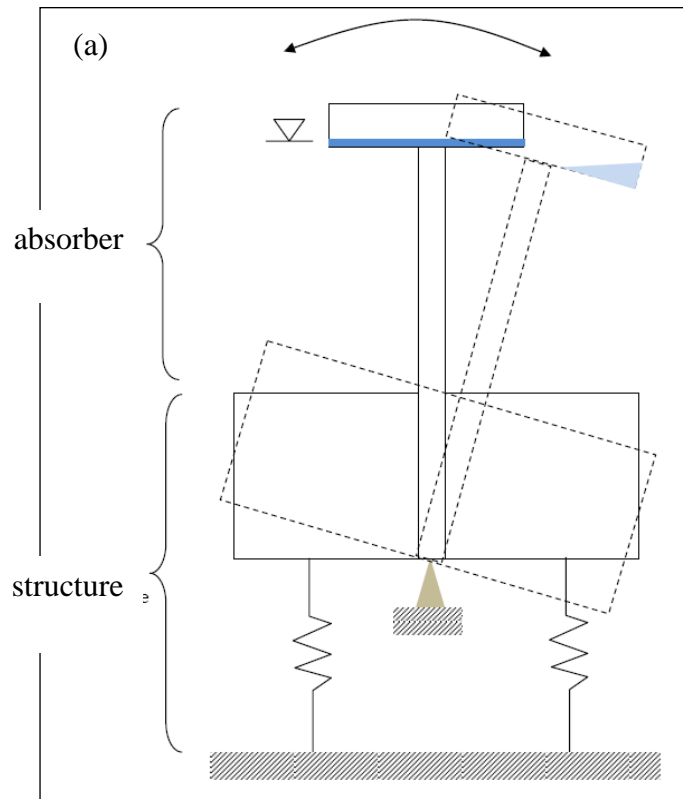


Figure 3.1: (a) Schematic and (b) photograph of the structure with the absorber.

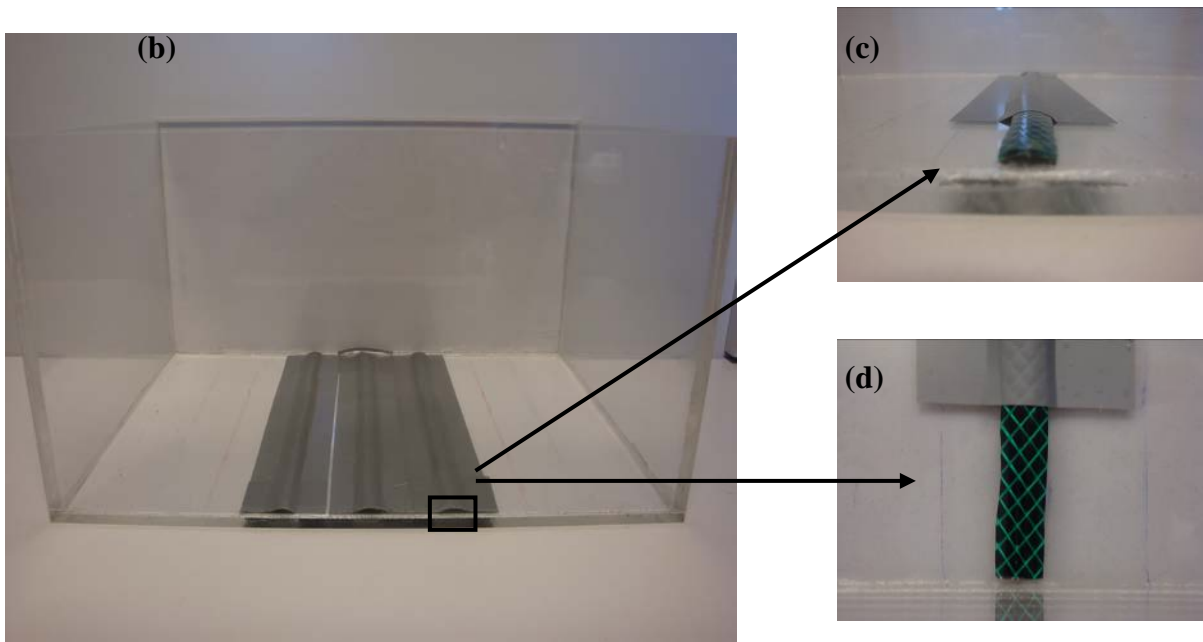
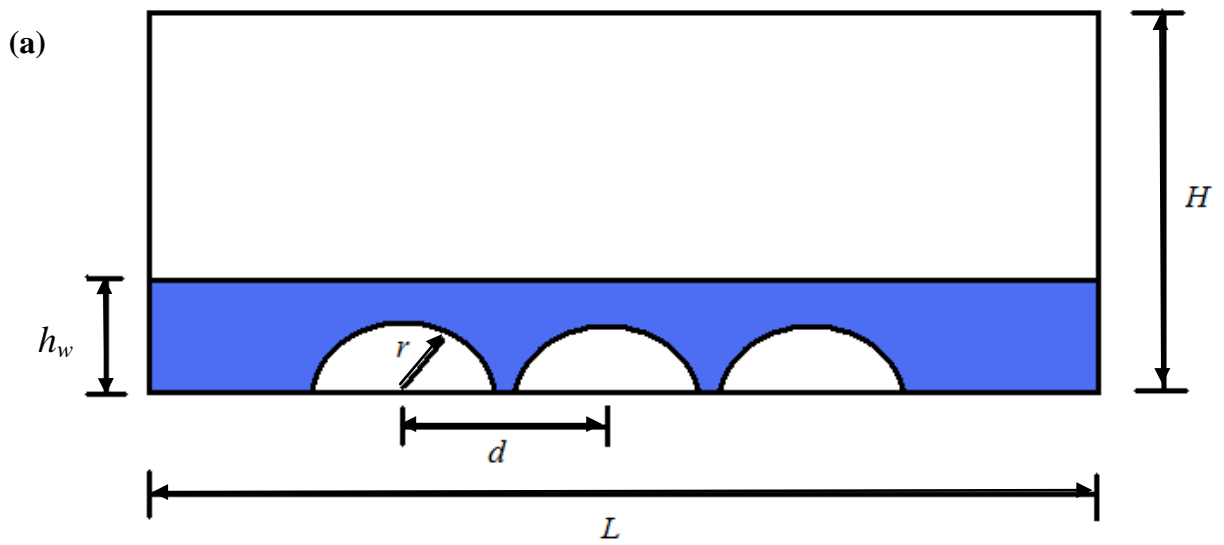


Figure 3.2: (a) Geometry of the rectangular absorber with 3 semi-circular obstructions (not to scale). (b) 3 semi-circular obstructions attached to the bottom centre of the rectangular container (distance between obstructions centre to centre is 42.5mm). (c) Front and (d) plan views of the semi-circular obstruction with section of tape removed.

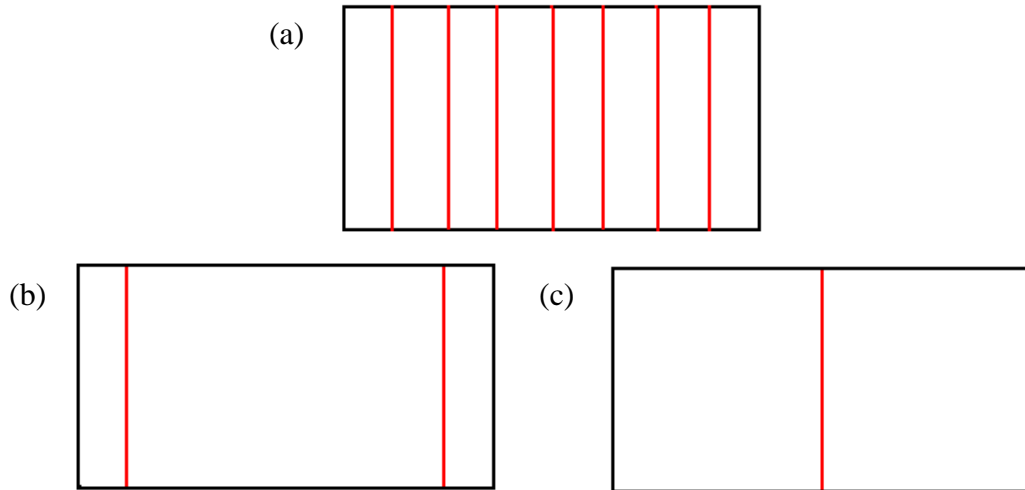


Figure 3.3: Schematic plan views of containers with obstructions attached (specified by red lines) for (a) 7 obstructions (even spaced), (b) 2 obstructions (1 obstruction 45 mm from each wall) and (c) 1 obstruction (centre).

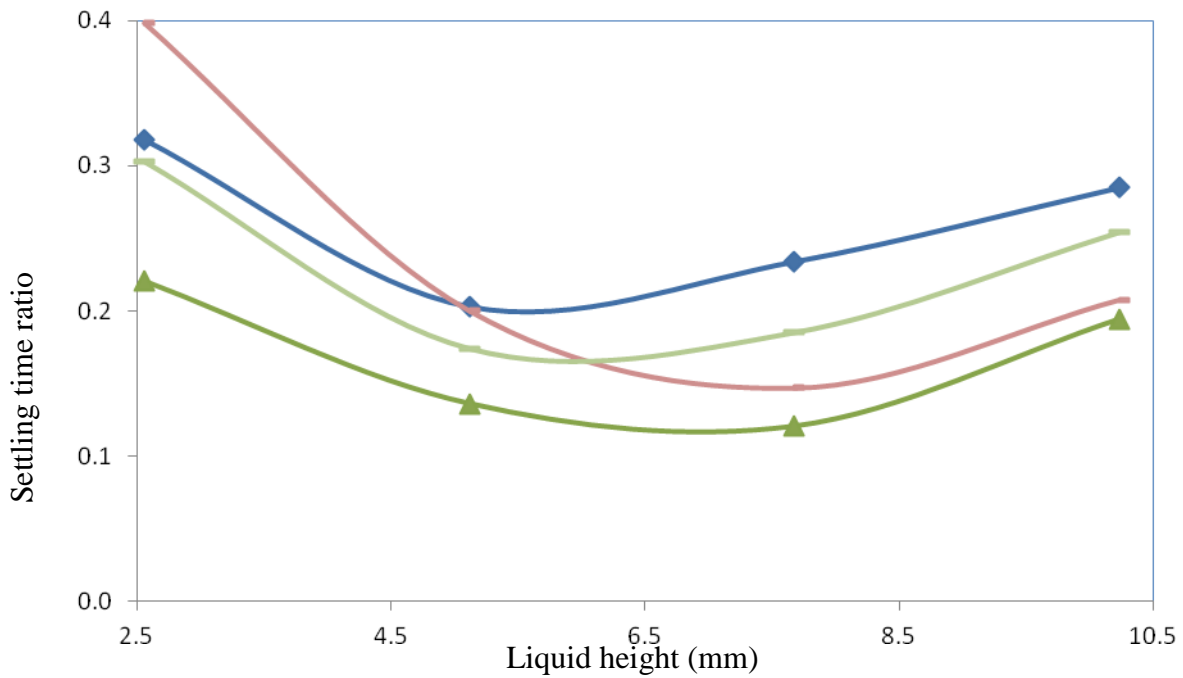


Figure 3.4: Settling time ratios for 0 obstructions (—◆—), 7 obstructions (—), 2 obstructions (sides) (—) and 1 obstruction (centre) (—▲—) with a 4 mm obstruction height from 2.6 mm to 10.2 mm liquid height.

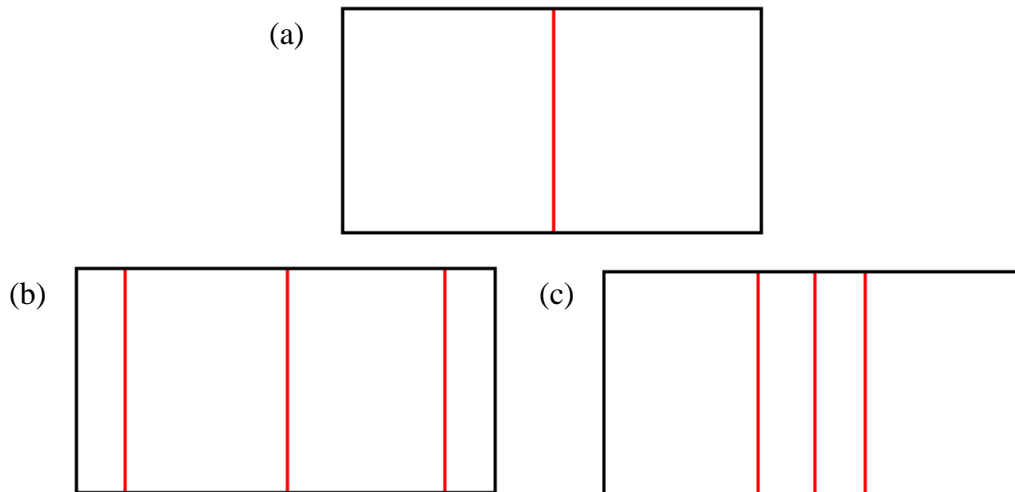


Figure 3.5: Schematic plan views of containers with obstructions attached (specified by red lines) for (a) 1 obstruction (centre), (b) 3 obstructions (1 obstruction centre, 2 obstructions (45 mm from each wall) and (c) 3 obstructions (centre, spaced 45 mm from centre obstruction).

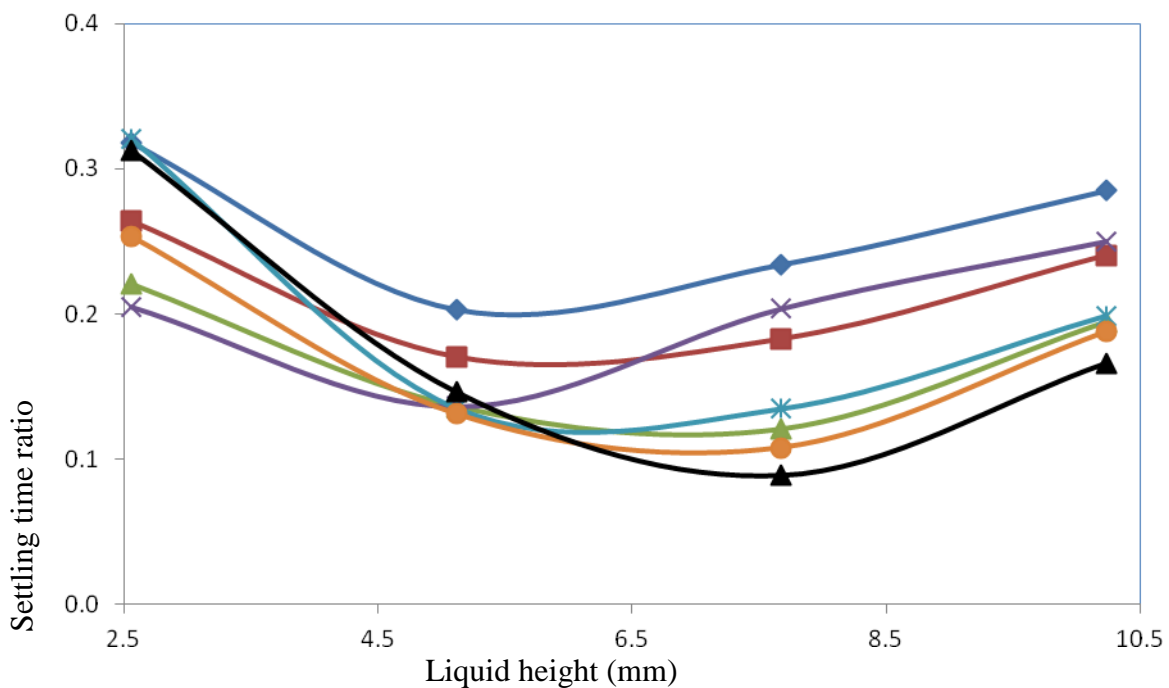


Figure 3.6: Same as Figure 3.4 but for 0 obstructions (◆), 1 obstructions (centre) (■), 3 obstructions (1 centre, 2 sides) (×) and 3 obstructions (centre) (●) with a 2 mm obstruction height and 1 obstructions (centre) (▲), 3 obstructions (1 centre, 2 sides) (◆) and 3 obstructions (centre) (▲) with a 4 mm obstruction height.

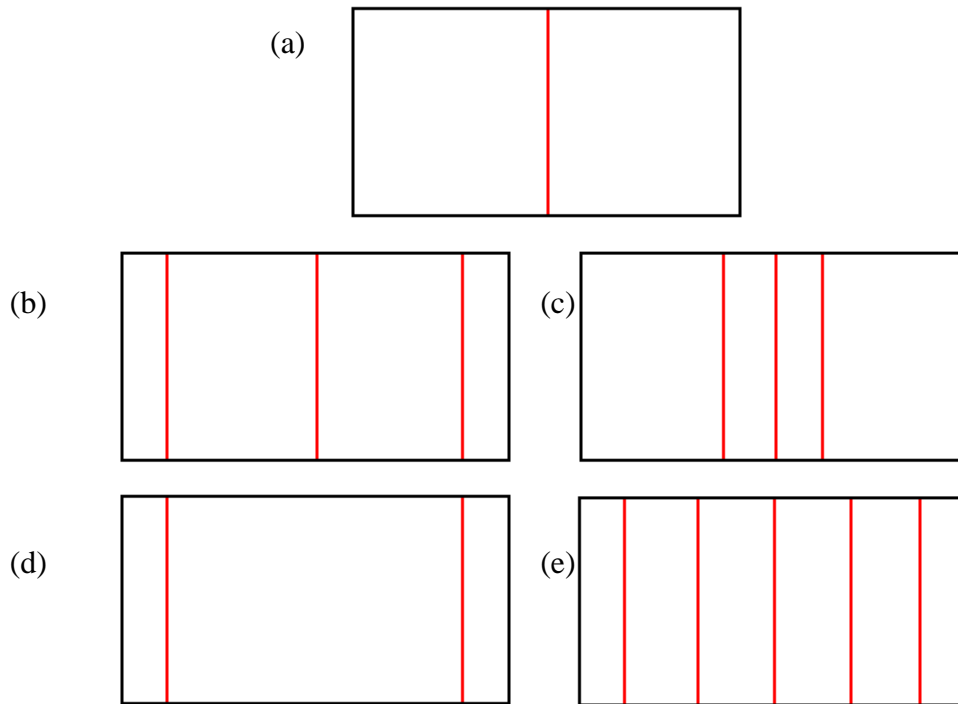


Figure 3.7: Schematic plan views of containers with obstructions attached (specified by red lines) for (a) 1 obstruction (centre), (b) 3 obstructions (1 obstruction centre, 2 obstructions spaced 45 mm from each wall), (c) 3 obstructions (centre, spaced 45 mm from centre obstruction), (d) 2 obstructions (45 mm from each wall) and (e) 5 obstructions (spaced evenly).

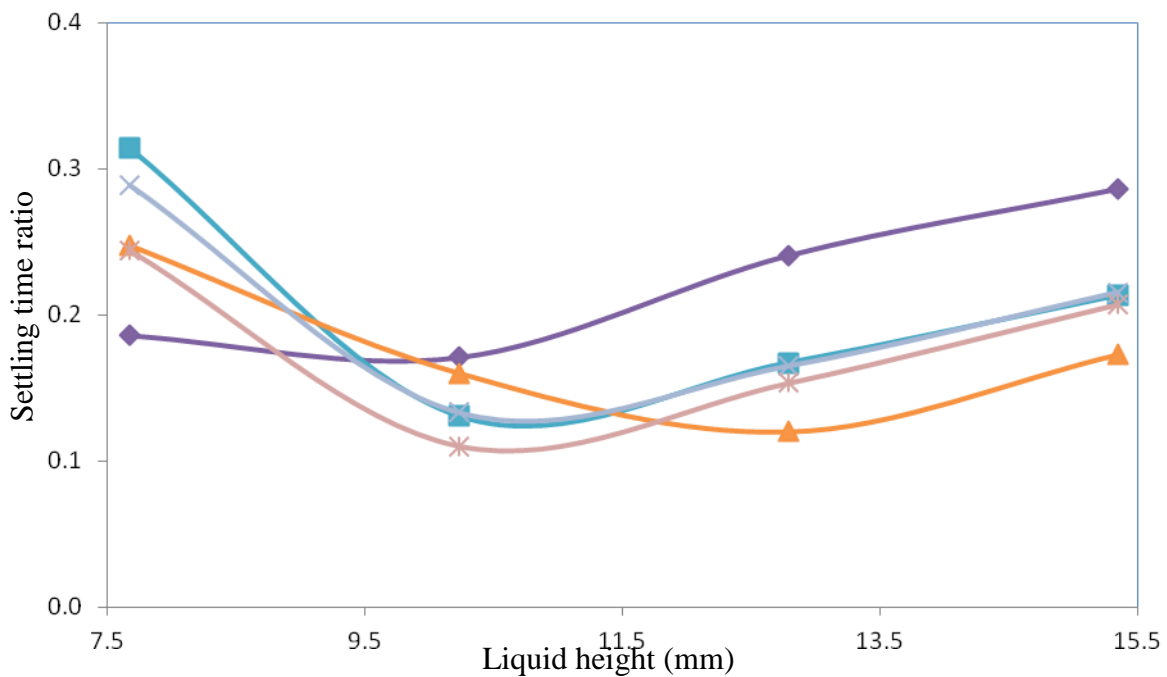


Figure 3.8: Settling time ratios for 2 obstructions (sides) (—◆—), 5 obstructions (—■—), 1 obstruction (centre) (—▲—), 3 obstructions (1 centre, 2 sides) (—×—) and 3 obstructions (centre) (—*—) with an 8 mm obstruction height at 7.7 mm to 15.3 mm liquid heights.

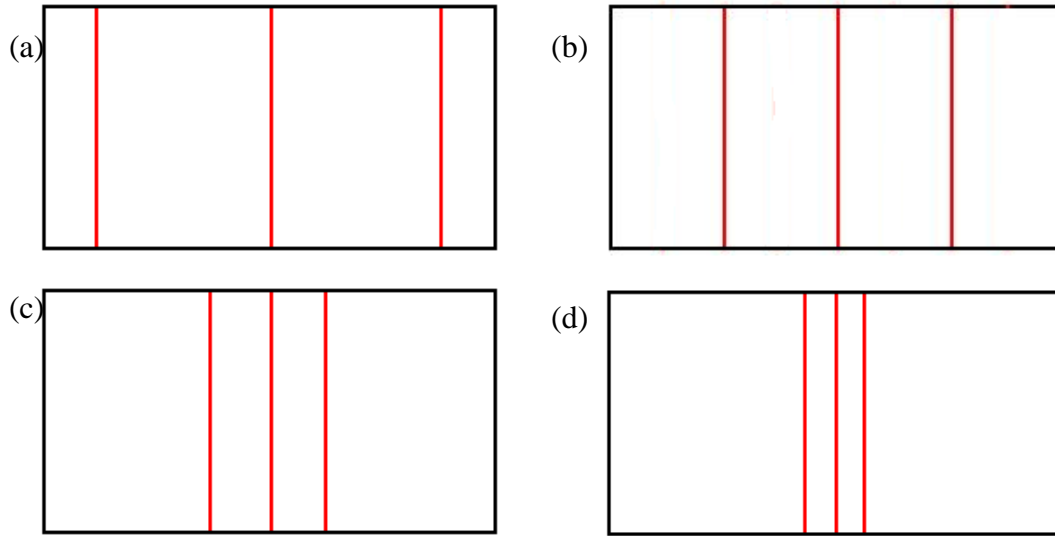


Figure 3.9: Schematic plan views of containers with obstructions attached (specified by red lines) for (a) 3 obstructions (1 obstruction centre, 2 obstructions spaced 45 mm from each wall), (b) 3 obstructions (spaced evenly), (c) 3 obstructions (centre, spaced 45 mm from centre obstruction) and (d) 3 obstructions (centre, spaced 22.5 mm from centre obstruction).

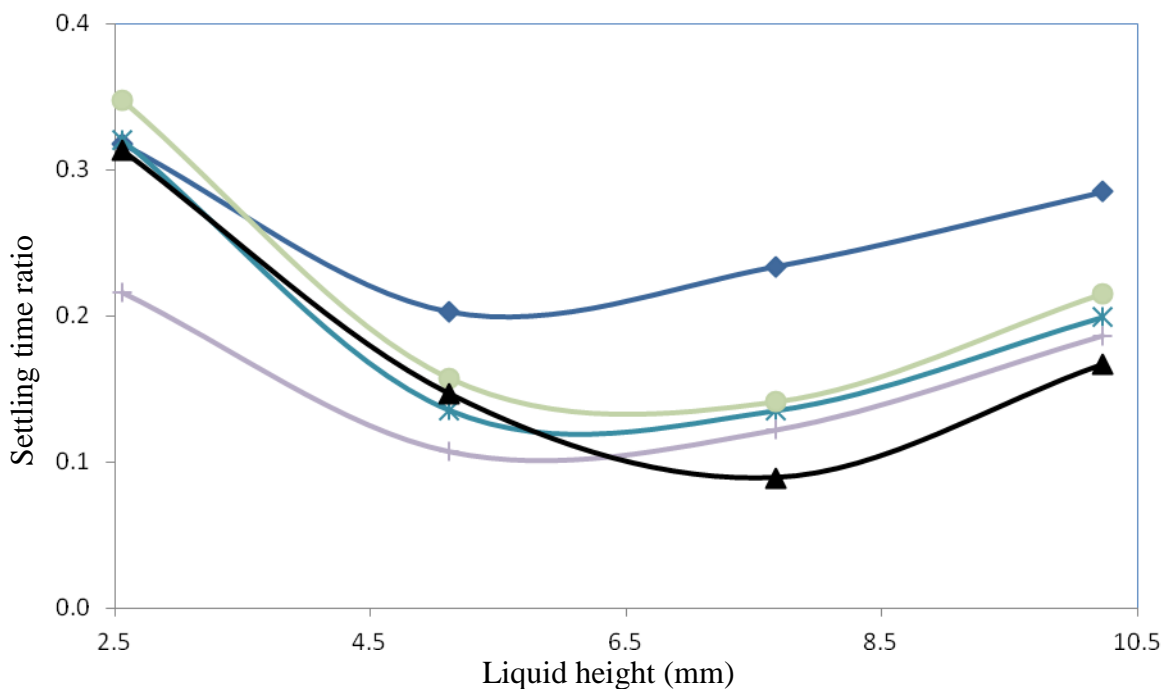


Figure 3.10: Same as Figure 3.4 but for 0 obstructions (◆), 3 obstructions (1 centre, 2 sides) (*), 3 obstruction (1 centre, 2 middle) (●), 3 obstructions (1 centre, 21.25 mm) (+) and 3 obstructions (centre) (▲) with a 4 mm obstruction height.

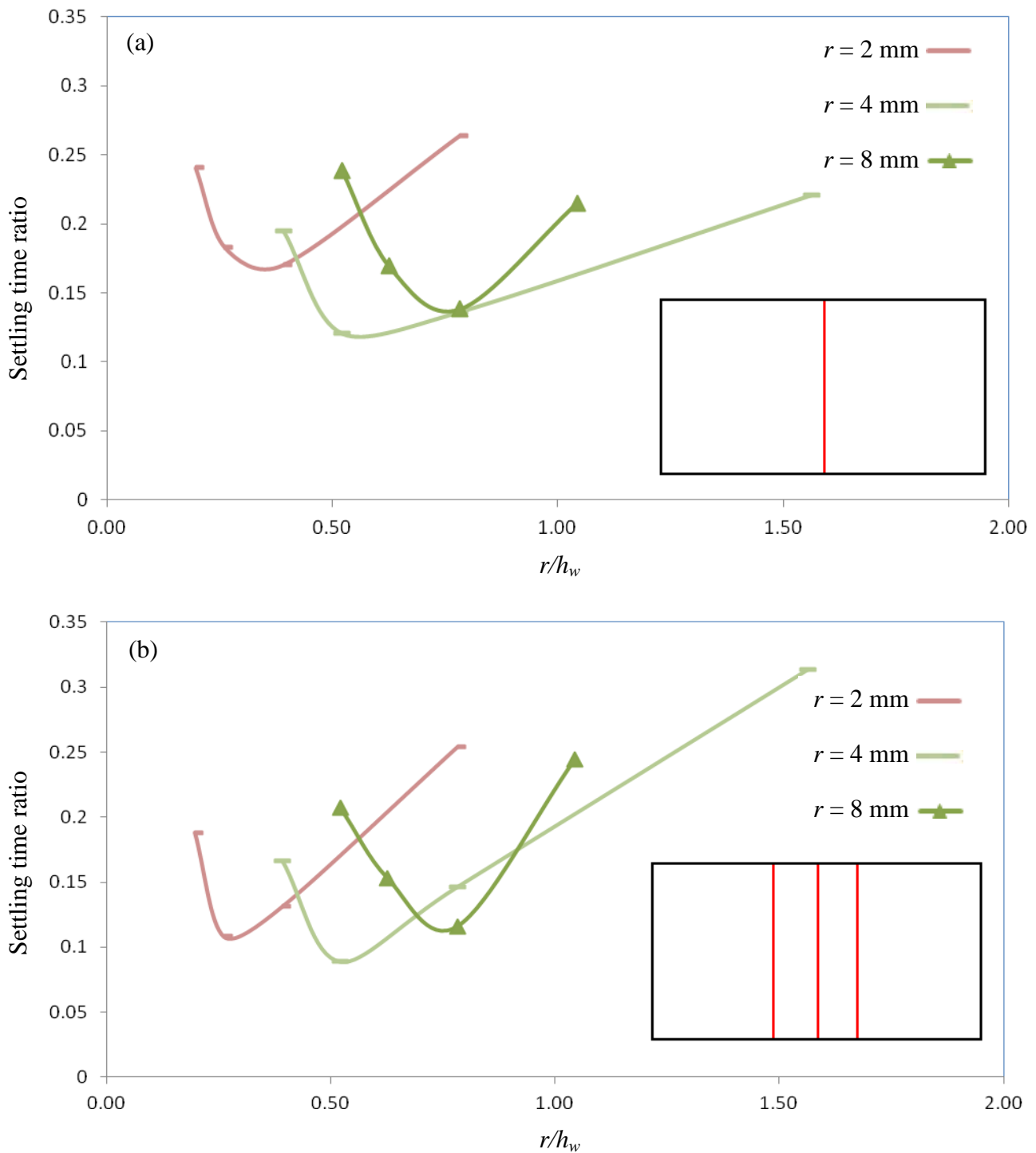


Figure 3.11: A summary of settling time ratios for cases with obstruction height to liquid height ratio (r/h_w) and obstruction heights (r) of 2 mm (—), 4 mm (—) and 8 mm (—). Inserts are schematic plan views of containers for cases in each figure with varying distance of obstruction to centre of container to free surface length ratio (d/L) of (a) 0 (1 obstruction in the centre), (b) 0.125 (3 obstructions in the centre with 42.5 mm spacing) and (c) 0.375 (3 obstructions with 127.5 mm spacing).

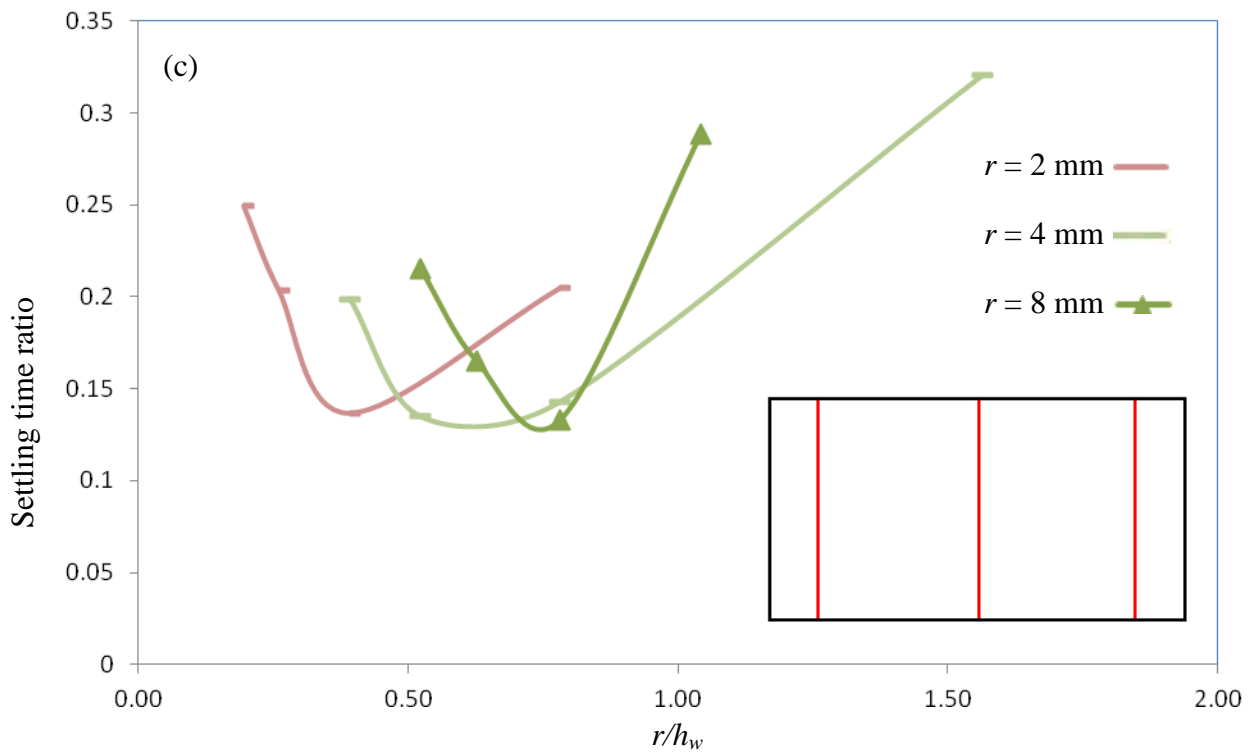


Figure 3.11: Continued.

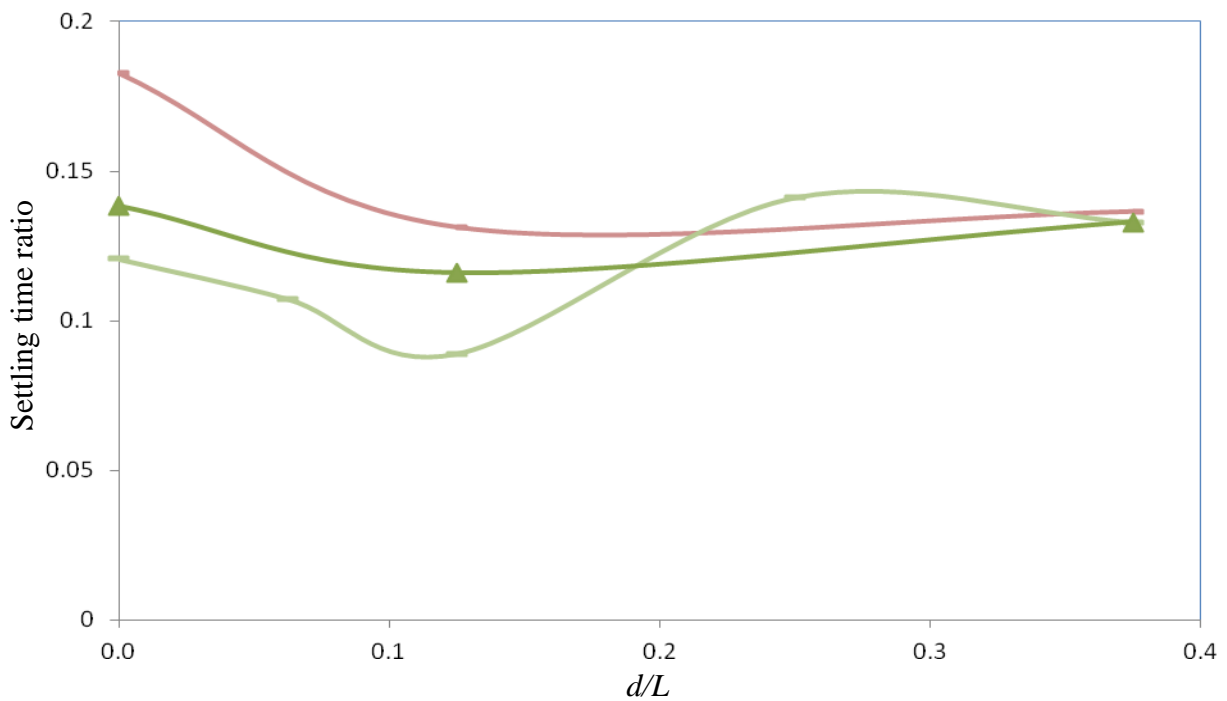


Figure 3.12: Variation of settling time ratio for distance of obstructions to centre of container to free surface length ratio (d/L) for obstruction height to liquid height ratio (r/h_w) of 0.4 ($r = 2 \text{ mm}$) (—), 0.5 ($r = 4 \text{ mm}$) (—) and 0.8 ($r = 8 \text{ mm}$) (—▲).

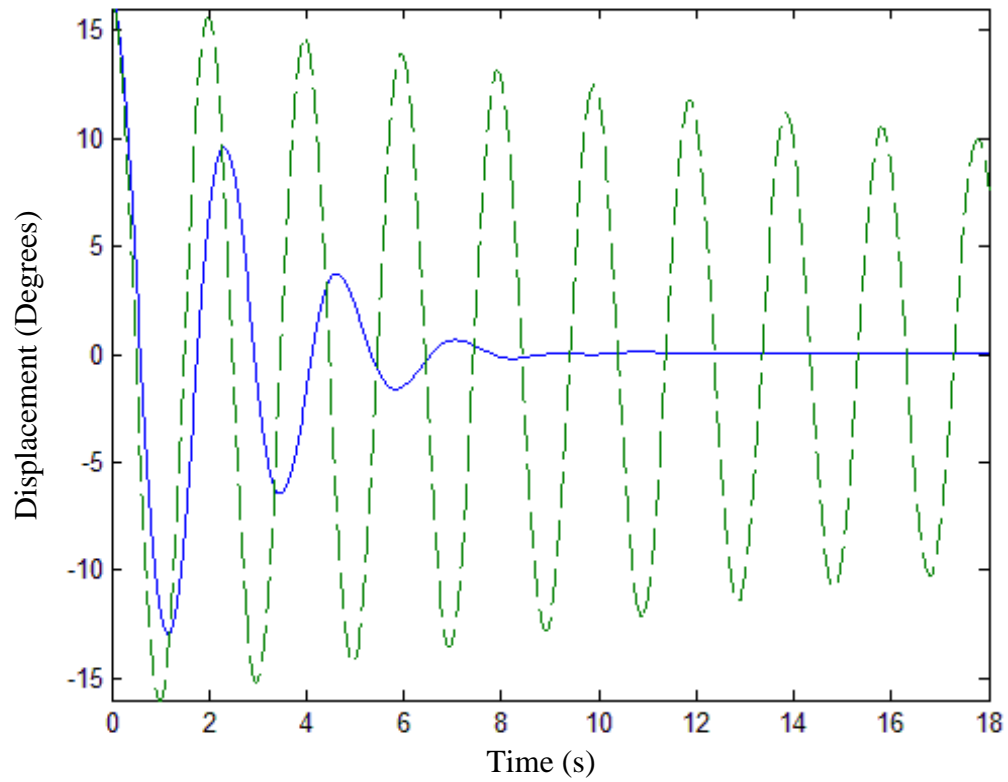


Figure 3.13: Displacement histories of uncontrolled (-----) and controlled (——) with the rectangular absorber with 3 semi-circular obstructions attached to the bottom centre of the container with obstruction height of 4 mm and a liquid height of 7.7 mm.

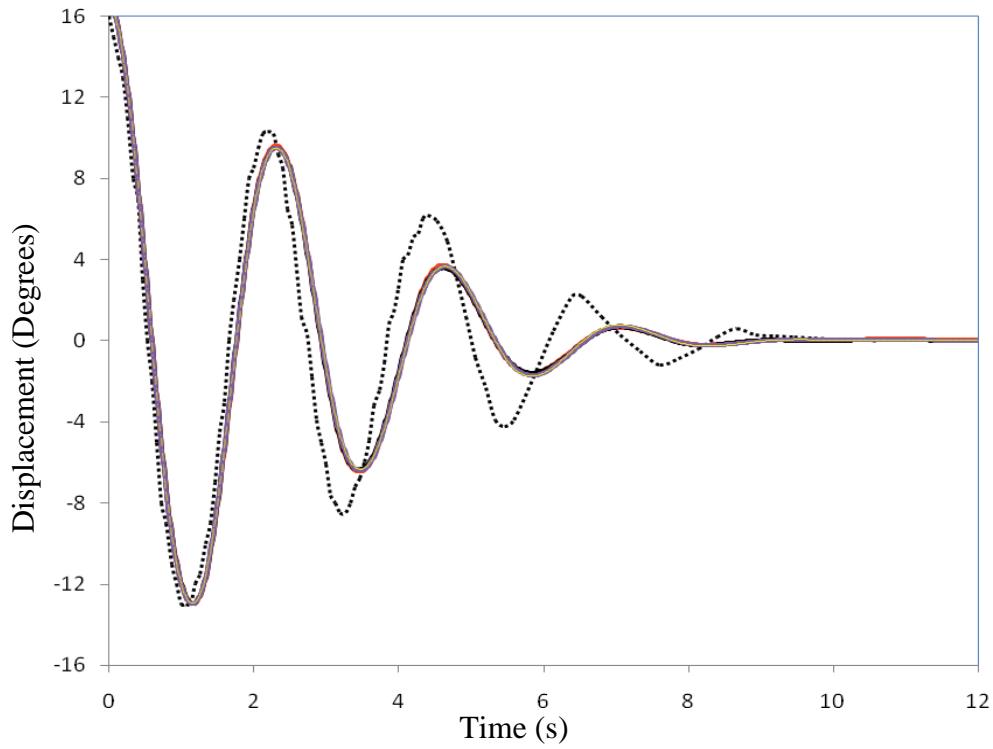


Figure 3.14: Displacement histories of the experimental observation (----) and numerical prediction with smoothing lengths of 1.2 (—), 1.6 (—), 2.0 (—) and 2.4 (—). Obstructions are the same as in Figure 3.13.

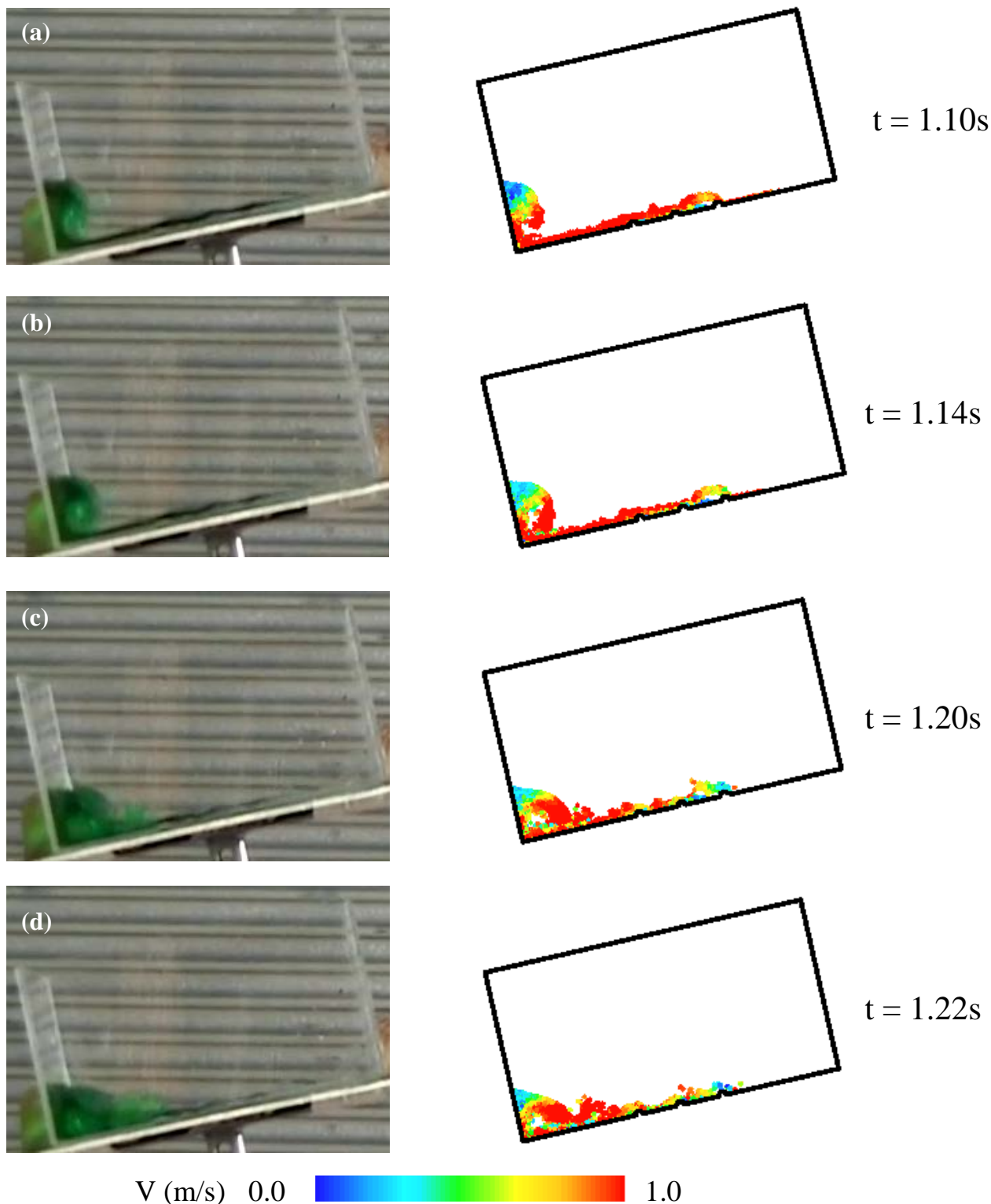


Figure 3.15: Still frames at areas of interest of free surface comparisons of water within a sloshing absorber controlling a structure. 3 semi-circular obstructions located in the bottom centre with obstruction height and spacing of 4 mm and 42.5 mm respectively, 16 degrees initial displacement and liquid height of 7.7 mm case is used for this comparison. Left column shows experimental observations. Right column shows numerical predictions obtained with SPH. Experimental error is 1/25 s (+/- 40 ms). Fixed velocity scale shows fluid particle velocity ranging from 0 to 1 m/s.

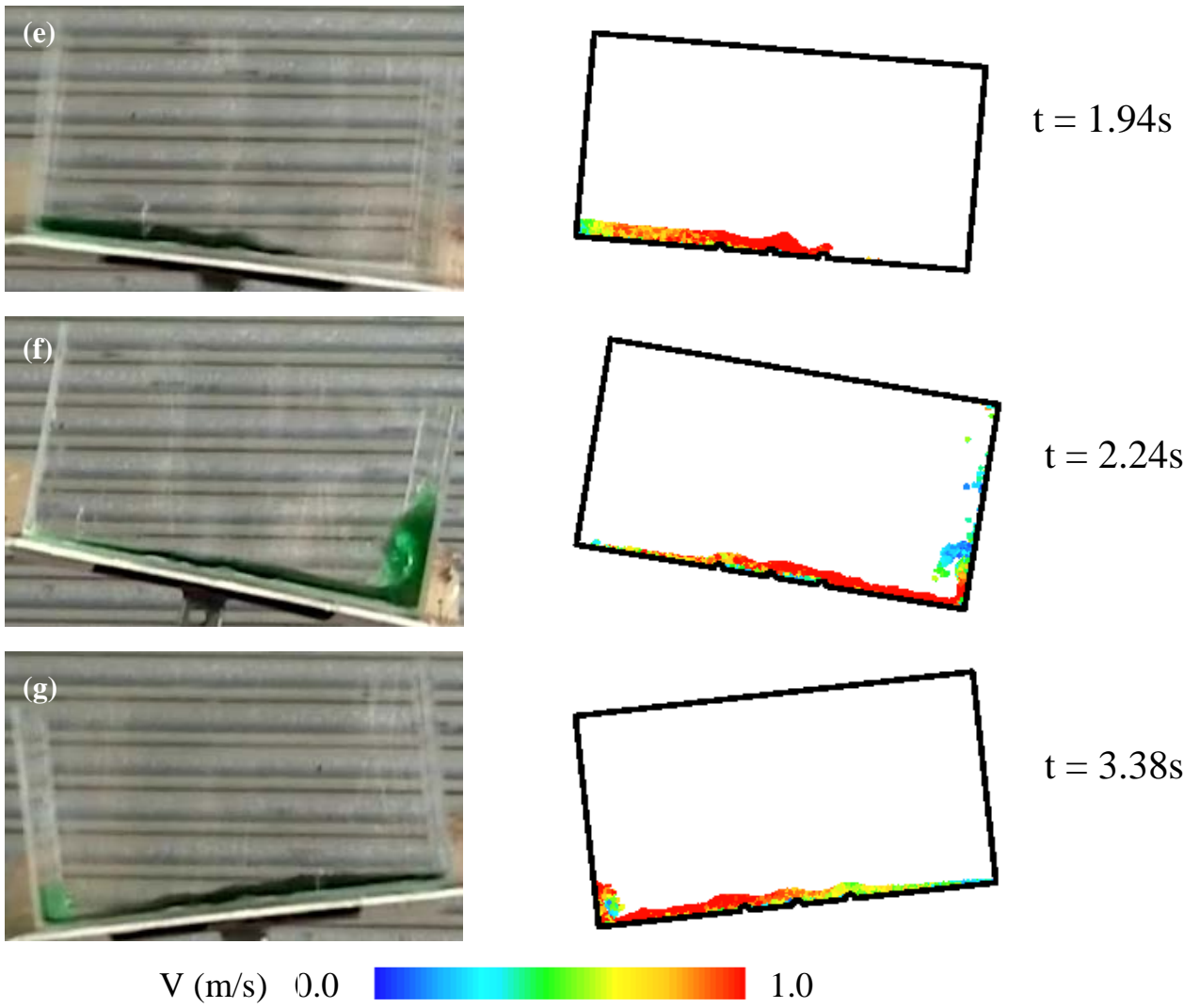
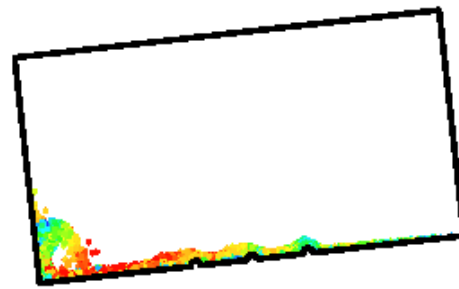
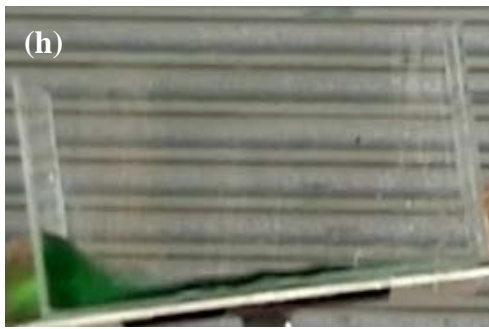
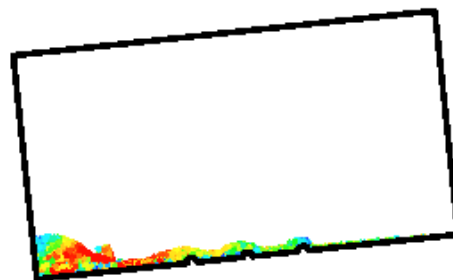


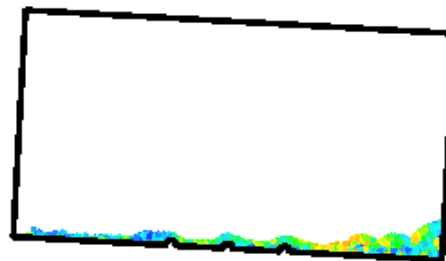
Figure 3.15: Continued.



$t = 3.52s$



$t = 3.60s$



$t = 4.84s$

$V \text{ (m/s)}$ 0.0  1.0

Figure 3.15: Continued

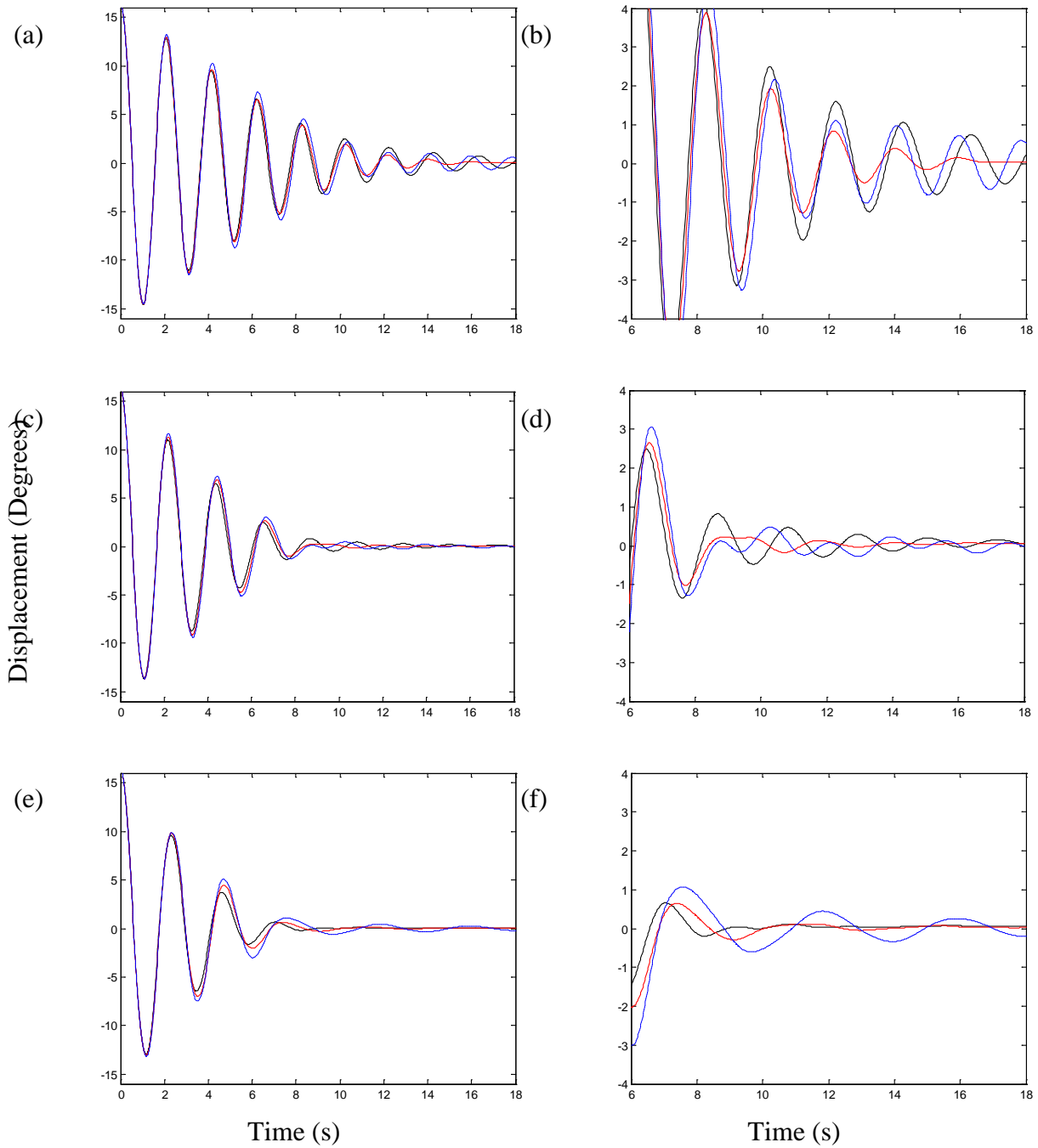


Figure 3.16: Displacement histories of the structure when coupled to rectangular shaped absorber without (— —) and with one (—) and 3 (—) semi-circular obstructions located in the centre (4 mm obstruction height) with obstruction spacing of 42.5 mm, 16 degrees initial displacement and liquid heights of (a) 2.6 mm, (c) 5.1 mm, (e) 7.7 mm, (g) 10.2 mm and (i) 12.8 mm. The right column displays the cases from the left column restricted to +/- 4 degrees displacement and time from 6 s to 18 s to focus on the effect of obstructions at small displacements (b) 2.6 mm, (d) 5.1 mm, (f) 7.7 mm, (h) 10.2 mm and (j) 12.8 mm.

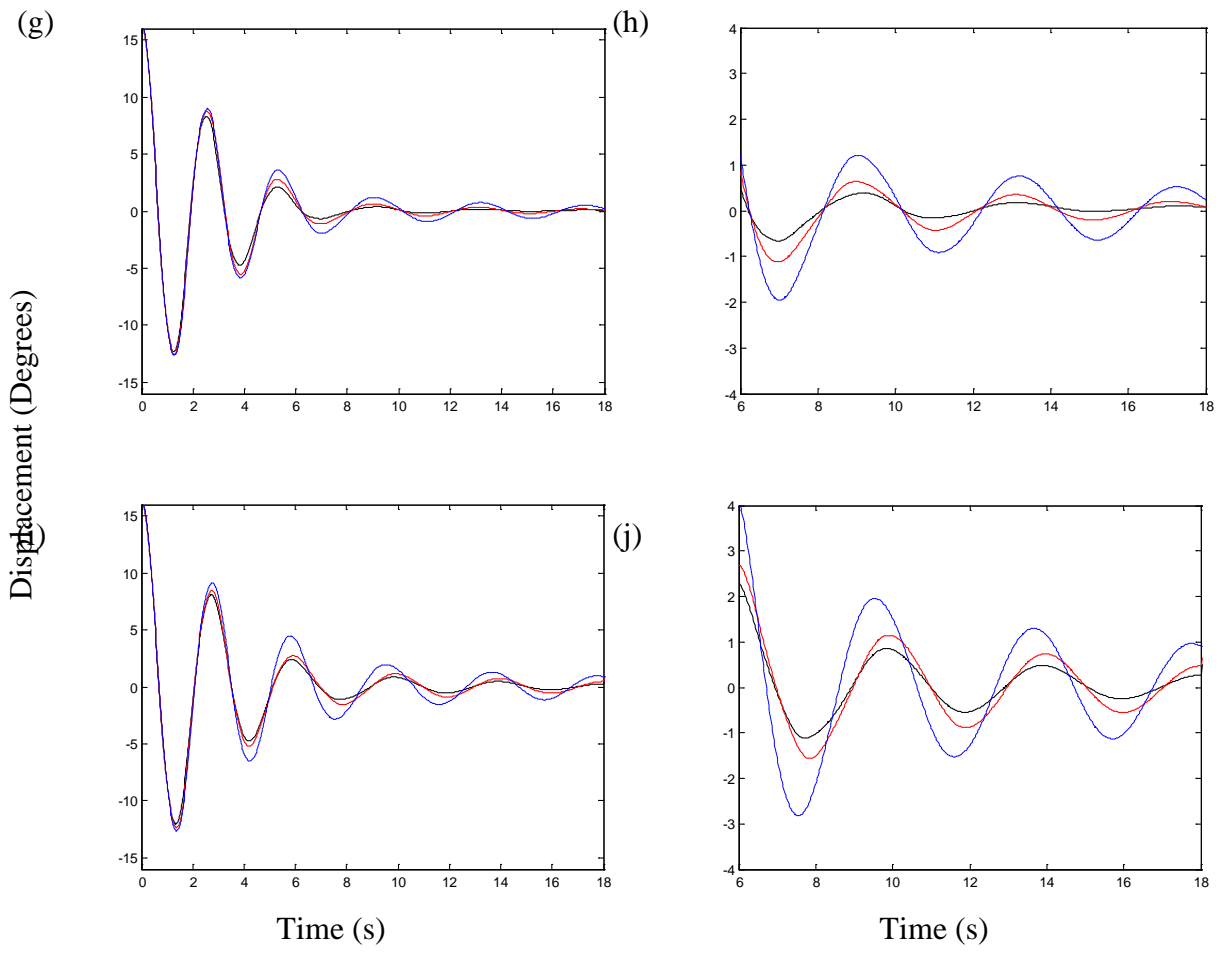


Figure 3.16: Continued.

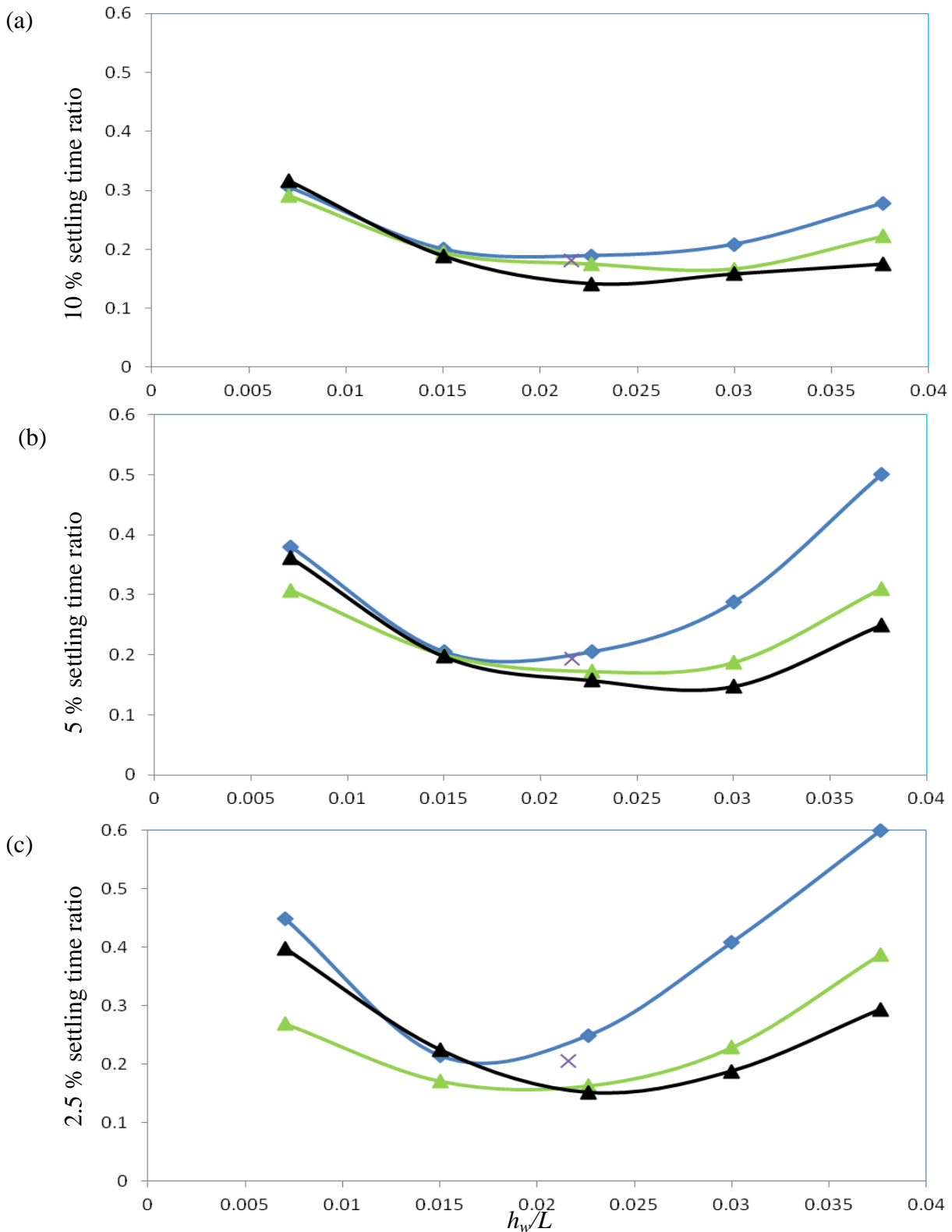


Figure 3.17: Variation of (a) 10 %, (b) 5 % and (c) 2.5 % settling time ratios with liquid height to free surface length ratio (h_w/L) for absorbers without (\blacklozenge) and with 1 (\blacktriangle) and 3 (\blacktriangle) obstructions. Settling times are taken from cases in Figure 3.14. The settling time ratio for the optimum case from (V.J. Modi and S.R. Munshi, 1998) with a d/L of 0 and an r/h_w of 0.75 ($r = 6$ mm) (\times) is also displayed for comparison.

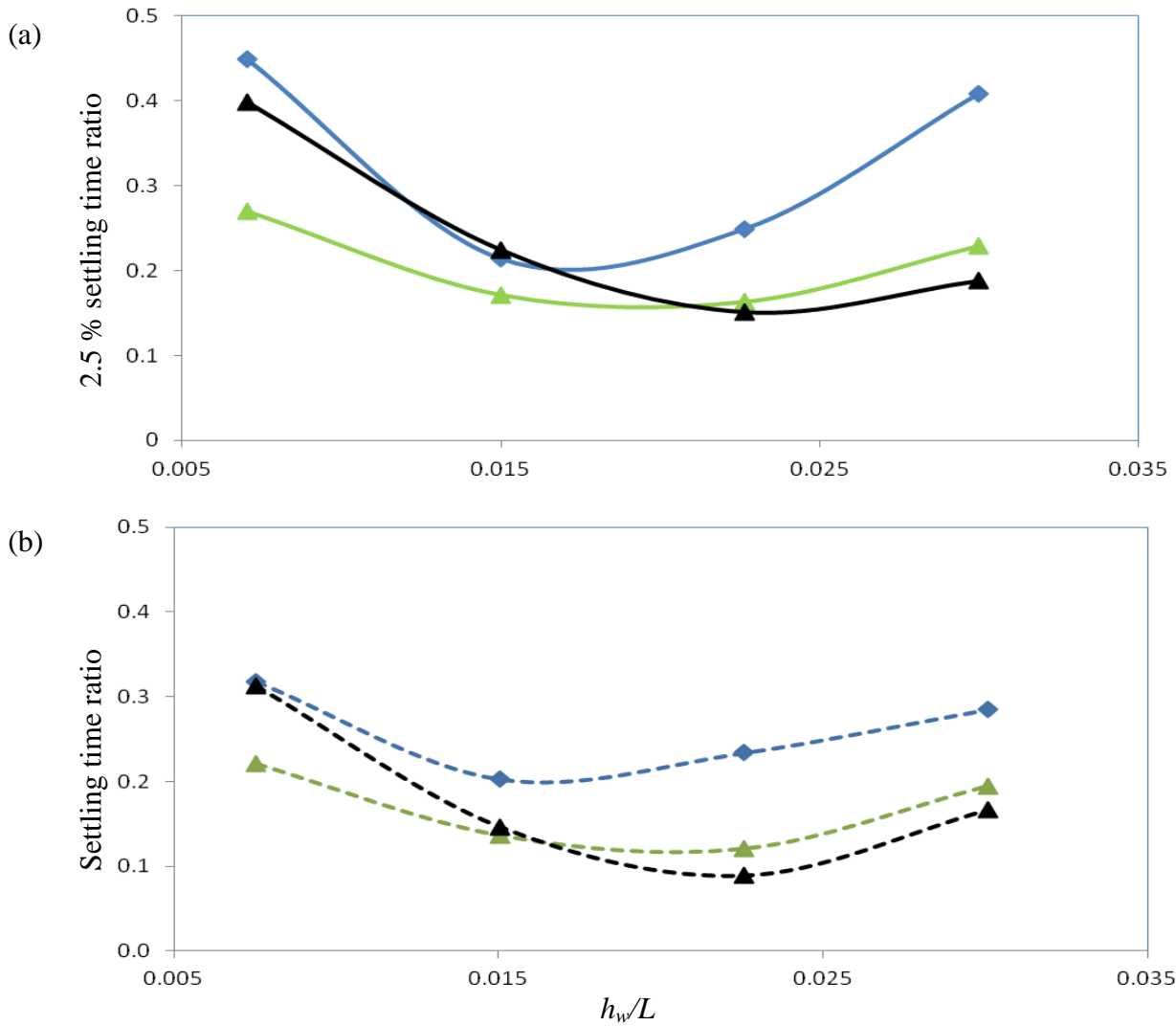


Figure 3.18: Variation of (a) numerical 2.5 % settling time ratios and (b) experimental settling time ratios with liquid height to free surface length ratio (h_w/L) for absorbers without (◆) and with 1 (▲) and 3 (▲) obstructions. Numerical and experimental settling time ratios are taken from cases in Figures 3.17(c) and 3.6, respectively.

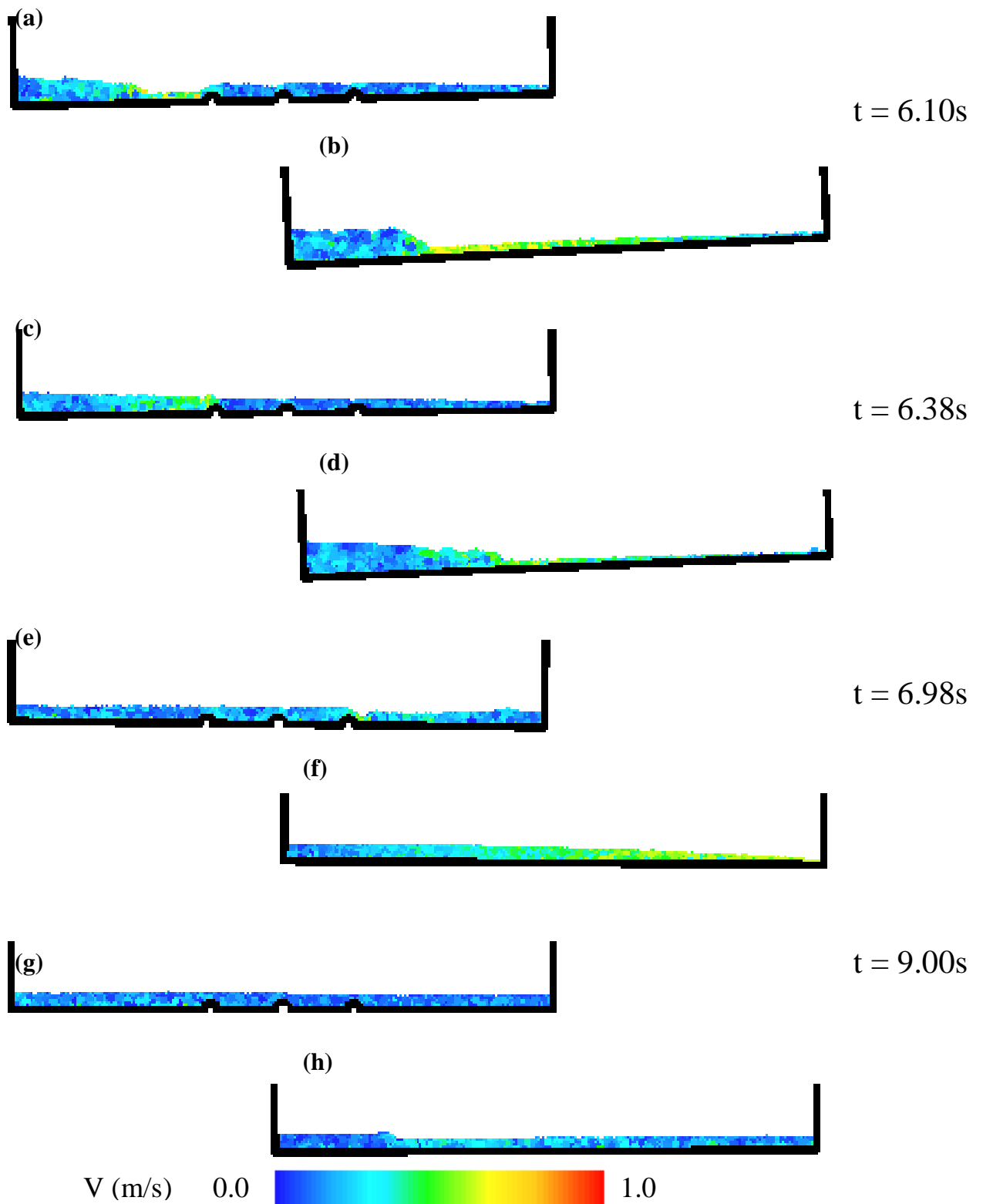


Figure 3.19: Still frames at areas of interest of liquid flow field comparisons of water within the lower half of a sloshing absorber controlling a structure. Left column shows 3 semi-circular obstructions located in the bottom centre with obstruction height and spacing of 4 mm and 42.5 mm respectively, 16 degrees initial displacement and liquid height of 7.7 mm case is used for this comparison. Right column shows same case without obstructions. Fixed velocity scale shows fluid particle velocity ranging from 0 to 1 m/s.

Chapter 4

A STUDY ON THE EFFECT OF INCLINATION ON A SLOSHING ABSORBER USING SPH

4.1 Introduction

Generally, a sloshing absorber achieves optimal energy dissipation through tuning when the frequency of the sloshing liquid matches the frequency at which the structure oscillates. Sloshing absorbers can be attached to large structures such as tall buildings and bridges to suppress excessive oscillations caused by wind or earthquake loads. As these loads are random in nature, a sloshing absorber that is effective over a range of structural frequencies is attractive for design purposes.

Chapters 2 and 3 gave evidence that shallow liquid level sloshing absorbers that produce travelling waves with severe velocity gradients are effective energy dissipaters. Along with the height of the liquid within the container, the length of the container is also a critical parameter of the liquid frequency. Therefore, while maintaining effective energy dissipation through shallow liquid levels, varying the liquid frequency of an absorber requires varying the length of the container.

Exploring the potential to increase energy dissipation through sloshing by varying the geometry of the common rectangular absorber base, has received little attention in the literature. These efforts have been limited to Gardarsson et al. (2001) and Olson and Reed (2001), where the base of the container was inclined to resemble wave energy (tsunami) dissipation at the shore of an ocean coastline. Also Modi and Akinturk (2002) and Modi et

al., (2003) investigated introducing two-dimensional wedge shaped obstacles in a rectangular absorber. They also presented steps and hole patterns cut in the wedges to resemble the natural dissipation effects that occur in rock and sand beds with incoming, breaking waves on the beach. All previous works gave superior energy dissipation when compared to the standard rectangular absorber.

Semercigil et al. (2013) varied the inclination of the common rectangular absorber, reducing the free surface of the liquid and exposing part of the base of the container. Varying the inclination of the container varies the static free surface length. As a result, the sloshing wave stretches and shrinks as it travels up and down the slope of the container. Consequently, there is potential for the inclination angle to be an effective tuning parameter, varying the effective wavelength, and therefore, the liquid frequency. Furthermore, there may be one inclination that dissipates energy effectively over a range of structural frequencies. As large structures oscillate at varying frequencies this is attractive for design purposes.

In this chapter, numerical predictions using Smoothed Particle Hydrodynamics (SPH) are validated with experimental observations from Semercigil et al. (2013). SPH is used to identify the effective energy dissipation characteristics for the absorber cases analysed and give details, such as liquid velocity flow fields, which are not possible through experimental observations. Numerical predictions using two rectangular absorbers are analysed at various inclination angles to determine if one case can produce effective energy dissipation over a range of structural frequencies. Semi-circular obstructions, that are similar to the obstructions in Chapters 2 and 3, are also attached to the base of the rectangular absorbers to explore the

potential to increase energy dissipation further. Numerical predictions to identify the physical events occurring within the absorber, that are responsible for effective energy dissipation, are the main focus of this work and reported in the form of design recommendations.

4.2 Numerical Model

Smoothed Particle Hydrodynamics (SPH) is used in this study to model the two-dimensional sloshing liquid and two absorber containers attached to the structure to be controlled. The two absorbers are used to provide identical energy dissipation characteristics within the liquid at both positive and negative displacements for inclination angles above 0 degrees. The same SPH code is used here as in chapter 2.

Experiments by Semercigil et al. (2013), were conducted as wind tunnel testing of the response of the section model of a suspension bridge. A line drawing and a photograph of these experiments are given in Figures 4.1(a) and 4.1(b). The numerical model of the two inclined containers attached to the bridge deck by two vertical poles is displayed in Figure 4.1(c) and is a structure configured as an inverted pendulum. This consists of a mechanical oscillator whose motion is designed to be rotational around a pivot point. Structural stiffness is provided by attached springs. Using an inverted pendulum configuration can significantly enhance the energy dissipation of a sloshing absorber compared to that experienced in pure translation (Lu et al., 2004). The two containers to accommodate the sloshing liquid are mounted on top 230 mm above the pivot point, displayed in Figure 4.1(c). They are spaced 75 mm apart from centre of each container to the pivot point in order to accommodate the railing in the centre of the model bridge deck. Water is used as the sloshing liquid with a density of 1000 kg m^{-3} and dynamic viscosity of 0.001 Pa s .

The two inclined rectangular sloshing absorbers, displayed in Figure 4.1, have a free surface length of 150 mm each to match the experimental setup. As a result, a liquid height of 7.9 mm was chosen using Equation 4.1 (Milne-Thomson, 1968) to have a sloshing frequency of approximately 0.85 Hz to match the structural frequency of the uncontrolled bridge and achieve tuning.

$$f = \frac{1}{2\pi} \sqrt{\frac{g\pi}{l} \tanh \frac{\pi h}{l}} \quad (4.1)$$

g , h and l represent the gravitational acceleration, fluid height and length of container respectively. Sloshing absorbers were analysed at structural frequencies of 0.85 Hz and 1.8 Hz for inclination angles 0, 8, 13, 20 and 26 degrees.

As the structure is excited, the containers on top are subjected to angular oscillations. To match the experimental setup, the uncontrolled structure has a mass moment of inertia of 0.141 kg m² and an equivalent viscous damping ratio of 1 %. The rectangular absorber's size for the numerical validation remains constant for the study with a length of 150 mm. Therefore the wavelength of the fluid or free surface length is also 150 mm.

For the frequency variation study, the two container's lengths are increased to 700 mm so it is possible at inclinations analysed for liquid frequencies, to match low oscillating frequencies produced by large structures as per Equation 4.1. This is because, at constant liquid height,

free surface length needs to increase when structural frequency is reduced. Large structures, such as high-rise buildings, can produce structural frequencies as low as 0.5 Hz (Wu et al. 2009). The frequency variation study uses containers with inclination angles 0, 1.5, 2.5, 4, 6, 8, 10 and 12 degrees for structural frequencies of 0.5, 0.7 and 0.9 Hz. The static free surface length is tuned at inclination angles 4, 8 and 12 degrees for structural frequencies 0.5, 0.7 and 0.9 Hz. Therefore, this range of inclination angles was chosen to cover the transition of tuned and un-tuned inclination angles at these three structural frequencies. Also, to achieve constant liquid to structure mass (moment of inertia) ratio with the experimental setup, the uncontrolled structure for the frequency variation study has a mass moment of inertia of 9.48 kg m^2 .

An SPH particle size of $0.8 \text{ mm} \times 0.8 \text{ mm}$ is suitable to model liquid height 7.9 mm for a structural frequency of 0.5 Hz as discussed in Appendix 2. This particle resolution is accurate enough to capture all flow characteristics without significantly increasing simulation run time. The number of fluid particles used for liquid height of 7.9 mm at free surface lengths 150 mm and 700 mm are about 3500 and 16700 respectively. Time stepping in this code is explicit and is limited by the Courant condition modified for the presence of viscosity, presented in Appendix 1. The time step used for integration is $1 \times 10^{-6} \text{ s}$.

To replicate the experimental initial conditions, the structure is offset from 0 degrees to an initial displacement of 2.4 degrees, over 2 seconds. The fluid within the container is then given 3 seconds to settle under gravity, in this position, until the liquid velocity approaches 0 m/s . The structure is then released to move and respond freely, exciting the fluid within the

container. The damping of the attached springs and control of the working fluid result in structural motions ceasing. The structure and fluid motion are recorded numerically.

A snapshot of the velocity contours, using SPH, at a particular marked instance for the 20 degree inclination case is displayed in Figure 4.2. Velocity scale runs from 0 m/s to 0.1 m/s. Liquid sloshing is observed within the two containers as the structure oscillates producing velocity gradients that contribute to energy dissipation. The SPH model provides further details, such as liquid velocity flow fields, that are unable to be achieved through experimental analysis. This valuable information helps to understand and optimise energy dissipation characteristics within the sloshing absorbers.

4.3 Numerical Predictions

In the following, SPH predictions are compared with experimental observations, from Semercigil et al. (2013). Then, cases with varying container inclinations are presented at select structural frequencies to analyse the rate of energy dissipation. Liquid velocity flow field snapshots for cases of particular interest are discussed. Finally, various obstruction setups are analysed in efforts to increase energy dissipation further.

4.3.1 Numerical Validation

Numerical and experimental displacement histories with a structural frequency of 1.8 Hz for uncontrolled, 0 (controlled), 8, 13, 20 and 26 degrees inclination are displayed in Figures

4.3(a) to 4.3(f). Almost identical displacement histories are achieved between the numerical and experimental cases for the uncontrolled case in Figure 4.3(a).

Increase in numerical damping is predicted for all controlled cases, displayed in Figures 4.3(b), 4.3(c), 4.3(d), 4.3(e) and 4.3(f). For numerical displacement histories of the cases with inclinations of 13, 20 and 26 degrees, in Figures 4.3(d), 4.3(e) and 4.3(f), enough excess energy dissipation is predicted to affect the structure's damped frequency, ω_d . As indicated in Equation (4.2) below, as ζ_{eq} increases, ω_d decreases.

$$\omega_d = \omega_n \sqrt{1 - \zeta_{eq}^2} \quad (4.2)$$

Where ω_n is the undamped natural frequency of the structure, and ζ_{eq} is the equivalent viscous damping ratio caused by energy dissipation within the fluid. This results in the developing phase difference between the predicted and experimentally observed structural displacement histories in Figures 4.3(d), 4.3(e) and 4.3(f).

As inclination increases from 0 degrees, the liquid settles to one side of the container, increasing the liquid height. Energy dissipation characteristics vary with the increased liquid height producing standing waves, instead of travelling waves, which occur at inclinations of 0 and 8 degrees at a structural frequency of 1.8 Hz. At this structural frequency, increases in liquid velocity are observed in the travelling waves with larger free surface deformation when compared to cases with lower structural frequencies.

Standing waves, which occur at inclinations above 8 degrees, possess lower energy dissipation characteristics than travelling waves. This is due to a reduction in liquid velocities and the liquid being less energetic with a calmer free surface. At these instances, the increase in numerical damping results in a phase difference between numerical and experimental displacement histories.

At inclinations of 0 and 8 degrees, although higher numerical damping is also predicted than observed experimentally, similar structural frequencies are produced between numerical and experimental cases. This is a result of SPH being able to accurately predict the timing and motion of the structure and the travelling waves, with increased liquid velocities and larger free surface deformation. The increase in artificial numerical damping that occurs at a structural frequency of 1.8 Hz is too high to validate the SPH model. As a result, a method to improve the accuracy of the numerical predictions is investigated next.

Increased numerical energy dissipation is related to artificial numerical damping associated with SPH, which relies on integration, as part of its smoothing procedure. This integration takes place from the centre of each fluid particle and has to do with its interaction with its neighbouring particles. As the particle size gets smaller, along with the corresponding smoothing length, the level of artificial damping is expected to diminish, at the expense of required computational effort. A particle size of 0.8 mm x 0.8 mm was initially chosen due to it achieving a successful validation analysis with experimental observations, at a similar shallow liquid height, for the case in Appendix 2 Resolution Study. However, due to this case

having a larger free surface length than compared to the case analysed in Appendix 2 Resolution Study unphysical results are numerically predicted, at this particle size. Therefore, a reduction in the particle size from 0.8 mm x 0.8 mm and 0.4 mm x 0.4 mm is analysed.

Numerical displacement histories of the case with no inclination, at a structural frequency of 1.8 Hz, are displayed in Figure 4.4 with particle sizes 0.8 mm x 0.8 mm and 0.4 mm x 0.4 mm. The artificial damping reduces slightly as particle size increases. Therefore, this gives confidence that SPH is able to achieve similar damping to the experiments by increasing the particle size further. A particle size of 0.4 mm x 0.4 mm for the cases with a free surface length of 150 mm has been determined to be at the edge of the practical limit with the currently available computational facility. Therefore, the particle size required to achieve acceptable damping, at a structural frequency of 1.8 Hz, is unable to be achieved. Halving the particles size increases the run time by 4 times.

Chapter 2 gave evidence that SPH was capable of achieving acceptable comparisons with a similar experimental (inverted pendulum) setup up to a structural frequency of 0.92 Hz. Therefore, a lower structural frequency of 0.85 Hz is now investigated, in order to be able to present information with acceptable accuracy. Numerical and experimental displacement histories with a structural frequency of 0.85 Hz for uncontrolled, 0 (controlled), 8, 13, 20 and 26 degrees inclination are displayed in Figure 4.5(a), (b), (c), (d), (e) and (f). Again almost identical displacement histories are achieved between the numerical and experimental cases for the uncontrolled case in Figure 4.5(a).

The container length of 150 mm was chosen so that the liquid frequency of 0.85 Hz, be tuned at an inclination of 0 degrees, as per Equation 4.1. As a result, the most effective case is at this inclination, dissipating the majority of the energy within the first three cycles from release in Figure 4.5(b). With effective tuning, the fluid travels out-of-phase with the structure, eliminating structural oscillations quickly, therefore controlling the structure.

As inclination increases, free surface length is reduced and tuning is lost, resulting in prolonged structure oscillations, displayed in Figures 4.5(c), (d), (e) and (f). Smaller amounts of liquid producing increased velocities are observed in these un-tuned cases, compared to the tuned case. The reduced amounts of high velocities in the liquid sloshing waves result in decreased energy dissipation at the wave-to-wall interactions. Consequently, the fluid is unable to dissipate the energy from the structure, transferring it back as a result, increasing the amount of time to cease oscillating. These observations are presented later, in Section 4.3.2, in the form of liquid velocity flow field snapshots.

Increasing the inclination of the container also varies the dissipation characteristics of one side of each container. The inclined cases' free surface stretches and shrinks as the structure oscillates, travelling up and down the sloped base of the container. Consequently, the wave travelling up and down the sloped base does not reach the wall of the opposing side of the container. Therefore, dissipation on this side of the container is limited to shearing between the travelling wave and container base. This differs from the 0 degree inclination case where wave-to-wall interactions occur at both walls of the container.

A small increase in numerical damping is also predicted for inclination cases above 0 degrees, at a structural frequency of 0.85 Hz, displayed in Figures 4.5(c), (d), (e) and (f). Also, minute phase differences occur between numerical and experimental displacement histories. This is again due to the increase in artificial numerical damping. However, even with these small variations, at a structural frequency of 0.85 Hz, SPH predictions show acceptable similarities with experimental observations.

Efforts to validate SPH at a structural frequency of 1.8 Hz were unsuccessful, due to the numerical damping being too high, due to limitations of the numerical tool at a high frequency. However, the numerical model is capable of producing quite acceptable comparisons to experiments at a structural frequency of 0.85 Hz. This critical observation gives confidence to explore numerically at lower structural frequencies, around 0.85 Hz, which are relevant frequencies in large structures (Wu et al. 2009).

4.3.2 Frequency Variation Study

As presented in the preceding section, although high artificial damping is could not be avoided using SPH for structural frequencies of 1.8 Hz and above, good agreement is possible between numerical and experimental displacement histories at a structural frequency of 0.85 Hz. This limitation may not be a critical issue as large structures, such as high-rise buildings, produce low structural frequencies around and below 0.85 Hz (Wu et al. 2009). Hence, new cases are now analysed numerically, at structural frequencies of 0.5 Hz, 0.7 Hz and 0.9Hz, to provide insight which may only be possible from the detailed information generated with simulations.

When the structural frequency is reduced, the free surface length is required to increase, for a constant liquid height, in order for liquid frequencies to match the lower structural frequencies, using Equation 4.1. The free surface length is increased to 700 mm, so it is possible for the sloshing frequency to match the lower structural frequencies for the inclination angles analysed. The uncontrolled structure now has a mass moment of inertia of 9.48 kg m^2 , to achieve constant liquid to structure mass moment of inertia ratio with the experimental setup.

Numerical displacement histories for cases with container lengths of 700 mm and inclinations of 0, 1.5, 2.5, 4, 6, 8, 10 and 12 degrees, for structural frequencies 0.5 Hz, 0.7 Hz and 0.9 Hz, are displayed in Figure 4.6(a), (b), (c), (d), (e), (f), (g) and (h). These inclination angles are chosen so the tuned cases that produce a static free surface length that has a sloshing frequency that matches the frequency of the structure, as per Equation 4.1, are within this range. The static free surface length is tuned at inclination angles 4, 8 and 12 degrees for structural frequencies 0.5, 0.7 and 0.9 Hz.

For cases with a structural frequency of 0.5 Hz, from inclinations 0 to 2.5 degrees in Figures 4.6(a) to 4.6(c), the rate of dissipation increases, reducing peak displacements faster. This is due to the free surface length approaching the tuned liquid frequency at 4 degrees inclination. These three cases all produce similar displacement histories.

At 4-degree inclination, the static free surface length is approximately 278 mm, which produces a liquid frequency equal to the structural frequency of 0.5 Hz in Figure 4.6(d). As inclination increases so does the static liquid height. Also, as the structure oscillates, the free surface length and liquid height vary as the liquid sloshes within the container. Therefore, by using Equation 4.1, the free surface length is determined using the original static liquid height from the configuration of a flat container. This equation is for a rectangular sloshing absorber. However, as the rectangular container is inclined, the liquid settles to one side of the container, producing a triangular sectioned static liquid profile. Despite this difference, the standard equation is still quite close in determining optimal energy dissipation through tuning as the 4 degree inclination case is the most effective, dissipating the majority of energy within 3 oscillations. For this particular case, the effectiveness seems to be related to the severe velocity gradients which occur in the breaking waves travelling on the slope of the container for longer durations than those of the other inclinations.

As observed in the Figure 4.6, when inclination increases past the tuned free surface length of 4 degrees of inclination, tuning is lost. This again results in increased peak displacements and longer time for the structure to cease oscillating for inclinations of 6, 8, 10 and 12 displayed in Figures 4.6(e) to 4.6(h).

Similar trends are observed for numerical displacement histories with structural frequencies of 0.7 Hz and 0.9 Hz as that for the 0.5 Hz in Figure 4.6. At a structural frequency of 0.7 Hz, tuning is achieved with a free surface length of about 200 mm, which occurs at an inclination of 8 degrees. At a structural frequency of 0.9 Hz, tuning is achieved with a free surface length

of approximately 155 mm, which occurs at an inclination of 12 degrees. At both structural frequencies, inclinations lower than the tuned case produce similar displacement histories, slightly dissipating increased amounts of energy, approaching the tuned case. For inclination cases above the tuned case, energy dissipation is reduced, resulting in increased peak displacements and longer time for the structure to cease oscillating. Larger amounts of liquid, producing increased velocities, are observed for tuned cases, when compared to the inclination cases that are not tuned. The increased amounts of high velocities in the liquid sloshing waves occur for longer durations and result in enhanced energy dissipation at the wave-to-wall interactions. Velocity flow field snapshots are presented in Section 4.3.4.2 to give evidence to these observations.

4.3.3 Summary of Performance

Performance summaries of 10 % and 5 % settling time ratios from cases in Figure 4.6 are displayed in Figures 4.7(a) and 4.7(b), respectively. A 10 % and 5 % settling time is the time for the peak displacement to decay within 10 % and 5 % of the initial displacement (of 2.4 degrees). Settling time ratio is the controlled (with liquid) case's settling time normalised by the uncontrolled (no liquid) case's settling time at each structural frequency. The 10 % and 5 % values are chosen only as some indication of performance, and are not absolute by any measure. Of course, an effective case dissipates its initial energy quickly, resulting in the shortest settling time ratio. All cases are similar between 10 % and 5 % settling time ratios. Therefore, only the 5 % settling time ratios are discussed next. All mentions of settling time ratio in the discussion of Figure 4.7, refer to 5 % settling time ratio.

The case with a structural frequency of 0.5 Hz produces its smallest settling time ratio at an inclination of 4 degrees of approximately 0.04. This is a substantial improvement of about 96 % compared to the uncontrolled case. At an inclination of 4 degrees the static free surface length is tuned so that the liquid sloshing frequency matches the structural frequency. At structural frequencies of 0.7 Hz and 0.9 Hz, the shortest settling time is produced one inclination below the tuned inclination, with the tuned inclination having a slightly higher settling time. This difference is likely due to determining the inclination angle using a static free surface length and flat container's static liquid height from the liquid frequency formula (Equation 4.1). However, using the inclined container's static liquid height in this formula produces a sloshing frequency closer to the frequency of the oscillating structure. While the free surface length varies as the structure oscillates, the inclination angle that produces the highest energy dissipation and shortest settling time is slightly lower than the tuned inclination.

For a structural frequency of 0.7 Hz, the shortest settling time ratio, of about 0.12, occurs at an inclination of 6 degrees, where the tuning inclination of 8 degrees produces a slightly higher settling time ratio of 0.145. Similarly, the shortest settling time ratio for a structural frequency of 0.9 Hz is about 0.21 and occurs at an inclination of 10 degrees, where the inclination is tuned at 12 degrees producing a settling time ratio of 0.25. These differences of 2.5 % and 4 % are quite small when comparing the difference of 29 % at a structural frequency of 0.5 Hz between inclinations 4 and 12 degrees.

The shortest settling time ratio for all structural frequencies is about 4 % that occurs at 0.5 Hz at an inclination of 4 degrees. This is an increase of about 56 % from the second shortest settling time ratio of about 9 % at the same structural frequency and an inclination of 2.5 degrees. At a structural frequency of 0.5 Hz, shorter settling times occur from inclination angles 0 to 4 degrees than any inclination case at structural frequencies 0.7 Hz and 0.9 Hz. An average settling time ratio of approximately 9 % occurs at a structural frequency of 0.5 Hz at inclination angles from 0 to 4 degrees. This significant improvement of 81 % over a range of inclinations, is attractive for design purposes. This is due to enhanced energy dissipation being achieved without having to be too precise on the installed inclination angle. As long as the inclination angle is 4 degrees or smaller at a structural frequency of 0.5 Hz, enhanced energy dissipation can be achieved.

Average 10 % and 5 % settling times ratios over the range of frequencies, analysed at each inclination are displayed in Figures 4.8(a) and 4.8(b), respectively. This is to determine which inclination case is the most effective over the range of structural frequencies analysed. Effective energy dissipation over a range of structural frequencies is essential for industrial applications where a structure's frequency can vary significantly. The most effective inclination angle of structural frequencies of 0.5 Hz to 0.9 Hz, for both 10 % and 5 % settling time ratios, is 4 degrees. This case produces the same average 10 % and 5 % settling time ratio of approximately 0.19 (19 %) or an improvement of 81 %.

A summary of performance for 10 % and 5 % settling time ratios with cases from Figures 4.7(a) and 4.7(b) are presented in Figures 4.9(a) and 4.9(b) with respect to liquid frequency

over structural frequency. Here, tuning is achieved when liquid frequency equals structural frequency or the value along the horizontal axis (f_L/f_s) is 1. All structural frequency cases show similar trends where settling time reduces as f_L/f_s increases from 0.2 to around 1. For f_L/f_s above 1, settling time increases. All structural frequencies produce shortest settling times of an f_L/f_s of approximately 0.8 to 1 or around the tuned inclination angle. Performance is enhanced at lower structural frequencies. As structural frequency increases so does settling time ratio, evenly at all inclination angles. This is possibly due to increased initial energy within the system at higher structural frequencies.

Overall, substantial improvements are observed at all inclination angles over structural frequencies 0.5 Hz to 0.9 Hz as compared to the uncontrolled cases. The liquid sloshing absorbers can be tuned to achieve optimal energy dissipation through inclination alone. This is achieved by inclining the containers to achieve static free surface lengths that produce a liquid sloshing frequency that matches the frequency of the structure to be controlled. The optimal inclination angle is 4 degrees producing the shortest average 10 % and 5 % settling time ratios over structural frequencies 0.5 Hz to 0.9 Hz. This is attractive for design purposes as effective energy dissipation over a range of structural frequencies is essential for industrial applications where a large structure's frequency can vary significantly. The inclination angle of 4 degrees is most effective at a structural frequency of 0.5 Hz where energy dissipation is enhanced by 96 % compared to the uncontrolled case.

4.3.4 Liquid Velocity Flow Fields

Here, a comparison between tuned and un-tuned cases is presented to describe differences in liquid motion and dissipation characteristics at an inclination angle of 0 degrees. Then comparisons are presented to give information on how liquid motion and dissipation characteristics vary between absorbers without and with inclination. Finally, tuned and un-tuned inclination cases are compared to show how increased amounts of energy are dissipated effectively for the inclined tuned case compared to the inclined un-tuned cases.

4.3.4.1 Energy dissipation Characteristics – Cases Without and With Inclination

In a liquid sloshing absorber, maximum energy dissipation is achieved when the wave-to-wall interaction occurs at 0 degrees structural displacement and the liquid and structure are travelling in opposing directions. This is due to the structure having maximum velocity at zero degrees displacement. Minimum momentum opposition is achieved when the wave-to-wall interaction occurs at 0 degrees structural displacement, and the liquid and structure are travelling in the same direction.

For a rectangular liquid sloshing absorber, tuning the sloshing frequency to match the frequency of the oscillating structure, using Equation 4.1, is the most common method to achieve maximum energy dissipation. Although this method produces effective energy dissipation, maximum energy dissipation (at 0 degrees displacement) cannot be achieved as the structure's motion pushes the liquid in the direction the structure oscillates. The cases around tuned, liquid frequency to structural frequency (f_L/f_s) of 0.8 to 1 produce wave-to-wall interactions that begin as the structure approaches peak displacement and finish around the

peak displacement. The structural displacement locations, where wave-to-wall interactions occur, for the un-tuned cases, vary depending on f_L/f_s . Wave-to-wall interactions can occur from around 0 degrees structural displacement, with the liquid and structure travelling in the same direction, producing minimum momentum opposition, or even not at all. All un-tuned cases consequently result in poor energy dissipation.

Liquid velocity flow field snapshots are displayed in Figures 4.10 and 4.11. The particular instances are chosen at displacement locations that show key areas where energy is dissipated effectively, through wave-to-wall interactions, for tuned cases. These instances occur when the structure is approaching peak displacements. Alternatively, these same locations also show where energy dissipation is reduced for the un-tuned case, compared to the tuned cases, where wave-to-wall interactions do not occur. After the structure is released from its initial (first negative) peak displacement, it rotates clockwise towards its first positive peak displacement. The structure approaches the first positive peak displacement for all cases in Figure 4.10 and approaches the second negative peak displacement for all cases in Figure 4.11. The instances given in this section occur within the first full cycle of oscillation where the majority of the energy is dissipated effectively for the tuned cases.

Three numerical cases are analysed in this section. The case with an inclination of 0 degrees and a structural frequency of 0.85 Hz, from Figure 4.5(b), is the tuned, no inclination case and is presented in Figure 4.10(a) and 4.11(a). This case is the only tuned, 0 degree inclination case analysed in this chapter and is also the most effective energy dissipater for all 0 degree inclination cases analysed. The case with a structural frequency of 0.5 Hz, with no inclination (not tuned), from Figures 4.6(a), is displayed in Figures 4.10(b) and 4.11(b).

These tuned and un-tuned cases are initially compared to show how liquid motion and dissipation characteristics vary for cases with no inclination.

Then, the un-tuned case with no inclination is compared to the case with an inclination angle of 4 degrees (tuned), at the same structural frequency of 0.5 Hz, from Figures 4.6(d), displayed in Figures 4.10(c) and 4.11(c). As a reminder, the 4 degree inclination case is the most effective energy dissipater for all cases analysed in this chapter. This comparison is analysed to give information on how liquid motion and dissipation characteristics vary between absorbers without and with inclination. Velocity colour scale indicates a range from 0 m/s (blue) to 0.1 m/s (red).

The container length is 150 mm for the case with a structural frequency of 0.85 Hz in Figures 4.10(a) and 4.11(a) and 700 mm for the cases with a structural frequency of 0.5 Hz in Figures 4.10(b), 4.10(c), 4.11(b) and 4.11(c). Although, these cases have different container sizes and are analysed at different structural frequencies, they both have the same liquid to structure mass moment of inertia ratio. Therefore, liquid velocity flow field snapshots at the structural locations where effective energy dissipation occurs for these cases are comparable.

The case with an inclination of 0 degrees, in Figure 4.10(a), is tuned with a liquid sloshing frequency matching the structural frequency of 0.85 Hz. High velocity gradients (in red) are observed as the structure approaches the first positive peak displacement, at 0.68 s, in the liquid travelling towards the right wall as the structure rotates clockwise. This results in increased energy dissipation at the right wave-to-wall interaction.

Alternatively, the case with no inclination and a structural frequency of 0.5 Hz in Figure 4.10(b) is not tuned. Therefore, the liquid is still travelling towards the right wall when the first structural positive peak displacement occurs at 1.08 s. The wave-to-wall interaction is consequently eliminated, resulting in poor energy dissipation.

The structure approaches its second negative peak displacement at 1.32 s, rotating anticlockwise in Figure 4.11(a). The high velocity wave (in red) travels towards the left wall again producing increased shear dissipation at the wave-to-wall interaction. The case that is not tuned approaches its second negative peak structural displacement at 1.6 s with the structure rotating anticlockwise, in Figure 4.11(b). Due to the case being so far out of tune the initial wave displayed in the Figure 4.10(b) is still travelling from left to right and does not reach the wall to dissipate energy. Therefore, energy dissipation efforts are reduced again.

The case with an inclination of 4 degrees and structural frequency of 0.5 Hz is displayed in Figures 4.10(c) and 4.11(c). The absorber inclination is tuned at 4 degrees, which has a static free surface length that produces a liquid frequency that matches the structural frequency. Energy dissipation characteristics vary when compared to the tuned, no inclination case in Figures 4.10(a) and 4.11(a). For the 4 degree inclination case, the majority of the liquid remains on one side of the container, exposing the base of the opposing side, displayed in Figure 4.10(c). The free surface varies as the structure oscillates, producing high velocities (in red) and increased energy dissipation through shear stress as the wave travels up and down the sloped base of the container. This wave does not reach the wall of the opposing side of the container. Therefore, dissipation on this near side of the container is limited to shearing between the travelling wave and container base. Wave breaking with severe velocity gradients is also observed in the right container, at 1.6 s, as the structure approaches its

second negative peak displacement travelling from right to left, contributing to dissipation efforts in Figure 4.11(c). Both the 4 degree inclination and no inclination cases prove to be effective in dissipating energy when tuned producing 5 % settling times of 4.5 s and 5.5 s respectively.

Similar quantities of high velocity (in red) liquid are observed, particularly in the left containers, in the un-tuned, 0 degree inclination case in Figure 4.10(b) and the tuned, 4 degree inclination case in Figure 4.10(c). This results in similar amounts of energy being dissipated through shearing of the liquid as the wave travels along the base of the container. However, as the absorber is un-tuned at an inclination of 0 degrees, the travelling wave does not reach the boundary, eliminating the wave-to-wall interaction, in both containers, in Figure 4.11(b). Whereas, the 4 degree inclination absorber is tuned so that the liquid travels back and produces increased energy dissipation at the wave-to-wall interaction, in the left container, in Figure 4.11(c).

SPH gives flow field behaviour producing velocity gradients in travelling waves and free surface deformation in the form of breaking waves. These details give valuable information that helps explain how energy dissipation should occur within the liquid of the sloshing absorber. Such details give confidence for the use of SPH to design liquid sloshing absorbers for structural control applications.

4.3.4.2 Energy Dissipation Characteristics – Inclined Tuned and Un-tuned Cases

Liquid velocity flow field snapshots for cases with a structural frequency of 0.7 Hz are displayed in Figures 4.12 to 4.17 to explain how energy dissipation characteristics vary between tuned and un-tuned cases at various inclination angles. The cases with a structural frequency of 0.7 Hz were chosen as they are best suited to cover a range that includes inclination angles below tuned (4 degrees), tuned (8 degrees) and above tuned (12 degrees). The cases with an inclination angle of 4 degrees are displayed in Figures 4.12(a) to 4.17(a), 8 degrees, displayed in Figures 4.12(b) to 4.17(b), and 12 degrees, displayed in Figures 4.12(c) to 4.17(c).

Six structural displacement locations were chosen to analyse the three inclination cases. The displacement locations consist of 0 degrees structure displacement and both positive and negative peak displacements. These instances were chosen as they are locations where liquid motion is of particular interest and give evidence to how effective energy dissipation occurs. In particular, structural peak displacements are where the wave-to-wall interactions of the tuned (8 degree inclination) case occur, producing effective energy dissipation. At approximately 0 degrees structural displacement, the un-tuned (12 degree inclination) case's wave-to-wall interaction occurs. As the liquid and structure are travelling in the same direction, a minimum of momentum opposition is achieved, resulting in poor energy dissipation.

The three inclination cases, at 0 degrees structural displacement are displayed in Figures 4.12(a), 4.12(b) and 4.12(c). These instances occur at 0.4 s, as the structure rotates clockwise, approaching the first positive peak displacement. Liquid velocities are high (displayed in red) for all cases, possessing high kinetic energy, as the structures have just been released and no previous wave-to-wall interactions to dissipate energy have yet occurred.

The first positive peak displacement occurs at 0.8 s for all three inclination cases, displayed in Figures 4.13(a), 4.13(b) and 4.13(c). The first wave-to-wall interaction occurs in the right container for all three cases as the structure approaches peak displacement. At this point in time, the cases with inclination angles of 4 degrees, in Figure 4.13(a) and 8 degrees, in Figure 4.13(b) have larger amounts of high velocity (in red) compared to those of the 12 degree inclination case in Figure 4.13(c). This gives evidence that the wave-to-wall interactions began later for the 4 and 8 degree inclination cases, than the 12 degree inclination case and energy is still being dissipated. As the 12 degree inclination case's wave-to-wall interaction occurs earlier, than the 4 and 8 degree inclination cases, energy dissipation efforts are not as effective.

Although, the tuned, 8 degree inclination case produces higher damping, at a structural frequency of 0.7 Hz, in Figure 4.6(f), the un-tuned, 4 degree inclination case produces a smaller first structural peak displacement, in Figure 4.6(d). This is due to the 4 degree inclination case's liquid mass being distributed over a larger section of the container base, as displayed in Figure 4.13(a), compared to the 8 degree inclination case, in Figure 4.13(b). The 8 degree inclination case's bulk of the liquid mass is located further away from the centre of

rotation and therefore, produces the larger first structural peak displacement. The 12 degree inclination case produces an even larger first peak displacement, in Figure 4.6(h), for this same reason.

At the second 0-degree structural displacement, high liquid velocities are still observed (in red) for all inclination cases, displayed in Figures 4.14(a), 4.14(b) and 4.14(c). As the structure rotates anti-clockwise, the 12 degree inclination case possesses the largest amount of high velocity liquid, in Figure 4.14(c). The larger amount of high velocity liquid gives evidence that the wave-to-wall interaction in the left container is beginning earlier for the 12 degree inclination case, than the cases with inclination angles of 4 degrees, in Figure 4.14(a) and 8 degrees, in Figure 4.14(b). Therefore, at 0 degrees structural displacement, the 12 degree inclination case produces minimum momentum opposition resulting in poor energy dissipation.

At the second negative peak displacement, cases with inclination angles of 4 degrees, in Figure 4.15(a) and 8 degrees, in Figure 4.15(b) again produce larger amounts of high velocity liquid than the 12 degree inclination case, in Figure 4.15(c). The speculations for the 12 degrees inclination case, at 0 degrees structural displacement, in Figure 4.14(c), agree with the liquid flow fields, in Figure 4.15(c), where the wave-to-wall interaction occurs earlier in the left container than the other inclination cases. As a result, less energy is dissipated, compared to the other inclination cases where the wave-to-wall interaction occurs closer to peak displacement.

The fifth 0-degree structural displacement occurs around 3.4 s, for all inclination cases, as the structural rotates clockwise, in Figures 4.16(a), 4.16(b) and 4.16(c). This instance was chosen as the tuned (8 degree inclination) case's higher damping produces peak displacements, in Figure 4.6(f), that are now smaller than the un-tuned case with an inclination of 4 degrees, in Figure 4.6(d). The case with an inclination of 12 degrees again produces the largest amount of high velocity liquid, in Figure 4.16(c), with the wave-to-wall interaction still occurring around 0 degrees structural displacement in the right container.

The 8 degree inclination case now produces a significantly larger amount of high velocity liquid, in Figure 4.16(b), compared to the 4 degree inclination case in Figure 4.16(a). This observation gives evidence that the wave-to-wall interaction, in the right container, is beginning earlier for the tuned, 8 degree inclination case than the un-tuned case with 4 degrees inclination, which should result in poorer energy dissipation. However, at the third positive peak displacement, the 4 degree inclination case has smaller amounts of high velocity liquid, in Figure 4.17(a) than compared to the 8 degree inclination case, in Figure 4.17(b). Therefore, the tuned, 8 degree inclination case produces larger amounts of high velocity liquid over a longer duration, resulting in increased energy dissipation at the wave-to-wall interactions.

The large amounts of high velocity liquid observed at the fifth 0-degree peak displacement for the case with 12 degrees inclination, in Figure 4.16(c), has been significantly reduced at the third positive peak displacement, in Figure 4.17(c). The wave-to-wall interactions continue to occur at 0 degrees peak displacement, producing minimum momentum opposition

and low damping. As a result, a longer time is required for the structure to cease oscillating, in Figure 4.6(h) compared to the cases with inclination angles of 4 degrees, in Figure 4.6(d) and 8 degrees, in Figure 4.6(f).

4.3.5 Inclination Cases with Obstructions

Following observations in the previous two chapters, attaching semi-circular obstructions to the base of a rectangular container enhances energy dissipation. Efforts to enhance dissipation further by attaching obstructions are presented here.

The first setup analysed is 1 obstruction located in the centre of the container base with 2 obstruction height cases of 2.4 mm and 5.9 mm. The 1 obstruction case was chosen as it was the most effective in Chapter 2. This is due to the travelling wave front possessing increased velocity gradients as the liquid travels over the obstruction, producing superior energy dissipation at the wave-to-wall interactions. Obstruction heights were chosen from optimum ratios suggested in Chapter 2 of obstruction radius over free surface length (r/L) of 1.6 % ($r = 2.4$ mm) and obstruction radius over liquid height (r/h_w) of 75 % ($r = 5.9$ mm). These optimum ratios, from Chapter 2, are for one obstruction case. However, due to having a fixed free surface length and liquid height, it is not possible to have both ratios agree simultaneously, for the inclination cases. Therefore, two obstruction height cases are analysed using one optimum ratio each, to determine which ratio is more effective.

Displacement histories of inclination cases at a structural frequency of 0.5 Hz from Figure 4.6 are compared with the same cases with a single obstruction attached at the centre base of the

two containers in Figure 4.18. The only obstruction case that ceases oscillating marginally faster than the case without obstructions is the case with no inclination in Figure 4.18(a). This agrees with conclusions from Chapters 2 and 3, for shallow liquid depths in a rectangular container with no inclination. Increased velocity gradients are observed as the liquid travels over the obstruction, producing superior energy dissipation at the wave-to-wall interactions. The optimum ratio, obstruction radius over liquid height (r/h_w), is marginally more effective than obstruction radius over free surface length (r/L) at an inclination of 0 degrees.

As inclination increases, the breaking wave travelling up the slope of the container becomes the main dissipater. The obstruction interrupts the breaking wave and although it dissipates energy at the wave-to-obstruction interaction, the liquid does not have sufficient energy to continue travelling up the slope due to gravity acting against the liquid. Therefore, overall energy dissipation from introducing the obstruction is lost with the absence of the breaking wave that travels up and down the slope of the container.

The addition of the obstruction produces an identical displacement history to the case without an obstruction as inclination increases above 4 degrees in Figures 4.18(c) and 4.18(d). This is because the breaking wave does not have enough velocity to travel up the steep incline to interact with the obstruction in the centre of the container. However, even by relocating the obstruction closer to the breaking wave, the 4 degree inclination case has given evidence that the obstruction could not increase energy dissipation.

From the conclusions made from the single obstruction results, efforts are now focused on exploring increased energy dissipated from the obstruction interrupting, instead of enhancing, the breaking wave. This is to be achieved through obstructions, evenly spaced, covering the base of the two containers. The semi-circular obstructions again have a height of 2.4 mm. A space of twice the obstruction height separates each obstruction along the base of the containers. Displacement histories of inclination cases at a structural frequency of 0.5 Hz from Figure 4.6 are compared with the same cases with the attached, evenly spaced obstructions in Figure 4.19. Inclination angles of 0, 1.5, 2.5, 4, 6 and 8 degrees are displayed in Figures 4.19(a), (b), (c), (d), (e) and (f).

As expected from conclusions in Chapter 3 for a container with no inclination, there are too many obstructions that interrupt the travelling wave, reducing liquid velocity. As a result, the energy dissipation at the wave-to-wall interactions is reduced and displacement amplitudes and settling time increase. Increased inclinations with evenly spaced obstructions are still investigated for the potential to enhance energy dissipation further, due to the dissipation characteristics changing. However, similar events occur increasing displacement amplitudes and settling times for all inclination cases. For any inclination above 0 degrees, the best performance occurs without obstructions.

Liquid velocity flow fields at a structural frequency of 0.5 Hz, repeated from Figure 4.10(c) and 4.10(f) are displayed in Figure 4.20(a) and 4.20(c). The same case with evenly spaced obstructions is displayed in Figure 4.20(b) and 4.20(d) to compare differences in liquid

motion by adding obstructions to the base of the inclined absorber. Again, velocity colour scale indicates a range from 0 m/s (blue) to 0.1 m/s (red).

Slight differences are observed in the proportion of high velocity liquid (in red) between cases without and with evenly spaced obstructions, approaching the first structural positive peak displacement, in Figures 4.20(a) and 4.20(b). A lower quantity of high velocity liquid is observed for the case with obstructions. This is due to the obstructions disrupting the wave travelling up the sloped container. Smaller velocities are also observed as the structure approaches its second negative peak displacement, in Figures 4.20(c) and 4.20(d), where larger breaking waves occur in the right container for the case without obstructions. Although energy is being dissipated through the wave-to-obstruction interactions, this case is not as effective as the case without obstructions. This is due to the increase velocity of the travelling waves producing superior shear dissipation with the smooth, sloped container base.

Enhanced energy dissipation is achieved without attached obstructions on the base of the absorber at inclination angles above 0 degrees. However, this study has given evidence that an absorber can produce effective dissipation over a range of structural frequencies by increasing the inclination angle of the containers alone. Therefore, potential to investigate increasing energy dissipation further at the wave-to-wall interactions, for inclination angles above 0 degrees, are promising. Possible ways to achieve increased energy dissipation at the wave-to-wall interactions include varying the angle or introducing semi-circular obstructions to the container walls. Reducing the height of the container roof so it assists in effecting the

motion of the liquid at wave-to-wall interaction could also produce increased energy dissipation at the wave-to-wall interactions.

4.4 Conclusions

Tuning a sloshing absorber is achieved when the frequency of the sloshing liquid matches the frequency of the oscillating structure to be controlled. Previous experimental work (Semercigil et al., 2013) investigated the potential to tune the absorber's container by varying the inclination angle alone, consequently varying the liquid free surface length and therefore liquid frequency. As a result, practical advantages could include having one inclination that dissipates energy effectively over a range of structural frequencies. This would be attractive for design purposes as large structures oscillate at varying frequencies. Numerical predictions to identify effective energy dissipation characteristics within the absorber are analysed in this chapter and give details, such as liquid velocity flow fields, which are not possible through experimental observations. Independent variables in this chapter consist of the absorber's inclination angle and structural frequencies, which range from 0 degrees to 26 degrees and 0.5 Hz to 1.8 Hz respectively. The dependant variable is settling time ratio and is used as the performance indicator to determine percentage improvement between cases.

Smoothed Particle Hydrodynamics (SPH) predictions are compared with experimental observations in the form of structural displacement histories. Acceptable comparisons between experimental and numerical displacement histories are achieved for cases with a structural frequency of 0.85 Hz. At structural frequencies of 1.8 Hz and above, a significant increase in virtual numerical damping occurs. Increasing the particle resolution by reducing

the particle size may amend this discrepancy. However, due to computational limitations, a particle size that is required to eliminate the virtual damping is currently unachievable practically. Therefore, the particle size used in this chapter is sufficient only to analyse cases with structural frequencies around 0.85 Hz and below. SPH gives liquid flow field behaviour, producing velocity gradients in travelling waves and free surface deformation in the form of breaking waves. These details give valuable information that helps explain how energy dissipation occurs within the liquid of the sloshing absorber, and give confidence to use SPH to design liquid sloshing absorbers for structural control applications.

Two rectangular containers, with fixed free surface lengths, can be tuned to achieve optimal energy dissipation at multiple structural frequencies, through varying only the container's inclination angle. For the case with no inclination, leading travelling waves at the liquid free surface occur with increased velocity gradients. This results in significant energy dissipation at the wave-to-wall interactions.

Increasing the inclination of the containers varies the dissipation characteristics of one side of each container. As the inclined container oscillates, the free surface length stretches and shrinks, with the wave travelling the sloped base of the container. The dissipation is limited to shearing between the travelling wave and container base, on one side of the container, as the wave travelling up the inclined base does not reach the opposite wall. The energy dissipation characteristics are different for the case with no inclination where wave-to-wall interactions occur at both walls of the container. However, as the inclination cases have a

variable free surface length, there is potential to produce effective energy dissipation over a range of structural frequencies.

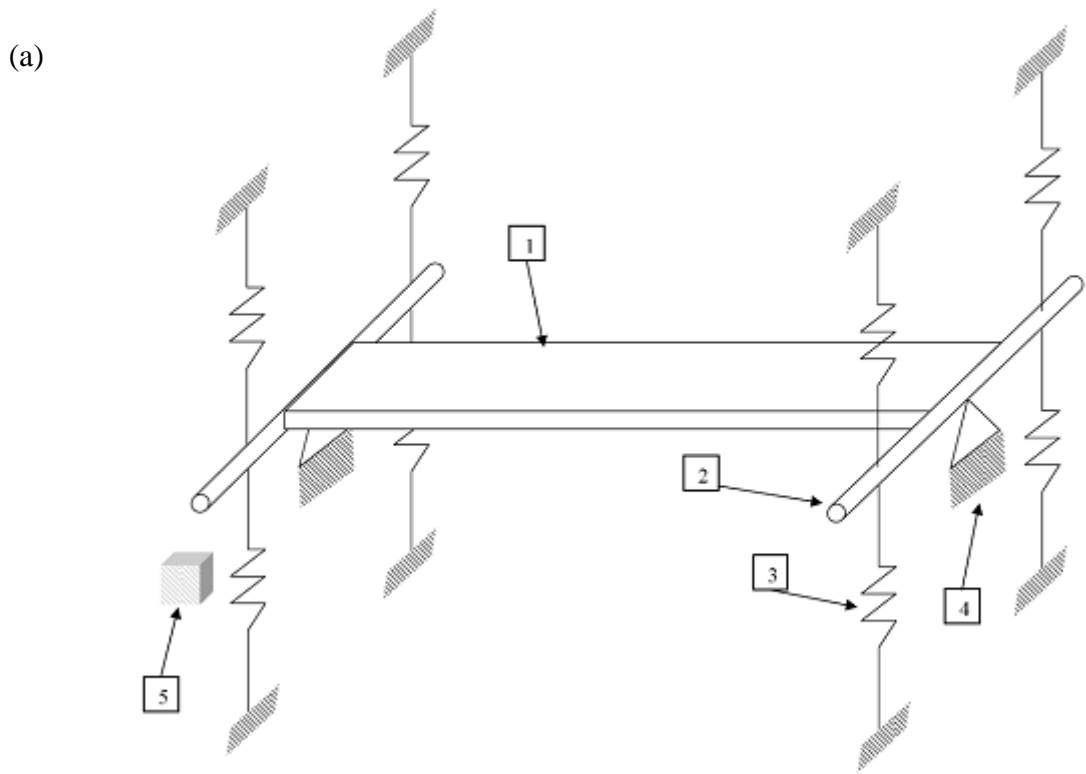
Although dissipation characteristics vary between flat and inclined containers, the most effective cases at each structural frequency occur around the inclination angle where the static free surface length is tuned. Tuning is achieved when the static free surface length produces a liquid sloshing frequency that matches the frequency of the structure. For structural frequencies 0.5 Hz to 0.9 Hz, an inclination angle of 4 degrees is the most effective energy dissipater, producing significant increases in energy dissipation. This is attractive for design purposes as effective energy dissipation over a range of structural frequencies is essential for industrial applications where a large structure's frequency can vary significantly. The inclination angle of 4 degrees is optimal at a structural frequency of 0.5 Hz where energy dissipation is enhanced by 96 % compared to the uncontrolled case.

In a liquid sloshing absorber, maximum energy dissipation is achieved when the wave-to-wall interaction occurs at 0 degrees of structural displacement, provided that the liquid and structure are travelling in opposite directions. Minimum momentum opposition occurs at the same structural displacement, with liquid and structure travelling in the same direction. For a rectangular liquid sloshing absorber, maximum energy dissipation cannot be achieved as the structure pushes the liquid in the same direction that the structure oscillates. However, effective energy dissipation is still achieved for the tuned cases with the wave-to-wall interactions occurring as the structure approaches peak displacements. Larger amounts of high velocity liquid are observed for longer durations in the tuned cases, than those compared

to the un-tuned cases, producing increased energy dissipation at the wave-to-wall interactions.

The structural displacement locations where the un-tuned cases' wave-to-wall interactions occur vary, depending on the ratio of liquid frequency to structural frequency (f_L/f_s). For the cases analysed in this chapter, un-tuned cases' wave-to-wall interactions occurred at 0 degree structural displacement, with the liquid and structure travelling in the same directions, producing minimum momentum opposition to not occurring at all. However, all un-tuned cases produced poorer energy dissipation compared to the cases around the tuned inclination angle (f_L/f_s of 0.8 to 1).

Limited attempts to increase energy dissipation through attaching semi-circular obstructions to the container's base for inclinations above 0 degrees proved unsuccessful. This is due to the obstructions interrupting the travelling wave. Although energy is dissipated at the wave-to-obstruction interactions, superior shear dissipation is achieved through increased amounts of high velocity waves travelling up and down the smooth, sloped container base. Instead, efforts to increase energy dissipation further at the wave-to-wall interactions would be worthwhile for future work. Varying the angle of the container walls, reducing the height of the container roof and introducing semi-circular obstructions to the container walls are possible ways of increasing energy dissipation through effecting the wave-to-wall interaction.



1: Bridge deck, 2: rigid arms to connect springs, 3: springs, 4: knife edge to ensure angular response and 5: a stop block used for consistent initial displacement in transient vibration tests.

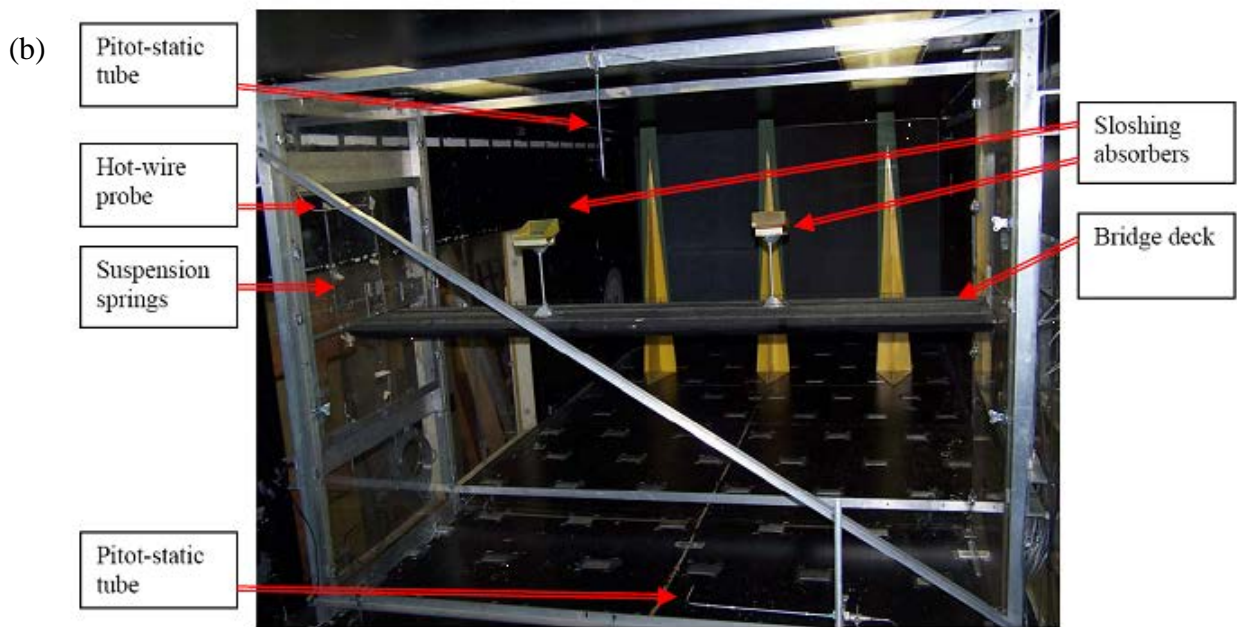


Figure 4.1: An (a) isometric line drawing and (b) photograph of the experimental setup in the wind tunnel, looking upstream. (c) Numerical model of the two inclined containers attached to the bridge deck by two vertical poles. A simplified end view is shown, for clarity.

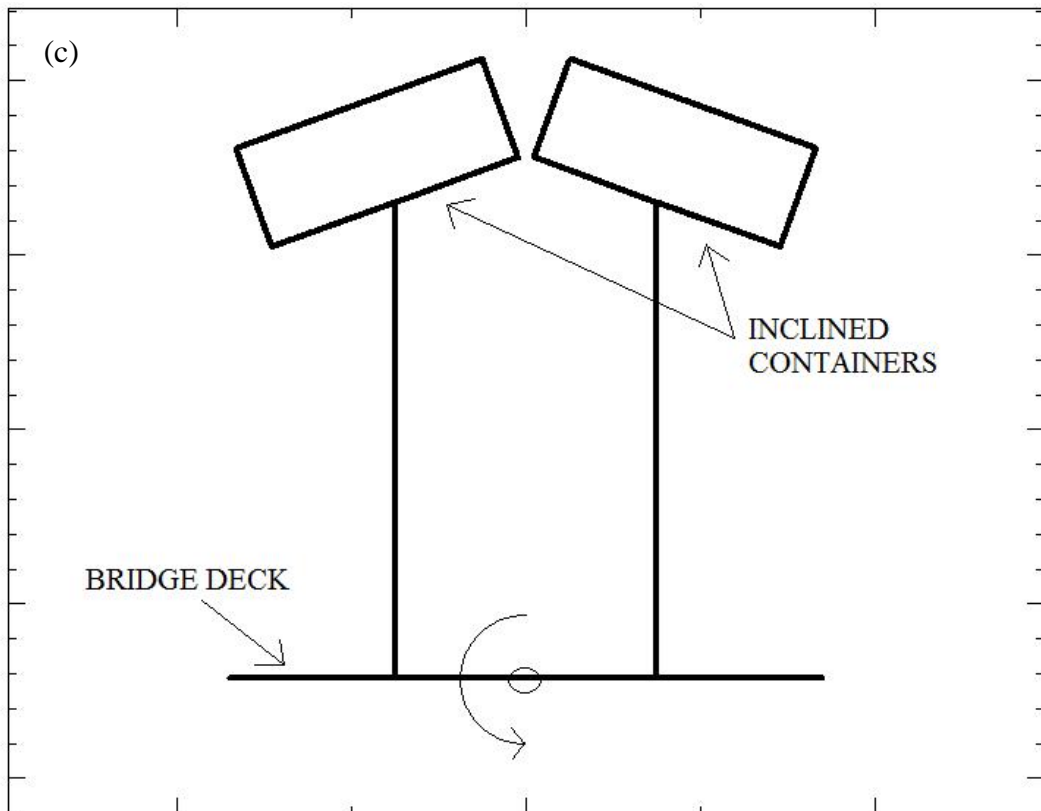


Figure 4.1: Continued.

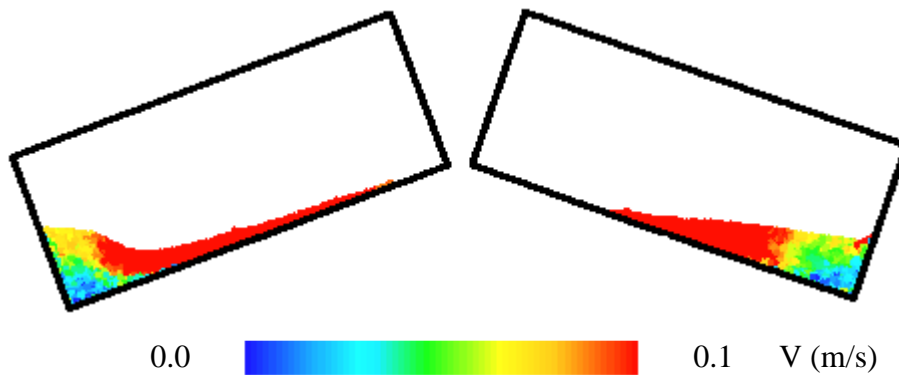


Figure 4.2: A snapshot of the velocity contours at a particular marked instance for the 20 degree inclination case. Liquid sloshing occurs within the two containers as the structure oscillates. Velocity scale runs from 0 m/s to 0.1 m/s.

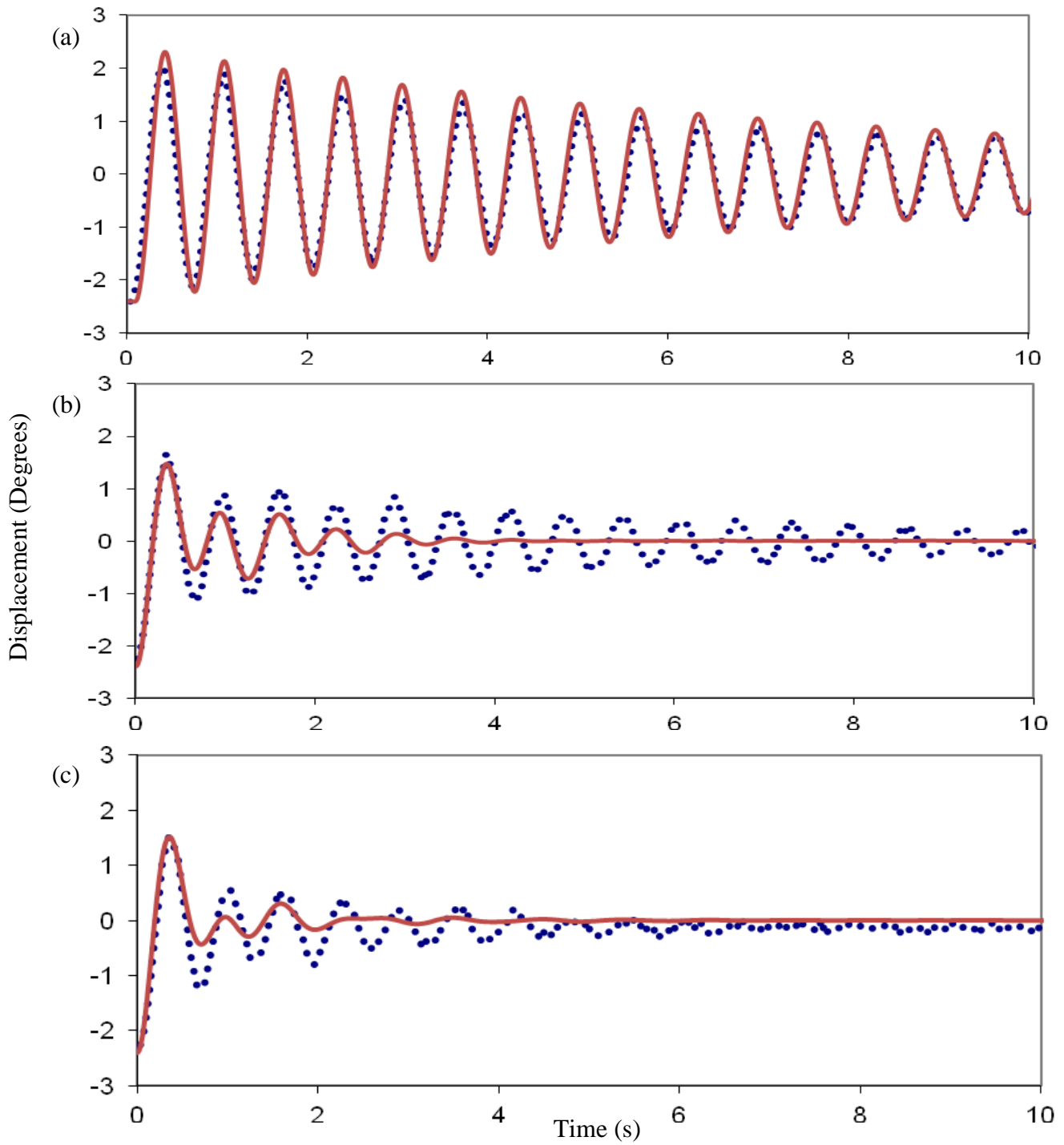


Figure 4.3: Numerical (—) and experimental (•••) displacement histories for 2 containers with free surface (L) of 150 mm at structural frequency of 1.8 Hz (a) uncontrolled and at inclinations (b) 0, (c) 8, (d) 13, (e) 20 and (f) 26 degrees. (Tuned at 13 degrees (c))

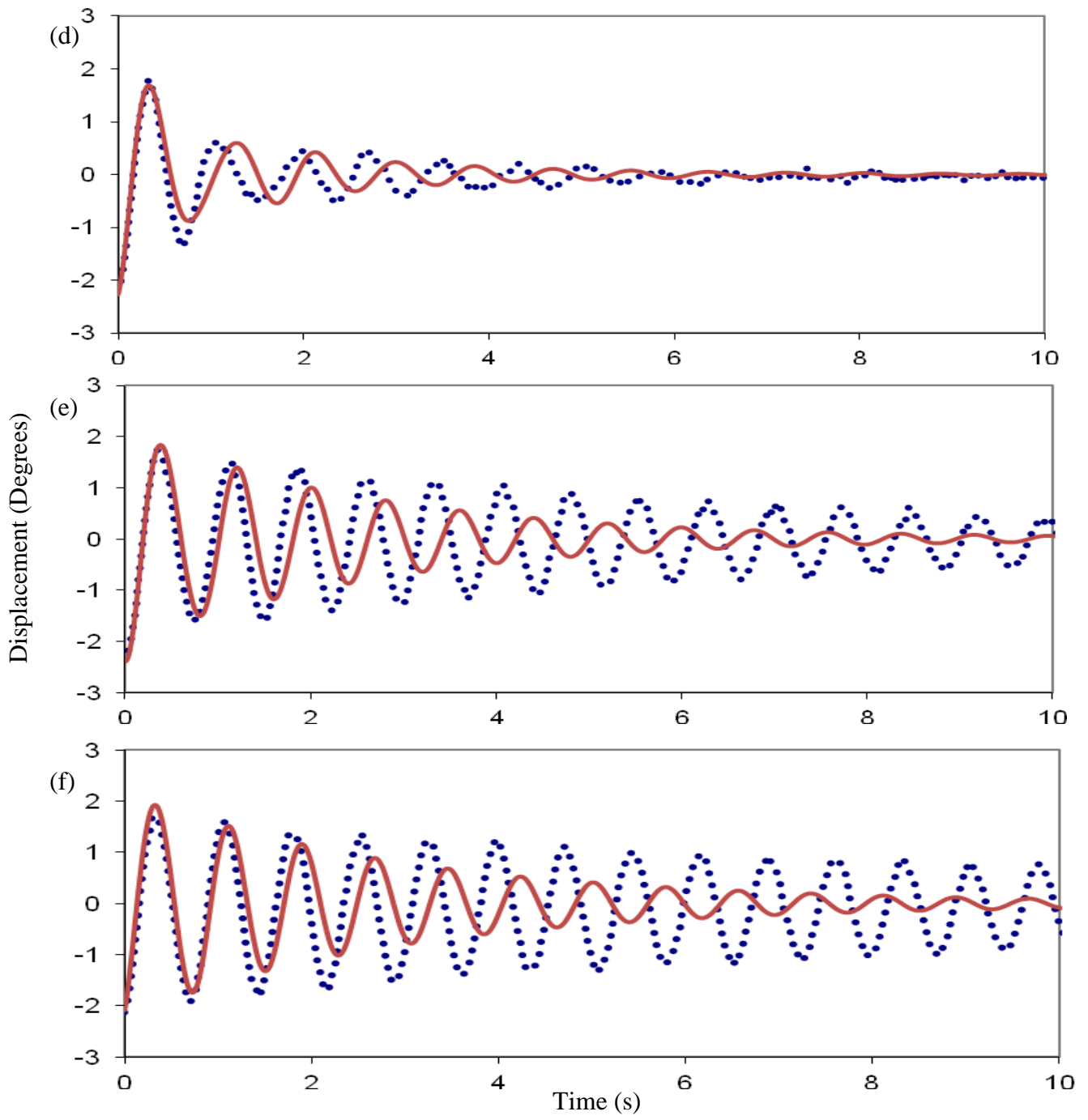


Figure 4.3: Continued.

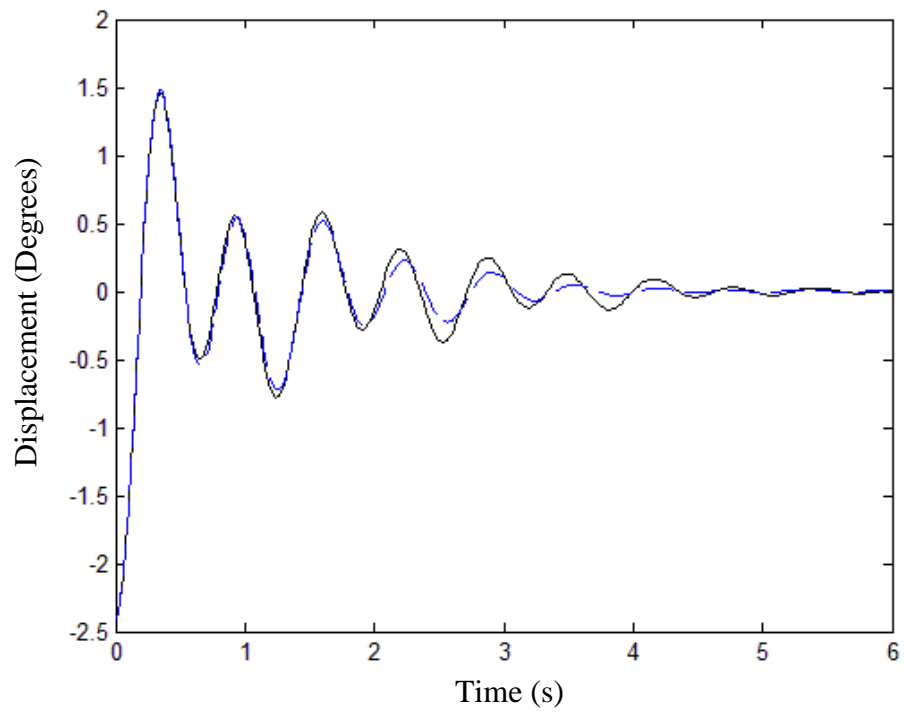


Figure 4.4: Numerical displacement histories of the 0 degree inclination case at a structural frequency of 1.8Hz with particle sizes 0.8 mm x 0.8 mm (— —) from Figure 4.3(b), and 0.4 mm x 0.4 mm (—).

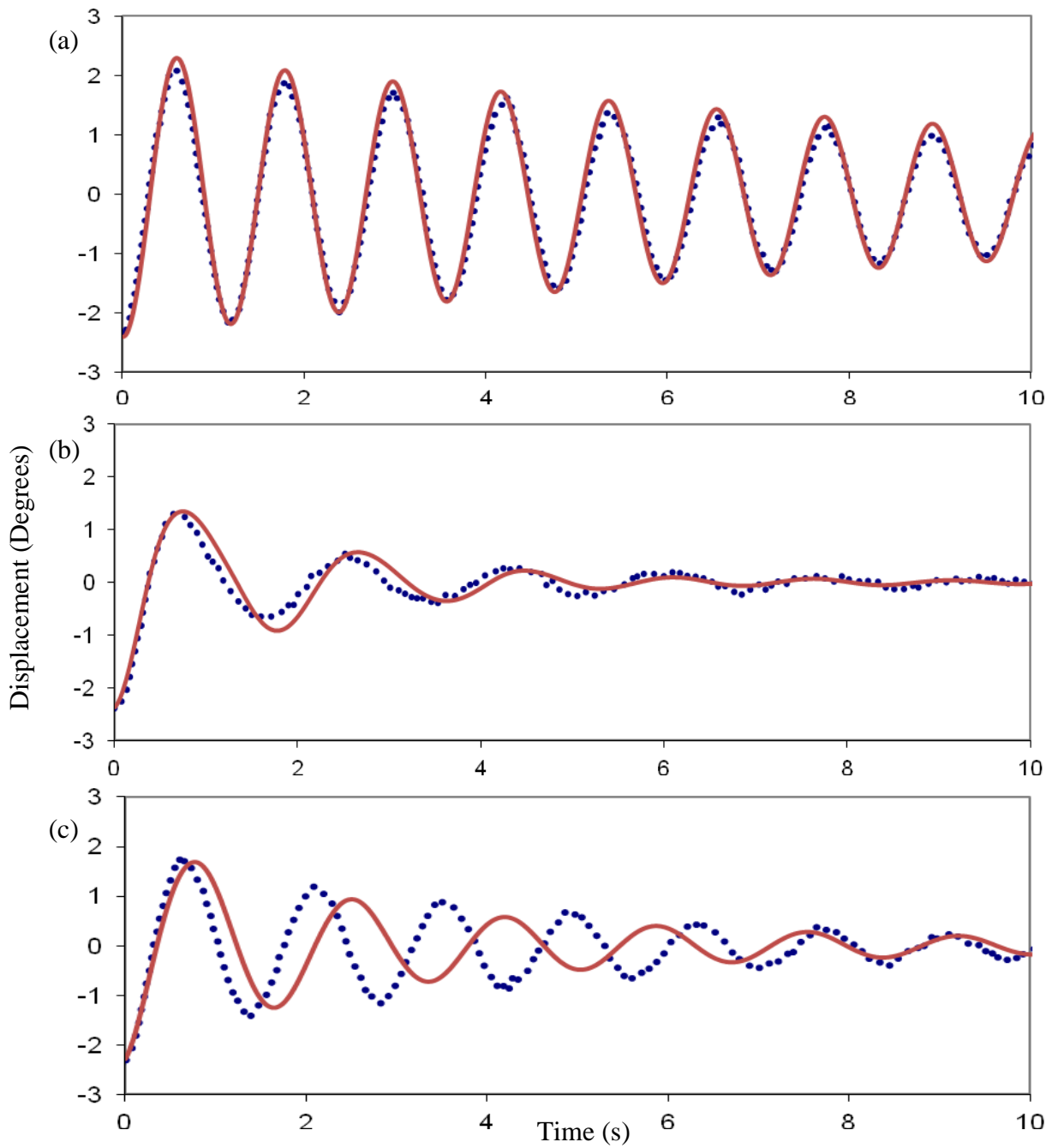


Figure 4.5: Same as Figure 4.3 but for a structural frequency of 0.85 Hz. (Tuned at 0 degrees (b))

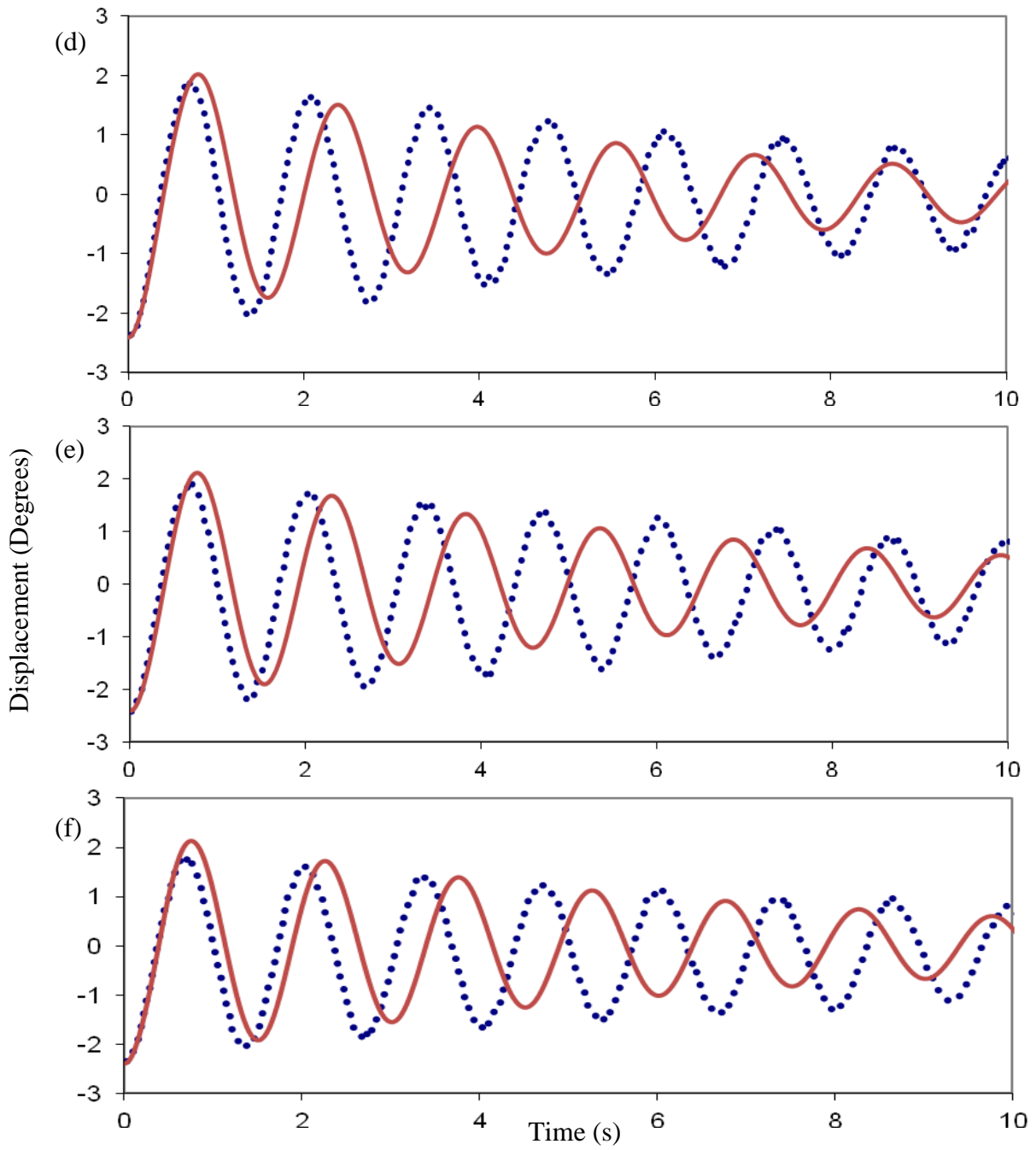


Figure 4.5: Continued.

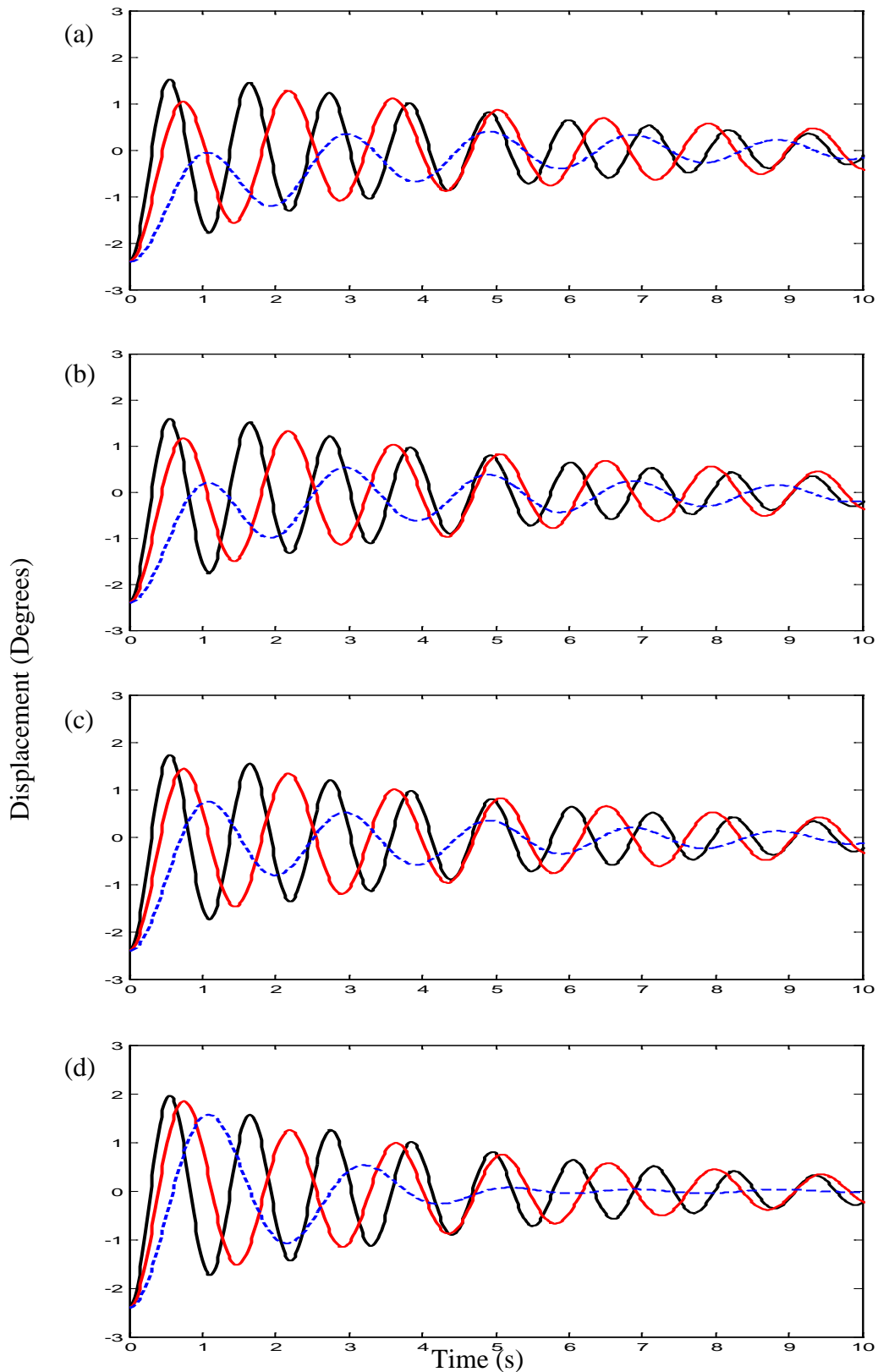


Figure 4.6: Numerical displacement histories for 2 containers with free surface (L) of 700mm at inclinations (a) 0, (b) 1.5, (c) 2.5, (d) 4, (e) 6, (f) 8, (g) 10 and (h) 12 degrees for structural frequencies of 0.5Hz (— —), 0.7Hz (—) and 0.9Hz (—). Structural frequencies of 0.5Hz, 0.7Hz and 0.9Hz are tuned at 4 (d), 8 (f) and 12 (h) degree inclinations respectively.

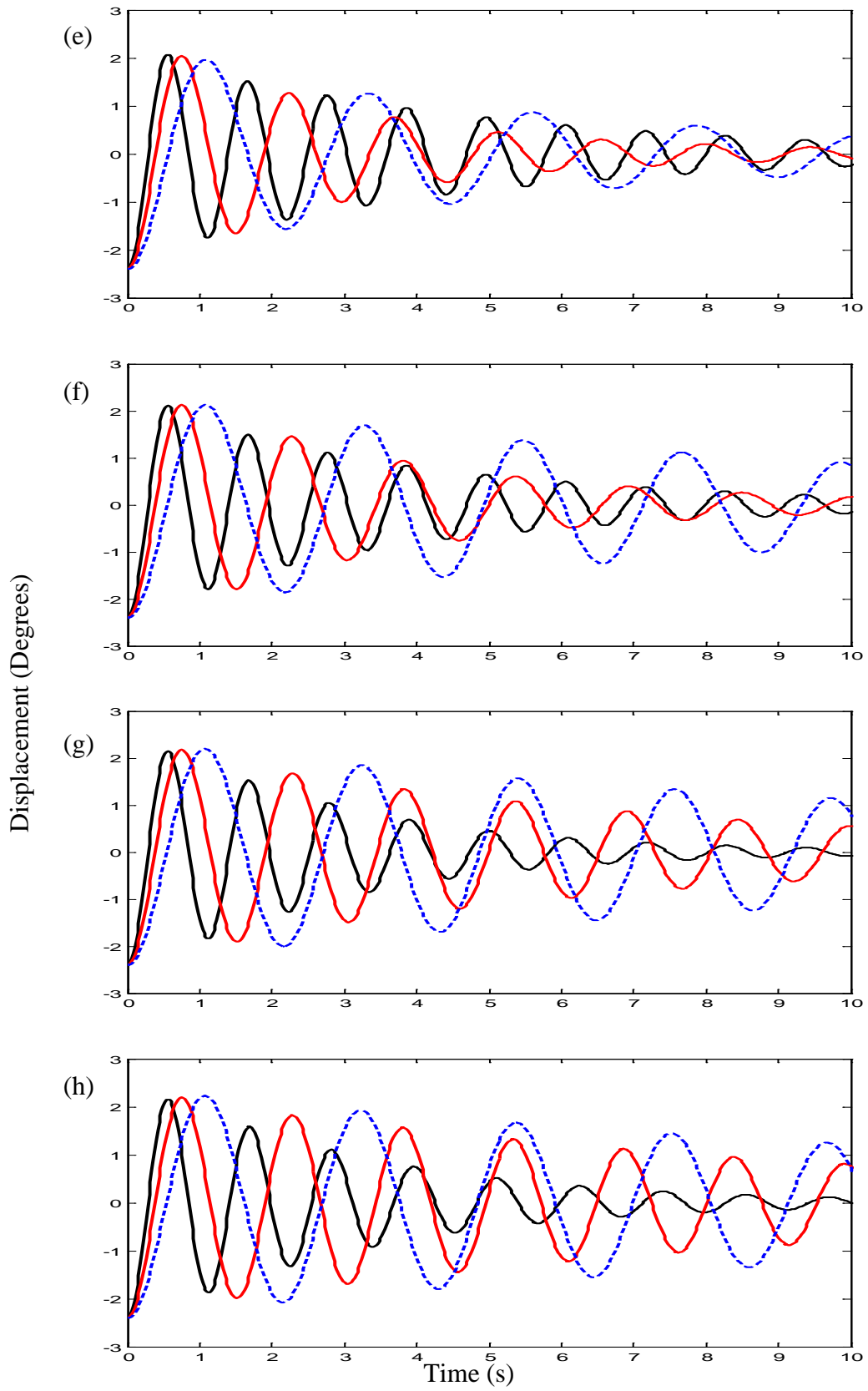


Figure 4.6: Continued.

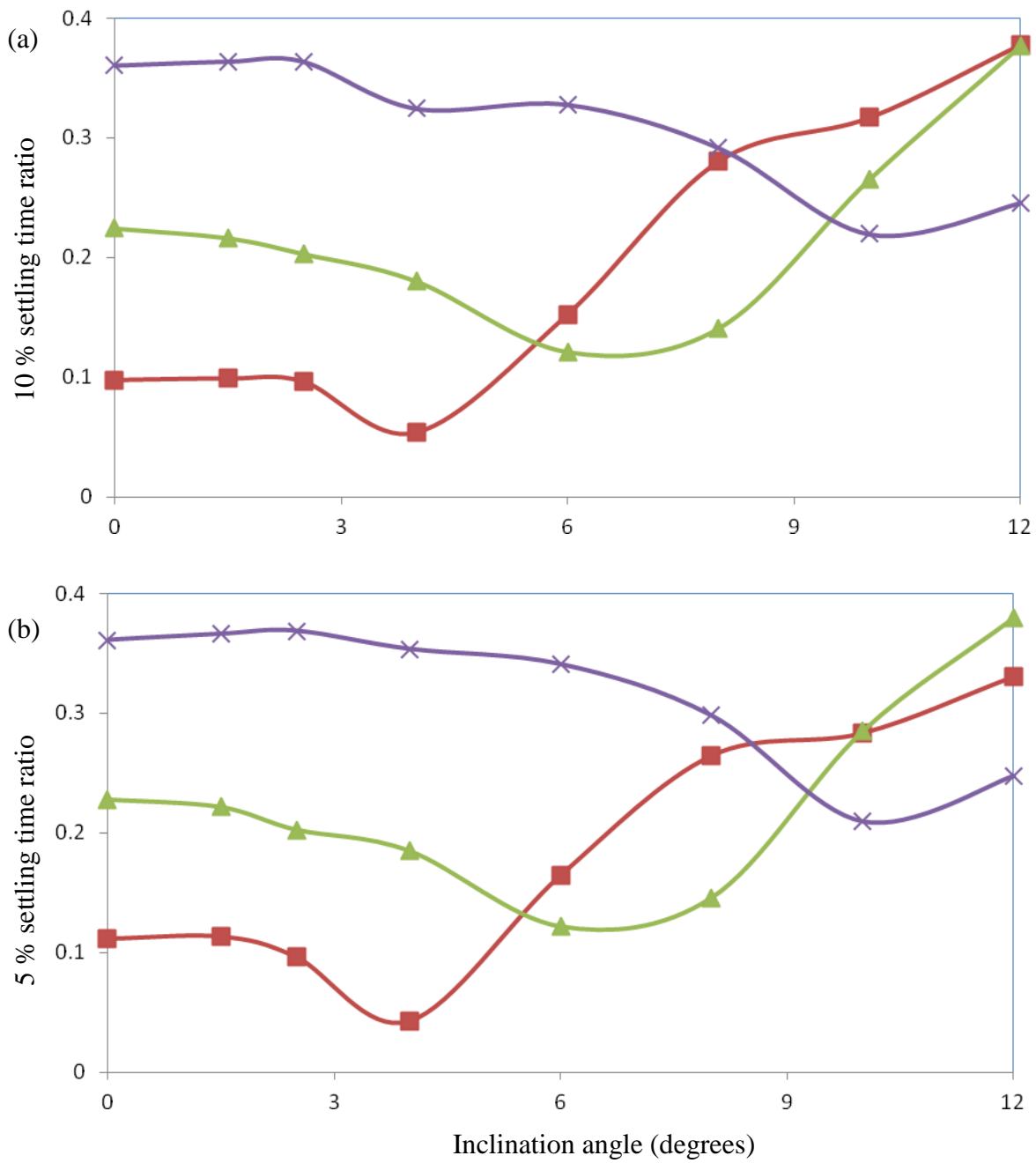


Figure 4.7: (a) 10 % and (b) 5 % settling times ratios for cases with structural frequencies 0.5 Hz (—■—), 0.7 Hz (—▲—) and 0.9 Hz (—×—), from Figure 4.6.

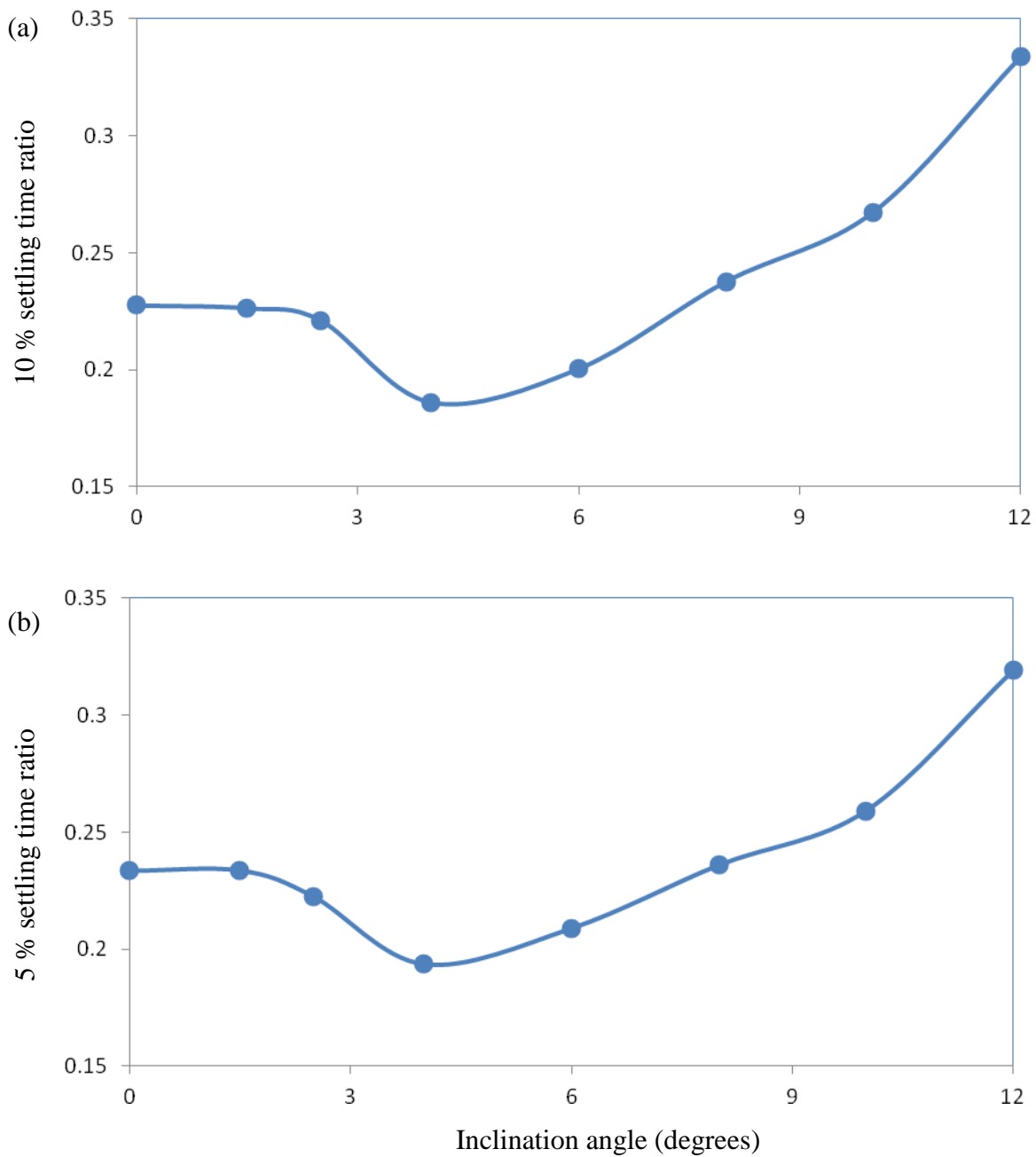


Figure 4.8: Average (a) 10 % and (b) 5 % settling time ratios over structural frequencies 0.5 Hz, 0.7 Hz and 0.9 Hz, for cases from Figure 4.6.

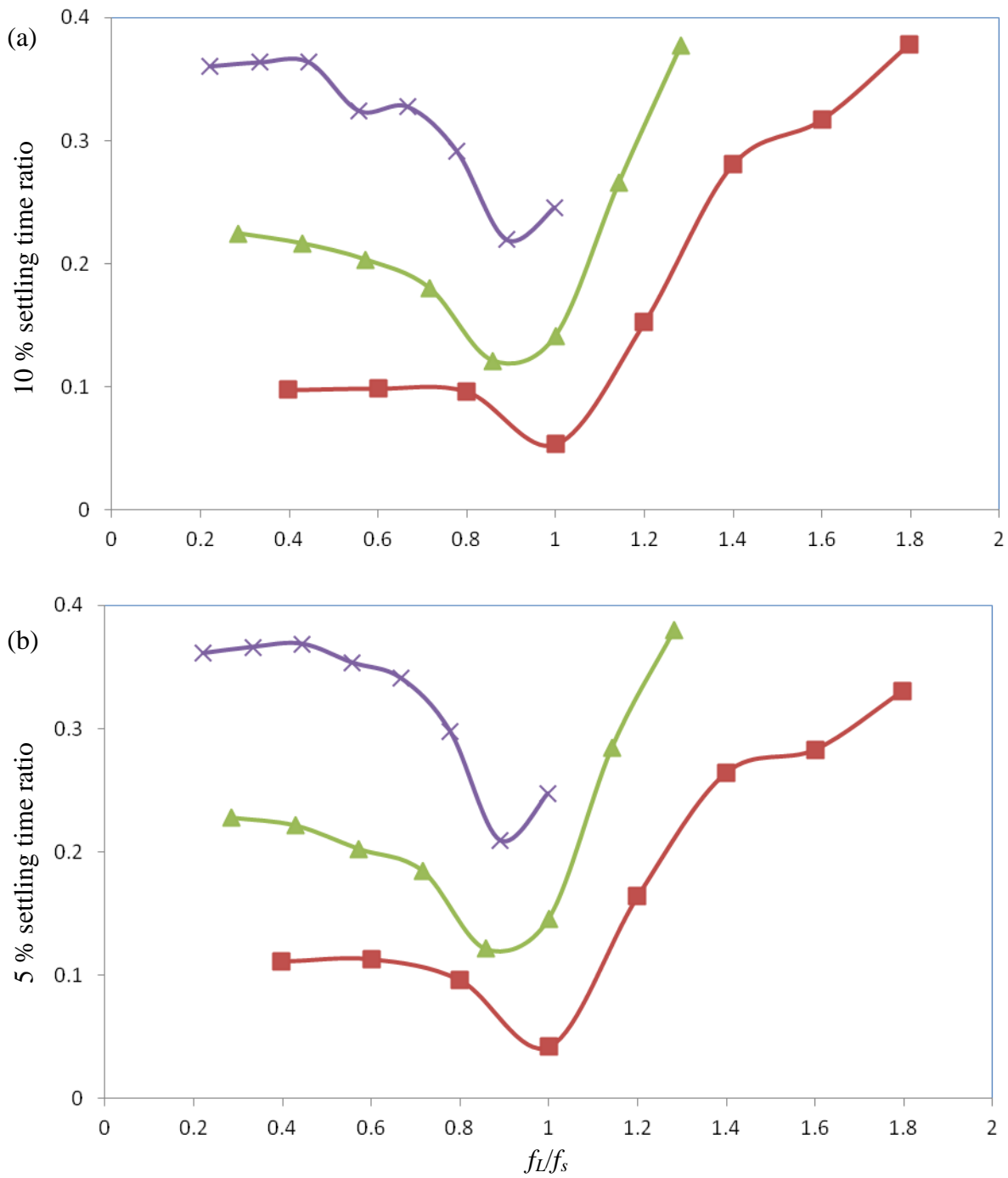


Figure 4.9: (a) 10 % and (b) 5 % settling time ratios with respect to liquid frequency to natural frequency (f_L/f_s) for cases in Figures 4.7(a) and (b).

Approaching first positive peak displacement

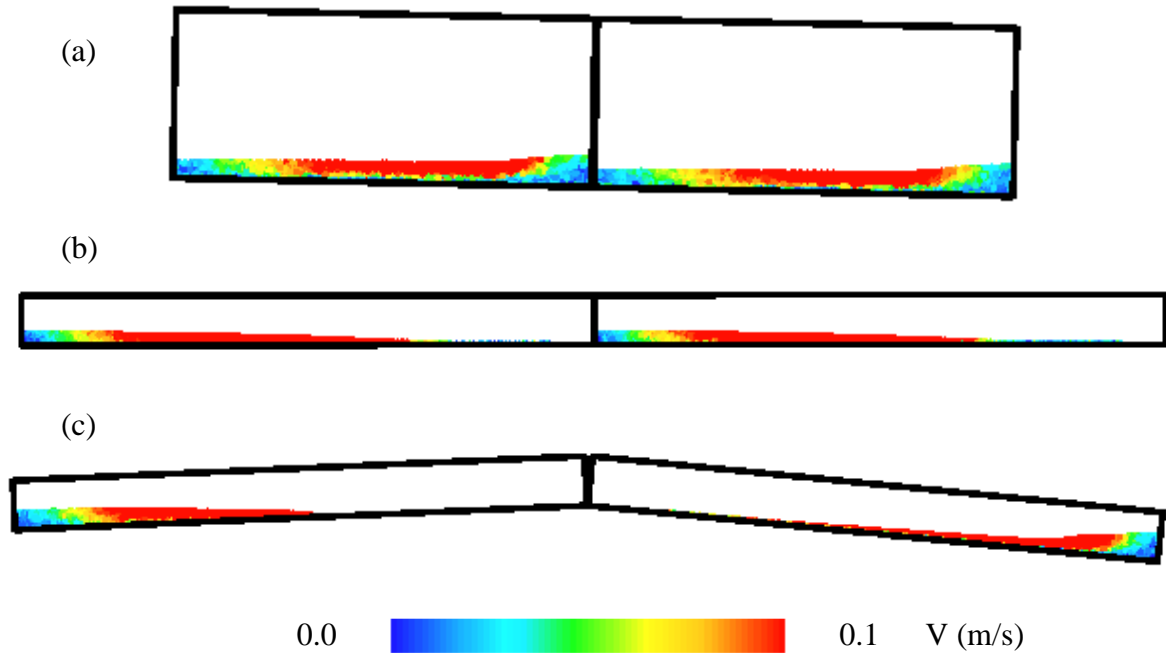


Figure 4.10: Liquid velocity flow field snapshots approaching first positive structural peak displacement. (a) for 0 degree inclination from Figure 4.5(b) with a structural frequency of 0.85 Hz, (b) for 0 degree inclination from Figure 4.6(a) with a structural frequency of 0.5 Hz, (c) for 4 degrees inclination from Figure 4.6(d) with a structural frequency of 0.5 Hz.

Approaching second negative peak displacement

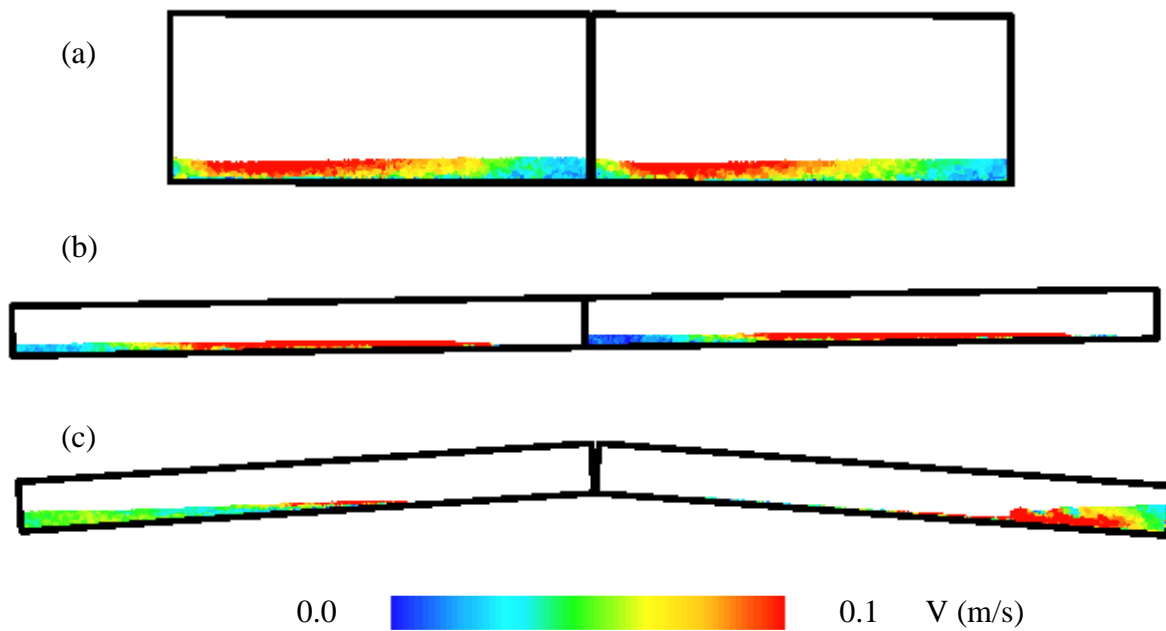


Figure 4.11: Same cases as Figure 4.10 except approaching second negative structural peak displacement.

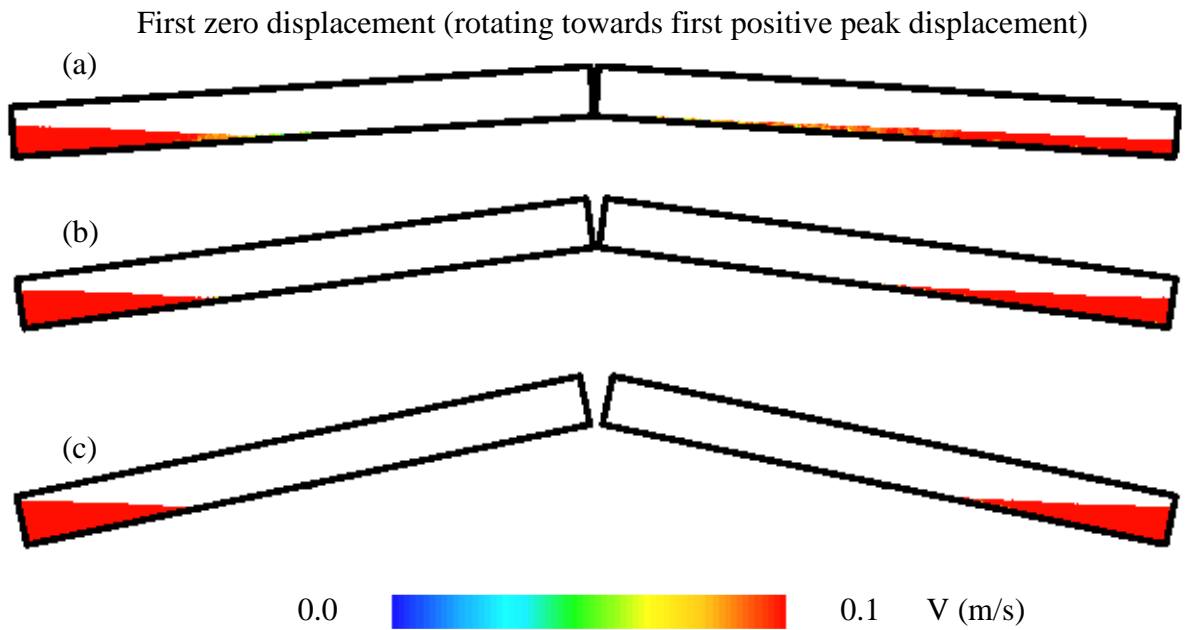


Figure 4.12: Liquid velocity flow field snapshots at first zero structural displacement for cases with a structural frequency of 0.7 Hz. (a) for 4 degree inclination from Figure 4.6(d), (b) for 8 degree (tuned) inclination from Figure 4.6(f) and (c) for 12 degrees inclination from Figure 4.6(h).

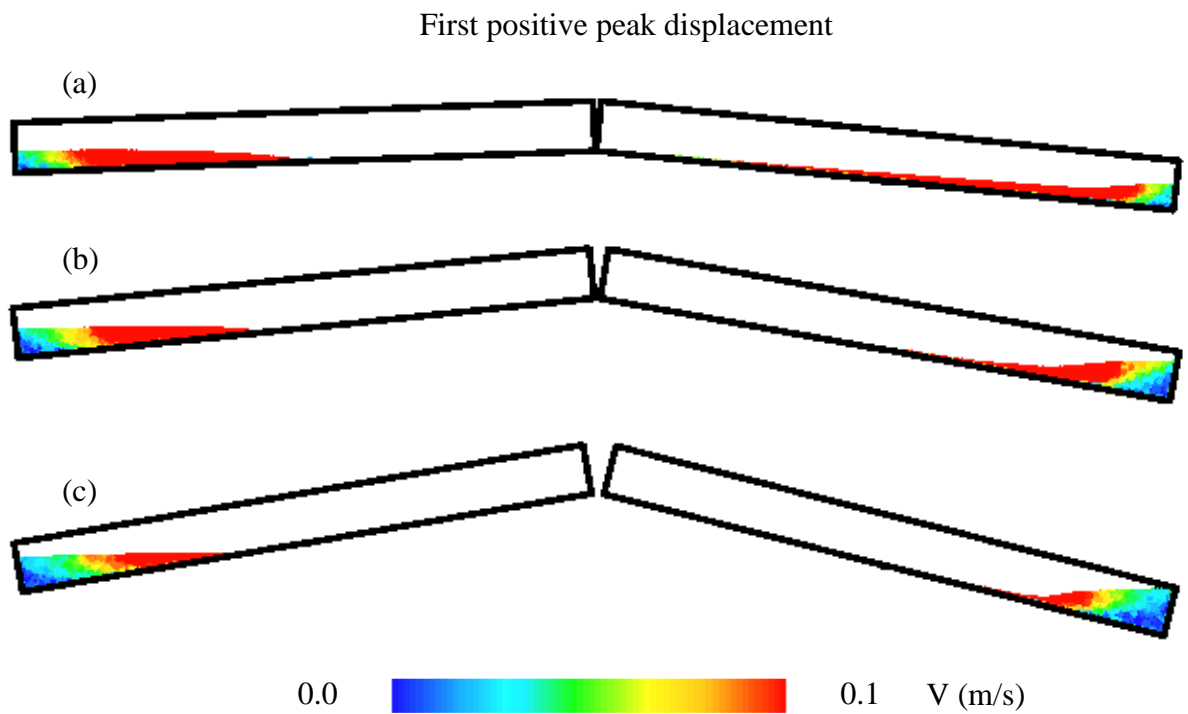


Figure 4.13: Same cases as Figure 4.12 except at first positive structural peak displacement.

Second zero displacement (rotating towards second negative peak displacement)

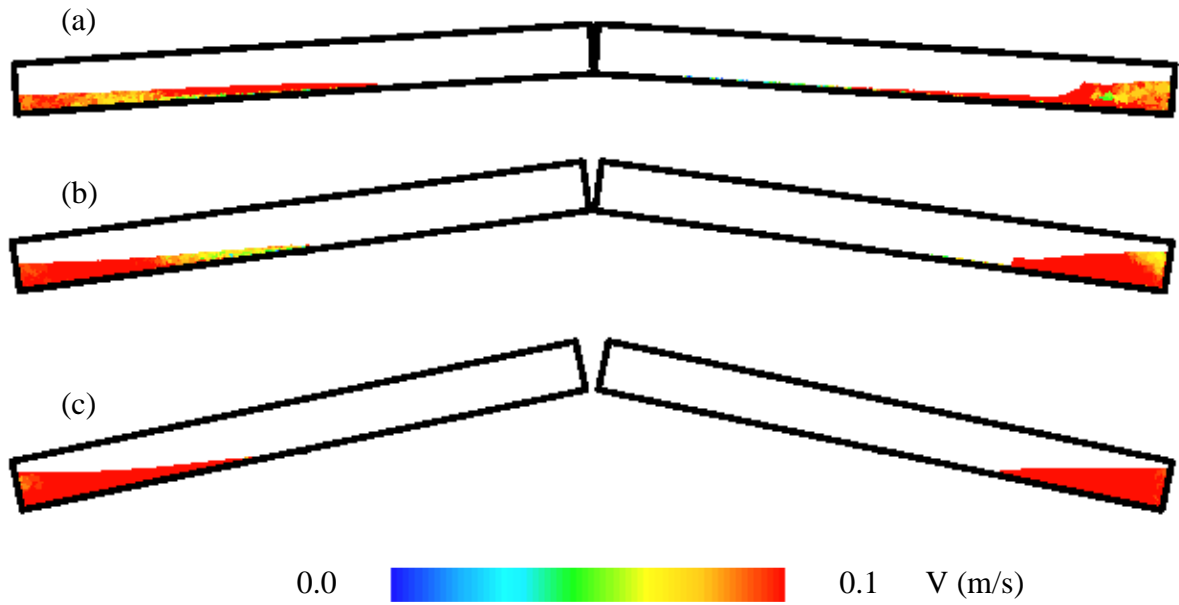


Figure 4.14: Same cases as Figure 4.12 except at second zero structural displacement.

Second negative peak displacement

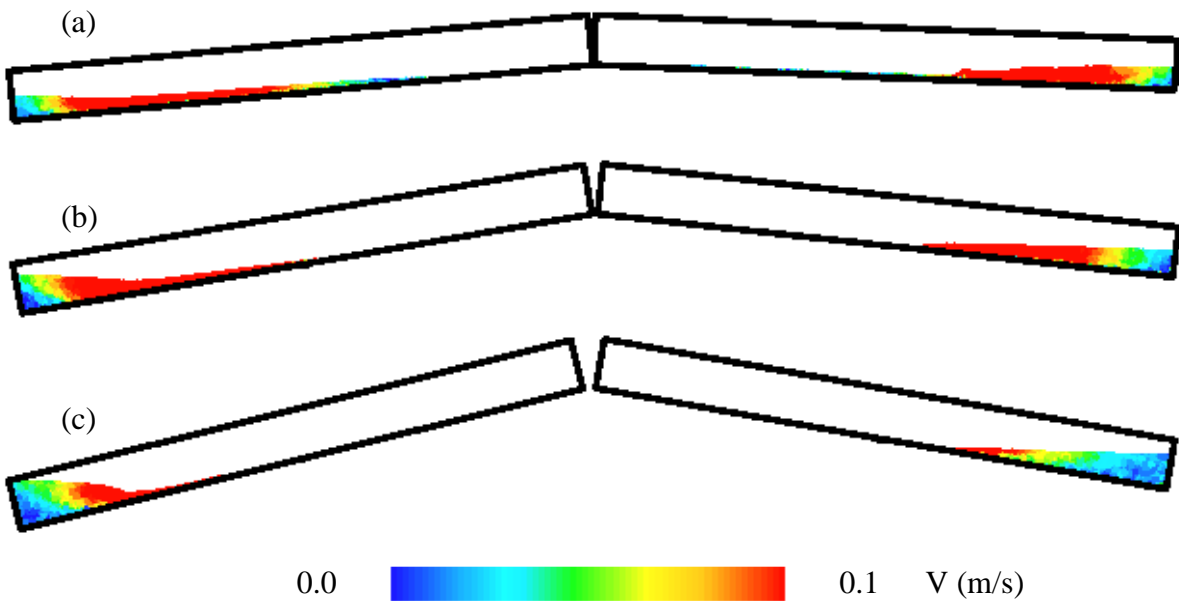


Figure 4.15: Same cases as Figure 4.12 except at second negative structural peak displacement.

Fifth zero displacement (rotating towards third positive peak displacement)

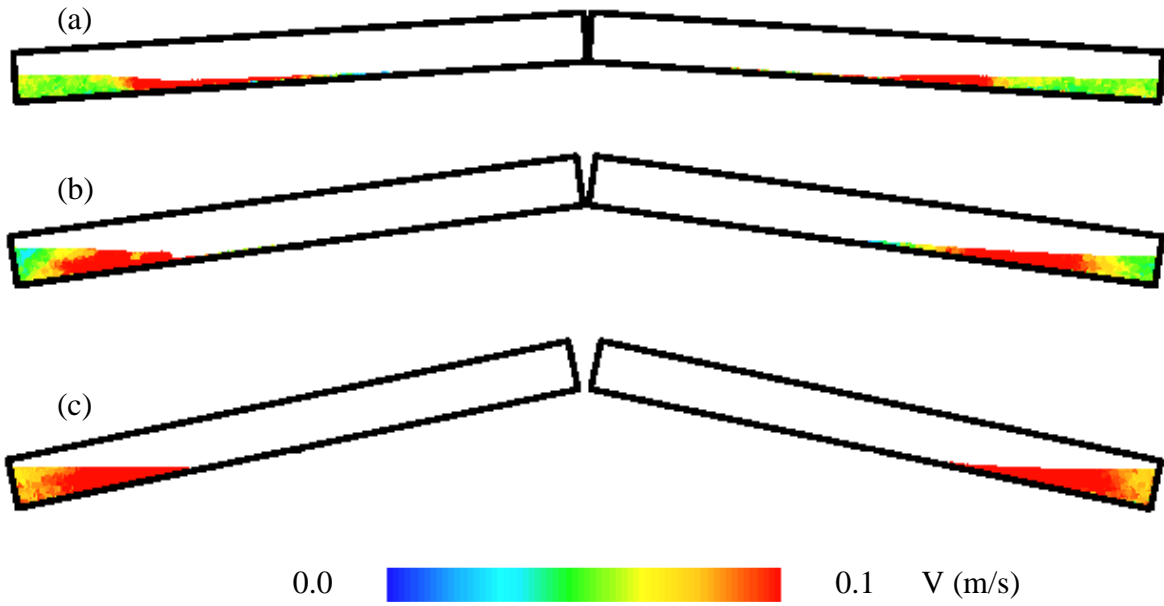


Figure 4.16: Same cases as Figure 4.12 except at fifth zero structural displacement.

Third positive peak displacement

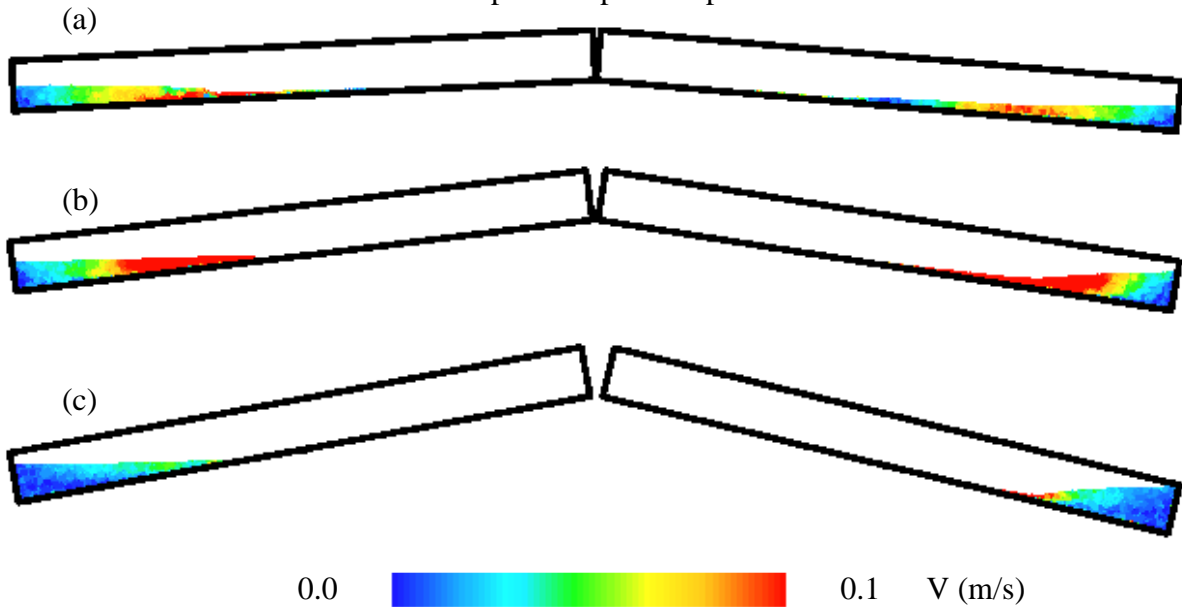


Figure 4.17: Same cases as Figure 4.12 except at third positive structural peak displacement.

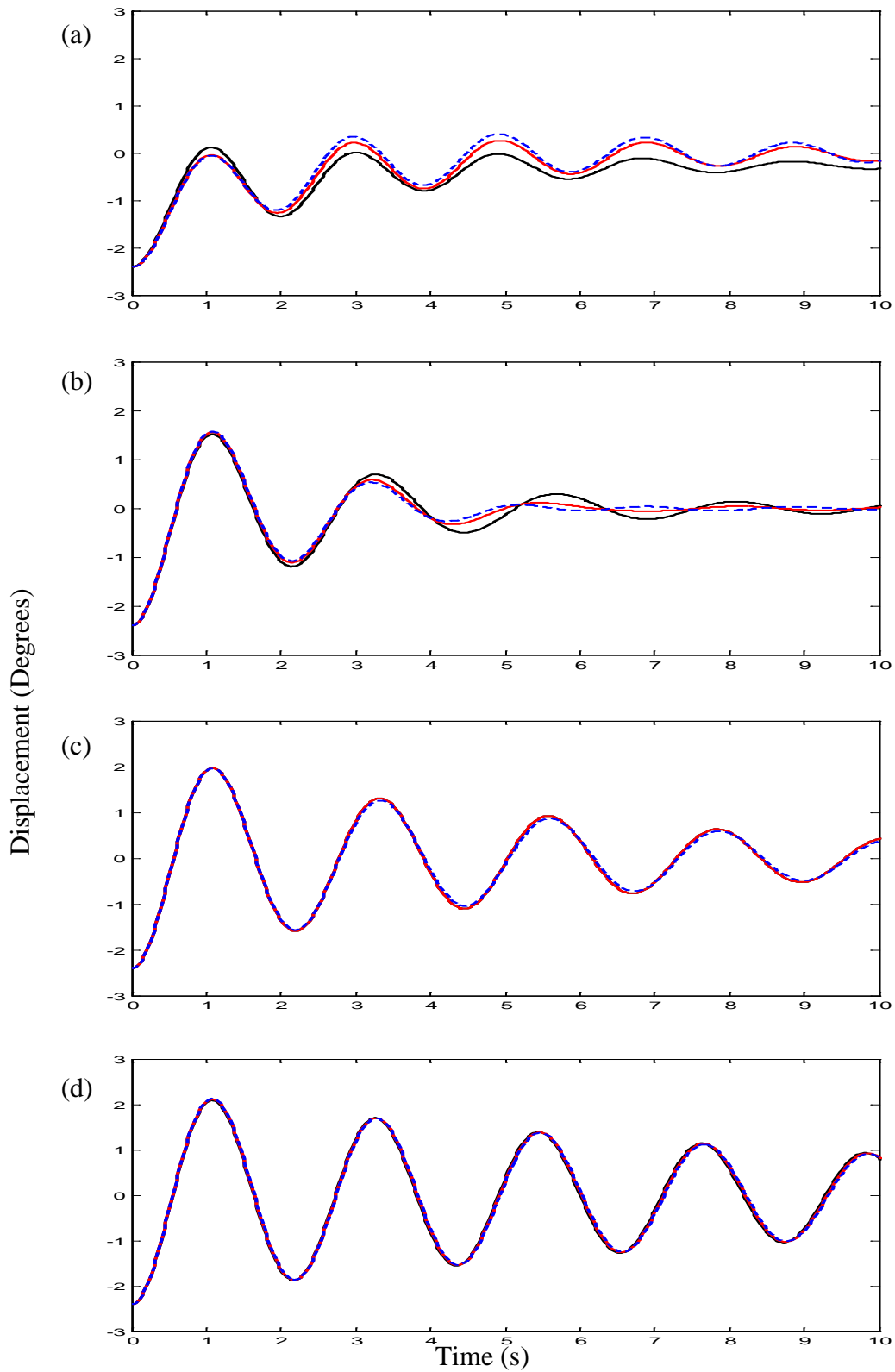


Figure 4.18: Same cases as in Figure 4.6 (— —) without obstructions and with a single semi-circular obstruction located in the centre base of the container with obstruction radius of 2.4 mm (—) and 5.9 mm (—) for inclinations (a) 0, (b) 4, (c) 6 and (d) 8 degrees. (Tuned at 4 degrees (b))

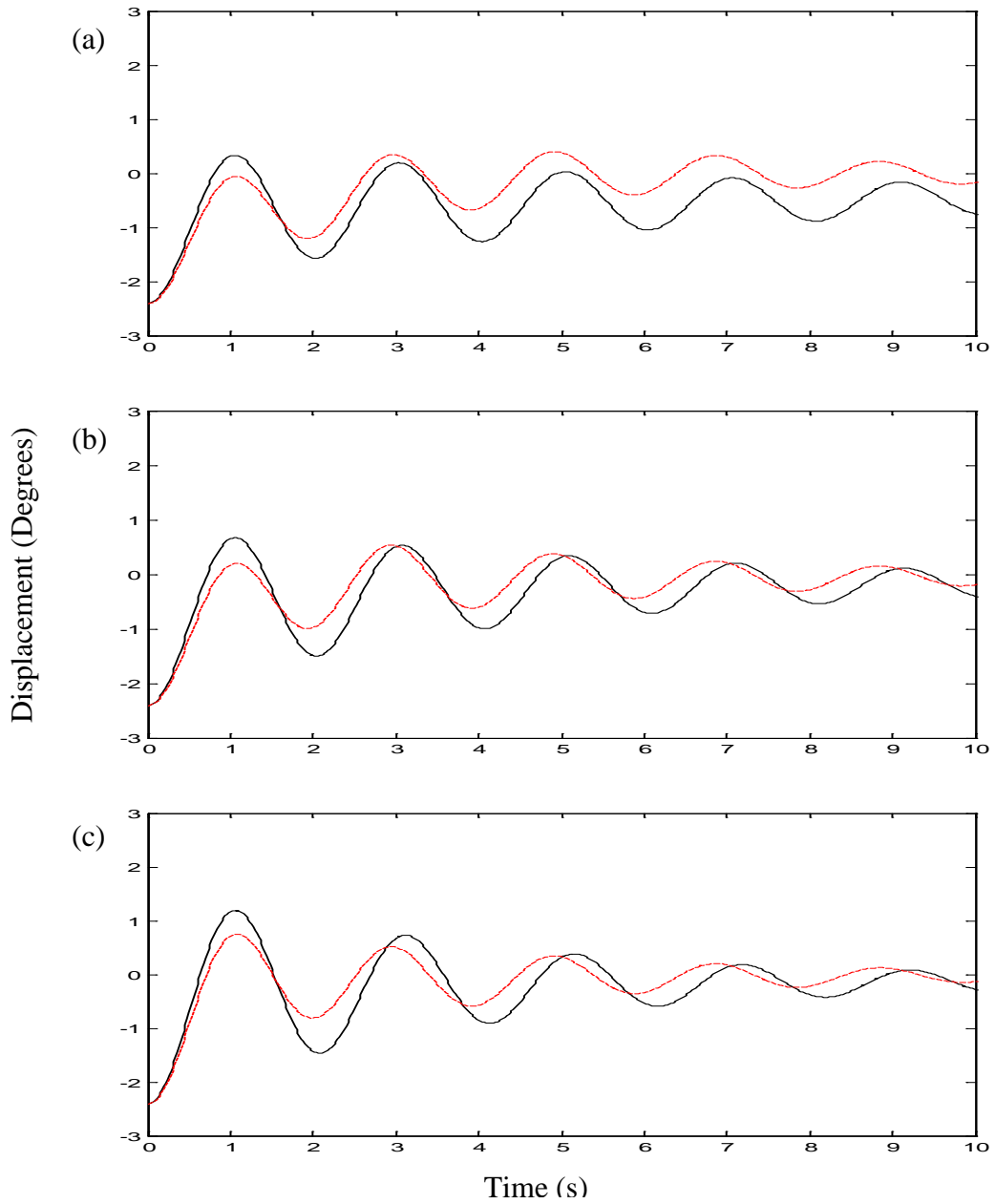


Figure 4.19: Same cases as in Figure 4.6 (— —) without obstructions and with evenly spaced semi-circular obstructions (—) with obstruction radius of 2.4 mm for inclinations (a) 0, (b) 1.5, (c) 2.5, (d) 4, (e) 6 and (f) 8 degrees. (Tuned at 4 degrees (d))

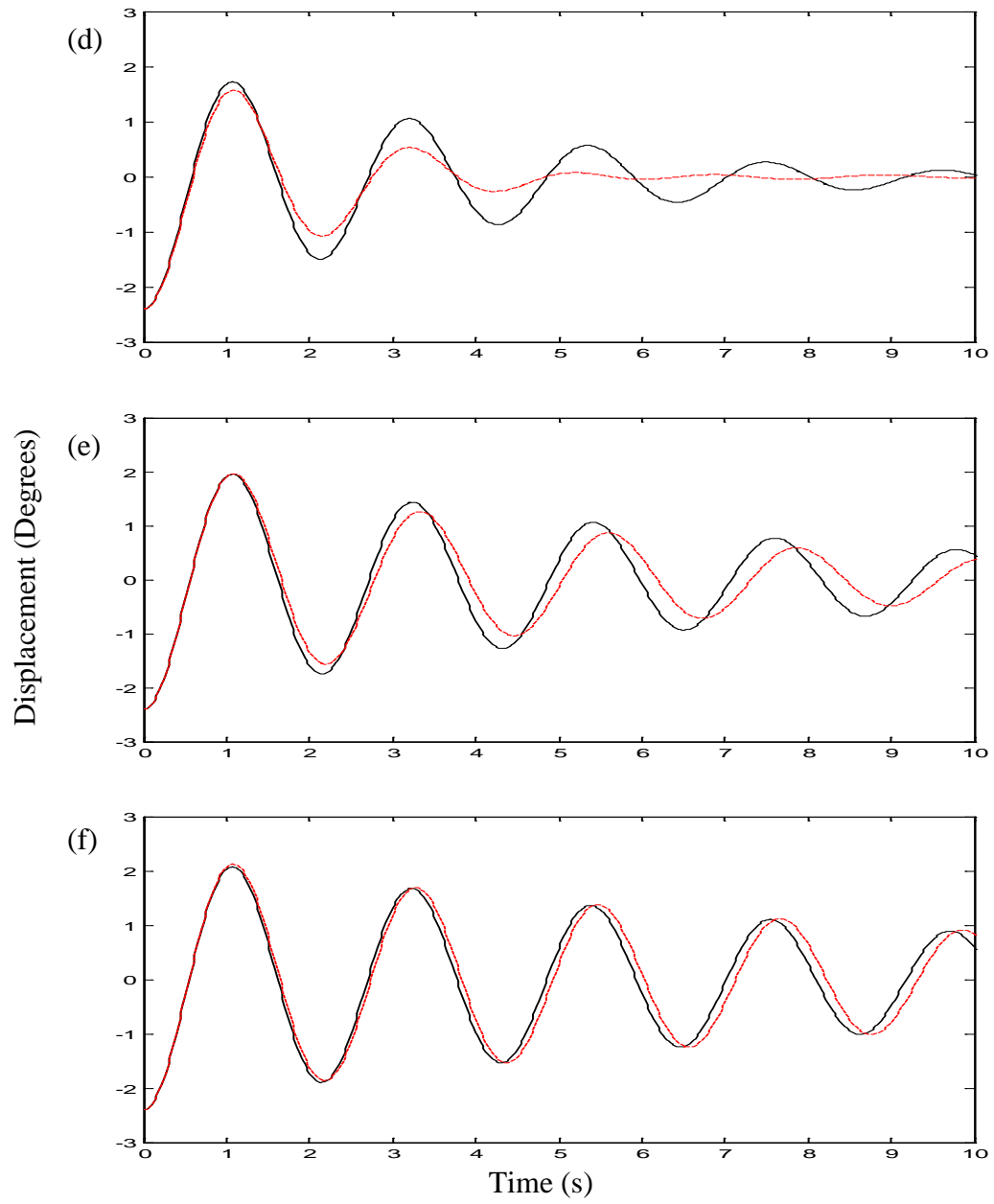


Figure 4.19: Continued.

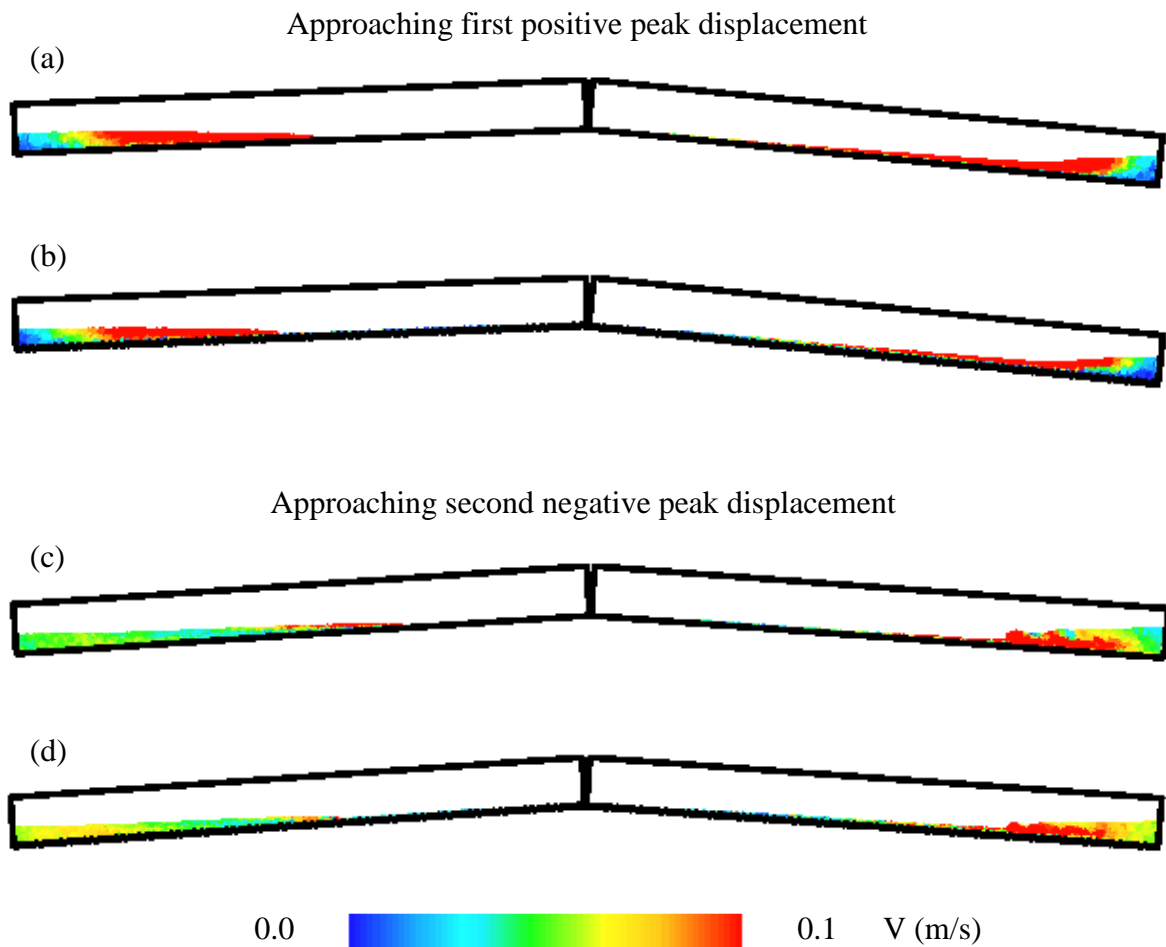


Figure 4.20: Liquid velocity flow field snapshots with a structural frequency of 0.5 Hz. (a) and (c) for 4 degrees inclination (repeated from Figure 4.10(c) and 4.11(c)), (b) and (d) for 4 degrees inclination with evenly spaced obstructions with a obstruction height of 2.4 mm from Figure 4.19(d).

Chapter 5

SLOSHING AND ENERGY DISSIPATION IN AN EGG: SPH SIMULATIONS AND EXPERIMENTS

5.1 Introduction

A hen's egg seems to have evolved to efficiently dissipate energy to protect its embryo using sloshing of its liquid content. Hence, the potential to implement the egg's unique properties as a sloshing absorber for structural control, is the main focus of this chapter. Exploring the shape of the liquid container has received little attention in the literature. These limited works have been on cylindrical (T. Ikeda and R. A. Ibrahim, 2005) and trapezoidal shapes (A. Marsh, et al., 2011). (G. So and S.E. Semercigil, 2004) presented the egg as an effective energy dissipater through experimental observations. (A. Marsh et al., 2012) further explored an egg shaped cylinder.

A hen's egg uses liquid sloshing to efficiently dissipate energy to protect its embryo. When boiled, the egg's content is solidified, and sloshing is eliminated. In Reference (G. So and S.E. Semercigil, 2004), experimental observations are reported on the transient oscillations of an egg after it is released from its vertical position. A boiled egg requires approximately 10 times longer to cease oscillating as compared to a raw one. This observation is repeated in Figure 5.1 where the history of the angular oscillations of the shell are indicated with solid and dashed lines for a raw and a boiled egg, respectively. Hence, a raw egg clearly represents design opportunities as an effective energy dissipater while keeping its white and the yolk in separate membranes. Separate membranes allow the opportunity for the white and the yolk to

oscillate out of phase from each other, and out of phase from the oscillations of the eggshell. Physical structure of a hen's egg is shown in Figure 5.2.

Experimental observations in Reference (G. So and S.E. Semercigil, 2004) further suggest that replacing the content of an egg with water can enhance energy dissipation. This observation is critical, as it isolates the shape of the shell to be the significant parameter, rather than the complicated physiology of its content. Surprisingly, the egg seems to be relatively insensitive to fill level of its content, having similar stopping times from 20% to 100% fill levels (G. So and S.E. Semercigil, 2004). This last observation makes the egg attractive for design purposes, as the performance of a conventional rectangular absorber varies quite significantly from deep and shallow liquid levels (A. Marsh et al., 2010).

Similar to the investigation reported in (A. Marsh et al., 2012), numerical predictions in this study are performed using the Smoothed Particle Hydrodynamics (SPH) technique. Due to prohibitive computational requirements, the earlier attempt to study sloshing in an egg shell had to be limited to two dimensions, namely to that of a cylinder with an egg shaped cross section (A. Marsh et al., 2012). Here, this earlier work is extended into three dimensions. The three dimensional model has also enabled direct comparisons with the experimental observations of (G. So and S.E. Semercigil, 2004) for validation purposes. In addition, the SPH model has provided further details of the flow inside an egg which are not possible to observe experimentally. Such details include the mode of energy dissipation for different fill levels, and the effect of liquid viscosity. From chapters 2 and 3, superior energy dissipation is observed by attaching semi-circular obstructions to the base of an absorber. The potential to

increase dissipation further is explored by adding these obstructions to the inner egg shell. Finally, insensitivity to different fill levels inside an egg's shell, implies a form of self tuning. Self tuning is an intriguing concept in structural dynamics, if understood, providing wealth of design possibilities. An attempt in this direction is briefly presented here.

5.2 Numerical Model

A geometric model of the egg shell shown in Figure 5.3 (A. Marsh et al., 2010), generated with same dimensions as reported in Reference (G. So and S.E. Semercigil, 2004). The length of the two axes of the shell are 58 mm and 44 mm. The eggshell has a mass of 5 g. It has a total liquid volume of 50 ml, excluding the air pocket of approximately 2 ml. Water is used as the sloshing liquid with a density and dynamic viscosity of 1000 kg/m^3 and 0.001 Pa s , respectively.

The liquid, eggshell, walls and horizontal surface all have a particle size of 0.8 mm by 0.8 mm by 0.8mm. This particle size was chosen as it produces enough resolution to model the liquid's complex free surface shapes while not demanding excessive computational time unnecessarily (Appendix 2). The shell is made up of 23,660 particles, whereas the volume fraction of 1 requires 116,334 fluid particles. A typical run with a volume fraction of 1 requires approximately 7 days, on a single node of a dual 3.2 GHz Intel Xeon processor.

Each test begins with the egg held in a vertical position on a flat horizontal surface for one second, so the liquid content attains an initial state of rest. The egg is then released and its

history of its transient oscillations is observed until the initial potential energy is dissipated. Similar to the earlier experiments (G. So and S.E. Semercigil, 2004), two vertical walls were modelled to restrict the motion of the shell in one plane.

5.3 Discussion

Here, SPH predictions are compared with earlier experimental observations first. Then, a summary of cases is presented for the effect of viscosity on the rate of energy dissipation. Following that, a study to increase dissipation further by introducing semi-circular obstructions to the inner egg shell is given. Finally, the current state of investigation on the self-tuning process in an egg shell is presented briefly.

5.3.1 Comparison of experimental and numerical observations

Numerical and experimental displacement histories of the egg are presented in Figure 5.4 for volume fractions of 0.2, 0.4, 0.6, 0.8 and 1. As a reminder, full egg contains a small air pocket of 4% of the total volume, to still allow for sloshing to occur.

One general trend of the experimental observations in Figure 5.4, is that the first quarter cycle of oscillations takes substantially longer than the following cycles. This difference is due to the sliding that takes place immediately following the release. After this initial lunge, angular oscillations continue in a rocking mode. Hence, the effective coefficient of friction at the contact is very much likely to be a time-variant property. In addition, the outer shell of the egg, being a natural material, has a variable surface roughness. As a result, the contact

surface must experience a variable coefficient of friction as the location of the point of contact changes, as the egg shell oscillates.

A variable coefficient of friction is not possible to either quantify reliably or to implement in the existing capability of the numerical model. What is attempted in this study is to conduct the simulations with two different coefficients of friction of 0.01 and 0.05. The objective is to bracket the behaviour of the egg with the assumption that the true coefficient of friction is no smaller than 0.01 and no larger than 0.05 at any time. The two coefficients of 0.01 and 0.05 were chosen to resemble a low contact surface friction (E. Altuntaş and A. Şekeroğlu, 2008). The tests were designed on hard surfaces to reduce energy dissipation through friction, ensuring that the energy dissipation is mainly from the working fluid.

Numerically predicted displacement histories in Figure 5.4, generally have a higher rate of energy dissipation than that of the experiments. This faster dissipation results in smaller peak displacements and longer natural periods. Such behaviour is especially noticeable during the first half cycle of oscillations. The reason for predicting a higher rate of dissipation is to do with artificial numerical damping associated with the model. SPH (Smoothed Particle Hydrodynamics) relies on integration, as part of its smoothing procedure. This integration takes place from the centre of each fluid particle and has to do with its interaction with its neighbouring particles. As the particle size gets smaller, along with the corresponding smoothing length, the level of artificial damping is expected to diminish, at the expense of required computational effort. A 0.8 mm particle size with a smoothing length 1.2 times this size, has been determined to be at the edge of the practical limit with the currently available

computational facility. Halving the particles size increases the run time by 16 times (J.J. Monaghan, 1992) (P. Cleary and M. Prakash, 2004).

Numerically predicted displacement histories suggest close correspondence to the experimental observations, especially for the volume fractions of 0.4 to 0.8 in Figure 5.4(b) to 4(d), ceasing oscillations within 2 periods. For the other two volume fractions, 0.2 in Figure 5.4(a) and 1 in Figure 5.4(e), experimental observations suggest small amplitude oscillations sustained past 1s. These small oscillations are not observed in the simulations, due to numerical artificial damping. Although there are differences in peak displacement magnitudes and damped natural frequency, the level of similarities between the numerical and experimental observations gives confidence to the relevance of numerical simulations.

Animations of the numerical predictions indicate that the two lower volume fractions (0.2 and 0.4) have large free surface deformation with breaking travelling waves that dissipate energy. In contrast, the highest fraction of 1 has minimal free surface, and energy dissipation takes place solely through shearing of the liquid at the wall. These trends are in agreement with (A. Marsh et al., 2012) where modelling had to be restricted to two-dimensional geometry of an egg cylinder, due to then prohibitive computational requirements. Direct comparisons between two and three dimensional cases are not undertaken due to the three-dimensional egg and two-dimensional egg cylinder being different geometries that produce different damping characteristics.

A summary of the cases in Figure 5.4 are given in Figure 5.5(a) and 5.5(b) for different volume fractions. In these figures, the vertical axis represents the 10 % and 5 % settling times, as the time for the peak displacement to decay within 10 % and 5 % of the initial displacement (of 90 degrees). 10 % and 5 % values are chosen as some indication of performance, and they are not absolute by any measure. Of course, an effective case dissipates its initial energy quickly, resulting in the shortest settling time.

Both for 10 % and 5 % settling times, experimental values are within quite close agreement with the numerical predictions. With an approximately linear variation, settling times get shorter with increasing volume fraction. The exception to this close agreement is at the two extreme values of 0.2 and 1 volume fractions where the experimental observations indicate some remnant energy which causes small oscillations once the significant portion of the initial energy is quickly dissipated. In Figure 5.5(a), 10 % settling, the remnant energy is small enough to indicate a discrepancy only at 0.2 volume fraction. For the more severe case of 5 % settling, both 0.2 and 1 volume fractions suggest longer experimental times than what could be predicted. As discussed earlier, the cause for not being able to predict these small oscillations closely is the presence of artificial damping due to smoothing the spatial distributions in SPH.

The initial potential energy of an egg, in the upright position, is presented in Figure 5.5(c) for different volume fractions. A higher volume corresponds to larger mass. In addition, the net hydrostatic head is larger as the height of the centre of mass increases with volume fraction. Hence, the imposed potential energy to be dissipated increases with volume fraction as

suggested in Figure 5.5(c). As a result, due to the settling times being similar for all volume fractions, higher volume fractions are more effective dissipaters. Therefore, the most effective energy dissipation takes place between the liquid and the wall, since there is minimal free surface deformation at higher volume fractions. Such a determination may be significant in attempts to enhance the dissipation capabilities of a natural egg.

5.3.2 *Effect of Viscosity*

Following the observations of the preceding section, free surface deformation and the wall shear seem to be the primary sources of dissipation for the low and high fill levels, respectively. As a result, volume fractions of 0.2 and 1 are analysed here as the variation in energy dissipation characteristics between shallow and deep liquid levels is most noticeable. The settling times are comparable for all fill levels and the amount of initial potential energy to be dissipated clearly increases with the fill level, making higher fill levels in an egg faster dissipaters. Hence, encouraging shear dissipation seems to be promising to enhance the performance of an egg shaped container. To this end, a summary of an extensive case study is presented here to investigate the effect of liquid viscosity on the rate of energy dissipation.

Displacement histories of an egg for varying viscosities are presented in Figure 5.6, in two columns of three rows. The first column, Figures 5.6(a) to 5.6(c), corresponds to the volume fraction of 0.2. The second column, Figures 5.6(d) to 5.6(f), corresponds to the volume fraction of 1. Three different viscosities of 0.001 Pa s, 0.1 Pa s and 1 Pa s are used in each of the three rows, in descending order. A friction coefficient of 0.01 remains constant for all cases. Figures 5.6(a), 5.6(c), 5.6(d) and 5.6(f) have red circles, marking instances where

liquid velocity field snapshots are taken for further discussion. These snapshots are given in Figures 5.7 and 5.8 for volume fractions of 0.2 and 1, respectively.

Viscosity of 0.001 Pa s for 0.2 volume fraction, possesses reasonably good energy dissipation capabilities, with a 10% settling time of 1.1 s as shown in Figure 5.6(a), repeated from Figure 5.4(a). With a viscosity of 0.1 Pa s, the 10% settling time marginally improves to about 0.9 s, as shown in Figure 5.6(b). However, when the liquid's viscosity is increased to 1 Pa s in Figure 5.6(c), the liquid is too viscous to slosh. The liquid mass settles at the base of the egg, restricting it to slowly move towards its resting position, rather than oscillating about this position of minimum potential energy, resulting in a poor rate of dissipation.

The snapshots of the velocity field in Figure 5.7, when the shell of the egg is removed for clarity, correspond to the four instances marked in Figures 5.6(a) and 5.6(c). The first column, Figures 5.7(a) to 5.7(d), correspond to Figure 5.6(a), viscosity of 0.001 Pa s. The second column, Figures 5.7(e) to 5.7(h), correspond to Figures 5.6(c), viscosity of 1 Pa s. The coloured scale shows liquid particle velocity ranging from 0 (blue) to 0.3m/s (red).

Severe velocity gradients in the liquid are marked in Figures 5.7(a) and 5.7(c), for 0.001 Pa s. Free surface deformation with highly energetic liquid, is particularly noticeable in Figure 5.7(b). Any instant after about 1.1 s is marked in shades of blue, as a result of having dissipated most of the available energy. In contrast, no free surface deformation and no sharp gradients occur for the 1 Pa s viscosity case in Figures 5.7(e) to 5.7(h). The egg very gradually moves to its rest position, taking a significantly longer time to dissipate the

available energy than that of the lowest viscosity case. Since free surface discontinuities are the main form of energy dissipation for shallow levels, increase of viscosity may be detrimental for a volume fraction of 0.2.

Displacement histories for the largest volume fraction of 1, in Figures 5.6(d) to 5.6(f), show remarkably similar settling times for all viscosities, dissipating the available energy within 0.8 s. This seeming insensitivity to drastically different fluid viscosities, may be reasoned with the help of the snapshots in Figure 5.8.

Figure 5.8 is formatted similar to Figure 5.7, with 0.001 Pa s in the first column, and 1 Pa s in the second column, at the marked instances in Figures 5.6(d) and 5.6(f). Low viscosity cases in the first column have minimal surface deformation, similar to those in the second column. With the exception of the first snapshot at 0.25 s, the surface velocities are higher in the second column, for the higher viscosity. In addition, the higher viscosity seems to enforce a more orderly velocity field than those in the first column. In the second column, the velocity field is stratified clearly, from the smallest to the largest value in bands, from the contact point to the free surface. In the first column, this stratification is less orderly with sharper gradients in the field, away from the walls. These disorderly intrusions of slowly moving particles in a fast moving field, and fast particles in slow fields, have to be responsible for large shear. However, without the benefit of these pockets of shear deformations away from the wall, the large viscosity case is able to move faster next to the wall, and make up for the absence of any sharp gradients in the field.

5.3.3 *The Effects of Obstructions*

Efforts to increase the rate of energy dissipation further are explored by introducing semi-circular surface roughness elements (obstructions) around the inner shell of the egg. Chapters 2 and 3 suggest that attaching obstructions to the base of the rectangular absorber, increased energy dissipation significantly at shallow liquid depths. As a result, 0.2 volume fraction is analysed. A volume fraction of 1 is also analysed to determine how the obstructions effect energy dissipation at the highest volume fraction where wall shear is the main energy dissipation characteristic.

Two obstruction cases consisting of 1 and 2 semi-circular obstructions with 4 mm radii displayed in Figures 5.9(a) and 5.9(b). These obstructions are attached to the short axis of symmetry of the egg. The lower obstruction's centre is attached 22 mm (r_1 in Figure 5.3) from the base of the egg. The higher obstruction's centre is attached 18 mm from the top of the egg. The locations for the obstructions were chosen to be around the side of the egg (r_2 in Figure 5.3) as it spends the majority of its time oscillating around this radius. As a result, the liquid spends most of its time in this area and therefore will produce the most wave-to-obstruction interactions. The obstruction radius was chosen to have a ratio of obstruction radius over liquid height to Chapter 3's most effective energy dissipater obstruction case of r/h of about 52%. The liquid height (h) at 0.2 volume fraction is approximately 8 mm. As a result, with an obstruction radius (r) of 4 mm, r/h is about 50%.

Exploring the effects of liquid viscosity in the previous section did not increase the rate of energy dissipation. However, wave-to-obstruction interactions produce increased velocity gradients within the liquid significantly increasing energy dissipation. Increasing the liquid

viscosity produces higher liquid velocities at the surface at high volume fractions. As a result, there may be potential to increase dissipation further through the combination of the attached obstructions and effect of viscosity. Therefore, a range of viscosities 0.001, 0.1 and 1 Pa s (the same viscosities used in 5.4.2 Effects of Viscosity) are analysed at volume fractions of 0.2 and 1 to show the interaction between the effect of obstructions and viscosities at these volume fractions.

Displacement histories for viscosities 0.001, 0.1 and 1 Pa s are displayed in Figure 5.10. The 1 obstruction case is analysed at 0.2 volume fraction in Figures 5.10(a) to 5.10(c) and 1 volume fraction in Figures 5.10(d) to 5.10(f). Comparisons are made with the same volume fraction and viscosity cases without obstructions presented previously in Figure 5.6. Slight improvements are achieved by introducing the obstruction for 0.2 volume fraction with viscosity 0.001 Pa s in Figure 5.10(a). These improvements occur within the first two oscillations where peak displacements are reduced as compared to the no obstruction case. This is due to energy being dissipated as the sloshing wave travels over the obstruction, creating severe velocity gradients, reducing the displacement amplitudes of the egg faster.

Displacement histories for 0.2 volume fraction with and without the obstruction attached are similar for viscosities 0.1 Pa s and 1.0 Pa s in Figures 5.10(b) and 5.10(c). As the viscosity increases, the fluid becomes too thick to slosh, therefore, becoming ineffective energy dissipater. Energy dissipation is slightly reduced by the introduction of the obstruction at 1 volume fraction, for all viscosities in Figures 5.10(d) to 5.10(f).

At a volume fraction of 1, the addition of the obstruction also gives minimal differences at all viscosities in Figures 5.10(d) to 5.10(f). The location where the obstruction is cut out of the

egg shell produces a slight rocking motion as it interacts with the ground, while the egg oscillates, resulting in a minor increase in displacement amplitude at all viscosities in Figure 5.10(d) to 5.10(f). These small oscillations are only observed at a volume fraction of 1 as the increase in distribution of liquid mass and therefore potential energy slightly enhances the rocking motion.

Displacement histories for the same viscosities in Figure 5.10 are presented in Figure 5.11 for the 2 obstruction case in Figures 5.11(a) to 5.11(c) and the case without obstructions in Figures 5.11(d) to 5.11(f). The most effective case is 0.2 volume fraction, with viscosity of 0.001 Pa s, in Figure 5.11(a). Introducing the second obstruction increases energy dissipation further, eliminating oscillations within 0.8 s, approximately half the time of the case without obstructions. Increased amounts of energy within the sloshing wave are dissipated with the presence of the two obstructions. An explanation of how the obstructions dissipate energy within the liquid is given later in the form of liquid velocity field snapshots. Introducing the second obstruction also increases dissipation for viscosity 0.1 Pa s in Figure 5.11(b) eliminating oscillations at about 1.1 s, 0.6 s quicker than the case without obstructions. Similarly for the 1 obstruction case, the 2 obstruction case at a volume fraction of 0.2 and viscosity of 1.0 Pa s gives very poor energy dissipation with the liquid being too thick to slosh in Figure 5.11(c).

Energy dissipation worsens for a volume fraction of 1 by introducing 2 obstructions for all viscosities displayed in Figures 5.11(d) to 5.11(f). The slight rocking motion that was observed previously for the 1 obstruction cases occurs twice as frequently with 2 obstructions, producing increased amounts of displacement amplitude. Wider displacement amplitudes also occur, particularly at the first peak displacement, at around 0.5 s, in Figures

5.11(d) to 5.11(f). This occurs as the higher located obstruction becomes in contact with the ground at the first peak displacement. The egg balances in this position for a slightly longer period of time compared to the case without obstructions before oscillating back towards 0 degrees displacement. Slight phase differences occur at all viscosities for the 2 obstruction cases, in Figures 5.11(d) to 5.11(f). This is due to the difference in the distribution of the liquid mass within the egg. The egg without obstructions is able to occupy the space, where the 2 obstructions are located, with liquid. The added liquid mass, close to the egg's shell, encourages the egg to oscillate faster. As a result, the cases with 2 obstructions at all viscosities become worse energy dissipaters requiring increased amounts of time to cease oscillating.

Liquid velocity field snapshots are displayed in Figure 5.12 for 0.2 volume fraction with a viscosity of 0.001 Pa s. The 2 obstruction case is presented in the left column Figures 5.12(a) to 5.12(d) and the case without obstruction in Figures 5.12(e) to 5.12(h). Each frame corresponds to the relevant instances that occur within the first second in Figure 5.11(a). Fixed velocity scale shows liquid particle velocity ranging from 0 (blue) to 0.3m/s (red).

High velocity gradients are displayed in Figures 5.12(a) and 5.12(b) as the sloshing wave travels over the first obstruction at times 0.45 s and 0.47 s. At these times for the case without obstructions the travelling wave has already approached the smaller radius (top) of the egg at high velocity in Figures 5.12(e) and 5.12(f). As a result, a larger peak displacement is produced at 0.47 s in Figure 5.11(a) compared to the case with obstructions. Velocity gradients are also observed in Figures 5.12(c) and 5.12(d) as the sloshing wave continues and travels over the second obstruction at times 0.57 s and 0.62 s. These severe velocity gradients within the liquid give evidence of substantial amounts energy dissipation as a result of the

obstructions. The 2 obstructions dissipate the majority of the energy as the egg ceases oscillating shortly after at 0.8 s. At these times for the case without obstructions the travelling wave has interacted with the smaller radius (top) of the egg. However, energy stored within the structure is still too high and is given back to the fluid causing the travelling wave to continue from right to left in Figures 5.12(g) and 5.12(h).

5.3.4 Tuning - A Frequency study

The performance of an egg to dissipate energy is relatively insensitive to vastly varying fill levels, as suggested earlier in Figures 5.4 and 5.5. This insensitivity may be related to a form of self tuning. At each level of fill, due to varying cross section of the egg, as the static depth of the liquid changes, there may be some compensation from the corresponding free surface length to maintain tuning. In addition, both the depth of liquid and the free surface length are variable parameters as the egg oscillates. Initially, the upright egg has the deepest static level and shortest surface length. In contrast, the liquid depth is smallest, and the surface length is longest when the egg is horizontal. As the egg is released from its initial upright position, the depth of liquid and the length of the free surface vary within these two limits.

What is presented in this section is a summary of the efforts to explore self tuning. To this end, the structure of the shell and the liquid inside the shell are treated independent of each other. The objective in this treatment is to observe the values of structural natural frequency of the shell and the liquid sloshing frequency. The coincidence of these two frequencies indicates tuning.

The frequency of the shell is estimated from the simplified pendulum analogy, $(g/r)^{1/2}$, where g is the gravitational acceleration, and r the local radius at the point of contact. Remembering the geometry of the egg in Figure 5.3, r varies from 22 mm (upright) to 44 mm (horizontal) and to 14 mm (inverted).

The sloshing frequency of the liquid is obtained from numerical simulations after giving the egg an initial disturbance and then maintaining the shell at either one of the three positions (upright, horizontal or inverted). As the liquid sloshes in a stationary shell, the history of the total kinetic energy is recorded. The frequency is then obtained from the Fourier transformation of the history of the kinetic energy. The frequency content of the kinetic energy changes marginally depending on the observation time, smaller values being close to the beginning. Hence, the process of capturing the sloshing frequency is repeated with several different windows for each case, to record the possible variation.

The natural frequency of the empty shell and the sloshing frequency of the liquid in a stationary shell are presented in Figure 5.13 for different fill levels. Vertical error bars for the sloshing frequencies represent the variation due to different observations windows mentioned earlier. Figures 5.13(a) to 5.13(c) correspond to the vertical, horizontal and upright positions of the egg. Out of these three positions, the upright egg case in Figure 5.13(a) is relevant during the initial stages. The inverted egg in Figure 5.13(c) is rarely of any significance. The horizontal position in Figure 5.13(b), on the other hand, covers the vast majority of the oscillations of the shell.

In Figure 5.13(b), for the radius of the horizontal egg, by some design of nature, it seems that the frequencies of the empty shell and the liquid in the stationary shell are in close correspondence for all fill levels. The upright and the inverted positions, on the other hand, seem to have consistently lower sloshing frequencies than the frequencies of the shell. This difference is as large as 100% for the inverted egg in Figure 5.13(c). However, since both of these last two cases have limited opportunity to have any significant effect, the egg must be able to maintain tuning for different levels of its liquid fill.

In Figure 5.14, variation of the frequency of the egg are given for different fill levels for both the experimental observations (\blacktriangle) and the numerical predictions with 0.01 (\blacklozenge) and 0.05 (\blacksquare) friction coefficients. These values are extracted from the histories in Figure 5.4. It should be emphasized that these frequencies are given in an average sense, since there is possibility of contributions from all three radii of contact. However, the horizontal position has the largest contribution, resulting in frequencies in the same order of magnitude as those in Figure 5.13(b). The experimental values are represented with a shaded band in Figure 5.14, as extensive judgement had to be exercised for their prediction. In general, the numerically predicted frequencies are in quite close correspondence to those of the experiments.

5.4 Conclusions

A natural hen's egg seems to have evolved with the capability to quickly dissipate energy through sloshing of its liquid content to protect the embryo. Understanding such a process may have practical implications in engineering devices to protect structures from excessive damaging oscillations. Numerical simulations are presented in this chapter and compared with experimental observations, to study the process of dissipation in an egg.

Smoothed Particle Hydrodynamics (SPH) is ideally suitable to represent such complex free surface flows. Through numerical simulations, it is possible to identify excessive surface deformations to be responsible for dissipation for low liquid levels in an egg shell. High liquid levels, however, dissipate energy with shear close to the wall.

Although the initial potential energy is dissipated in comparable times at all fill levels, an egg with a higher fill level is a more effective dissipater due to having larger potential energy at the start. The relative insensitivity at high fill levels to varying the viscosity of the sloshing liquid is an additional benefit. This trend may also provide design incentives to enhance the dissipation capability of a natural egg with structural modifications.

Introducing 2 semi-circular obstructions to the inner shell of an egg produce superior energy dissipation at a volume fraction of 0.2 using water as the sloshing liquid. The increase in dissipation results in the egg ceasing oscillations in approximately half the time than the case

without obstructions. This is a result of the wave-to-obstruction interactions producing severe velocity gradients within the liquid, dissipating increased amounts of energy.

An exploratory investigation is also presented into the possible self-tuning of an egg to maintain effectiveness at vastly different fill levels. Due to its unique shape, it seems that an egg is able to maintain tuning between the sloshing of its liquid content and the structural oscillations of its shell. This simple building block of nature has lessons to structural engineers in search for an effective and simple structural controller. Hence, continued efforts are certainly worthwhile.

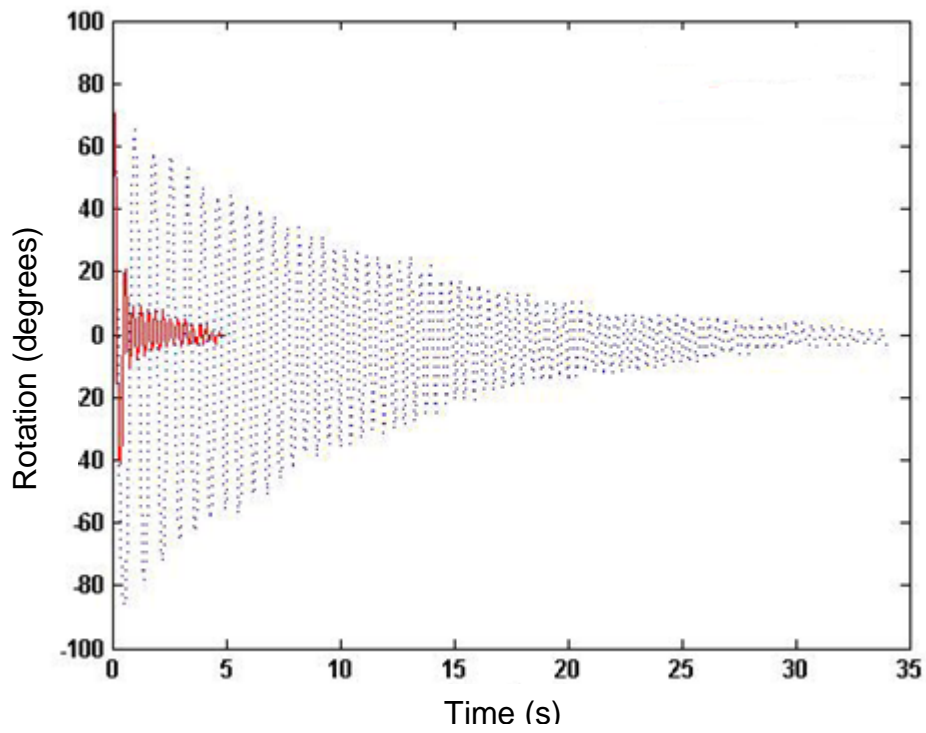


Figure 5.1: Angular displacement history of an egg when raw (—) and boiled (---) from (G. So and S.E. Semercigil, 2004).

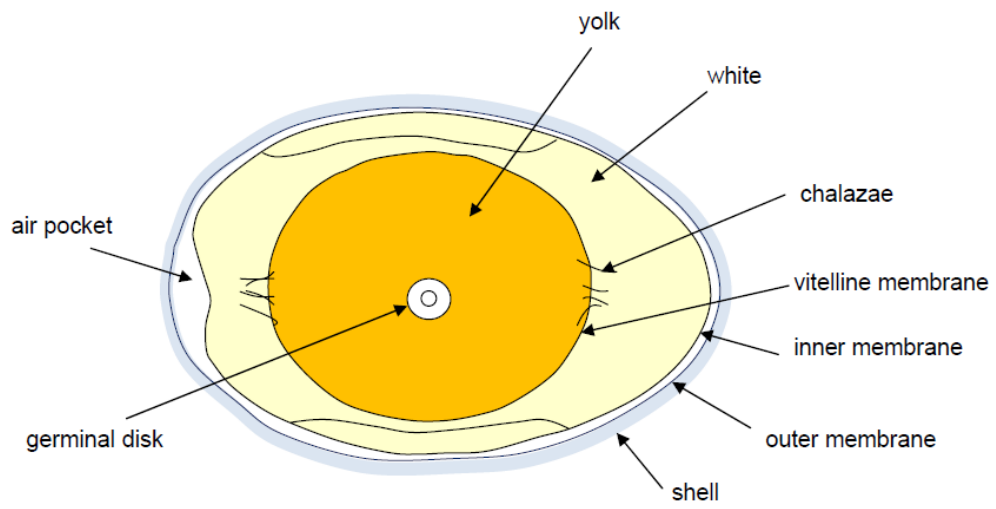


Figure 5.2: Physiology of egg (Avian Sciences Net, 2012).

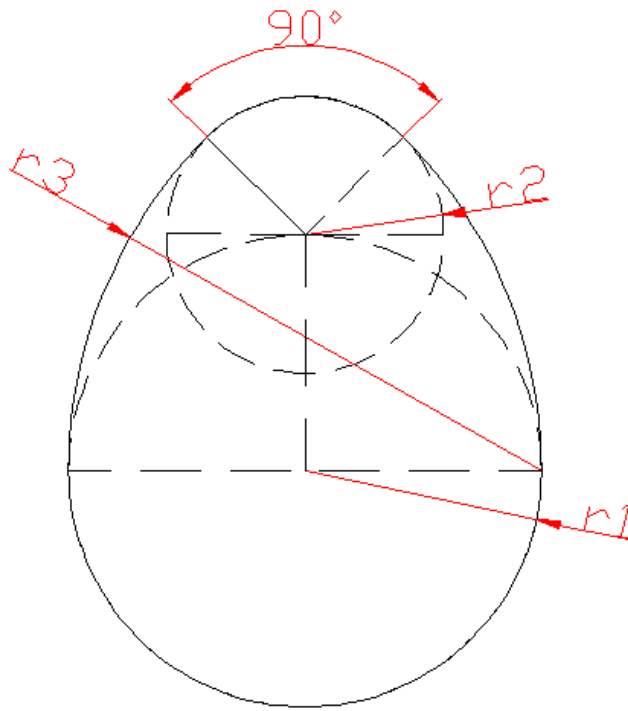


Figure 5.3: Geometry of an egg (A. Marsh et al., 2012).
 $r_1 = 22$ mm (vertical), $r_2 = 14$ mm (inverted) and $r_3 = 44$ mm (horizontal).

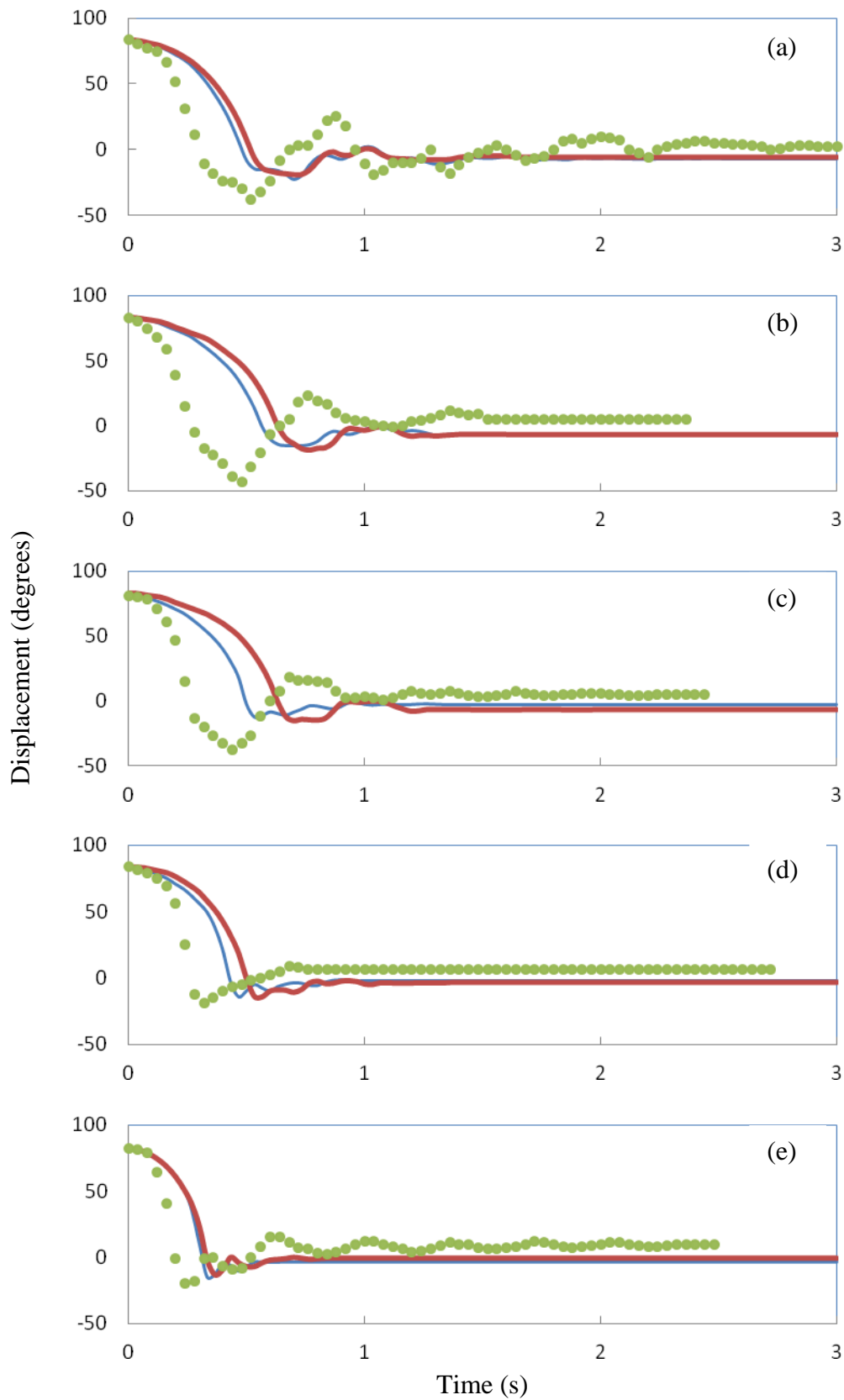


Figure 5.4: Displacement histories for numerical egg friction coefficient of 0.01 (blue thin), 0.05 (red thick) and experimental observations (green dot) for (a) 0.2, (b) 0.4, (c) 0.6, (d) 0.8 and (e) 1 volume fractions.

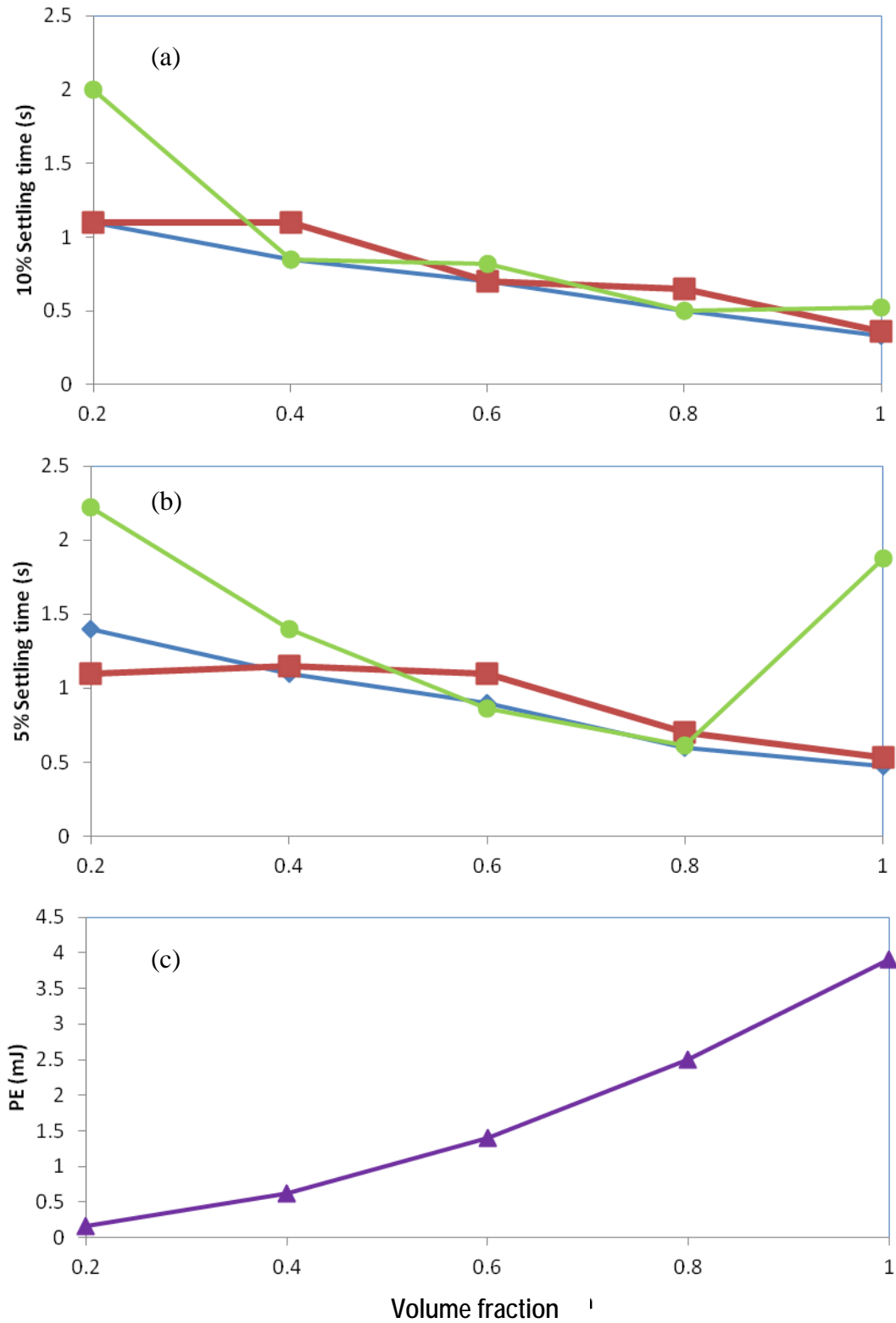


Figure 5.5: Variation of (a) 10% and (b) 5% settling time and (c) initial potential energy (\blacktriangle) with volume fraction. Settling times given for experimental cases (\bullet) and numerical ones with friction coefficient of 0.01 (\blacklozenge) and 0.05 (\blacksquare).

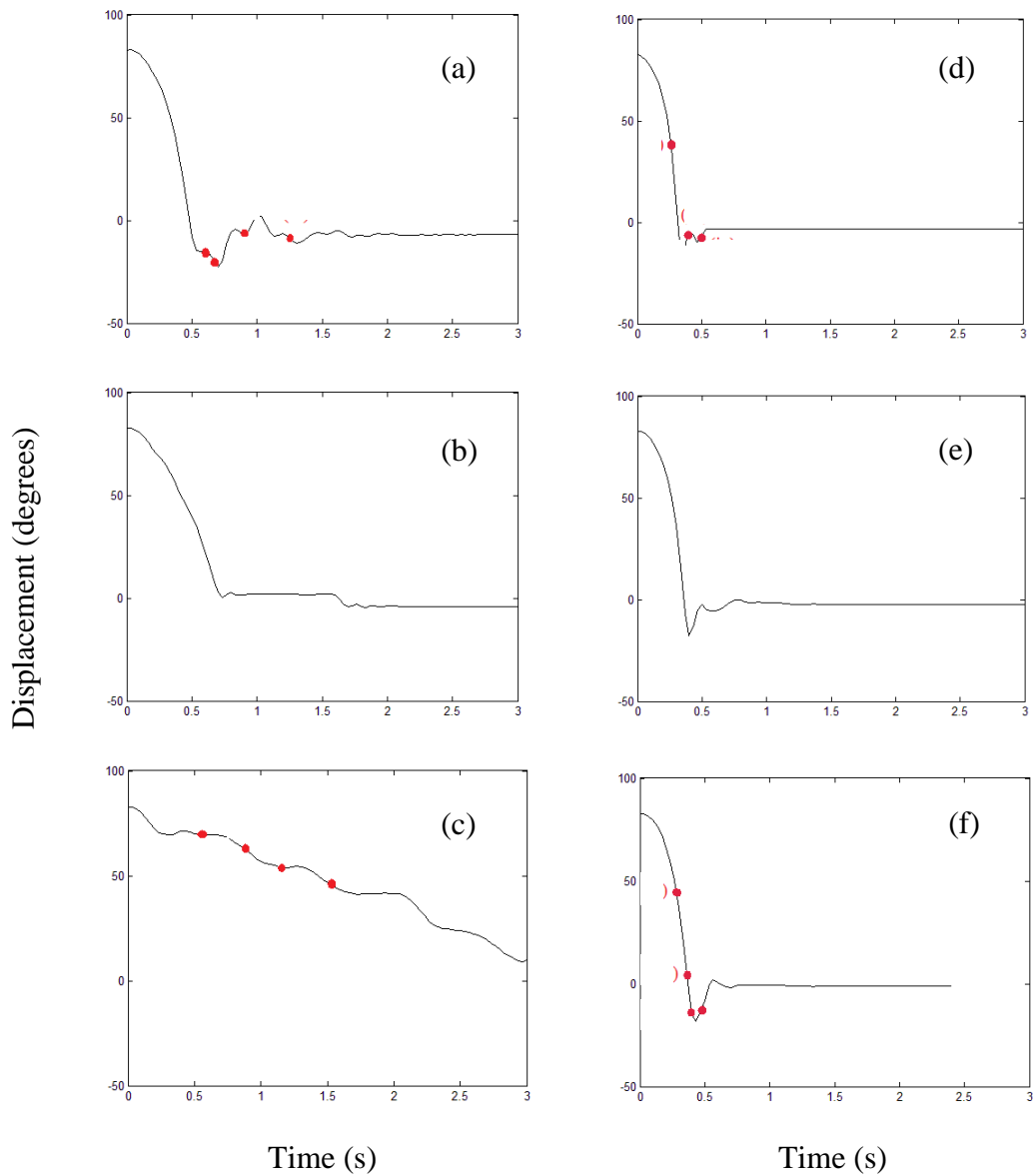


Figure 5.6: Numerical displacement histories for friction coefficient of 0.01, 0.2 volume fraction and a viscosity of (a) 0.001 Pa s, (b) 0.1 Pa s, (c) 1.0 Pa s; and 1.0 volume fraction and a viscosity of (d) 0.001 Pa s, (e) 0.1 Pa s and (f) 1.0 Pa s. Red dots correspond to the instants of the snapshots in Figure 5.7 and 5.8.

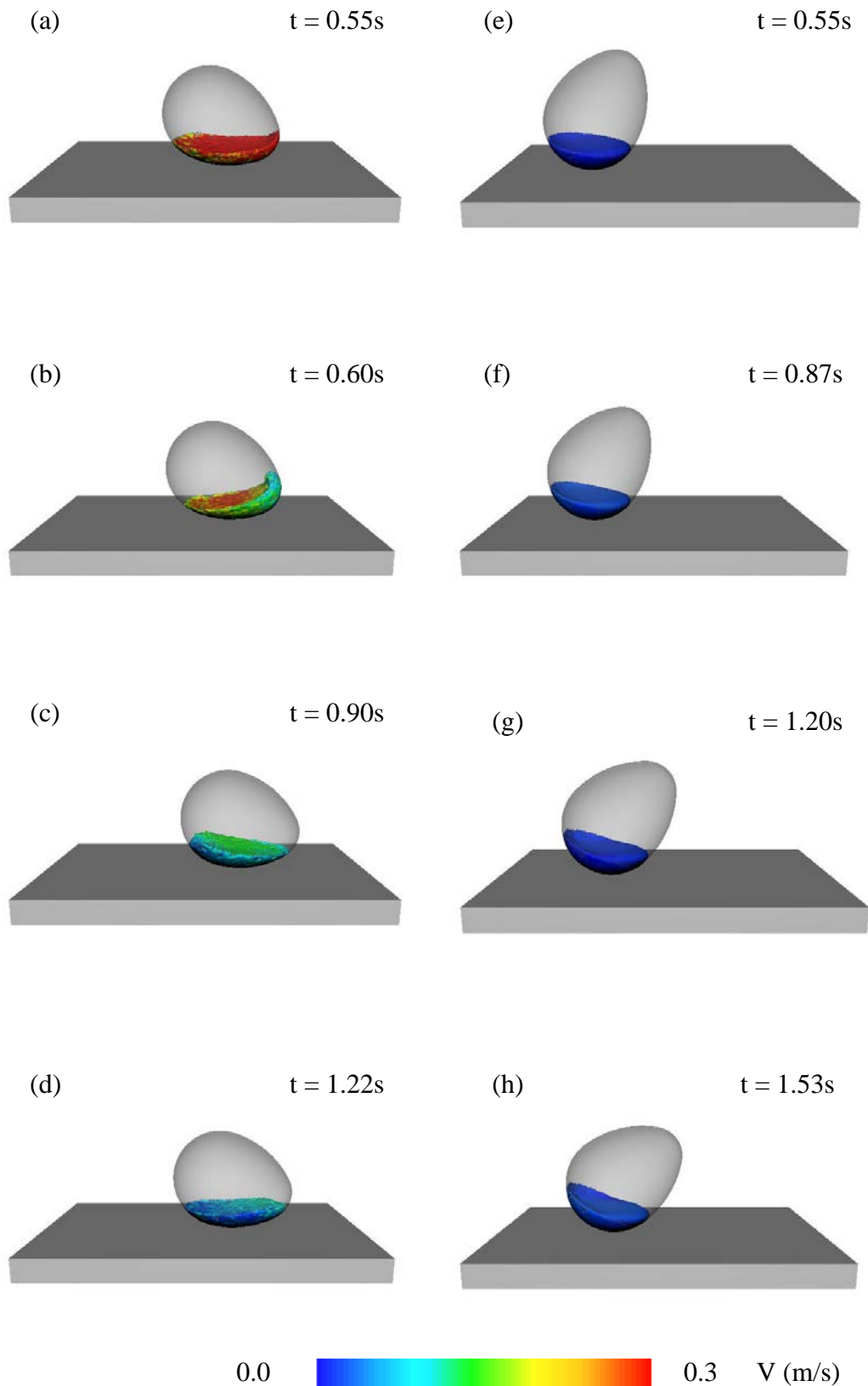


Figure 5.7: Liquid velocity flow field snapshots corresponding to marked instances in Figure 5.6 for 0.2 volume fraction. (a) to (d) for viscosity of 0.001 Pa s, and (e) to (h) for viscosity of 1.0 Pa s. Velocity colour scale range from 0 m/s (blue) to 0.3 m/s (red).

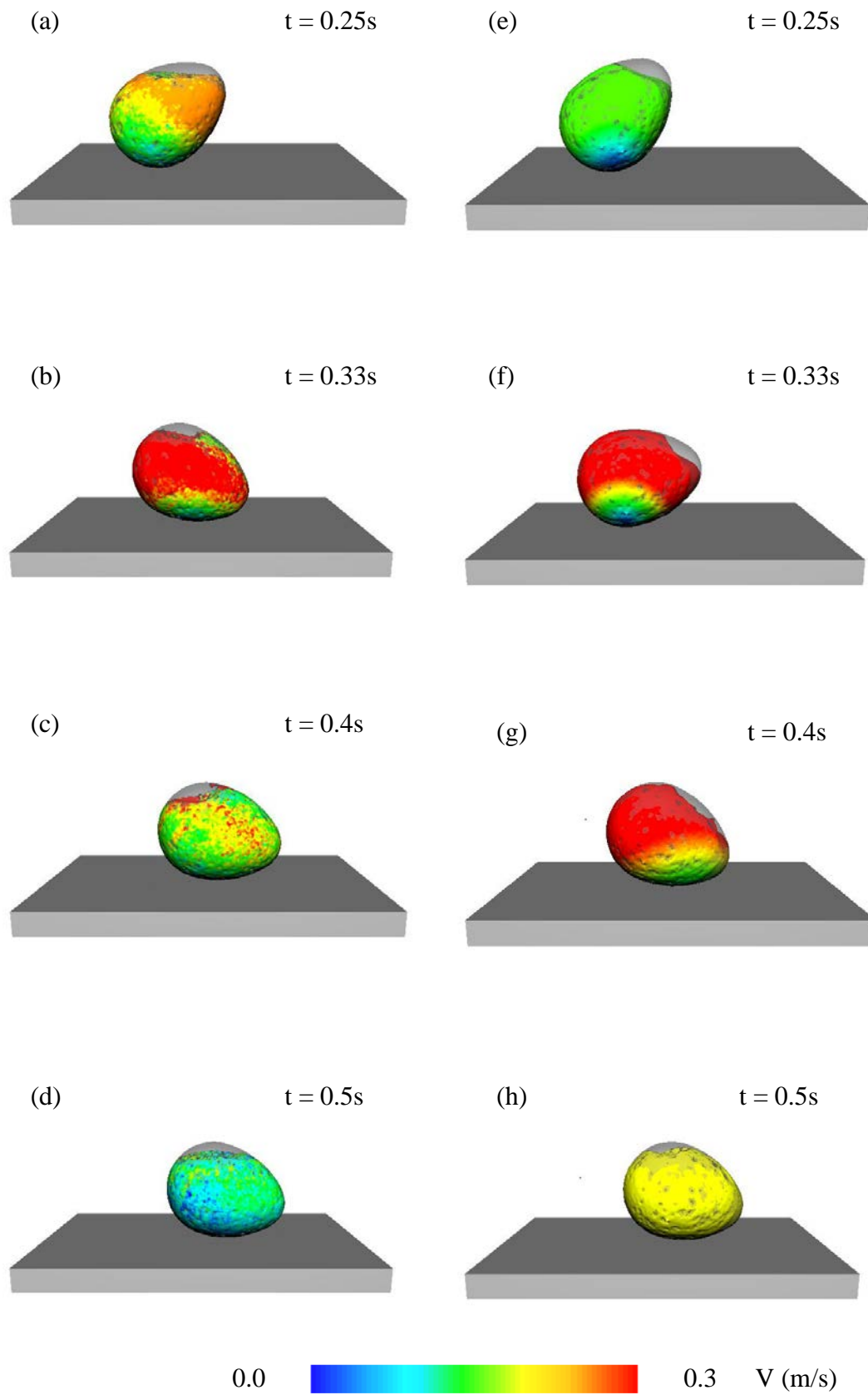


Figure 5.8: Same as in Figure 7, but for 1 volume fraction.

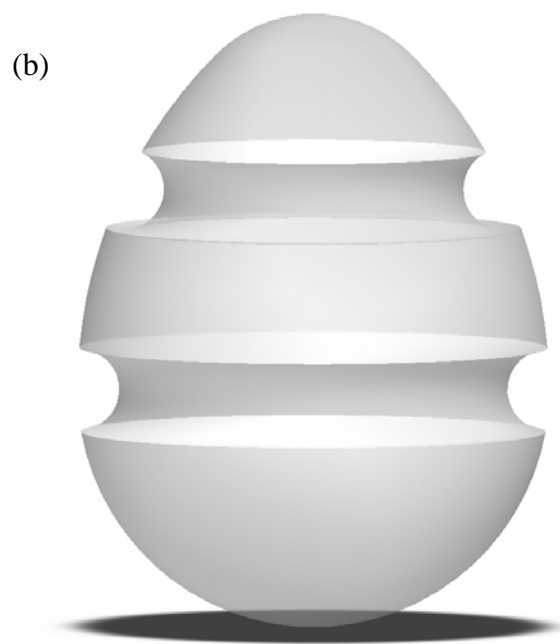
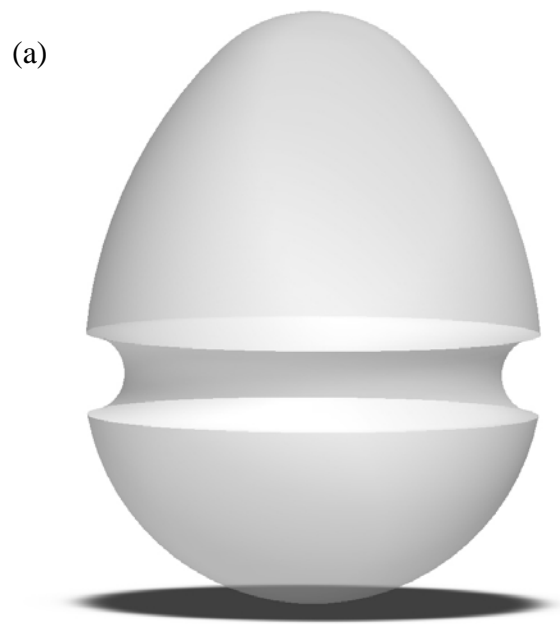


Figure 5.9: Egg geometry for 1 (a) and 2 (b) semi-circular obstruction cases with radius 4 mm.

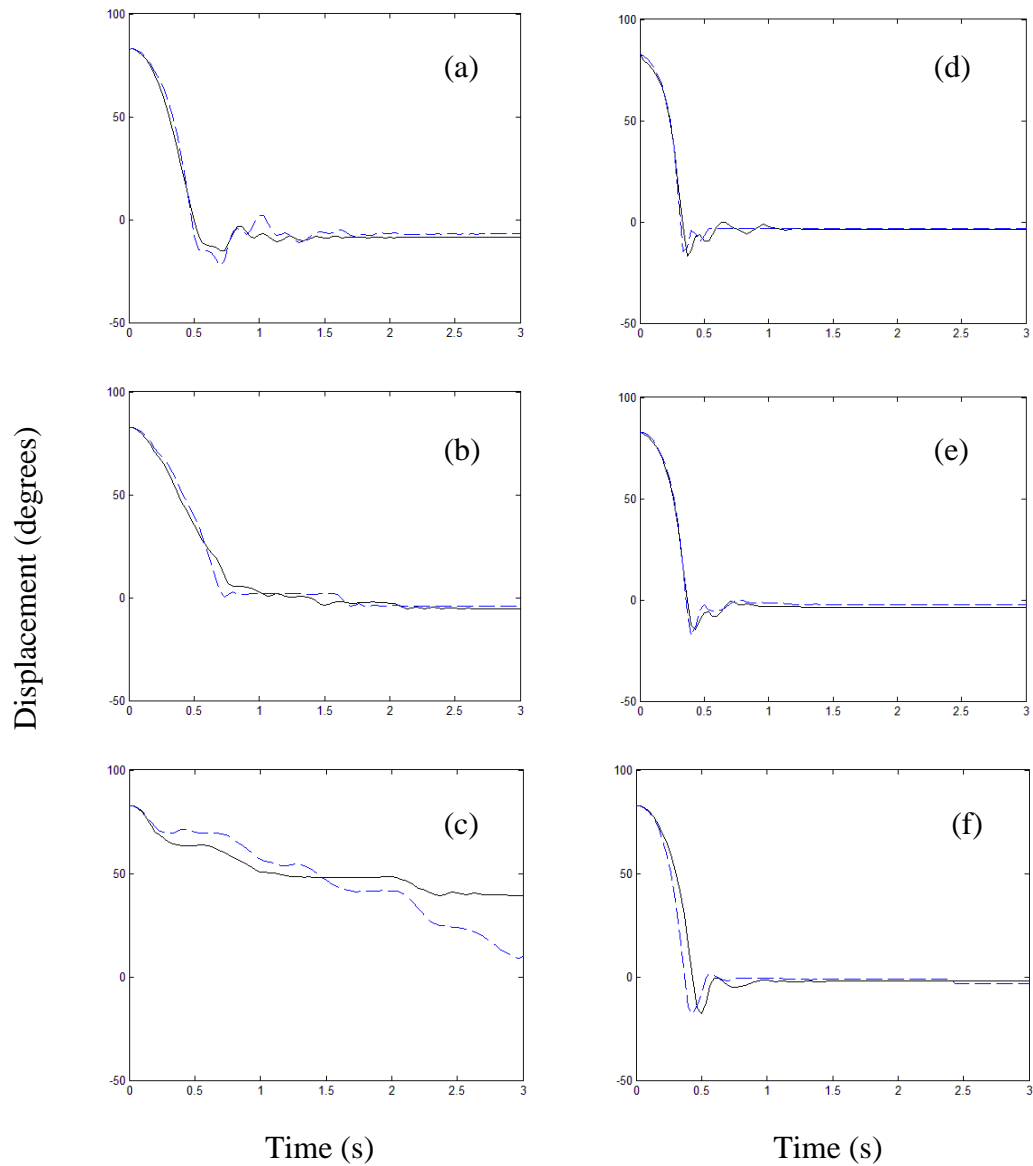


Figure 5.10: Numerical displacement histories without (-----) and with 1 semi-circular obstruction (—) with radius 4 mm and friction coefficient of 0.01, 0.2 volume fraction and a viscosity of (a) 0.001 Pa s, (b) 0.1 Pa s, (c) 1.0 Pa s; and 1.0 volume fraction and a viscosity of (d) 0.001 Pa s, (e) 0.1 Pa s and (f) 1.0 Pa s.

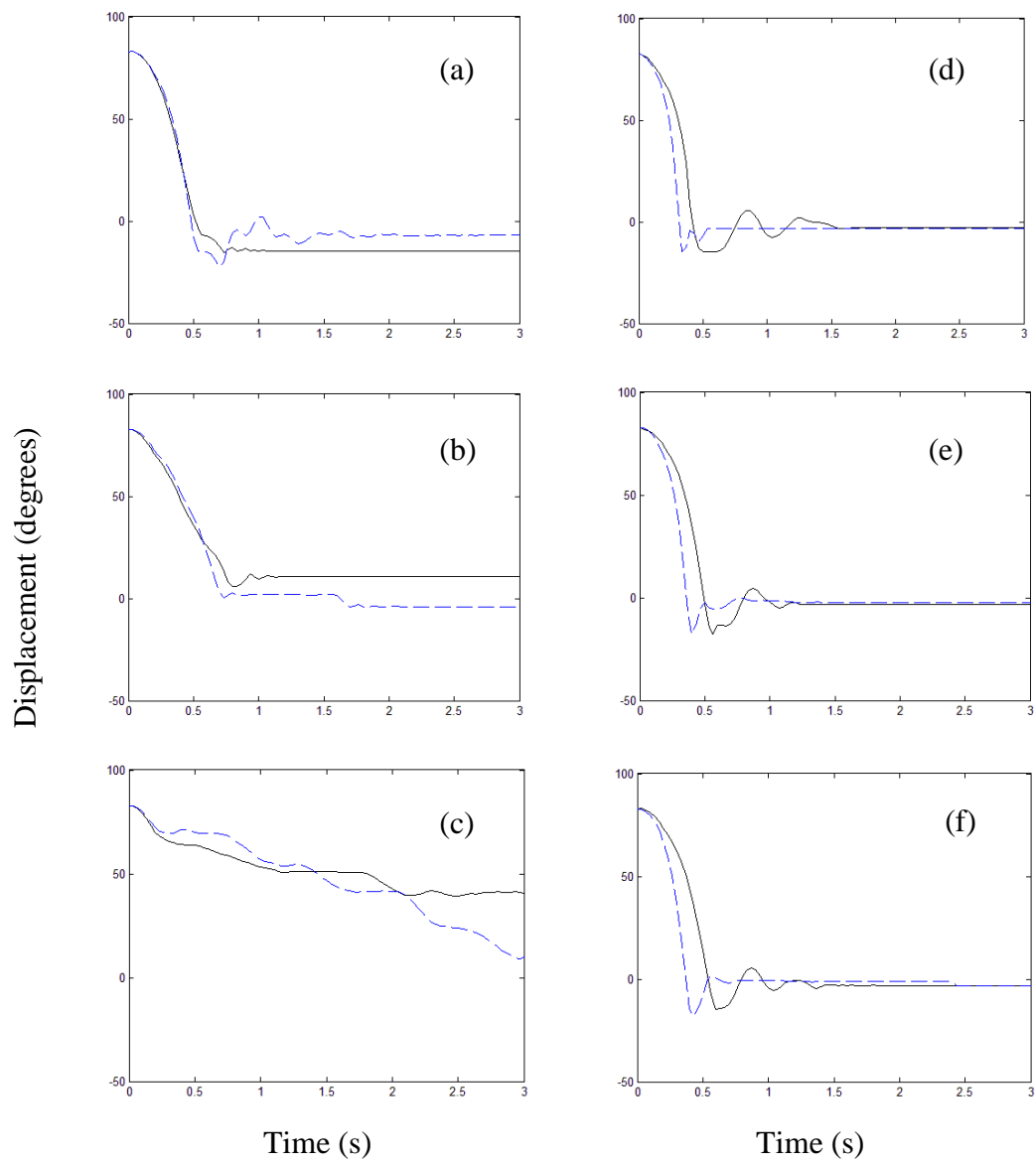


Figure 5.11: Same as Figure 5.10 but for 2 semi-circular obstructions (—) with radius 4 mm.

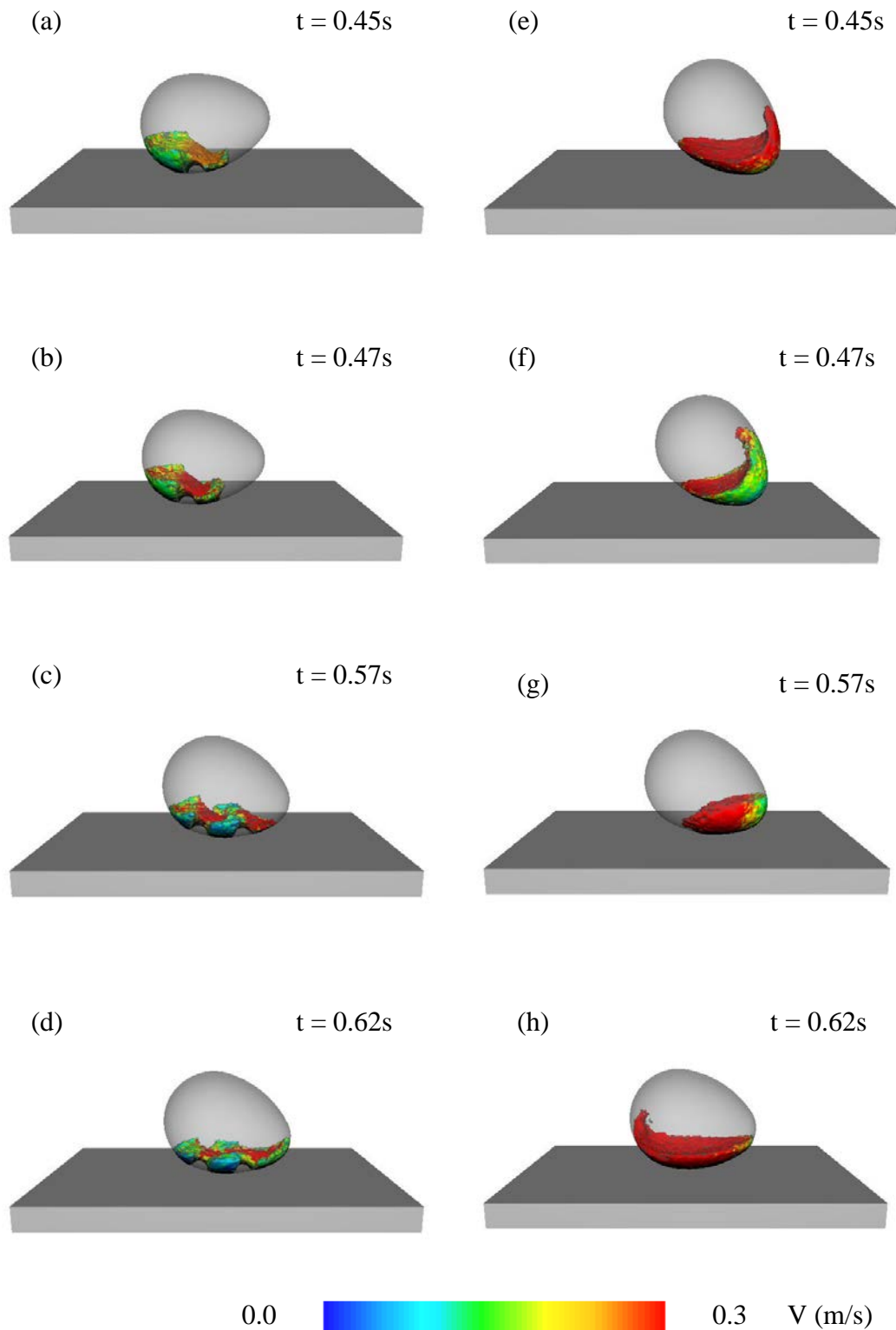


Figure 5.12: Liquid velocity flow field snapshots for 0.2 volume fraction. (a) to (d) for 2 semi-circular obstructions with 4 mm radius and (e) to (h) without obstruction case. Velocity colour scale indicates a range from 0 m/s (blue) to 0.3 m/s (red).

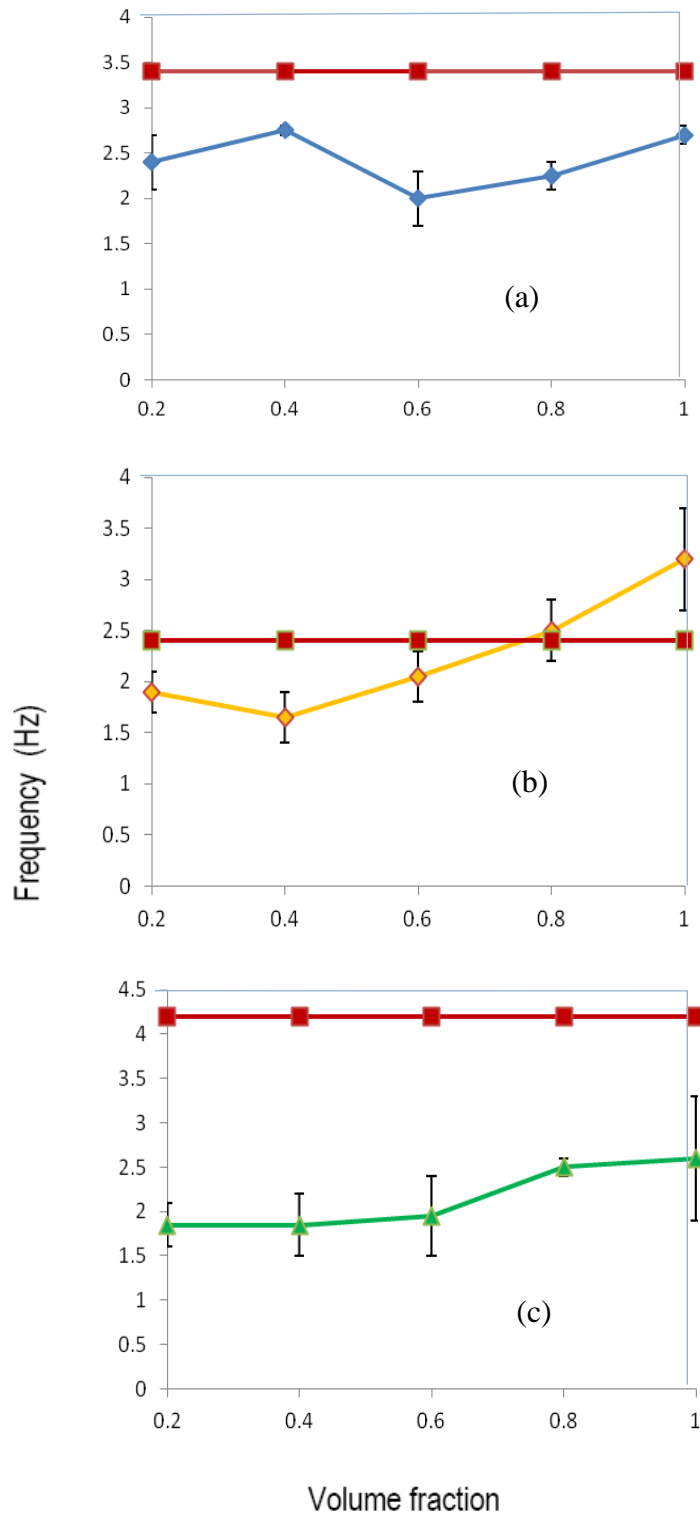


Figure 5.13: Variation of the structural (■) and liquid frequencies for different fill levels and for (a) upright (◆), (b) horizontal (◇) and (c) inverted (▲) positions of the egg.

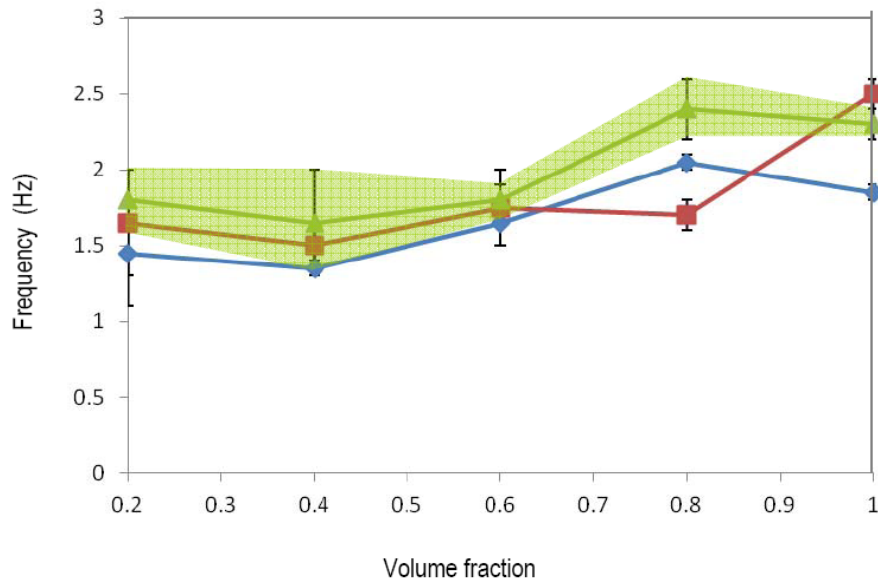


Figure 5.14: Variation of the experimental (▲) and numerical (0.01 friction coefficient ◆, 0.05 friction coefficient ■) structural frequency with volume fraction.

Chapter 6

CONCLUSION

The primary objective of this thesis is to investigate the potential to improve the design of sloshing absorbers through attaching surface roughness elements (obstructions) to the absorbers. The potential to increase energy dissipation through intentionally induced liquid sloshing within an absorber for structural control purposes is presented. Shallow liquid level sloshing absorbers are the main focus of this thesis. This is because low-level liquid absorbers produce travelling sloshing waves with superior energy dissipation capability, as opposed to deep-level liquids with sustained standing sloshing waves.

Large structures, such as tall buildings and bridges, are subject to wind and earthquake loads, which can cause them to oscillate at varying magnitudes. As these loads are random in nature, a sloshing absorber that is effective over a range of structural frequencies and initial displacement amplitudes is attractive for design purposes. Liquid sloshing absorbers using suggested optimum ratios, from Modi and Munshi (1998), to maximize energy dissipation are presented in Chapter 2, using Smoothed Particle Hydrodynamics (SPH). These sloshing absorbers are analysed over a range of structural frequencies and initial displacement amplitudes. Energy dissipation is enhanced with the introduction of semi-circular obstructions attached to the base of a rectangular sloshing absorber.

The case with 1 obstruction has an optimum ratio of obstruction height to liquid height (r/h_w) of 0.75, from Modi and Munshi (1998). This case increases energy dissipation evenly over

structural frequencies of 0.36 Hz to 0.92 Hz compared to the optimum case without an obstruction, from Modi and Munshi (1998). Improvements of up to 60 % are achieved with the introduction of an optimum obstruction. Introducing an obstruction, using optimum ratios, to ‘tuned’ liquid height cases increases energy dissipation significantly. A substantial increase in energy dissipation also occurs with an attached optimum obstruction when varying the initial displacement amplitude. Therefore, attaching 1 obstruction to the centre of the absorber’s base, with an r/h_w of 0.75 is recommended for structural applications.

Investigating the full potential of the effects of surface roughness elements (obstructions) was the main focus of Chapter 3. In general introducing obstructions close to the centre of the absorber improves the effectiveness of structural control and is consequently recommended. The central obstructions, increase shear energy dissipation due to wave-to-obstruction interactions. Also increases in liquid velocity as the wave travels over the obstruction, resulting in superior energy dissipation at the wave-to-wall interactions. Hence, small in-phase structural oscillations are eliminated.

Overall, both 1 and 3 obstruction cases give significantly increased energy dissipation over a range of liquid heights analysed when compared to the case without obstructions. The optimum case with 3 obstructions dissipates energy approximately 40 % faster than the same case without obstructions and about 30 % faster than the most effective case without obstructions. The most effective 3 obstruction case ceases structural oscillations 54 % faster than the same case without obstructions. This is a significant increase as the optimum obstruction case, from Modi and Munshi (1998), only produces an increase in energy

dissipation of about 20 % by attaching an obstruction, at an initial displacement of 16 degrees.

Displacement history comparisons between experimental observations and numerical predictions were promising. Slight variations were seen in predicted peak amplitude and frequency of structural oscillations. Increasing the smoothing length and using a gradient of kernel approximation for the boundary treatment proved insignificant. Very accurate free surface shape comparisons were achieved between experimental observations and numerical predictions using SPH. As a result, SPH is a competent design tool and is recommended to be used to further investigate energy dissipation in liquid sloshing absorbers.

In Chapter 4, numerical predictions are validated with previous experimental results, from Semercigil et al. (2013), to further investigate tuning a sloshing absorber through varying the inclination angle of the container. Varying the inclination angle alone consequently varies the liquid free surface length and therefore liquid frequency. Tuning a sloshing absorber is achieved when the liquid sloshing frequency equals the structural frequency. Therefore, practical advantages could include having one inclination that dissipates energy effectively over a range of structural frequencies. This would be attractive for design purposes as large structures oscillate at varying frequencies. Numerical predictions identify effective energy dissipation characteristics and give details, such as liquid velocity flow fields, which are not possible through experimental observations. Liquid sloshing absorbers with fixed free surface lengths are able to be tuned to achieve optimal energy dissipation at multiple structural frequencies through varying only the container's inclination angle.

At an inclination of 0 degrees, leading travelling waves at the liquid free surface occur with increased velocity gradients. This results in significant energy dissipation occurring at the wave-to-wall interactions. Increasing the inclination of the containers varies the dissipation characteristics of one side of each container. As the container is inclined, the liquid settles to one side of the container, exposing the base of the opposing side. The free surface varies as the structure oscillates, travelling up and down the sloped base of the container. Consequently, the wave travelling up and down the slope base does not reach the wall of the opposing side of the container. Therefore, dissipation on this side of the container is limited to shearing between the travelling wave and container base. This differs from the 0 degree inclination case where wave-to-wall interactions occur at both walls of the container. However, the variable free surface length of the inclined container possesses the potential to achieve effective energy dissipation over a range of structural frequencies.

Although dissipation characteristics vary between flat and inclined containers, the most effective cases at each structural frequency occur around the inclination angle where tuning of the static free surface length is achieved. For structural frequencies 0.5 Hz to 0.9 Hz, an inclination angle of 4 degrees is the most effective energy dissipater, producing significant increases in energy dissipation by 81 % compared to uncontrolled cases. This is attractive for design purposes as effective energy dissipation over a range of structural frequencies is essential for industrial applications where a large structure's frequency can vary significantly and is therefore recommended for structural applications. The inclination angle of 4 degrees is optimal at a structural frequency of 0.5 Hz where energy dissipation is enhanced by 96 % compared to the uncontrolled case.

Limited attempts to increase energy dissipation through attaching semi-circular obstructions to the container's base for inclinations above 0 degrees proved unsuccessful. This is due to the obstructions interrupting the travelling wave. Although energy is dissipated at the wave-to-obstruction interactions, superior shear dissipation is achieved through increased amounts of high velocity waves travelling up and down the smooth, sloped container base.

The novel concept of implementing the geometry of a hen's egg as a sloshing absorber is analysed in Chapter 5. The egg's unique, natural shape shows great potential producing high damping characteristics. Although the initial potential energy is dissipated in comparable times at all fill levels, an egg with a higher fill level is a more effective dissipater due to having larger initial potential energy and is therefore recommended. The relative insensitivity at high fill levels to varying the viscosity of the sloshing liquid is an additional benefit. This trend may also provide design incentives to enhance the dissipation capability of a natural egg with structural modifications.

Introducing 2 semi-circular obstructions to the inner shell of an egg produce superior energy dissipation at a volume fraction of 0.2 using water as the sloshing liquid. The increase in dissipation results in the egg ceasing oscillations in approximately half the time than the case without obstructions. This is a result of the wave-to-obstruction interactions producing severe velocity gradients within the liquid, dissipating increased amounts of energy.

An exploratory investigation is also presented into the possible self-tuning of an egg to maintain effectiveness at vastly different fill levels. Due to its unique shape, it seems that an egg is able to maintain tuning between the sloshing of its liquid content and the structural oscillations of its shell. This simple building block of nature has lessons to structural engineers in search for an effective and simple structural controller. Hence, continued efforts are certainly worthwhile.

REFERENCES

Altuntaş, E., Şekeroğlu, A., 2008, Effect of Egg Shape Index on Mechanical Properties of Chicken Eggs. *Journal of Food Engineering*, 85, 606-612.

Anderson, J.G., Semercigil, S.E. and Turan, Ö.F., 2000, A Standing-Wave Type Sloshing Absorber to Control Transient Oscillations, *Journal of Sound and Vibration*, 232, 838-856.

Avian Sciences Net, <http://ag.ansc.purdue.edu/poultry/class.htm>, Accessed February 14, 2012.

Banerji, B., Murudi, M., Shah, A.H., Poppelwell, N. 2000. Tuned Liquid Dampers for Controlling Earthquake Response of Structures, *Earthquake Engineering and Structural Dynamics*, 29, 587-602.

Blevins, R.D., 1979, *Formulas for Natural Frequency and Mode Shape*, Van Nostrand Reinhold Company, New York.

Cleary, P.W., 1998, Modelling Confined Multimaterial Heat and Mass Flows using SPH, *Appl. Math. Modelling*, 22, 981-993.

Cleary P.W., Prakash, M., 2004, Discrete Element Modelling and Smooth Particle Hydrodynamics: Potential in the Environment Sciences, *Phil. Transaction of Royal Society*, 362, 2003-2030.

Cleary, P.W., Prakash, M., Ha, J., Stokes, N., Scott, C., 2007, Smooth Particle Hydrodynamics: Status and Future Potential. *Progress in Computational Fluid Dynamics*, 7, 70-90.

Colagrossi, A., Palladino, F., Greco, M., Lugni, C., & Faltinsen, O.M., 2004, Experimental and Numerical Investigation of 2D Sloshing: Scenarios Near the Critical Filling Depth, In *Proc. 19th International Workshop on Water Waves and Floating Body*, Cortona, Italy.

Colagrossi, A., Palladino, F., Greco, M., Lugni, C., Faltinsen, O.M., 2006, Experimental and Numerical Investigation of 2D Sloshing with Slamming, In *Proc. 21st International Workshop on Water Waves and Floating Body*, Loughborough, England.

Cummins, C.J., Silvester, T.B. and Cleary, P.W., 2012, Three-dimensional Wave Impact on a Rigid Structure using Smoothed Particle Hydrodynamics, *International Journal of Numerical Methods in Fluids*, 68, 1471-1496.

Forbes, L. K, 1988, Critical Free-surface Flow over a Semi-circular Obstruction, *Journal of Engineering Mathematics* 22, 3-13.

Gardarsson, S., Yeh, H. and Reed, D., 2001, Behavior of Sloped-Bottom Tuned Liquid Dampers, *Journal of Engineering Mechanics*, March, 266-271.

Gingold, R.A., Monaghan, J.J., 1977, *Mon. Not. R. Astron. Soc.*, 181, 375.

Lucy, L.B., 1977, *Astron. J.*, 82, 1013.

Gradinscak, M., Semercigil, S.E. and Turan, Ö.F., 2002, Design of Flexible Containers for Sloshing Control, *Proceedings of ASME FEDSM*, Montreal, Quebec, Canada.

Guzel, B., Prakash, M., Semercigil, S.E., & Turan, Ö.F., 2005, Energy Dissipation with Sloshing for Absorber Design, *International Mechanical Engineering Congress and Exposition*, IMECE2005-79838.

Ikeda, T., Ibrahim, R.A., 2005, Nonlinear Random Responses of a Structure Parametrically Coupled with Liquid Sloshing in a Cylindrical Tank. *Journal of Sound and Vibration*, 284, 75-102.

Kaneko, S., and Mizota, Y., 2000, Dynamic Modeling of Deepwater-Type Cylindrical Tuned Liquid Damper with a Submerged Net, *Journal of Pressure Vessel Technology*, 122, 96-104.

Kareem, A. 1990. Reduction of Wind Induced Motion Utilising a Tuned Sloshing Damper, *Journal of Wind Engineering and Industrial Aerodynamics*, 36, 725-737.

Kline, S.J., and F.A. McClintock, 1953, Describing Uncertainties in Single-Sample Experiments, *Mechanical Engineering*, 75, 3-8.

Lu, M.L., Poppelwell, N., Shah, A.H., Chan, J.K., 2004, Nutation Damper Undergoing a Coupled Motion, *Journal of Vibration and Control*, 10, 1313-1334.

Marsh, A.P., Prakash, M., Semercigil, S.E., Turan, Ö.T., 2009, A Study of Sloshing Absorber Geometry for Structural Control with SPH, 4th international SPHERIC Workshop, Nantes, France, 232-239.

Marsh, A.P., Prakash, M., Semercigil, S.E., Turan, Ö.F., 2010, A Numerical Investigation of Energy Dissipation with a Shallow Depth Sloshing Absorber, *Applied Mathematical Modelling*, 34, 2941-57.

Marsh, A.P., 2010, Design of Effective Traveling-Wave Sloshing Absorbers for Structural Control, Ph.D. Thesis, Victoria University.

Marsh, A., Prakash, M., Semercigil, S.E., Turan, Ö.F., 2011, A Study of Sloshing Absorber Geometry for Structural Control with SPH. *Journal of Fluids and Structures*, 27(8), 1165-1181.

Marsh, A., Prakash, M., Semercigil, S.E., Turan, Ö.F., 2012, An Investigation and Modelling of Energy Dissipation through Sloshing in an Egg-shaped Shell, *Journal of Sound and Vibration*, 330(26), 6287-6295.

Milne-Thomson, L.M., 1968, *Theoretical Hydrodynamics*, 5th ed., Macmillan Press, London, 426-463.

Modi, V.J., Welt, F. & Seto, M.L., 1996, Control of Wind Induced Instabilities through Application of Nutation Dampers: A Brief Overview, *Engineering Structures*, 17, 626-638.

Modi, V.J., Munshi, S.R., 1998, An Efficient Liquid Sloshing Damper for Vibration Control, *Journal of Fluids and Structures*, 12, 1055-1071.

Modi, V.J., Akinturk, A., 2002, An Efficient Liquid Sloshing Damper for Control of Wind-induced Instabilities, *Journal of Wind Engineering and Industrial Aerodynamics*, 90, 1907-1918.

Modi, V.J., Akinturk, A., and Tse, W., 2003, A Family of Efficient Sloshing Liquid Dampers for Suppression of Wind-induced Instabilities, *Journal of Vibration and Control*, 9, 361-386.

Monaghan, J.J., 1992, Smoothed Particle Hydrodynamics, *Ann. Rev. Astron. Astrophys.* 30, 543-574.

Monaghan, J.J., 1994, Simulating Free Surface Flows with SPH, *J. Computat. Phys.* 110, 399-406.

Olsen, D.E. and Reed, D.A., 2001, A Nonlinear Numerical Model for Sloped-bottom Tuned Liquid Dampers, *Earthquake Engineering and Structural Dynamics*, 30, 731-743.

Semercigil, S.E., Turan, Ö.F., Kopp, G.A., & Terres-Nicoli, J.M., 2013, A Sloshing Absorber for Limiting Torsional Buffeting Oscillations of a Long Span Bridge Deck. Submitted to the *Journal of Sound and Vibration*.

So, G., Semercigil, S.E., 2004, A Note on a Natural Sloshing Absorber for Vibration Control. *Journal of Sound and Vibration*, 269, 1119-1127.

Tamura, Y., Kohsaka, R., Nakamura, O., Miyashita, K., Modi, V.J., 1996, Wind-induced Responses of an Airport Tower – Efficiency of a Tuned Liquid Damper, *Journal of Wind Engineering*, 65, 121-131.

Wu, J., Chang, C. and Lin, Y., 2009, Optimal Designs for Non-uniform Tuned Liquid Column Dampers in Horizontal Motion, *Journal of Sound and Vibration*, 326, 104-122.

Young-Kyu, J, 2004, Structural Behaviour of Water Sloshing Damper with Embossments Subject to Random Excitation, Canadian Journal of Civil Engineering, 31, 120- 132.

APPENDIX 1

SMOOTHED PARTICLE HYDRODYNAMICS

In this appendix, a description of the Smoothed Particle Hydrodynamics (SPH) method is given. The SPH method was first developed by Gingold and Monaghan (1977) and independently by Lucy (1977). An in depth description of the SPH method can also be found here (J.J. Monaghan, 1992).

SPH is a Lagrangian continuum method used for solving systems of partial differential equations (PDEs). SPH is also a mesh-free particle based method used to model fluid flows. The fluid particles are discretized and the properties of these particles are attributed to their centres. The method tracks the fluid particles over continuous interpolated fields. SPH uses an interpolation kernel function to smooth the properties of these particles such as density, velocity and pressure over the interpolated fields. The SPH code used for this thesis was developed by the CSIRO (Commonwealth Scientific and Industrial Research Organisation) Division of Mathematics, Informatics and Statistics.

The interpolated value of any field A at position r is approximated using Equation (A1) where each particle ' b ' has properties mass m_b , position r_b , density ρ_b , and velocity v_b .

$$A(r) = \sum_b m_b \frac{A_b}{\rho_b} W(r - r_b, h) \quad (\text{A1})$$

W is the interpolation kernel and A_b is the value of A at position r_b . The smoothing length is denoted by h and is the region in which the smoothing function operates. In this thesis a

smoothing length of 1.2 times the particle separation is used unless otherwise stated where the particle separation is equal to the particle length in one direction. The smoothing function allows approximations to the properties of the fluid particles to be calculated. As a result the smoothing function determines the gradients of these fluid properties given by Equation (A2) for the function A .

$$\nabla A(r) = \sum_b m_b \frac{A_b}{\rho_b} \nabla W(r - r_b, h) \quad (\text{A2})$$

The SPH continuity equation is given by Equation (A3) from Monaghan (1992, 1994).

$$\frac{d\rho_a}{dt} = \sum_b m_b (v_a - v_b) \nabla W_{ab}, \quad (\text{A3})$$

where $W_{ab} = W(r_{ab}, h)$ which is the interpolation kernel and is evaluated for the distance $|r_{ab}|$ where r_{ab} is the position vector from particle 'b' to particle 'a' given by $r_{ab} = r_a - r_b$.

The SPH momentum equation is given in Equation (A4) from Cleary (1998).

$$\frac{dv_a}{dt} = - \sum_b m_b \left[\left(\frac{P_b}{\rho_b^2} + \frac{P_a}{\rho_a^2} \right) - \frac{\xi}{\rho_a \rho_b} \frac{4\mu_a \mu_b}{(\mu_a + \mu_b)} \frac{v_{ab} r_{ab}}{(r_{ab}^2 + \eta^2)} \right] \nabla_a W_{ab} + g \quad (\text{A4})$$

P_a and μ_a are pressure and viscosity of particle 'a'. $v_{ab} = v_a - v_b$ and g is the gravitational acceleration. Here η is a parameter used to smooth out the singularity at $r_{ab} = 0$.

The time-step for the simulations in this thesis is given in Equation (A5) and is limited to the Courant condition modified for the presence of viscosity.

$$\Delta t = \min_a \left\{ \frac{0.5h}{c_s + 2\xi\mu_a / h\rho_a} \right\}, \quad (\text{A5})$$

where c_s is the local speed of sound. A time step of 1×10^{-6} s remains constant for the thesis.

SPH, being a compressible method, is used near the incompressible limit and therefore a speed of sound that is significantly larger than the velocity scales in the flow is chosen. The equation of state, governing the relationship between particle density and fluid pressure is given in Equation (A6) where P is the magnitude of the pressure.

$$P = P_0 \left[\left(\frac{\rho}{\rho_0} \right)^\gamma - 1 \right], \quad (\text{A6})$$

where P_0 is the reference pressure and ρ_0 is the reference density. The exponent $\gamma = 7$ is used for water.

Particles are modeled in SPH representing solid boundaries. These solid particles are assigned properties including density, mass and velocity. The boundary particles exert forces on the fluid particles with two approximations used to calculate the force in this thesis. The Lennard-Jones type forcing is the most common form used in this thesis. This is the cheapest form as it only requires a single layer of particles at the boundary. The force in this

approximation acts in the normal direction to the boundary particles and is given in Equation (A7).

$$F_{LJ} = -24\varepsilon \left[2 \left(\frac{\sigma^{12}}{r^{13}} \right) - \left(\frac{\sigma^6}{r^7} \right) \right] , \quad (A7)$$

where ε , σ and r are the depth of the potential well, distance at which the inter-particle potential is zero and distance between the particles respectively. Each particle's force is interpolated creating a smoothly defined repulsive boundary force aiming at restricting penetration of the boundary by the fluid particles.

The gradient of kernel approximation is the second forcing type used in this thesis and is only analysed in Chapter 3. This form is more expensive than the previous approximation as it requires 3 or more layers of boundary particles, which evolve their densities and are included in the summations of the continuity and momentum equations. In Chapter 3, a smoothing length of 2.4 times the particle separation is used requiring 3 layers of particles at the boundary to achieve an accurate representation.

The Improved Euler Integration Scheme is used for all simulations in this thesis. This is a numerical procedure for solving ordinary differential equations with a given initial value. The procedure to calculating the initial value problem is given in Equation (A8) and (A9).

$$y'(t) = f(t, y(t)) \quad , \quad (A8)$$

$$y(t_0) = y_0 \quad , \quad (A9)$$

The trapezoidal scheme is given in Equation (A10).

$$y_{i+1} = y_i + \frac{h}{2}[f(t_i, y_i) + f(t_{i+1}, y_{i+1})] , \quad (\text{A10})$$

where h is the step size. Predicting y_{i+1} using Euler's method, a more accurate approximation can be made. Setting $y_{i+1} = y_i + hf(t_i, y_i)$ in the right side of Equation (A10) the Improved Euler's Integration Scheme is produced given in Equation (A11).

$$y_{i+1} = y_i + \frac{h}{2}[f(t_i, y_i) + f(t_i + h, y_i + hf(t_i, y_i))] , \quad (\text{A11})$$

where $t_{i+1} = t_i + h$. This is an improvement as it uses the trapezoid scheme, compared to Euler's method, which uses a rectangle.

APPENDIX 2

RESOLUTION STUDY

In this appendix, the accuracy of the numerical predictions using Smoothed Particle Hydrodynamics (SPH) is investigated by varying the particle size. The particle sizes are analysed to determine when resolution independence occurs and what particle size is capable of predicting accurate liquid behaviour without significantly increasing computational time unnecessarily.

Two-dimensional particle sizes of 0.4 mm x 0.4 mm (0.16 mm²), 0.8 mm x 0.8 mm (0.64 mm²) and 1.2 mm x 1.2 mm (1.44 mm²) are analysed requiring approximately 15300, 3800 and 1400 particles respectively to discretize the liquid. The case with 3 obstructions located in the bottom centre of the container and a liquid height of 7.7 mm is used from chapter 3. The 7.7 mm liquid height was chosen for this resolution study as it was around the most common liquid height used throughout the thesis, being approximately 8 mm (mainly in Chapters 2, 3 and 4). By choosing the most commonly used liquid height the potential to study a resolution that satisfies the majority of the chapters can be achieved.

Displacement histories for 0.16 mm², 0.64 mm² and 1.44 mm² are displayed in Figure A2.1. The initial conditions for all resolution cases are the same with the structure having an initial displacement of 16 degrees. The structure is then released exciting the liquid within the container and allowing the structure to move and respond freely. Resolution dependence is

achieved with particle size cases 0.16 mm^2 and 0.64 mm^2 having very similar displacement histories. However, the displacement history of the case with a particle size of 1.44 mm^2 differs with increased amplitude and marginally larger natural frequency or shorter period of oscillation. From this, 0.16 mm^2 and 0.64 mm^2 particle sizes are both acceptable resolutions to be used.

Liquid free surface shape snapshots of experimental observations and numerical predictions are displayed in Figures A2.2(a) to (f). Instances analysed were chosen due to particular points of interest. These included wave-to-wall interactions where liquid was most energetic and wave-to-obstruction interactions to determine how the liquid interacted with the obstructions. The first two cycles of motion of the container are compared due to the liquid being most energetic within the first two cycles.

Experimental liquid free surface snapshots are displayed in Figures A2.2(a), (e), (i), (m), (q) and (u) that occur at 1.14 s, 1.22 s, 1.94 s, 2.24 s, 3.38 s and 4.84 s as indicated in the top left hand corner of each figure. Numerical prediction snapshots for 0.16 mm^2 , 0.64 mm^2 and 1.44 mm^2 particle areas are displayed in the remaining figures at the same instances in time as the experimental snapshots. Particle sizes for these numerical predictions are indicated in the top right hand corner of the figures. The liquid velocity in the simulations ranges from 0 to 1 m/s as displayed in the fixed colour scale at the bottom of the figure.

The first wave-to-wall interaction occurs at 1.14 s with the liquid travelling from right to left. A hydraulic jump occurs with large free surface deformation, in Figure A2.1(a). Significant

swirling occurs close to the left container wall as the liquid falls due to gravity. The swirling pattern is captured effectively by particle sizes 0.16 mm^2 in Figure A2.2(b) and 0.64 mm^2 in Figure A2.2(c). However the resolution is not high enough for particle size 1.44 mm^2 in Figure A2.1(d) to notice the swirling pattern. As particle size increases, swirling becomes less defined and velocity gradients displayed in the colour range are not as steep as a result. This issue also occurs in Figure A2.1(h) at 1.22 s as the wave continues to fall.

After the first wave-to-wall interaction, the liquid then travels from left to right. The interaction from the effect of the obstructions is displayed in Figures A2.2(i) at 1.94 s. Predicted liquid particle velocities are seen to be dependent on resolution. A higher proportion of the liquid is coloured red for the particle size 1.44 mm^2 in Figure A2.2(l) due to the increase in liquid velocity causing a larger natural frequency displayed in Figure A2.1.

The first wave-to-wall interaction on the right wall is displayed in Figure A2.2(m) as the liquid continues to travel from left to right. A hydraulic jump occurs with large free surface deformation and swirling. Again swirling is predicted by 0.16 mm^2 in Figure A2.2(n) and 0.64 mm^2 in Figure A2.2(o). As resolution decreases the liquid free surface becomes less smooth. This is noticed for particle size 1.44 mm^2 Figure A2.2(p) with the liquid on the left side of the container not being able to predict the smooth liquid free surface in the experiment.

At 3.38 s, the liquid's travelling wave begins to interact with the left container wall in Figure A2.2(q). This is predicted numerically for all particle sizes. However for particle size 1.44

mm² in Figure A2.2(t) the wave occurring at the wall is more developed and the right side of the container base is exposed. This is due to the larger portion of the liquid having a high velocity displayed previously causing a larger natural frequency and increased amplitude displayed in Figure A2.1. The second wave to wall interaction on the right wall is displayed in Figure A2.2(u). Liquid free surface is predicted for particle sizes 0.16 mm² in Figure A2.2(v) and 0.64 mm² in Figure A2.2(w). Liquid distribution is again dependent on resolution with majority of the left base of the container exposed for particle size 1.44 mm² in Figure A2.2(x).

For a liquid height of 7.7 mm particle sizes 0.16 mm² and 0.64 mm² accurately predicted energetic wave-to-wall interactions with large liquid free surface deformation. However, particle size 1.44 mm² did not have a high enough resolution to predict swirling occurring during the wave-to-wall interactions and less smooth free surface flows. Also, increased liquid velocities were seen in higher proportions of the liquid (coloured red) for the particle size 1.44 mm² causing a larger natural frequency and increased amplitude. Hence, both particle sizes 0.16 mm² and 0.64 mm² would be suitable resolutions to use for this liquid height.

Liquid heights from 2.6 mm to 12.8 mm are analysed in Chapter 3. When liquid is extremely shallow, predicted liquid distribution and travelling wavefront positions differ at low resolution. This is because particle size affects the liquid's ability to spread across the container surface (A. Marsh et al., 2010). Therefore, extra computational time is sacrificed to achieve accurate liquid behaviour at such extremely shallow liquid heights. Chapter 3 uses

the smallest container of all the chapters, resulting in the reduced amount of particles required to achieve the same liquid heights. Also, using the smaller container allows the case with the deepest liquid height of 12.8 mm to be within the practical limit with the currently available computational facility. As a result, for consistency a particle size of 0.16 mm^2 was used for all simulations in chapter 3.

In chapter 2, liquid heights from 7.2 mm to 47.2 mm are analysed. A particle size of 0.16 mm^2 is used for liquid heights below 8 mm. As liquid heights are substantially deeper and the container is larger than the sloshing absorbers analysed in Chapter 3, a particle size of 0.64 mm^2 is used for liquid heights of 8 mm and above. The same particle size was also used in Chapter 4 for a liquid height of 7.9 mm. In both Chapters 2 and 4, larger containers are used compared to Chapter 3, resulting in an increased amount of liquid particles required to achieve the same liquid height. However, this Resolution Study has given evidence that a particle size of 0.64 mm^2 is suitable to predict accurate liquid behaviour while remaining within the practical limit with the currently available computational facility.

Three-dimensional simulations are undertaken in Chapter 5. As a result, up to 5 times the amount of particles are required compared to the highest amount of particles used for the two-dimensional simulations. Therefore, a $0.8 \text{ mm} \times 0.8 \text{ mm} \times 0.8 \text{ mm}$ (0.512 mm^3) particle size, has been determined to be at the edge of the practical limit with the currently available computational facility. Halving the particles size increases the run time by 16 times for the three-dimensional simulations (J.J. Monaghan, 1992) (P. Cleary and M. Prakash, 2004). A

particle size of 0.512 mm^3 gave close correspondence between three-dimensional numerically predicted displacement histories and experimental observations.

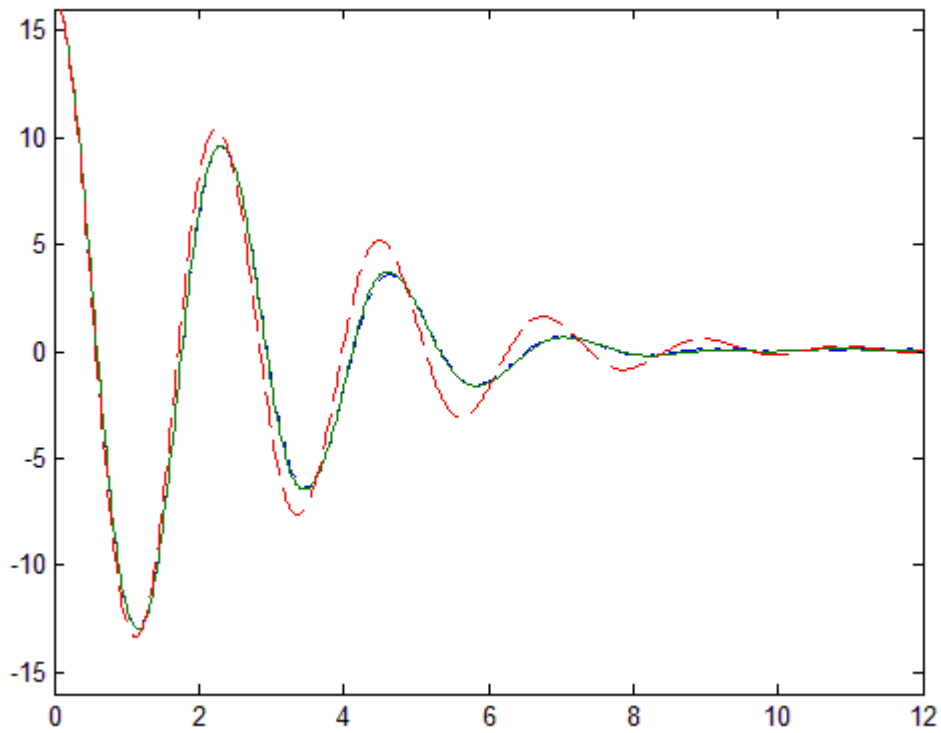
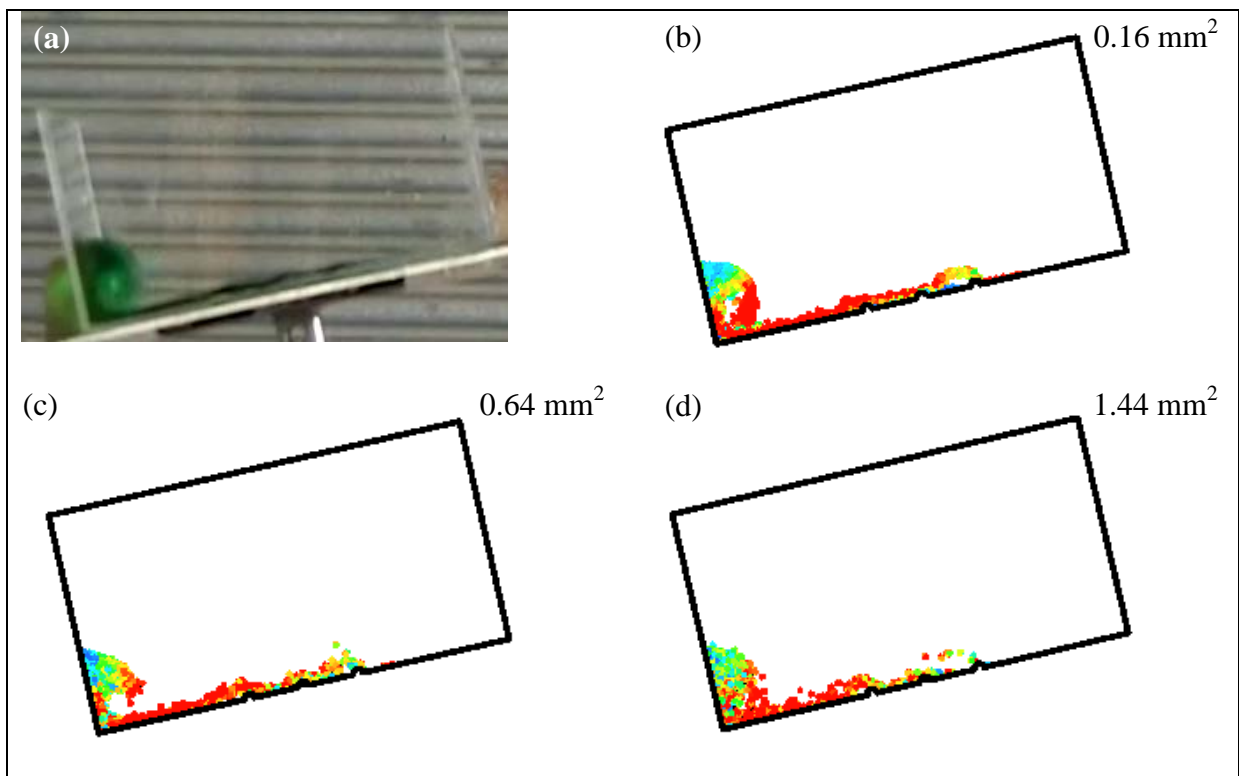


Figure A2.1. Transient displacement histories of numerical predictions with 0.16 mm^2 (—), 0.64 mm^2 (---) and 1.44 mm^2 (- - -) particle sizes. Obstruction case used is three semi-circle obstructions with a 4mm obstruction height and a 7.7mm liquid depth, with a 16° initial displacement.

t = 1.14 s



t = 1.22 s

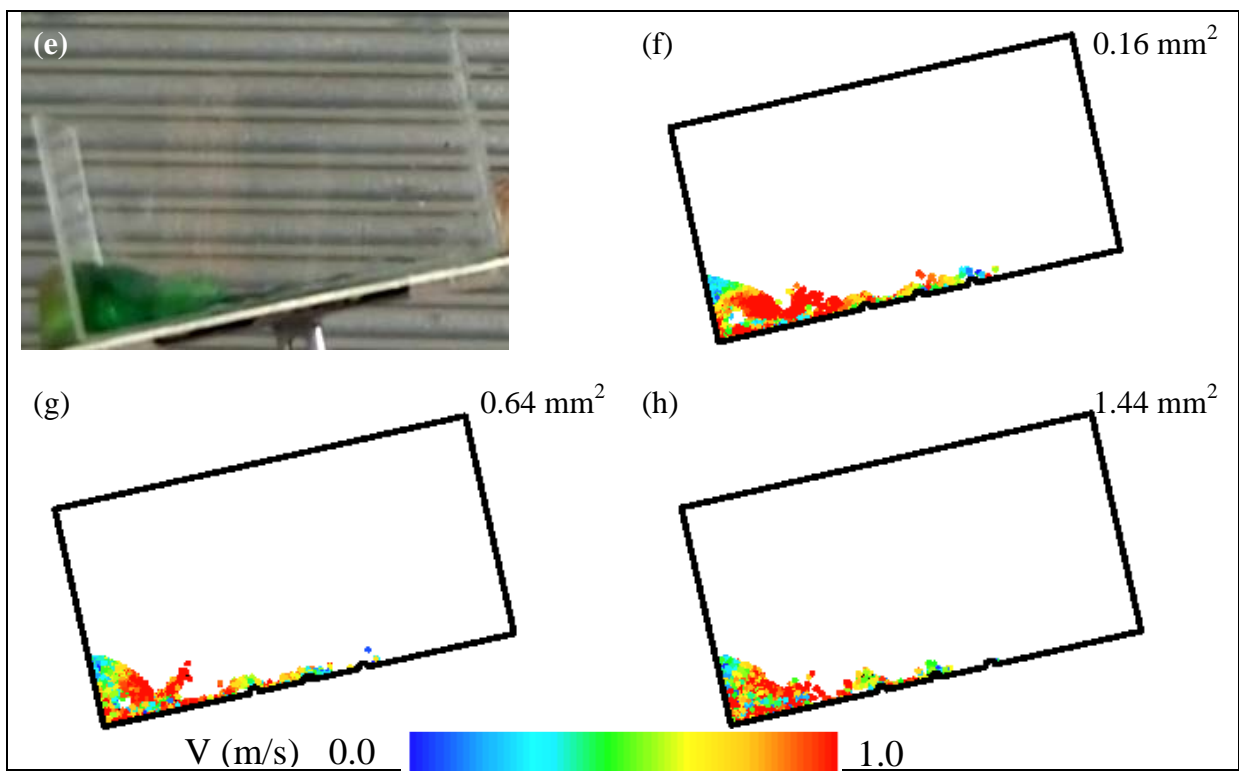
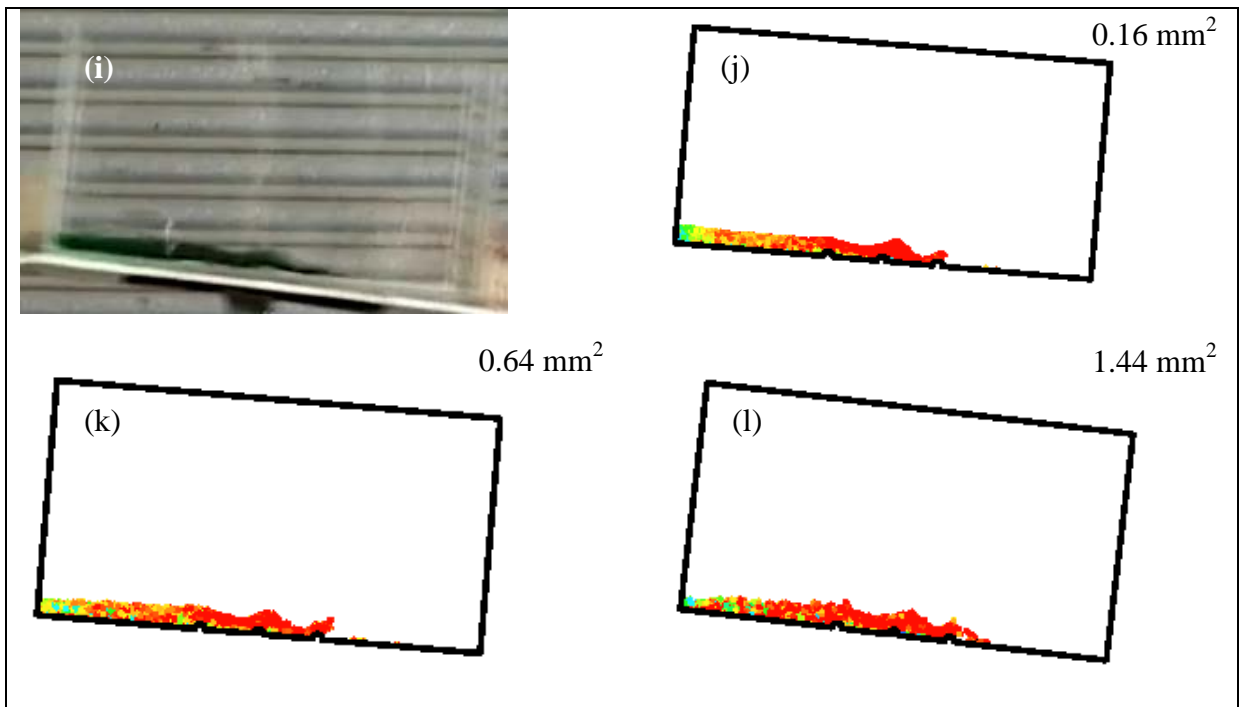
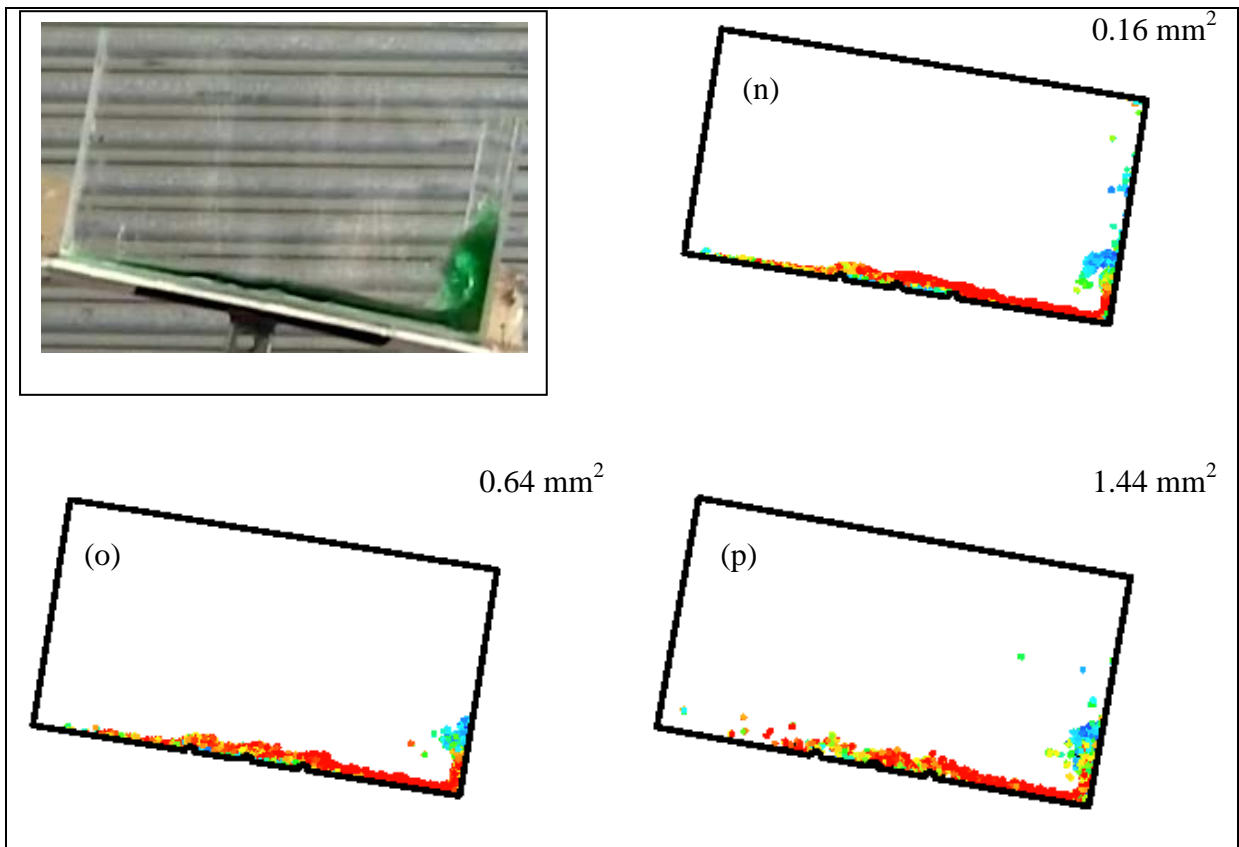


Figure A2.2. Free surface comparisons between experimental observations, and numerical predictions obtained with particle sizes of 0.16 mm², 0.64 mm² and 1.44 mm². Particle size is marked at bottom right corner of frames. Fixed velocity scale shows liquid particle velocity ranging from 0 to 1m/s.

t = 1.94 s

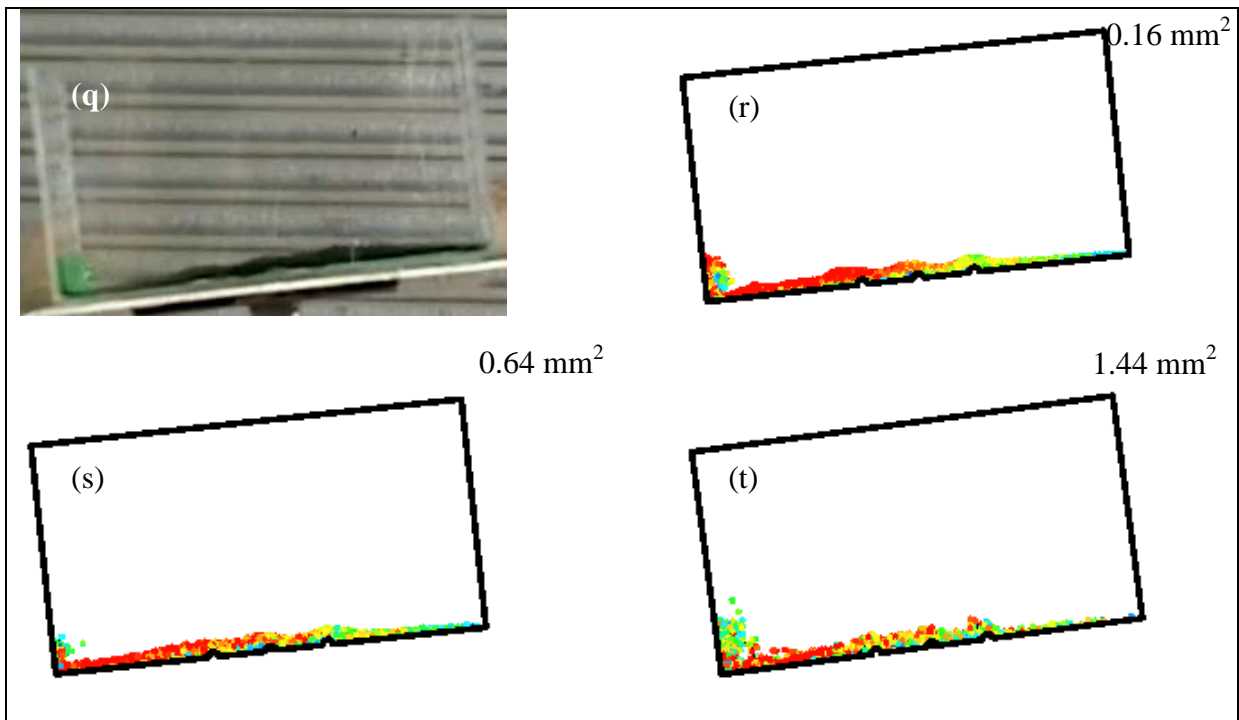


t = 2.24 s

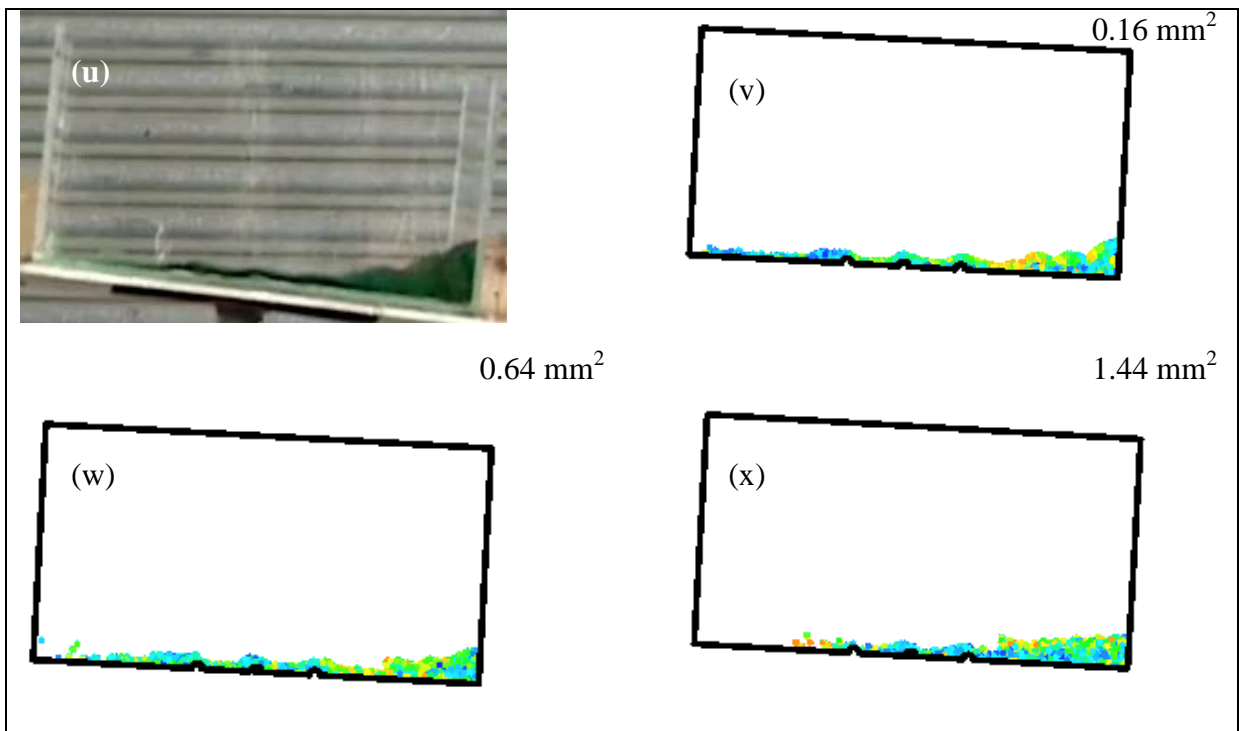


V (m/s) 0.0  1.0
Figure A2.2. Continued.

t = 3.38 s



t = 4.84 s



V (m/s) 0.0  1.0

Figure A2.2. Continued.